Embryonic stem cell-derived macrophages

–

A novel approach to developing anti-inflammatory macrophages for cell therapy

Noémie Caroline J. Nkejabega

A thesis submitted for the degree of Doctor of Philosophy

The University of Edinburgh

2013

DECLARATION

I declare that the work presented in this thesis is my own and has not previously been published or presented towards another higher degree except where clearly acknowledged as such in the text.

16.10.2013

Noémie Caroline J. Nkejabega Dated

ABSTRACT

Ischemia/reperfusion injury (IRI) is a major cause of acute kidney injury (AKI) that is associated with high morbidity and mortality. Macrophages (Mφ) are multifunctional cells involved in the initiation, progression and resolution of kidney inflammation response. The enzyme hemeoxygenase-1 (HO-1) is upregulated in response to cell stress and metabolises heme-containing proteins to carbon monoxide (CO) and bilirubin that possess anti-apoptotic and anti-oxidant properties. Previous work has shown that Mφ can be used as therapeutic vectors with the administration of bone marrow-derived macrophages (BMDM) overexpressing HO-1 being protective in murine renal IRI (Ferenbach et al., 2010). However, these studies used primary BMDM that are inherently heterogeneous with the genetic manipulation achieved by adenoviral transduction that is not suitable for use in patients. Previous work has shown that pure Mφ populations may be generated from murine and human embryonic stem cells (ESC) *in vitro*, providing an essentially limitless source of Mφ that can be derived from genetically manipulated cells. This project has adopted an ESC approach to develop anti-inflammatory ESC-derived macrophages (ESDM) overexpressing HO-1 for therapeutic use in experimental models of AKI. We successfully generated Mφ from ESC and demonstrate that ESDM are comparable to BMDM in all properties that we tested. ESDM are large mononuclear cells and express Mφ cell surface markers ($F4/80^{high}$ $CD11b^{high}$ $CD11c^{high}$ MHC class II^{low}). ESDM are phagocytic and produce pro-inflammatory mediators when activated by lipopolysaccharide and interferon-γ (LPS and IFNγ).

ESC were then genetically manipulated to overexpress HO-1 under the control of the constitutive pCAG promoter. Our results suggest that a high level of constitutive HO-1 overexpression in ESC impacts on ESC number, self-renewal and Mφ

differentiation. Thus, we decided to generate ESC that overexpress HO-1 under an inducible promoter using the A2lox.cre system. HO-1 inducible ESC exhibited significant HO-1 up-regulation and generated F4/80^{high} CD11b^{high} CD11c^{int} MHC II^{low} ESDM. However, HO-1 inducibility by doxycycline (Dox) was lost following both ESDM differentiation and RA induced differentiation of ESC. A similar loss of Dox-induced gene expression following ESDM differentiation or RA induced cell differentiation was found in ESC expressing a control eGFP transgene under the control of the same inducible promoter.

In view of the difficulties encountered using the inducible systems, a pharmacological approach using treatment with the potent HO-1 inducer hemearginate (HA) was used to upregulate HO-1 expression in ESDM. HA treatment significantly upregulated HO-1 expression by ESDM. HA treatment modulated ESDM phagocytosis and the production and gene expression of both pro- and anti-inflammatory mediators (NO, TNFα, IL-10 and IL-6) following LPS and IFNγ stimulation. Intravenous injection of fluorescently labelled ESDM directly after inducing renal IRI resulted in the localisation of the ESDM to solid organs and preferential homing to the injured kidney at the 1 hour time point indicating their potential for use in cell therapy.

In conclusion, we were able to generate functional Mφ from ESC. The differentiation of ESC to Mφ resulted in the loss of inducible gene expression and pharmacological HO-1 induction was used. HA treated ESDM present promising anti-inflammatory properties *in vitro* and home to the injured kidney in a model of murine IRI *in vivo*. Further experiments are still needed to determine if HA treated ESDM exert anti-inflammatory properties *in vivo*. However, our findings are a strong platform for future studies of the translational potential of using modified ESDM in cell therapy.

The best way out is always through.

R. Frost

Acknowledgements

It would not have been possible to write this thesis without the help and support of the kind people around me, to only some of whom, in no specific order, it is possible to give particular mention here.

I would like to express my utmost gratitude to my supervisor, Professor Jeremy Hughes for his continuous support during my PhD.
Dear Jeremy, for your "half full glass" vision of Life, patience with all my doubts, infectious enthusiasm, and immense knowledge, I shout Thank you! Merci! Diolch! Meeting you was pure serendipity! And today, at the end of my PhD journey, I can tell that you're the Best supervisor I could have had.

I would also like to thank Professor Lesley Forrester and Dr David Kluth for their encouragement and insightful comments.

Thanks to Dr Richard Axton, Helen Taylor and Julie Wilson for their precious help. Ms Rachel Victoria Richardson and Ms Joena Bal for their eager contribution.

Dear Spike, if it wasn't for you, I'd never have landed in Edinburgh!
Chère Grande Chef, Nathalie, si tu n'étais pas aussi sympa/bavarde, je n'aurais jamais atterri à Edimbourg!

I acknowledge the Medical Research Council UK that provided me with financial support for this research through an MRC PhD Studentship.

À ma Famille…
BONNE ANNÉÉÉÉE aux Assumani! Mon irremplaçable Marraine, Mon beau(dineux) Tonton et mes couz : Zaïna, Antoine et Marie-So !
À Luc & Nicole
À Anne & Fred & Antoine

Mais aussi à…
My dear friends, Catherine and Lindsay, You ROCK! Can't describe how happy I am we found each other! Edinburgh wouldn't be Edinburgh without you. Love you to bits! See you around the world! xxx
Marie d'être la plus géniale des potes, Fred & Sarah et Mathieu & Perrine pour les soupers/encouragements/…, Andréa -surtout de m'avoir présenté Fran, Mahmoud for your unconditional Luv, Nathalie Caron & ses filles de m'avoir sorti de mon trou, Brenda & Beano Hughes for being so welcoming while I was writing the last lines of this work, my fellow PIG lab mates especially Katie, Jillian, Alicja and Al Dane for the stimulating discussions and for all the fun we've had in the last three years^{+}.
Ryanair, Skype, Facebook, and all the mice who gave their life to Science…

Et puis surtout…

À Papoun & Mutti,

Merci pour la liberté que vous m'avez accordée, pour cette éducation maintes fois critiquée, pour ces mots qui m'ont souvent poussée, parfois freinée… Merci d'avoir contribué à faire de moi qui je suis aujourd'hui et surtout de m'encourager à aimer cette personne. Je vous aime.

À Maïté,

Pour ton humeur changeante, qui me permet de savourer intensément tes câlins spontanés, tes « ma sœuuuur », tes sourires,... Grandir à tes côtés ma sœur, c'est grandir tout court. Je t'aime et je suis fière de la femme que tu deviens.

À Gilles,

Je craquerais bien pour l'occasion, mais il ne faut pas exagérer non plus! Gilles tu es, et Gilles tu resteras, rien que pour moi! Pti frère, mes voyages, la solitude, les doutes… Tu sais que ça a été très dur. Mais rien que pour les liens que la distance a resserrés entre nous, je recommencerais ! C'est apaisant de (enfin) me sentir proche de toi, je t'aime.

À toi, mon Fran…

Table of Contents

DECLARATION 2

ABSTRACT 3

ACKNOWLEDGEMENTS 6

TABLE OF CONTENTS 9

FIGURES 17

TABLES 24

LIST OF ABBREVIATIONS 25

CHAPTER 1. INTRODUCTION 29

1.1 THE KIDNEY 29

1.1.1 Anatomy of the kidney *29*

1.1.2 Kidney vasculature *32*

1.2 RENAL FAILURE 35

1.2.1 Pathophysiology of ischaemic acute kidney injury *38*

1.2.1.1 Proximal tubule alterations and injury 40

1.2.1.2 Haemodynamic changes 40

1.2.1.3 Cellular death 41

1.2.1.4 Microvascular alterations 42

1.2.1.5 Inflammatory response 44

1.3 THE HEMEOXYGENASE SYSTEM 48

1.3.1 Hemeoxygenase-1 and the kidney *52*

1.3.1.1 Hemeoxygenase-1 in ischaemic acute kidney injury 53

1.3.2 Strategies of hemeoxygenase-1 up-regulation as therapy in models of renal inflammation *54*

1.3.2.1 Pharmacological induction of hemeoxygenase-1 54

1.3.2.2 HO-1 gene therapy 58

1.3.3 Kidney gene therapy *62*

1.3.4 Alternatives to direct targeting of HO-1 ..... *64*

1.4 MACROPHAGES 65

1.4.1 Macrophages cell therapy in renal inflammation and ischaemic acute kidney injury *68*

1.4.2 Macrophages as vector for HO-1 therapy in renal inflammation and ischaemic acute kidney injury *70*

1.5 EMBRYONIC STEM CELLS 71

1.5.1 Embryonic stem cell derived macrophages *73*

1.6 HYPOTHESIS 76

1.7 AIMS 76

CHAPTER 2. MATERIAL AND METHODS **77**

2.1 MATERIALS AND REAGENTS 77

2.2 EMBRYONIC STEM CELLS 77

2.2.1 E14 IV cell line *77*

2.2.2. A2lox.cre cell line *77*

2.2.3 Embryonic stem cell self-renewal–alkaline phosphatase activity assay *80*

2.2.4 Retinoic acid – embryonic stem cell differentiation assay *83*

2.2.5 Embryonic stem cell cryopreservation *83*

2.3 PREPARATION OF MACROPHAGES, DENDRITIC CELLS AND MONOCYTES 83

2.3.1 Preparation of L929-Conditioned Medium *83*

2.3.2 Preparation of embryonic stem cell-derived macrophages *84*

2.3.3 Preparation of bone marrow derived macrophages *88*

2.3.4 Preparation of bone marrow derived dendritic cells *88*

2.3.5 Purification of bone marrow monocytes *89*

2.4 CHARACTERISATION OF MACROPHAGES 90

2.4.1 Cytospin followed by Diff-quick staining *90*

2.4.2 Immunohistochemistry analysis of cells *90*

2.4.3 Flow cytometry *91*

2.4.4 Phagocytosis assay *94*

2.4.4.1 Flow cytometry analysis of phagocytosis of fluorescent latex beads 94

2.4.4.2 Preparation of apoptotic thymocytes 95

2.4.4.3 Fluorescent microscopy analysis of phagocytosis of apoptotic thymocytes 95

2.4.5 Macrophage activation: LPS and IFNγ stimulation *98*

2.4.5.1 Nitric oxide measurement 98

2.4.5.2 Enzyme Linked Immunosorbent Assay 100

2.5 INDUCTION OF HEMEOXYGENASE-1 EXPRESSION 101

2.5.1 Pharmacological induction of hemeoxygenase-1 expression *101*

2.5.2 Genetically engineered induction of hemeoxygenase-1 expression *101*

2.5.2.1 Constitutive overexpression of hemeoxygenase-1 under the pCAG promoter 101

2.5.2.2 Tetracycline inducible system: using the A2lox.cre embryonic stem cell line 102

2.6 DETECTION OF HEMEOXYGENASE-1 PROTEIN 102

2.6.1 Western blotting *102*

2.6.2 Flow cytometry analysis of intracellular hemeoxygenase-1 expression *105*

2.7 DETECTION OF HEMEOXYGENASE-1 GENE EXPRESSION 105

2.7.1 RNA extraction *105*

2.7.2 DNase treatment *106*

2.7.3 Reverse transcriptase PCR *106*

2.7.4 Quantitative real time PCR *107*

2.8 MURINE MODEL OF RENAL ISCHAEMIA/REPERFUSION INJURY 109

2.8.1 Characterisation of ischaemic injury *110*

2.8.1.1 Assessment of renal histology 110

2.8.1.2 Immunohistochemistry of tissue sections 112

2.8.1.3 Assessment of renal function 114

2.9 IN VIVO LOCALISATION OF EMBRYONIC STEM CELL-DERIVED MACROPHAGES 114

2.9.1 PKH26 dye labelling of macrophages *114*

2.9.2 Localisation of macrophages following renal ischaemia/reperfusion injury *116*

2.10 STATISTICAL ANALYSIS 116

CHAPTER 3. DERIVING AND PHENOTYPING EMBRYONIC STEM CELL-DERIVED MACROPHAGES 117

3.1 INTRODUCTION 117

3.2 PHENOTYPING EMBRYONIC STEM CELL-DERIVED MACROPHAGES 118

3.2.1 Embryonic stem cell-derived macrophages exhibit a macrophage-like morphology 118

3.2.2 Embryonic stem cell-derived macrophages express macrophage cell surface markers .. 122

3.2.3 Embryonic stem cell-derived macrophages phagocytose latex beads 127

3.2.4 Embryonic stem cell-derived macrophages respond to a pro-inflammatory stimulus 133

3.3 ANALYSIS OF EMBRYONIC STEM CELL-DERIVED MACROPHAGE DIFFERENTIATION 135

3.3.1 Phenotyping the embryonic stem cell-derived macrophage progenitor cells isolated from embryoid body culture supernatants. 135

3.3.1.1 Embryonic stem cell-derived macrophage progenitor cells acquire a macrophage-like morphology with maturity 136

3.3.1.2 Embryonic stem cell-derived macrophage progenitor cells do not express the stem cell marker Oct4 139

3.3.1.3 Embryonic stem cell-derived macrophage progenitor cells express the macrophage cell surface markers F4/80 and CD11b 139

3.3.1.4 Embryonic stem cell-derived macrophage progenitor cells are phagocytic 149

CHAPTER 4. CONSTITUTIVE AND INDUCIBLE OVEREXPRESSION OF HEMEOXYGENASE-1 IN EMBRYONIC STEM CELLS AND EMBRYONIC STEM CELL-DERIVED MACROPHAGES 153

4.1 INTRODUCTION 153

4.2 CONSTITUTIVE OVER EXPRESSION OF HEMEOXYGENASE-1: THE PCAG SYSTEM 154

4.2.1 Embryonic stem cells constitutively overexpress hemeoxygenase-1 under the exogenous pCAG promoter 154

4.2.2 Random integration of pCAG-HO-1 adversely affects the ability of embryonic stem cells to self-renew 156

4.2.3 Random integration of the pCAG-HO-1 plasmid can affect the differentiation of embryonic stem cell-derived macrophages 160

4.3 SUMMARY 1 165

4.4 TETRACYCLINE INDUCIBLE OVER-EXPRESSION OF HEMEOXYGENASE-1: THE A2LOX.CRE CELL LINE INDUCIBLE SYSTEM. 166

4.4.1 Hemeoxygenase-1 inducible embryonic stem cells overexpress hemeoxygenase-1 following doxycycline treatment *166*

4.4.2 Inducible Hemeoxygenase-1 expression has no effect on the self-renewal properties of the inducible embryonic stem cells *169*

4.4.3 The generation of hemeoxygenase-1 inducible embryonic stem cell-derived macrophages from the genetically modified stem cell line *169*

4.4.3.1 Hemeoxygenase-1 inducible embryonic stem cell-derived macrophages exhibit a large mononuclear cell morphology 171

4.4.3.2 Hemeoxygenase-1 inducible embryonic stem cell-derived macrophages express macrophage cell surface markers 174

4.4.3.3 Inducible hemeoxygenase-1 embryonic stem cell-derived macrophages do not overexpress hemeoxygenase-1 following doxycycline treatment 174

4.5 INVESTIGATING THE LOSS OF HEMEOXYGENASE-1 INDUCIBILITY IN GENETICALLY MODIFIED HEMEOXYGENASE-1 INDUCIBLE EMBRYONIC STEM CELL-DERIVED MACROPHAGES. 178

4.5.1 Increasing the dose of Doxycycline does not restore inducible hemeoxygenase-1 expression in embryonic stem cell derived macrophages *178*

4.5.2 The ability of Dox to induce hemeoxygenase-1 overexpression is diminished during macrophage differentiation *180*

4.5.3 The loss of inducibility is specific to the A2lox.cre cell line and not related to the hemeoxygenase-1 cDNA insert. *182*

4.5.4 The loss of Dox inducibility is not specific to process of cellular differentiation to macrophages *188*

4.6 SUMMARY 199

CHAPTER 5. PHARMACOLOGICAL INDUCTION OF HEMEOXYGENASE-1: HEME ARGINATE TREATMENT OF ESDM. 200

5.1 INTRODUCTION 200

5.2 HEME ARGINATE MODULATES THE POTENTIAL OF EMBRYONIC STEM CELLS TO UNDERGO SELF-RENEWAL 200

5.3 HEME ARGINATE SIGNIFICANTLY UPREGULATES THE EXPRESSION OF HEMEOXYGENASE-1 BY EMBRYONIC STEM CELL-DERIVED MACROPHAGES 203

5.4 STUDY OF THE EFFECT OF HEME ARGINATE EXPOSURE UPON THE PHENOTYPE OF EMBRYONIC STEM CELL-DERIVED MACROPHAGES 205

5.4.1 The duration of heme arginate exposure has an impact on the level of expression of hemeoxygenase-1 by Embryonic Stem Cell-Derived Macrophages 208

5.4.2 The effect of heme arginate treatment upon the phenotype of embryonic stem cell-derived macrophages 210

5.4.1.1 Heme arginate does not influence the yield of embryonic stem cell-derived macrophages 210

5.4.1.2 Heme arginate treated embryonic stem cell-derived macrophages exhibit a macrophage-like morphology 212

5.4.1.3 Exposure to heme arginate during embryonic stem cell-derived macrophage differentiation modulates expression of CD11b and CD11c 215

5.4.1.4.Heme arginate treated macrophages are significantly more phagocytic 217

5.4.1.5 Heme arginate modulates the response of embryonic stem cell-derived macrophages to pro-inflammatory stimuli 224

5.4.1.5.1 Heme arginate treated embryonic stem cell-derived macrophages produce less nitric oxide following treatment with LPS and IFNγ 224

5.4.1.5.2 Prolonged HA exposure significantly downregulates iNOS gene expression following stimulation with LPS and IFNγ 225

5.4.1.5.3 Prolonged heme arginate exposure significantly downregulates TNFα production by embryonic stem cell-derived macrophages following LPS and IFNγ stimulation 228

5.4.1.5.4 Heme arginate has no impact on TNFα gene expression by embryonic stem cell-derived macrophages following LPS and IFNγ stimulation 228

5.4.1.5.5 Embryonic stem cell-derived macrophages treated with heme arginate for 24h produce significantly more IL-10 following LPS and IFNγ stimulation 231

5.4.1.5.6 Prolonged heme arginate exposure significantly downregulates IL-10 gene expression by embryonic stem cell-derived macrophages following LPS and IFNγ stimulation *231*

5.4.1.5.7 Heme arginate exposure of embryonic stem cell-derived macrophages downregulates IL-6 and IL-1β mRNA expression following LPS and IFNγ stimulation but does not modulate IL-12 mRNA expression *234*

5.5 SUMMARY 236

CHAPTER 6. DEVELOPMENT OF A MODEL OF ACUTE KIDNEY INJURY IN 129/P2 MICE AND THE LOCALISATION OF EMBRYONIC STEM CELL DERIVED MACROPHAGES *IN VIVO* **237**

6.1 INTRODUCTION 237

6.2 THE SEVERITY OF ACUTE KIDNEY INJURY IN 129/P2 MICE IS INFLUENCED BY GENDER AND DURATION OF ISCHAEMIA. 238

6.2.1 The severity of acute tubular necrosis is dependent on gender and the duration of the ischaemic period *240*

6.2.2 The severity of renal failure is dependent on mouse gender and the duration of the ischaemic insult. *244*

6.2.3 The number of F4/80 positive interstitial macrophages in the medulla of 129/P2 mice is dependent on gender *248*

6.2.4 Medullary influx of F4/80 positive macrophages is not evident in 129/P2 mice 24 hours following renal ischaemia reperfusion *248*

6.3 *IN VIVO* LOCALISATION OF EMBRYONIC STEM CELL DERIVED MACROPHAGES 251

6.3.1 Embryonic stem cell-derived macrophages localise to solid organs one hour post renal ischaemia reperfusion injury *251*

6.3.2 Control and heme arginate treated embryonic stem cell-derived macrophages preferentially home to the injured kidney one hour post renal ischaemia reperfusion injury .. *253*

6.4 SUMMARY 256

CHAPTER 7. DISCUSSION & FUTURE WORK **257**

7.1 DERIVING AND PHENOTYPING EMBRYONIC STEM CELL-DERIVED MACROPHAGES. 257

7.2 CONSTITUTIVE AND INDUCIBLE OVEREXPRESSION OF HEMEOXYGENASE-1 IN EMBRYONIC STEM CELLS AND EMBRYONIC STEM CELL-DERIVED MACROPHAGES. 260

7.3 PHARMACOLOGICAL INDUCTION OF HEMEOXYGENASE-1: HEME ARGINATE TREATMENT OF ESDM. 264

7.4 DEVELOPMENT OF A MODEL OF ACUTE KIDNEY INJURY IN 129/P2 MICE AND THE LOCALISATION OF EMBRYONIC STEM CELL DERIVED MACROPHAGES IN VIVO 268

8. CONCLUSION 271

Figures

FIGURE 1: STANDARD NOMENCLATURE FOR STRUCTURES OF THE NEPHRON. 31

FIGURE 2: RENAL VASCULATURE 34

FIGURE 3: LOCALISATION OF ACUTE KIDNEY INJURY CAUSES. 37

FIGURE 4: KEY EVENTS ASSOCIATED WITH RENAL ISCHEMIA/REPERFUSION INJURY. 39

FIGURE 5: INTERACTION OF HEMOXYGENASE-1 WITH THE SUBSTRATE HEME RESULTS IN THREE END PRODUCTS: CARBON MONOXIDE (CO), BILIRUBIN AND Fe^{2+} THAT STIMULATES THE UPREGULATION OF FERRITIN. 49

FIGURE 6: POTENTIAL ROUTES OF GENE DELIVERY TO THE KIDNEY 63

FIGURE 7: CYTOKINES PRODUCED BY IMMUNE CELLS CAN GIVE RISE TO DISTINCT MURINE Mφ POPULATIONS 67

FIGURE 8: EMBRYONIC STEM CELLS ORIGINATE AS INNER MASS CELLS WITHIN A BLASTOCYST. 72

FIGURE 9: THE A2LOX.CRE EMBRYONIC STEM CELL LINE. 79

FIGURE 10: MICROSCOPIC EXAMINATION OF ALKALINE PHOSPHATASE ACTIVITY ASSAY. 82

FIGURE 11: METHOD FOR THE DIFFERENTIATION OF EMBRYONIC STEM CELLS INTO MACROPHAGES. ... 86

FIGURE 12: REPRESENTATIVE PICTURES OF CELLS GENERATED DURING THE EMBRYONIC STEM CELL-DERIVED MACROPHAGE DIFFERENTIATION. 87

FIGURE 13: VISUAL ASSESSMENT OF MACROPHAGE PHAGOCYTOSIS OF APOPTOTIC THYMOCYTES UNDER FLUORESCENT MICROSCOPE 97

FIGURE 14: GRIESS REACTION ASSAY FOLLOWING LPS AND IFN-γ ACTIVATION OF MACROPHAGES. ... 99

FIGURE 15: THE OUTER STRIPE OF THE OUTER MEDULLA (OSOM) IS ONE OF FOUR KIDNEY REGIONS. 111

FIGURE 16: PKH26 LABELLED EMBRYONIC STEM CELL-DERIVED MACROPHAGES. 115

FIGURE 17: EMBRYONIC STEM CELL-DERIVED MACROPHAGES EXHIBIT A MACROPHAGE-LIKE MORPHOLOGY. 119

FIGURE 18: EMBRYONIC STEM CELL-DERIVED MACROPHAGES EXHIBIT SIMILAR SIZE BUT HIGHER GRANULARITY THAN BONE MARROW DERIVED MACROPHAGES 121

FIGURE 19: DAY 7 EMBRYONIC STEM CELL-DERIVED AND BONE MARROW DERIVED MACROPHAGES EXHIBIT COMPARABLE EXPRESSION OF F4/80 AND CD11B BY FLOW CYTOMETRY. 123

FIGURE 20: FLOW CYTOMETRIC ANALYSIS OF F4/80, CD11B, CD11C AND MHC CLASS II EXPRESSION OF DAY 7 ESDM, BMDM AND BMDC. 125

FIGURE 21: EMBRYONIC STEM CELL-DERIVED MACROPHAGES AND BONE MARROW DERIVED MACROPHAGES EXHIBIT COMPARABLE CELL SURFACE EXPRESSION OF F4/80, CD11B, CD11C AND MHC II. 126

FIGURE 22: FLOW CYTOMETRIC ANALYSIS OF THE PHAGOCYTOSIS OF FLUORESCENT GREEN LATEX BEADS BY F4/80 POSITIVE MACROPHAGES. 129

FIGURE 23: EMBRYONIC STEM CELL-DERIVED MACROPHAGES AND BONE-MARROW-DERIVED MACROPHAGES EXHIBIT COMPARABLE PHAGOCYTOSIS OF FLUORESCENT LATEX BEADS. 130

FIGURE 24: MICROSCOPIC ANALYSIS OF FLUORESCENT GREEN LATEX BEAD PHAGOCYTOSIS BY CELL TRACKER ORANGE LABELLED EMBRYONIC STEM CELL-DERIVED AND BONE MARROW DERIVED MACROPHAGES. 131

FIGURE 25: PERCENTAGE PHAGOCYTOSIS AND PHAGOCYTIC INDEX OF EMBRYONIC STEM CELL-DERIVED AND BONE MARROW DERIVED MACROPHAGES FOLLOWING INCUBATION WITH FLUORESCENT LATEX BEADS. 132

FIGURE 26: EMBRYONIC STEM CELL-DERIVED MACROPHAGES ARE ACTIVATED BY LPS/IFNγ STIMULATION AND RELEASE NITRIC OXIDE. 134

FIGURE 27: QUALITATIVE ASSESSMENT OF CELL MORPHOLOGY BY LIGHT MICROSCOPY. 137

FIGURE 28: MATURATION OF EMBRYONIC STEM CELL-DERIVED MACROPHAGE PROGENITOR CELLS. . 138

FIGURE 29: EMBRYONIC STEM CELL-DERIVED MACROPHAGE PROGENITOR CELLS AND EMBRYONIC STEM CELL-DERIVED MACROPHAGES DO NOT EXPRESS THE STEM CELL MARKER OCT4. 140

FIGURE 30: EMBRYONIC STEM CELL-DERIVED MACROPHAGE PROGENITOR CELLS EXPRESS F4/80. 141

FIGURE 31: EMBRYONIC STEM CELL-DERIVED MACROPHAGE PROGENITOR CELLS (EPC) EXPRESS CD11B. 142

FIGURE 32: DAY 14 AND DAY 16 EMBRYONIC STEM CELL-DERIVED MACROPHAGE PROGENITOR CELLS HARVESTS PRODUCE THE HIGHEST CELL YIELDS. 144

FIGURE 33: EMBRYONIC STEM CELL-DERIVED MACROPHAGE PROGENITOR CELLS EXHIBIT DUAL EXPRESSION OF THE MACROPHAGE CELL SURFACE MARKERS F4/80 AND CD11B THAT INCREASES WITH CELL MATURITY. 146

FIGURE 34: EMBRYONIC STEM CELL-DERIVED MACROPHAGE PROGENITOR CELLS EXHIBIT EXPRESSION OF THE CELL SURFACE MARKER CD11C THAT INCREASES WITH CELL MATURITY. 147

FIGURE 35: COMPARISON OF THE CELL SURFACE EXPRESSION OF F4/80, CD11B, CD11C AND MHC CLASS II BY BONE MARROW MONOCYTES, D14 AND D16 EMBRYONIC STEM CELL-DERIVED MACROPHAGE PROGENITOR CELLS AND EMBRYONIC STEM CELL-DERIVED MACROPHAGES. 148

FIGURE 36: EMBRYONIC STEM CELL-DERIVED MACROPHAGE PROGENITOR CELLS ARE ABLE TO PHAGOCYTOSE GREEN FLUORESCENT BEADS. 150

FIGURE 37: STABLE EMBRYONIC STEM CELL LINES OVEREXPRESSING HEMEOXYGENASE-1 UNDER THE CONSTITUTIVE PCAG PROMOTER 155

FIGURE 38: GENERAL STEM CELL CONDITION IS IMPAIRED FOLLOWING INSERTION OF A PCAG-HO-1 VECTOR INTO THE GENOME OF THE CELLS. 158

FIGURE 39: THE RANDOM INTEGRATION OF PCAG-HO-1 REDUCES EMBRYONIC STEM CELL SELF-RENEWAL ABILITY AND PROMOTES CELL DIFFERENTIATION. 159

FIGURE 40: A VARIABLE NUMBER OF ADHERENT CELLS ARE GENERATED BY THE EMBRYONIC STEM CELL-DERIVED MACROPHAGE PROTOCOL FOLLOWING GENETIC MODIFICATION OF EMBRYONIC STEM CELLS. 162

FIGURE 41: CELL MORPHOLOGY OF DAY 7 E14IV, HO-1/2 AND HO-1/5 EMBRYONIC STEM CELL-DERIVED MACROPHAGES 163

FIGURE 42: FLOW CYTOMETRIC ANALYSIS OF CELL SURFACE MARKER EXPRESSION OF DAY 7 EMBRYONIC STEM CELL-DERIVED MACROPHAGES DERIVED FROM E14 IV AND HO-1/2 CELL LINES. 164

FIGURE 43: USE OF THE A2LOX.CRE EMBRYONIC STEM CELL LINE TO GENERATE HO-1^{IND} EMBRYONIC STEM CELLS. 167

FIGURE 44: DOXYCYCLINE INDUCES HEMEOXYGENASE-1 OVEREXPRESSION IN THE INDUCIBLE EMBRYONIC STEM CELLS 168

FIGURE 45: INDUCIBLE HEMEOXYGENASE-1 EXPRESSION HAS NO EFFECT ON THE SELF-RENEWAL PROPERTIES OF THE INDUCIBLE EMBRYONIC STEM CELLS. 170

FIGURE 46: CONTROL INDUCIBLE AND HEMEOXYGENASE-1 INDUCIBLE EMBRYONIC STEM CELL-DERIVED MACROPHAGES EXHIBIT A MACROPHAGE-LIKE MORPHOLOGY 172

FIGURE 47: REPRESENTATIVE SSC AND FSC FLOW ANALYSIS HISTOGRAMS OF CTRL^{IND} AND HO-1^{IND} EMBRYONIC STEM CELL-DERIVED MACROPHAGES. 173

FIGURE 48: HEMEOXYGENASE-1 INDUCIBLE EMBRYONIC STEM CELL-DERIVED MACROPHAGES EXPRESS CELL SURFACE MARKERS F4/80 AND CD11B. 175

FIGURE 49: INDUCIBLE EMBRYONIC STEM CELL-DERIVED MACROPHAGES ARE F4/80^{HIGH} CD11B^{HIGH} CD11C^{MED} MHC CLASS II^{LOW}. 176

FIGURE 50: HEMEOXYGENASE-1 INDUCIBLE EMBRYONIC STEM CELL-DERIVED MACROPHAGES DO NOT INDUCE HEMEOXYGENASE-1 OVEREXPRESSION FOLLOWING DOXYCYCLINE TREATMENT. 177

FIGURE 51: INCREASING THE DOSE OF DOXYCYCLINE DOES NOT RESTORE INDUCIBLE HEMEOXYGENASE-1 EXPRESSION IN GENETICALLY MODIFIED EMBRYONIC STEM CELL-DERIVED MACROPHAGES. 179

FIGURE 52: INDUCIBLE HEMEOXYGENASE-1 EXPRESSION DECREASES FROM DAY 4 OF EMBRYOID BODY FORMATION AND DISAPPEARS BY DAY 10. 181

FIGURE 53: THE PERCENTAGE OF EGFP POSITIVE EGFP^{IND} CELLS DECREASES AS EMBRYONIC STEM CELLS UNDERGO DIFFERENTIATION TO MACROPHAGES. 184

FIGURE 54: THE PERCENTAGE OF EGFP POSITIVE MAML-EGFP^{IND} CELLS FALLS AS EMBRYONIC STEM CELLS UNDERGO DIFFERENTIATION TO MACROPHAGES. 185

FIGURE 55: THE MEAN FLUORESCENCE INTENSITY OF EGFP DECREASES EARLY DURING CELL DIFFERENTIATION. 186

FIGURE 56: EMBRYONIC STEM CELL-DERIVED MACROPHAGES ARE AUTOFLUORESCENT. 187

FIGURE 57: THE MORPHOLOGY OF RETINOIC ACID TREATED EMBRYONIC STEM CELLS IS DIFFERENT TO EMBRYONIC STEM CELLS CULTURED IN LEUKAEMIA INHIBITORY FACTOR. 190

FIGURE 58: RETINOIC ACID TREATED EMBRYONIC STEM CELLS UNDERGO DIFFERENTIATION AND DO NOT EXPRESS THE STEM CELL MARKER OCT 4. 191

FIGURE 59: GENE EXPRESSION OF NANOG GENE IS SILENCED FOLLOWING RETINOIC ACID TREATMENT OF GENETICALLY MODIFIED EMBRYONIC STEM CELLS. 192

FIGURE 60: METHOD FOR THE ASSESSMENT OF INDUCIBLE EXPRESSION OF HO-1 AND EGFP OF OUR VARIOUS ESC CLONES FOLLOWING RETINOIC ACID TREATMENT AND DOXYCYCLINE STIMULATION. 194

FIGURE 61: RETINOIC ACID DIFFERENTIATED EMBRYONIC STEM CELLS DO NOT EXPRESS INDUCIBLE HEMEOXYGENASE-1 FOLLOWING DOXYCYCLINE STIMULATION. 195

FIGURE 62: THE PERCENTAGE OF EGFP POSITIVE CELLS DECREASES FOLLOWING RETINOIC ACID DIFFERENTIATION OF EGFP^{IND} ESC AND MAML-EGFP^{IND} ESC. 197

FIGURE 63: MEAN FLUORESCENCE INTENSITY OF EGFP DECREASES FOLLOWING RETINOIC ACID DIFFERENTIATION. 198

FIGURE 64: HEME ARGINATE MODULATES THE POTENTIAL OF EMBRYONIC STEM CELL TO SELF-RENEW. 202

FIGURE 65: HEME ARGINATE INCREASES EXPRESSION OF HEMEOXYGENASE-1 BY EMBRYONIC STEM CELL-DERIVED MACROPHAGE. 204

FIGURE 66: HEME ARGINATE TREATMENT PROTOCOLS 206

FIGURE 67: EXPERIMENTAL DESIGN FOR THE STUDY OF THE EFFECT OF SHORT OR PROLONGED HEME ARGINATE TREATMENT UPON THE PHENOTYPE AND FUNCTION OF EMBRYONIC STEM CELL-DERIVED MACROPHAGES 207

FIGURE 68: SHORT OR PROLONGED EXPOSURE TO HEME ARGINATE SIGNIFICANTLY UPREGULATES HEMEOXYGENASE-1 EXPRESSION. 209

FIGURE 69: SHORT OR PROLONGED EXPOSURE TO HEME ARGINATE DOES NOT INFLUENCE THE YIELD OF EMBRYONIC STEM CELL-DERIVED MACROPHAGES. 211

FIGURE 70: HEME ARGINATE TREATED EMBRYONIC STEM CELL-DERIVED MACROPHAGES EXHIBIT A MACROPHAGE-LIKE MORPHOLOGY 213

FIGURE 71: FSC AND SSC ANALYSIS BY FLOW CYTOMETRY: HEME ARGINATE DOES NOT INFLUENCE EMBRYONIC STEM CELL-DERIVED MACROPHAGE SIZE OR GRANULARITY. 214

FIGURE 72: EXPOSURE TO HEME ARGINATE DURING EMBRYONIC STEM CELL-DERIVED MACROPHAGE DIFFERENTIATION MODULATES EXPRESSION OF CD11B AND CD11C. 216

FIGURE 73: ASSESSMENT OF MACROPHAGE PHAGOCYTOSIS OF APOPTOTIC THYMOCYTES BY FLUORESCENT MICROSCOPY. 218

FIGURE 74: CONTROL AND HEME ARGINATE TREATED EMBRYONIC STEM CELL-DERIVED MACROPHAGES PHAGOCYTOSE APOPTOTIC THYMOCYTES. 220

FIGURE 75: HEME ARGINATE TREATED EMBRYONIC STEM CELL-DERIVED MACROPHAGES EXHIBIT INCREASED PHAGOCYTOSIS OF APOPTOTIC THYMOCYTES..... 221

FIGURE 76: EXPOSURE TO HEME ARGINATE DURING EMBRYONIC STEM CELL-DERIVED MACROPHAGE DIFFERENTIATION INCREASES THE PHAGOCYTIC INDEX FOR APOPTOTIC THYMOCYTES. 223

FIGURE 77: HEME ARGINATE TREATED EMBRYONIC STEM CELL-DERIVED MACROPHAGES PRODUCE SIGNIFICANTLY LESS NITRIC OXIDE FOLLOWING LPS AND IFNγ ACTIVATION..... 226

FIGURE 78: PROLONGED HEME ARGINATE EXPOSURE OF EMBRYONIC STEM CELL-DERIVED MACROPHAGES SIGNIFICANTLY DOWNREGULATES INOS GENE EXPRESSION FOLLOWING LPS AND IFNγ STIMULATION. 227

FIGURE 79: PROLONGED HEME ARGINATE EXPOSURE OF EMBRYONIC STEM CELL-DERIVED MACROPHAGES SIGNIFICANTLY DOWNREGULATES TNFα PRODUCTION FOLLOWING LPS AND IFNγ STIMULATION. 229

FIGURE 80: HEME ARGINATE TREATMENT OF EMBRYONIC STEM CELL-DERIVED MACROPHAGES HAS NO SIGNIFICANT IMPACT ON TNFα GENE EXPRESSION FOLLOWING LPS AND IFNγ STIMULATION. 230

FIGURE 81: EMBRYONIC STEM CELL-DERIVED MACROPHAGES TREATED WITH HEME ARGINATE FOR 24H PRODUCE SIGNIFICANTLY MORE IL-10 FOLLOWING LPS AND IFNγ STIMULATION..... 232

FIGURE 82: PROLONGED HEME ARGINATE EXPOSURE OF EMBRYONIC STEM CELL-DERIVED MACROPHAGES SIGNIFICANTLY DOWNREGULATES IL-10 GENE EXPRESSION FOLLOWING LPS AND IFNγ STIMULATION. 233

FIGURE 83: HEME ARGINATE EXPOSURE DOWNREGULATES IL-6 AND IL-1β GENE EXPRESSION FOLLOWING LPS+IFNγ STIMULATION BUT HAS NO EFFECT ON IL-12..... 235

FIGURE 84: THE ISCHAEMIA/REPERFUSION INJURY MODEL IN THE 129/P2 STRAIN: DETERMINING THE EFFECTS OF GENDER AND THE DURATION OF ISCHAEMIA. 239

FIGURE 85: REPRESENTATIVE RENAL HISTOLOGY OF NORMAL KIDNEYS AND KIDNEYS 24 HOURS FOLLOWING RENAL ISCHAEMIA REPERFUSION INJURY. 241

FIGURE 86: THE SEVERITY OF KIDNEY INJURY FOLLOWING 20 MINUTES OF RENAL ISCHAEMIA REPERFUSION INJURY IS DEPENDENT ON GENDER. 242

FIGURE 87: ACUTE TUBULAR NECROSIS INCREASES WITH THE DURATION OF RENAL ISCHAEMIA REPERFUSION INJURY 243

FIGURE 88: 129/P2 FEMALES EXHIBIT HIGHER BASELINE SERUM CREATININE LEVELS THAN MALE MICE. 246

FIGURE 89: SEVERITY OF RENAL FUNCTION IMPAIRMENT IS DEPENDENT ON THE DURATION OF THE ISCHAEMIC INSULT. 247

FIGURE 90: IMMUNOHISTOCHEMISTRY STAINING OF F4/80 POSITIVE RESIDENT MACROPHAGES IN THE NON-INJURED MEDULLA OF 129/P2 MICE. 249

FIGURE 91: MEDULLAS OF 129/P2 MALE MICE EXHIBIT SIGNIFICANTLY HIGHER NUMBERS OF F4/80 POSITIVE INTERSTITIAL MACROPHAGES THAN FEMALE MICE. 250

FIGURE 92: EMBRYONIC STEM CELL DERIVED MACROPHAGES LOCALISE TO SOLID ORGANS 1H POST ISCHAEMIA/REPERFUSION INJURY 252

FIGURE 93: CONTROL AND HEMEOXYGENASE-1 OVEREXPRESSING EMBRYONIC STEM CELL-DERIVED MACROPHAGES HOME TO THE INJURED KIDNEY 1H POST RENAL ISCHAEMIA REPERFUSION INJURY. 255

Tables

TABLE 1: SUMMARY OF THE VARIOUS FUNCTIONS, TISSUE EXPRESSION AND REGULATION OF HEMEOXYGENASE ISOFORMS. 50

TABLE 2: BENEFICIAL EFFECTS OF PHARMACOLOGICALLY INDUCED HEMEOXYGENASE-1 OVEREXPRESSION IN EXPERIMENTAL MODELS OF RENAL DISEASE 57

TABLE 3: CELL BASED HO-1 DELIVERY SYSTEMS IN VARIOUS DISEASES MODELS 61

TABLE 4: MACROPHAGE CELL THERAPY IN EXPERIMENTAL RENAL DISEASE 69

TABLE 5: ESDM GENERAL PHYSIOLOGY STUDIES 75

TABLE 6: CONJUGATED PRIMARY ANTIBODIES USED FOR FLOW CYTOMETRIC ANALYSIS OF CELLS DERIVED FROM BONE MARROW OR EMBRYONIC STEM CELLS 93

TABLE 7: ANTIBODIES USED FOR WESTERN BLOTTING 104

TABLE 8: QPCR PRIMERS 108

TABLE 9: ANTIBODIES USED FOR IMMUNOHISTOCHEMISTRY 113

TABLE 10: SUMMARY TABLE OF ESC, MPC, ESDM AND BMDM PROPERTIES 151

List of Abbreviations

A	
AAV	Adeno-Associated Virus
Ab	Antibody
Ad	Adenovirus
AKI	Acute Kidney Injury
ANOVA	Analysis Of Variance
Anti-GMB	Anti-glomerular basement membrane
Anti-Thy1	Anti Thymocyte differentiation antigen 1
APC	Allophycocyanin
APCs	Antigen Presenting Cells
ARF	Acute Renal Failure
ATN	Acute Tubular Necrosis
B	
β	Beta
BMDC	Bone Marrow Derived Dendritic Cell
BMDM	Bone Marrow Derived Macrophage
BMM	Bone Marrow Monocytes
BSA	Bovine Serum Albumin
C	
°C	Degree Celsius
Ca	Calcium
CD11b	Cluster of Differentiation antigen 11b
CD11c	Cluster of Differentiation antigen 11c
cDNA	Complementary Deoxyribonucleic Acid
CI	Confidence Interval
CO	Carbon Monoxide
CO_2	Carbon Dioxide
$CoCl_2$	Cobalt Chloride
CoPP	Cobalt protoporphyrin
CORMs	Carbon monoxide-releasing molecules
COX	Cyclooxygenase
D	
DAB	3,3-Diaminobenzidine
DAPI	4',6-diamidino-2-phenylindole
DC	Dendritic Cell
DMEM/F12	Dulbecco's Modified Eagle Medium: Nutrient Mixture F-12
DMSO	Dimethyl Sulfoxide
Dox	Doxycycline
DT	Diphtheria Toxin
DTR	Diphtheria Toxin Receptor
E	
EB	Embryoid Body
EDTA	Ethylenediaminetetraacetic acid
eGFP	Enhanced green fluorescent protein
ELISA	Enzyme Linked Immunosorbent Assay
ESC	Embryonic Stem Cell
ESDM	Embryonic Stem Cell Derived Macrophage
EtOH	Ethanol
F	
FACS	Fluorescence Activated Cell Sorting

FCS	Fetal Calf Serum
FIHC	Fluorescent Immunohistochemitry
FITC	Fluorescein isothiocyanate
FSC	Forward Scatter
G	
G	Gauge
GFR	Glomerular filtration rate
GM-CSF	Granulocyte-macrophage colony-stimulating factor
GMEM	Glasgow Minimun Essential Medium
GN	Glomerulonephritis
H	
h	Hour
HA	Heme Arginase
H&E stain	Hematoxylin and Eosin stain
HBSS	Hank's Balanced Salt Solution
HEPES	4-(2-hydroxyethyl)-1-piperazineethanesulfonic acid
HO-1	Hemeoxygenase-1
HPF	High Power Field
HRP	Horseradish Peroxidase
I	
ICE	Inducible Cassette Exchange
IFNγ	Interferon Gamma
IgG	Immunoglobulin
IL-1RA	Interleukin 1 Receptor Antagonist
IHC	Immunohistochemistry
IL-3	Interleukin 3
IL-4	Interleukin 4
IL-10	Interleukin 10
IM	Inner Medulla
Ind	Inducible
iNOS	Inducible Nitric Oxide synthase
IRES	Internal ribosome entry site
IRI	Ischemia Reperfusion Injury
ISOM	Inner Stripe of the Outer Medulla
K	
κ	Kappa
L	
LC	Liposome Clodronate
LIF	Leukemia Inhibitory Factor
LPS	Lipopolysaccharide
M	
M	Molar
MAML	Mastermind-like
M-CSF	Macrophage Colony Stimulating Factor
MeOH	Methanol
MFI	Mean Fluorescence Intensity
Mg	Magnesium
MHC Class II	Major Histocompatibility Complex Class two
Min	Minute
ml	Milliliter
mm	Millimeter
mM	Millimolar

MPC	Macrophage Progenitor Cell
MSC	Mesenchymal Stem Cell
Mφ	Macrophage
µl	Microliter
µm	Micrometer
µM	Micromolar
N	
N/A	Non available
Na	Sodium
NaCl	Sodium Chloride
NEAA	Non Essential Amino Acids
NK	Natural Killer
nm	Nanometer
NO	Nitric Oxide
ns	Non significant
NTN	Nephrotoxic nephritis
O	
Oct4	Octamer-binding transcription factor 4
OM	Outer Medulla
OMBF	Outer medullary blood flow
OSOM	Outer Stripe of the Outer Medulla
P	
PBS	Phosphate Buffered Saline
PBS -/-	Phosphate Buffered Saline without calcium and magnesium
PE	Phycoerythrin
PerCP-Cy5.5	Peridinin-Chlorophyll Proteins-Cyanin 5.5
PLA2	Phospholipase A2
PMN	Polymorphonuclear leukocytes
P/S	Penicillin/Streptomycin
R	
RNA	Ribonucleic Acid
RNase	Ribonuclease
ROS	Reactive Oxygen Species
RT	Room Temperature
rtTA	Reverse tetracycline transactivator
RTU	Ready To Use
S	
SD	Standard Deviation
SDS	Sodium Dodecyl Sulfate
SDS-PAGE	Sodium Dodecyl Sulfate Polyacrylamide Gel Electrophoresis
SEM	Standard Error of the Mean
SSC	Side Scatter
T	
TBS	Tris Buffered Saline
TBS-T	Tris Buffered Saline-Tween
TC	Tissue Culture
TE	Trypsin EDTA
T_H	T helper cell
TNF-α	Tumor Necrosis Factor Alpha
TRE	Tet-Responsive Element
TVP	Trypsin Verene Phosphate

U

UTO	Urinary tract obstruction

V

vs	Versus

X

XD	Xanthine dehydrogenase
XO	Xanthine oxidase

Chapter 1. Introduction

This thesis will examine the anti-inflammatory properties of hemeoxygenase-1 over-expressing embryonic stem cell-derived macrophages (Mφ) and their potential to limit damage in renal ischemia/reperfusion injury, a devastating entity for which only supportive treatments are currently available.

1.1 The Kidney

Excretion is one of the basic life processes of all living organisms. In vertebrates, the urinary system consists of the kidneys, ureters, bladder and urethra. The kidneys are important organs and perform a number of vital homeostatic tasks such as the excretion of water, electrolytes, nitrogenous waste through urine production, regulation of blood pressure and blood volume, acid-base control as well as the synthesis and secretion of hormones such as renin and erythropoietin.

1.1.1 Anatomy of the kidney

The kidney has a complex architecture with many structures and is composed of various cell types. The kidney consists of two major regions:

(i) The outer region termed the renal cortex

(ii) The inner region termed the renal medulla.

Since structural differences within the kidney are of high importance in the pathophysiology studied in this thesis, i.e. ischaemia/reperfusion injury, a short anatomical overview is given below and illustrated in Figure 1.

Outer (OM) and inner (IM) zones are distinguished within the medulla with the OM being further subdivided into the outer stripe of the outer medulla (OSOM) and the

inner stripe of the outer medulla (ISOM). The nephron is the basic structural and functional unit of the organ and carries out nearly all its functions. Each nephron is made up of highly specialised cells with marked structural and functional differences.

Nephrons are composed of an initial filtering component, the renal corpuscule composed of a glomerulus and the Bowman's capsule, and a tubule specialised for reabsorption and secretion of solutes and water. Depending on the position of their glomerulus in the renal parenchyma and the length of their tubules, nephrons are classified as either cortical or juxtamedullary. Cortical nephrons give rise to long loops of Henle entering the inner medulla. The proximal tubule starts at the glomerulus and consists of an initial convoluted part also called the S1 and S2 segments, followed by a straight part termed the S3 segment. The transition from the proximal tubule to the thin descending limb of Henle's loop is abrupt. Closely after the hairpin turn, the thin limb continues into the thin ascending limb, which soon enlarges to become the thick ascending limb. The thick ascending limb represents the initial straight part of the distal tubule. It extends upwards through the outer medulla and the cortex to the glomerulus. The distal convoluted tubule begins beyond the macula densa and extends to the collecting duct.

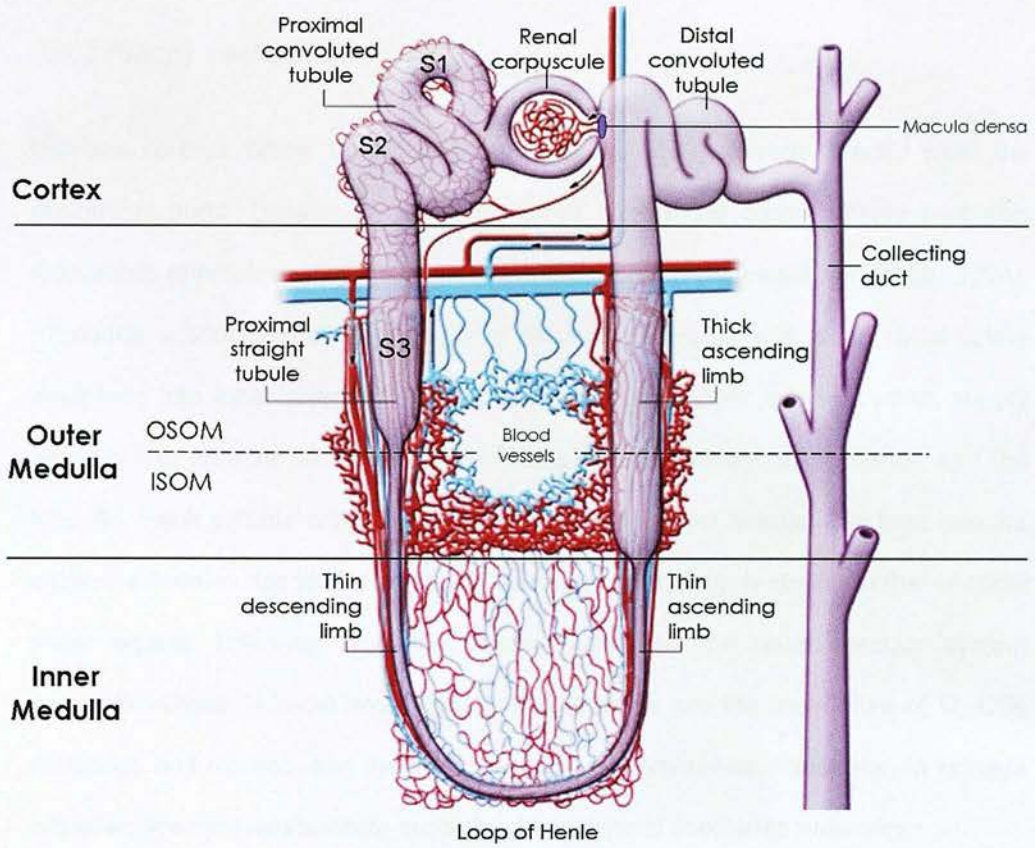

Figure 1: Standard nomenclature for structures of the nephron.

Anatomy of a cortical nephron with regions annotated. Vasculature is shown with capillaries in red and venous system in blue. (Modified from (Bonventre and Yang, 2011)

1.1.2 Kidney vasculature

Kidneys receive blood from the renal arteries, which branch directly from the abdominal aorta. Despite the relatively small size of the organ, kidney perfusion represents approximately 25% of total cardiac output (Friedewald and Rabb, 2004). Intrarenal vascularisation (Figure 2) is relatively complex with each renal artery branching into lobar arteries, dividing further into interlobar arteries, which supply blood to the arcuate arteries that run through the boundary of the cortex and the medulla. Each arcuate artery supplies several interlobular arteries that feed into the afferent arterioles. Up to that point, the renal arterial system is similar to that of other major organs. However, from the afferent arterioles, the renal vascular system becomes unique. In most organs, capillary networks are the main sites of O_2-CO_2 exchange and run between the artery-arteriole and venule-vein systems. In kidneys however, the microvasculature consists of two distinct capillaries networks:

- A highly specialised preliminary capillary network where blood filtration occurs, the glomerulus, which receives blood from an afferent arteriole
- A second capillary network arising from an efferent arteriole whose structure and role vary depending on its location.

In most cases, after leaving the glomerulus, efferent arterioles branch into a complex network of peritubular capillaries in close contact to the tubules in order to facilitate reabsorption of solutes etc. In the specific case of juxtamedullary glomeruli, the efferent arterioles are dividing into long thin walled vessels called the vasa recta. These vasa recta run vertically in the medulla and play an important role in ion and fluid exchanges.

The glomerulus filters the blood but does not deliver oxygen to tissues nor removes significant amount of CO_2. The main gaseous exchange happens in the secondary network where oxygen is delivered to the tubular cells of the cortex and medulla, which have a high demand due to their important metabolic activity.

After glomerular filtration and the nourishing of tubular cell have occured, the blood moves through a small network of venules that converge into interlobular veins. As with the arteriole distribution, veins follow the same pattern. Blood exits the kidney via the interlobular veins, the arcuate and the interlobar veins, which join to form the renal vein that enters the main circulation via the inferior vena cava.

A

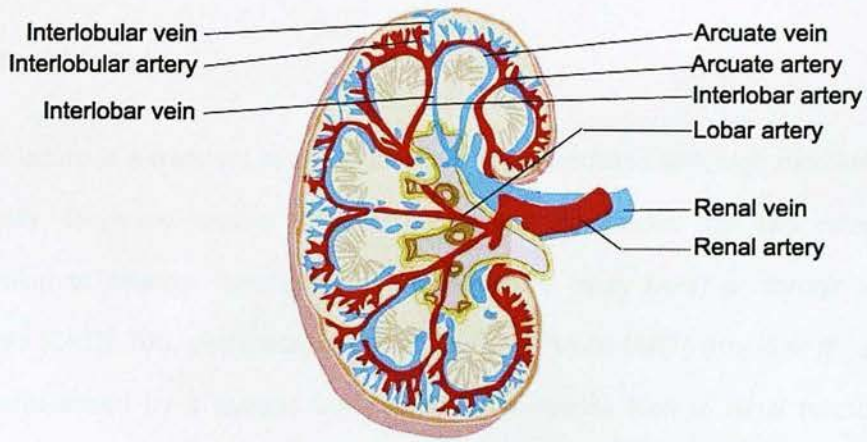

B

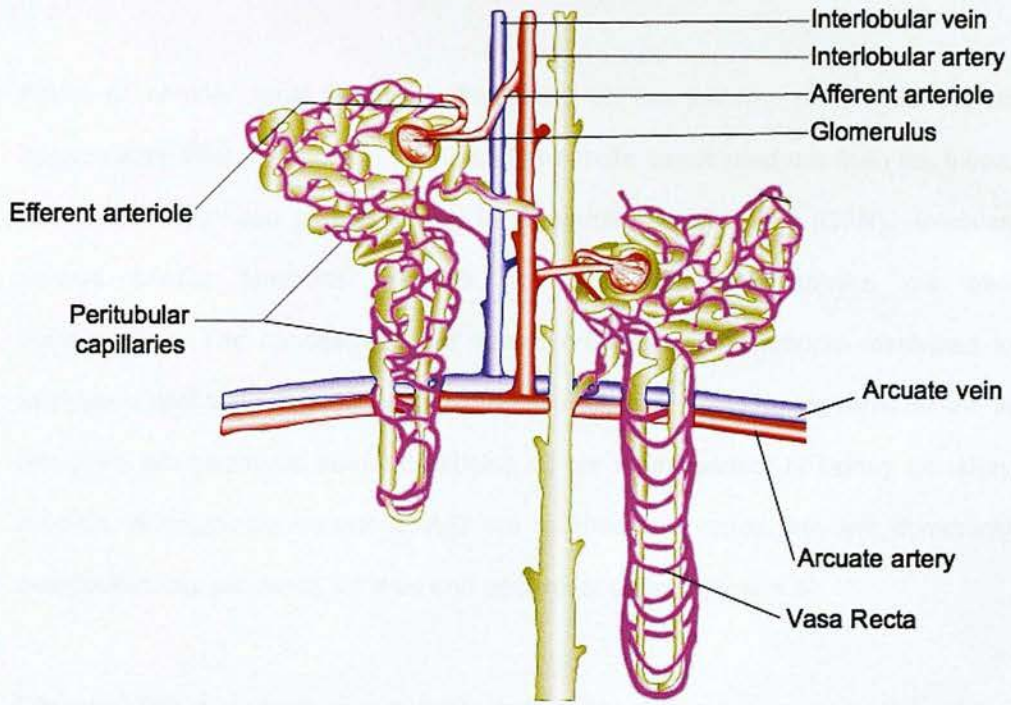

Figure 2: Renal Vasculature

A: The arterial system of the kidney is composed of a renal artery that branches into lobar arteries that further divide into interlobar arteries. These supply blood to the arcuate arteries that run through the boundary of the cortex and the medulla. **B:** Renal microcirculation. An afferent arteriole, branching from the interlobar artery, enters the glomerulus. The efferent arteriole then divides to form a complex peritubular capillary network surrounding the cortical tubules. In the case of juxtamedullary glomeruli, efferent arterioles give rise to vertically running vessels termed the vasa recta.

1.2 Renal failure

Renal failure is a frequent medical condition still associated with high morbidity and mortality. Diseases leading to renal failure can be divided into two categories according to whether they result in acute kidney injury (AKI) or chronic kidney disease (CKD). AKI, previously called acute renal failure (ARF) (Khalil et al., 2008), is characterized by a sudden but potentially reversible loss of renal function. In contrast, CKD is the progressive and irreversible loss in renal function.

Acute or chronic renal failure is the result of the inability of the kidneys to appropriately filter and excrete toxins and metabolic waste products from the blood. It is mainly described as a decrease in glomerular filtration rate (GFR). However, various tubular functions as well as intrarenal hemodynamics are also compromised. The concentration of serum creatinine is commonly measured to evaluate a decline in renal function as creatinine accumulates during renal failure. In this work, we measured serum creatinine as our main readout of kidney excretory function. Although the causes of AKI are multiple and varied they are commonly categorised into pre-renal, intrinsic and post-renal causes (Figure 3).

Pre-renal AKI is caused by a sudden and severe decrease or interruption of the renal blood flow brought about by varied conditions that result in a reduced blood volume or pressure (e.g. dehydration, bleeding), heart failure and renal artery stenosis (Blantz and Singh, 2011). Although pre-renal kidney dysfunction typically resolves if the underlying problem is dealt with (e.g. fluid administration), it can result in established intrinsic AKI if the low flow state is prolonged.

Intrinsic causes of AKI originate from direct damage to the kidneys by inflammation, toxins, drugs, infection and/or a prolonged reduction in the blood supply. Glomerulonephritis, acute tubular necrosis and acute interstitial nephritis may all cause intrinsic AKI (Choudhury, 2010).

Post-renal AKI is a consequence of an obstruction of urine flow due to extrinsic ureteric compression, an enlarged prostate, bilateral kidney stones or a urothelial or bladder tumour (Fujisawa et al., 2010).

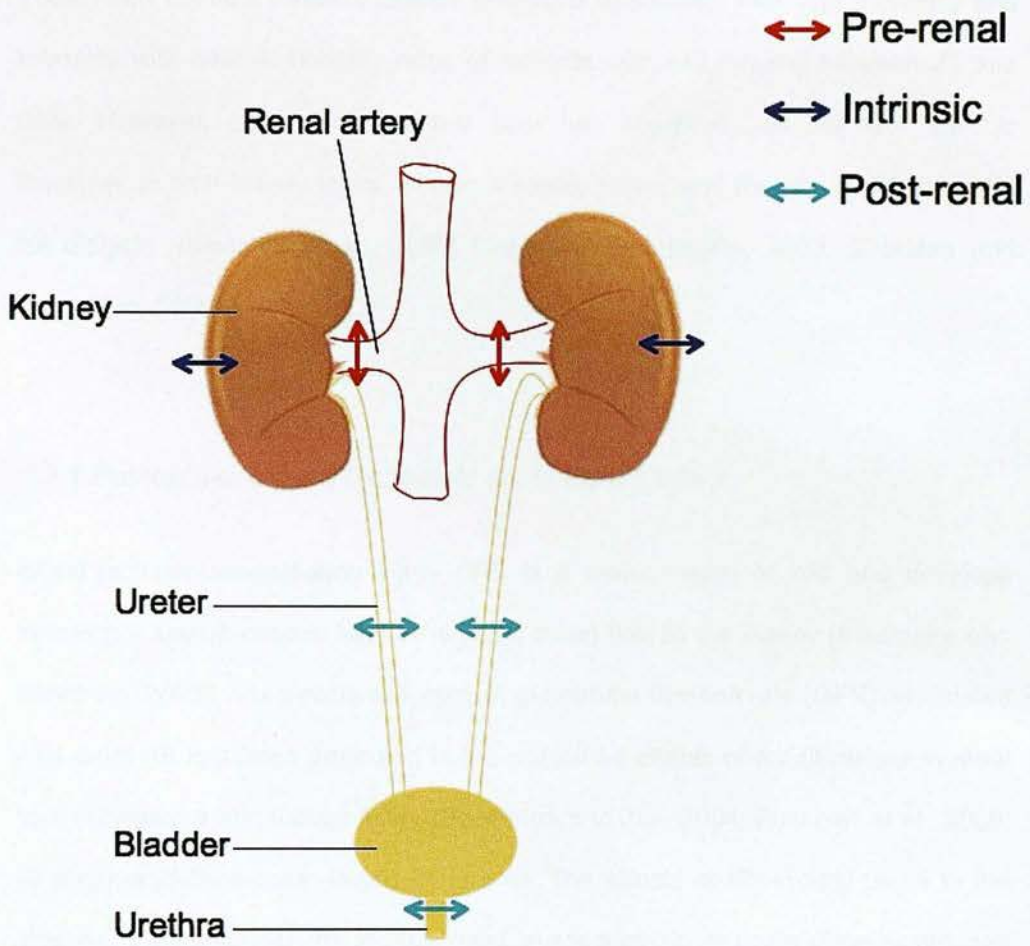

Figure 3: Localisation of acute kidney injury causes.

Pre-renal: sudden and severe drop in blood pressure or interruption of blood flow to the kidneys from severe injury or illness. **Intrinsic**: Direct damage to the kidneys by inflammation, toxins, drugs, infection or a reduced blood supply. **Post-renal**: Obstruction of the urine flow due to enlarged prostate, kidney stones, bladder tumour or injury.

Today, AKI is still a frequent clinical syndrome associated with high morbidity and mortality with overall mortality rates of patients with AKI ranging between 25 and 80%. However, although supportive care has improved, we still lack specific therapies to limit kidney injury, enhance kidney repair and thereby avoid the need for dialysis (Bussolati et al., 2008; Lieberthal and Nigam, 2000; Sheridan and Bonventre, 2000).

1.2.1 Pathophysiology of ischaemic acute kidney injury

Renal ischaemia/reperfusion injury (IRI) is a major cause of AKI and develops following a severe drop in total or regional blood flow to the kidney (Bonventre and Weinberg, 2003). The severe reduction in glomerular filtration rate (GFR) associated with renal IRI has been attributed to the combined effects of modifications in renal haemodynamics and tubular injury (Bonventre and Zuk, 2004; Bussolati et al., 2009; Sheridan and Bonventre, 2000) (Figure 4). The effects of IRI initially begin in the medulla, the region of the kidney most susceptible to hypoxia (Friedewald and Rabb, 2004). As the blood flow to the kidney decreases, the cells become increasingly hypoxic and undergo cell injury. This cellular injury triggers an inflammatory response resulting in endothelial cell activation and injury, enhanced endothelial cell-leukocyte adhesion, leukocyte recruitment and a compromised microvascular blood flow (Bonventre and Zuk, 2004; Kinsey et al., 2008; Sutton et al., 2002). In the following sections, we will discuss the major features of IRI.

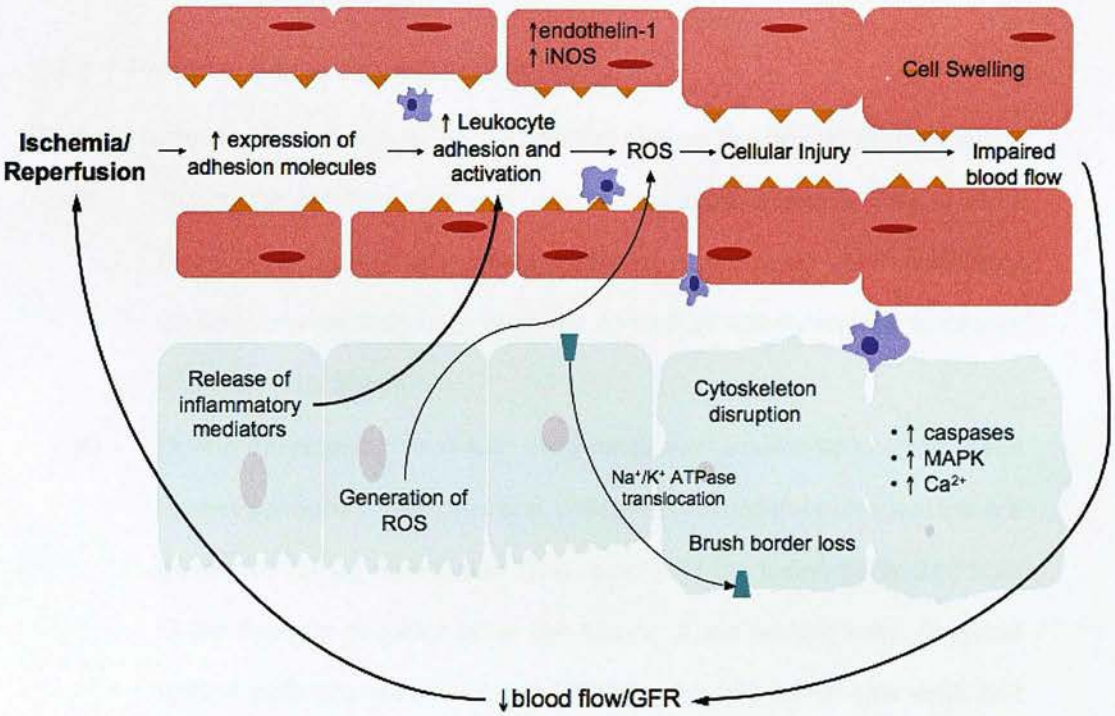

Figure 4: Key events associated with Renal Ischemia/Reperfusion injury.

While tissue injury is sustained during the initial ischaemic event, it is exacerbated by the robust inflammatory response that occurs during reperfusion. Inflammatory mediators are upregulated resulting in leukocyte recruitment and activation. Upregulated adhesion molecule expression increases endothelial-immune cell interactions with recruited leukocytes increasing injury by generating reactive oxygen species (ROS) and enhancing vascular tone. ROS directly injure many cytoskeletal and functional cellular components, causing, among other events, the redistribution of Na^+/K^+ ATPase. This results in the loss of the normal Na^+/K^+ gradients, increased intracellular Na^+, and subsequent cell swelling. Direct endothelial damage and abnormal vascular tone is a result of increased sensitivity to and release of vasoconstrictors such as endothelin-1. Increased nitric oxide (NO) is generated by inducible nitric oxide synthetase (iNOS), also exacerbates injury. Key regulators of apoptosis, such as caspases, are upregulated by these events, resulting in increased cell death.

1.2.1.1 Proximal tubule alterations and injury

IRI is characterised by two successive but distinct phases that lead to tissue injury:

(i) During the *initiation phase*, or ischaemic period, a severe drop in renal blood flow causes increasing hypoxia and cellular ATP depletion, creating diverse metabolic changes as well as morphological, functional and molecular alterations.

(ii) During the *reperfusion phase*, renal blood flow is restored and the tissue is re-oxygenated. This phase is critical as the most severe lesions are generated during reperfusion. The severity of the lesion generated from tissue hypoxia depends upon the nature of the tubular cells. Proximal tubular cells are particularly sensitive to hypoxia whilst glomeruli and collecting tubules are more resistant to a deficit in oxygen.

1.2.1.2 Haemodynamic changes

Cells undergo anaerobic metabolism during the ischaemic period resulting in impairment or total inhibition of the mitochondrial respiratory chain, a fall in ATP levels and an energy deficit. Cellular ATP depletion results in alteration of the cytoskeleton and the integrity of cellular junctions. Moreover, ATP depletion leads to tubular cell Na^+/K^+-ATPase dysfunction and loss of cellular polarisation with localisation from the basolateral surface to the apical membrane. The consequent intracellular Na^+ and water accumulation results in cell swelling that can cause tubular obstruction and backleak of fluid. In addition, the proximal tubular cells may undergo cell death by necrosis or apoptosis with cell debris forming casts that block the tubular lumen. Increased intratubular pressure alters vectorial transport by forcing fluid into the interstitium facilitating the development of interstitial oedema.

ATP depletion also disturbs calcium-dependent proteases, increases intracellular calcium concentration and reactive oxygen species (ROS) generation. Some calcium-dependent proteases can convert xanthine dehydrogenase (XD) to xanthine oxidase (XO). In the kidney, the most common form present is the XD that uses NAD^+ as electron acceptor to convert hypoxanthine (generated by ATP degradation) into xanthine and uric acid. However, during ischemia, XD is converted into XO, which can, during reperfusion, use oxygen as electron acceptor and generate the superoxide anion O_2^-: a biologically toxic ROS. Other well-known ROS include hydrogen peroxide (H_2O_2), hydroxyl radical (OH^-) and hypochlorous acid (HClO). Apart from XO, sources of ROS in kidneys include cyclo-oxygenases (COX), the mitochondrial electron transport chain and polymorphonuclear leukocytes (PMN). In normal physiological conditions, the multiple anti-oxidant systems (superoxide dismutase, catalase, glutathione peroxidase etc.) limit the potentially deleterious effects of ROS. However, in pathological conditions the oxidant/anti-oxidant equilibrium shifts towards exacerbated ROS production creating oxidative stress. During IRI, this oxidative stress is coupled to a nitrosative stress characterized by excess nitrite oxide (NO) production due to the over-expression of inducible nitric oxide synthase (iNOS). NO interacts with O_2^- to form the highly cytotoxic molecule peroxynitrite ($ONOO^-$). ROS generation and the resultant oxidative and nitrosative stress participate in the progression of ischaemia-associated tissue injury and inflammation and further impair kidney function.

1.2.1.3 Cellular death

There are two fundamental pathophysiological mechanisms of cellular death.

(i) Necrosis is a form of passive, traumatic cell death that results from acute cellular injury. It is characterized by the loss of membrane integrity, swelling and cellular fragmentation.

(ii) Apoptosis is a biologically conserved form of programmed cell death (Kerr et al., 1972). Biochemical events lead to characteristic cell changes including blebbing, cell shrinkage, and nuclear and DNA fragmentation leading to cellular death.

Apoptosis and necrosis generally co-exist after ischaemic injury and their relative importance depends on the severity of damage and cellular resilience. In contrast to necrosis, apoptosis requires energy. Thus, it is possible for a cell whose active self-destruction pathway has started to shift to necrosis in case of a severe ATP depletion (Eguchi et al., 1997).

1.2.1.4 Microvascular alterations

Impaired flow

In physiological conditions, the kidney is able to autoregulate its blood supply and its perfusion is naturally heterogeneous featuring a decreasing gradient from the cortex to the inner medulla. However, the renal blood flow can drop to 50% or more in the outer medulla following ischaemia. In these conditions, the kidney is no longer capable of autoregulating its blood supply leading to microvascular and hemodynamic alterations.

Renal vasoconstriction follows the activation of tubuloglomerular feedback. Indeed, the loss of proximal tubular cell polarity associated with the abnormal localisation of Na^+/K^+-ATPases pumps and altered tight junctions result in decreased Na^+ and Cl^- reabsorption by the proximal tubules. The increased concentration of these ions in

the macula densa region activates the tubuloglomerular feedback that reinforces vasoconstriction. Also, ischaemia induces the production of vasoconstrictor agents such as thromboxane A2 (TXA2), angiotensin II (Ang II) or endothelin-1 (ET-1), further exacerbating vasoconstriction.

Prolonged hypoxia also causes structural and biochemical injury to endothelial cells. Although the endothelial cell injury is generically similar to that of induced to tubules, there are two consequences that are specifically associated with endothelial cells:

(i) Increased endothelial permeability and

(ii) Leukocyte-endothelial cell interactions.

Permeability

ATP depletion and exposure to hypoxia leads to structural alteration of endothelial cells with destabilisation of intercellular interactions. This causes increased endothelial permeability that impairs its role as a physical barrier between plasma and the renal interstitium.

Leukocyte adhesion

Endothelial injury and activation result in increased expression of adhesion molecules such as selectins, integrins and members of the immunoglobulin superfamily such as intercellular adhesion molecule-1 (ICAM-1) and vascular cell adhesion molecule (VCAM). This increases leukocyte-endothelium adhesion and enables diapedesis across the endothelium and also contributes to impaired microvascular blood flow. Activated leukocytes are also pro-inflammatory and may further impair endothelial function by releasing cytokines, proteases and ROS.

1.2.1.5 Inflammatory response

A growing body of evidence indicates that inflammation plays a major role in ischaemic AKI. Various mediators produced by the 'maladaptive response' of proximal tubule to ischaemia amplify the inflammatory cascade, initiated by endothelial dysfunction. These include pro-inflammatory cytokines such as tumour necrosis factor α (TNF-α), interleukin-1 (IL-1) and IL-6 as well as chemotactic cytokines including macrophage inflammatory protein 1α (MIP-1α), monocyte chemotactic protein-1 (MCP-1), regulated upon activation normal T-cell expressed, and secreted (RANTES), and IL-8 (Bonventre and Yang, 2011). Several types of leukocyte have been implicated as potentially harmful in ischaemic AKI.

(i) Neutrophils

Neutrophils are the earliest leukocytes to infiltrate the post-ischaemic kidney. However, neutrophil depletion or blockade of their function provides partial functional protection in some but not all animal models (Fukuzawa et al., 2009; de Vries et al., 2003). Furthermore, neutrophils are not a prominent feature of ischaemic AKI in humans, casting doubts about the clinical significance of neutrophil infiltration (Devarajan, 2006).

(ii) Lymphocytes

The adaptive immune system also contributes to renal IRI. A role for T cells in the pathogenesis of kidney IRI has been established in *nu/nu* mice (which lack CD4 and CD8 T cells) and RAG-$1^{-/-}$ mice (lacking both B and T cells). *Nu/nu* mice exhibit tolerance to ischemia compared to wild-type controls whereas selective reconstitution with $CD4^+$ T cells restored kidney injury after IRI (Burne et al., 2001). Additionally, RAG-1 −/− mice were also protected from IRI and adoptive transfer of $CD4^+$ T cells from wild-type mice restored injury (Day et al., 2006). Interestingly,

transfer of $CD4^+$ T cells from IFN-γ −/− mice did not reconstitute injury suggesting a critical role for IFN-γ.

Other studies have focused on the role of regulatory T cells (Tregs) in ischaemic AKI. Tregs are a subtype of lymphocytes with strong immunosuppressive and anti-inflammatory properties and are identified by their expression of CD4 and CD25 and upregulation of FoxP3 (Akcay et al., 2009). Depletion of Tregs with an anti-CD25 monoclonal antibody resulted in greater accumulation of leukocytes and worsened kidney damage while Treg repletion significantly attenuated renal injury and leukocyte accumulation. However, transfer of IL-10 deficient Tregs did not prevent ischaemic injury suggesting an important role for IL-10 in their action (Kinsey et al., 2009).

B cell deficient mice are also protected from IRI (Burne-Taney et al., 2003). Unlike T cells, the adoptive transfer of purified B cells to these mice did not restore kidney injury after ischemia. Interestingly, susceptibility to ischemia could be re-established by serum transfer from wild-type animals. The authors suggest that lack of a circulating factor, possibly an immunoglobulin, may be responsible for the protection observed in B cell-deficient mice.

(iii) Mononuclear phagocytes

'Resident' mononuclear phagocytes (macrophages [Mφ] and dendritic cells) are present in all normal tissues with replacement via circulating monocytes derived from a bone marrow precursor. In the setting of acute or chronic kidney injury, the resident mononuclear phagocytes are supplemented by an influx of monocytes from the circulation, which themselves undergo activation and are capable of differentiating into functionally heterogeneous inflammatory Mφ and dendritic cells (Griffin, 2012). Different groups have shown that these cells play a somewhat

controversial role in AKI with experimental data suggesting both deleterious and protective functions (Ferenbach et al., 2012) and involvement in both the initiation and resolution phases of AKI (Kluth et al., 2004; Vinuesa et al., 2008). Today, two main systems have been developed for the purpose of selective *in vivo* depletion of Mφ in the hope to distinguish harmful from beneficial effects of these cells during AKI:

(i) The administration of liposomal clodronate (LC), which results in widespread death of phagocytic cells within 24–48 h and

(ii) Transgenic expression of the diphtheria toxin receptor (DTR) under the control of the CD11b or CD11c promoter has generated mice in which the administration of diphtheria toxin (DT) results in rapid death of CD11b+ monocytes/macrophages or CD11c+ macrophages/dendritic cells.

Although these depletion systems have allowed the role of $CD11b^+$ or $CD11c^+$ to be explored in various models of renal inflammation, the results have generated some interesting controversies. For instance, studies using LC administration to induce monocyte/Mφ apoptosis before IRI have demonstrated a protected phenotype, supporting the hypothesis that Mφ are deleterious in the initiation/propagation phase of renal IRI (Ferenbach et al., 2012). However, DT administration to CD11b-DTR mice had no effect upon the severity of AKI (Ferenbach et al., 2012). Depletion of $CD11c^+$ cells by administration of DT to CD11c-DTR mice prior to cisplatin-induced AKI (Tadagavadi and Reeves, 2010) was associated with exacerbated injury suggesting a protective effect of $CD11c^+$ cells. In contrast, depletion of $CD11c^+$ cells prior to ischaemic AKI (Li and Okusa, 2010) was associated with reduced injury suggesting a deleterious effect of $CD11c^+$ cells.

Concerning the recovery phase of renal IRI, Mφ appear essential for appropriate resolution and repair of tissue integrity with depletion of macrophages by LC or DT being retarding recovery (Day et al., 2006; Jo et al., 2006; Lin et al., 2010).

These contrasting results suggest the existence of injurious and reparative Mφ phenotypes (see later) and highlight the complexity of interpreting data from depletion studies (Griffin, 2012).

1.3 The hemeoxygenase system

Heme (iron protoporphyrin IX) is the chelate complex of an iron atom (Fe^{2+}) and four porphyrin ligand groups (Beri and Chandra, 1993). Despite the vital importance of heme molecules in biological processes, an excess of free heme can cause cell damage and tissue injury since heme induces ROS formation and oxidative stress (Wagener et al., 2003). Cellular homeostasis therefore depends on tight control of the amount of free heme in the microenvironment.

Hemeoxygenase (HO) was originally characterized in 1968 (Tenhunen et al., 1969). HO is an ubiquitous inducible stress-response protein and serves a major metabolic function in heme turnover. HO is the rate limiting enzyme in the catabolism of the heme containing porphyrin ring to equimolar amounts of biliverdin (rapidly converted to bilirubin by biliverdin reductase), carbon monoxide (CO) and free iron (Fe^{2+}) which leads to the induction of the iron-binding protein ferritin (Abraham and Kappas, 2008; Otterbein et al., 2003; Wagener et al., 2003) (Figure 5).

To date, three HO isoforms have been identified: Hemeoxygenase-1 (also called heat shock protein 32 [HSP32]), HO-2 and HO-3, (Maines et al., 1986; Tenhunen et al., 1969; William et al., 1997). All HO isoforms are highly conserved among species in evolution and their various functions, tissue distribution and inducers of expression can be found in Table 1.

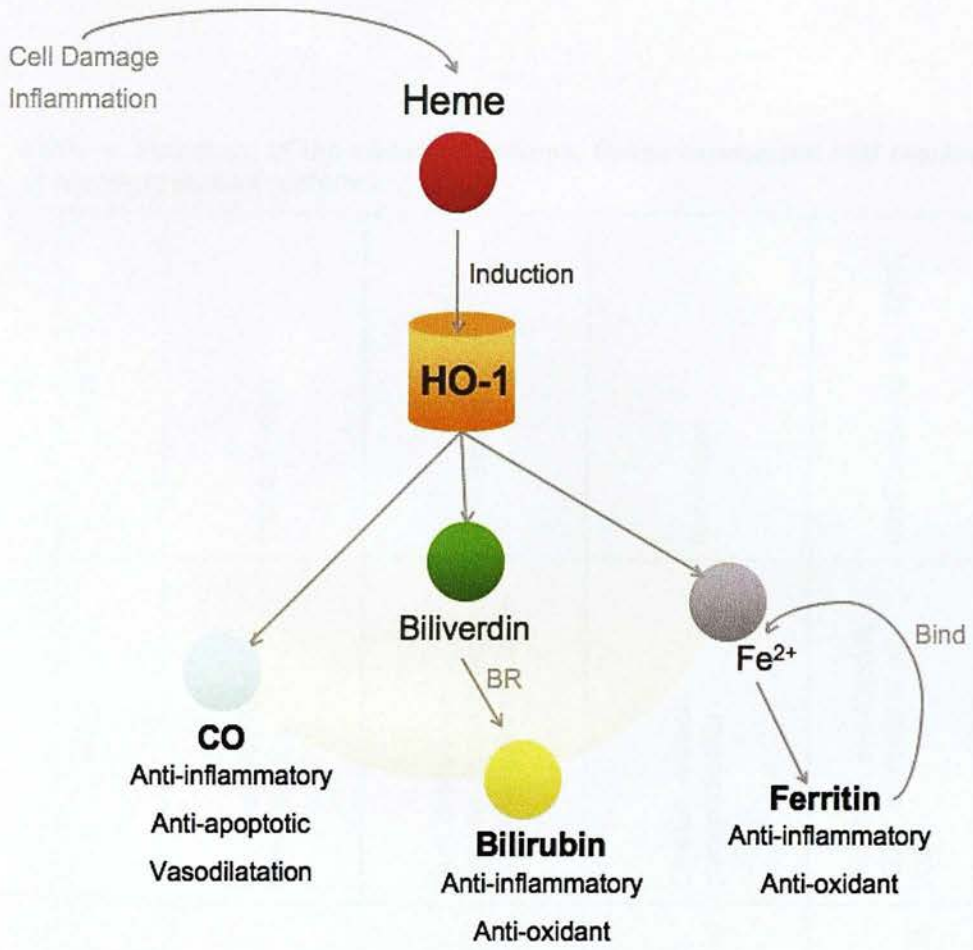

Figure 5: Interaction of Hemoxygenase-1 with the substrate heme results in three end products: carbon monoxide (CO), bilirubin and Fe^{2+} that stimulates the upregulation of ferritin.

Hemeoxygenase-1 catalyses the breakdown of heme into equimolar amounts of CO, free iron (Fe^{2+}) and biliverdin. Biliverdin is subsequently converted to bilirubin through the action of the enzyme biliverdin reductase (BR). Free iron induces ferritin synthesis that can then bind the potentially harmful free iron.

Table 1: Summary of the various functions, tissue expression and regulation of hemeoxygenase isoforms.

	HO-1	HO-2	HO-3
Main functions	Heme degradation Cytoprotection	Heme degradation Heme binding	Heme binding
Constitutive tissue expression	Spleen and liver	Most tissues but expression levels are higher in brain and testis	Most tissues
Inducers of expression	Heme, pro-inflammatory cytokines, hypoxia, hyperoxia, ultraviolet-A radiation, bacterial endotoxins	Opiates, adrenal glucocorticoids	Not known
References	(Lin et al., 2007; Ryter and Choi, 2002; Ryter and Choi, 2009; Soares and Bach, 2009)	(Abraham and Kappas, 2008; Wagener et al., 2003)	(McCoubrey et al., 1997)

Hemoxygenase-1 is the isoform that responds promptly and vigorously to diverse stimuli and has been shown to have cytoprotective effects in various inflammatory models (Inguaggiato et al., 2001; Lin et al., 2007). Interestingly, the only two human cases reported to lack HO-1 enzymatic activity died of an inflammatory syndrome at a young age (Kawashima et al., 2002; Radhakrishnan et al., 2011) whilst HO-1-deficient mice develop a chronic inflammatory state that progresses with age (Poss and Tonegawa, 1997). It is suggested that the clearance of pro-oxidant heme and the anti-oxidant and anti-inflammatory properties of its catabolic products account for the crucial cytoprotective properties of HO-1 (Nath, 2006).

Once regarded as a metabolic waste product, CO is now recognised to exert anti-inflammatory, anti-apoptotic and anti-proliferative properties at low concentration. CO influences a number of signalling pathways, targets NADPH oxidases, which regulate intracellular ROS production and influences the mitogen-activated protein kinases (MAPK) as well as transcription factors such as NF kappa-B (NF-κB). CO is also involved in vasoregulation via its influence on the soluble guanylate cyclase (sGC) pathways and calcium-dependent potassium channels (KCa) (Otterbein et al., 2003; Ryter and Choi, 2009).

Biliverdin and bilirubin are potent anti-oxidants as they can directly scavenge ROS and reduce ROS production, thus reduce cellular damage. These bile pigments are associated with the anti-oxidative function of HO-1 (Pae et al., 2008; Ryter and Choi, 2009).

Free iron, another heme catabolite, is known to generate ROS and may act as a catalyst of deleterious pro-oxidant reactions if it accumulates in the cell.

Interestingly, Fe^{2+} released by the HO-1 reaction can stimulate ferritin synthesis which sequesters reactive iron, and thus contributes indirectly to cytoprotection (Ryter and Tyrrell, 2000). Suttner and Dennery acknowledged a beneficial threshold of HO-1 overexpression related to the accumulation of reactive iron released by heme catabolism (Suttner and Dennery, 1999). Low HO-1 expression, low cellular heme and low iron may allow for decreased oxidative injury, whereas excessive accumulation of reactive iron at high HO-1 expression results in increased oxidative stress, cytotoxicity and abnormal cellular proliferation (Suttner and Dennery, 1999).

More recently, Kinderlerer and colleagues identified an additional cytoprotective action of HO-1, showing that HO-1 expression enhances vascular endothelial resistance to complement-mediated injury through the induction of the complement inhibitory protein decay-accelerating factor (DAF) (Kinderlerer et al., 2009).

1.3.1 Hemeoxygenase-1 and the kidney

HO-1 basal expression is relatively low throughout the kidney with HO-1 localising predominantly in the cortical proximal and distal tubules and medullary collecting tubules and loops of Henle (Da Silva et al., 2001). However, being an inducible enzyme, HO-1 is clearly upregulated in case of stress. The protective effects of HO-1 upregulation have proved to be beneficial in different models of IRI including brain (Nimura et al., 1996), gut (Attuwaybi et al., 2003), liver (Xue et al., 2007), heart (Akamatsu et al., 2004) and kidney (Salom et al., 2007). HO-1 induction also improved long term graft outcome in rat renal allografts (Tullius et al., 2001) and protected cardiac grafts from transplant associated IRI (Akamatsu et al., 2004). The reported cases of HO-1 human deficiency, who both died in childhood, were

characterised by systemic inflammation, anemia, thrombocytosis, coagulation abnormality, elevated serum levels of ferritin and heme and low serum bilirubin concentration in addition to a mesangial proliferative glomerulonephritis and an irregular distribution of foamy macrophages with iron pigments (Kawashima et al., 2002; Radhakrishnan et al., 2011).

1.3.1.1 Hemeoxygenase-1 in ischaemic acute kidney injury

As previously discussed, ischaemic AKI is due to a period of significantly reduced renal perfusion. Renal dysfunction has been attributed in part to the generation of ROS and rapid release of heme by injured cells. As the rate-limiting enzyme in the degradation of heme, HO-1 is induced following an ischaemic insult to the kidney. Indeed, HO-1 mRNA levels and enzyme activity increase significantly in rodent models of IRI. Interestingly, the inhibition of HO-1 activity by tin protoporphyrin resulted in worse renal function and increased intracellular heme content in these animals (Shimizu et al., 2000). Studies of AKI on HO-1 -/- mice showed significant renovascular hypertension and worsen renal function following IRI compared to HO-1 +/- mice (Wiesel et al., 2001).

Although these studied suggest that endogenous HO-1 is protective, the enzyme does not provide complete renoprotection and prevention from progression to renal failure. Thus, strategies to upregulate HO-1 expression are being studied in an attempt to improve the renoprotective capabilities of this cytoprotective enzyme (Chung and Perrella, 2004).

1.3.2 Strategies of hemeoxygenase-1 up-regulation as therapy in models of renal inflammation

Several strategies are currently being developed to harness HO-1 in inflammatory disease. To date, many groups have studied the beneficial efficacy of HO-1 induction on various models of renal diseases such as AKI, glomerulonephritis (GN), drug induced nephrotoxicity and autoimmune renal diseases. Various approaches are being studied and whilst pharmacological induction of HO-1 by heme derivatives, dietary antioxidants, or currently available drugs is a promising near-term approach, HO-1 gene delivery is a long-term therapeutic goal. The various available methods of HO-1 overexpression will be discussed in the following sections.

1.3.2.1 Pharmacological induction of hemeoxygenase-1

Overexpression of HO-1 has been primarily studied with the use of numerous pharmacological agents. Amongst these compounds, metalloporphyrins are widely recognised as potent HO-1 inducers. These molecules result in the complexing of metals such as Fe^{2+}, Co^{2+}, Zn^{2+} and Sn^{2+} by the natural precursor of heme, protoporphyrin IX (Ryter et al., 2006). Hemin (trade name Panhematin®) is the iron (Fe^{2+}) containing metalloporphyrin approved by the FDA[1] and widely used in the USA as treatment for acute porphyria. However, in its current commercial form, hemin is sold as a lyophilised powder that needs to be reconstituted with albumin immediately prior to intravenous administration to avoid formation of degradation

---

[1] And List of Orphan Products Designation and Approvals. Source: http://www.fda.gov/ohrms/dockets/dailys/00/mar00/030100/lst0094.pdf

products that could potentially be injurious to patients (Anderson et al., 2006). Paradoxically, some metalloporphyrins, such as tin protoporphyrin IX (SnPPIX) and zinc protoporphyrin IX (ZnPPIX), are used as effective competitive inhibitors of HO-1 activity (Sardana and Kappas, 1987). HO-1 activity inhibition by SnPPIX and ZnPPIX often results in the loss of the protected phenotype and increased damage to the tissues (Shimizu et al., 2000).

Chemical agents such as heme arginate (HA, trade name Normosang®) are also potent HO-1 inducers. HA is a stable heme and L-arginine compound (Tenhunen R et al., 1987), approved by the FDA[2]. The addition of L-arginine to the heme molecule prevents its rapid degradation in solution and so HA is currently given intravenously in the treatment acute porphyria and related neuropathies (Diot et al., 2007).

Statins, a widely used class of drugs to reduce cholesterol levels, are capable of inducing HO-1 expression. However, the use of statins as HO-1 inducers is at the centre of a controversy since the induction is not universally observed and it remains unclear whether HO-1 upregulation by the compounds is actually protective for humans (Durante, 2010; Golomb and Evans, 2008).

In the race to discover the best HO-1 inducer, scientists also turned to natural compounds such as curcumin, the active ingredient in the spice turmeric (Curcuma longa). *In vitro* and *in vivo* animal studies have shown that curcumin induces HO-1

---

[2] And List of Orphan Products Designation and Approvals. Source: http://www.fda.gov/ohrms/dockets/dailys/00/mar00/030100/lst0094.pdf

and also possess anti-tumour (Ströfer et al., 2011), anti-oxidant, anti-ischaemic (Yang et al., 2009) and anti-inflammatory properties (Zhong et al., 2011) while clinical trials in humans are underway (Hatcher et al., 2008).

Various groups have shown that the pharmacological induction of HO-1 exerted renoprotection against ischaemic renal injury, cisplatin induced nephrotoxicity, acute glomerulonephritis and renal transplant rejection (Table 2). However, there are some challenges associated with the use of pharmacological HO-1 inducers.

Firstly, as pharmacological HO-1 induction results in a general HO-1 upregulation, it might engender non-specific effects that could potentially counteract the therapeutic effects associated with HO-1 upregulation. Secondly, as sustained high level of HO-1 expression might increase oxygen cytotoxicity and cellular injury, the induction and duration of HO-1 expression must be carefully titrated (Suttner and Dennery, 1999). Furthermore, HO-1 inducibility is largely modulated by polymorphisms in the promoter region that may limit the efficacy of pharmacological HO-1 inducers in certain patient populations (Durante, 2010).

Table 2: Beneficial effects of pharmacologically induced hemeoxygenase-1 overexpression in experimental models of renal disease

Model (Species)	HO-1 inducer	Effects	Reference
IRI (Mouse)	Heme Arginate (30mg/kg)	↓Serum creatinine ↓ATN	(Ferenbach et al., 2011)
IRI (Tullius et al.)	Cerivastatin (0.5mg/kg)	↓Serum creatinine ↓ATN	(Gueler et al., 2007)
$HgCl_2$ nephrotoxicity (Tullius et al.)	Hemin (30mg/kg)	↓Serum creatinine ↓Blood urea nitrogen ↓ATN	(Yoneya et al., 2000)
Cisplatin nephrotoxicity (Human)	Hemin (20mg/kg)	↓Proximal tubules apoptosis and necrosis *in vitro*	(Shiraishi et al., 2000)
Membranous GN (Mouse)	CoPPIX (100µmol/kg)	↓Proteinuria ↓Glomerular lesions ↓Immune complex deposition ↑IL-10	(Wu et al., 2008)
Anti-Thy1 GN (Tullius et al.)	Curcumin (10-200mg/kg)	↓Proteinuria ↓Fibrosis	(Gaedeke et al., 2005)
Lupus GN (Mouse)	Hemin (100µmol/kg)	↓Proteinuria ↓Glomerular lesions ↓Immune complex deposition ↓NO ↓ Serum IFNγ ↓IgG anti-double-stranded DNA antibody levels	(Takeda et al., 2004)
Anti-GBM GN (Tullius et al.)	Hemin (30µmol/kg)	↓Proteinuria ↓NO	(Datta et al., 1999)
Unilateral ureteric obstruction (Tullius et al.)	Hemin (10mg/kg)	↓Proteinuria ↓Albuminuria ↓ TNFα, IL-1β, IFNγ, IL-6, IL-2 ↑IL-10 ↓Fibrosis	(Correa-Costa et al., 2010)

1.3.2.2 HO-1 gene therapy

HO-1 gene therapy is a rapidly evolving field in medical research. Various experimental techniques using viral, non-viral and cellular vectors have been described and employed on different models. However, successful and functional HO-1 gene transfer always requires that:

(i) The gene is delivered into a safe vector and

(ii) The delivery is site and organ specific (Abraham, 2003).

In the following section, we will describe available gene delivery techniques, their beneficial effects on models of inflammation and possible routes of administration in renal disease.

Viral Vectors

Viruses such as adenoviruses, retroviruses, lentiviruses and adeno-associated viruses (AAV) are commonly used as viral vectors for gene therapy. Indeed, these viruses have evolved specialised molecular mechanisms to efficiently transport their genomes inside infected cells. Gene therapy trials have used that characteristic to deliver the gene of interest to host cells. However, problems of viral gene therapy include innate and immune barriers to vector delivery, vector toxicity and the lack of sustained therapeutic gene expression. Immune response to viruses impedes gene delivery to target cells and can cause severe complications. In one of the early gene therapy trials in 1999 this led to the death of a patient who was treated with an adenoviral vector (Marshall, 1999). In the case of retroviruses and lentiviruses, random integration of the gene of interest into the host's genome can disturb the function of cellular genes and eventually lead to cancer (Hacein-Bey-Abina S., 2003). AAV are known to have site-specific integration that could eliminate the

concern for random insertional mutagenesis but are still at risk of an immune response.

While immune responses and insertional mutagenesis pose obstacles, various groups are now making progress by modifying existing protocols to overcome these hurdles (Herzog et al., 2010). For example, AAV vector capsids are being engineered to be more resistant to neutralising antibodies, to transduce target cells more efficiently and to show enhanced tropism for specific tissues (Zhong et al., 2008). Other protocols include transient immune suppression or modulation to prevent adaptive responses against capsid or transgene derived antigen (Sack and Herzog, 2009).

Non-Viral Vectors

Non-viral gene delivery vectors typically consist of DNA or RNA, which may be delivered to the target cell usually with the aid of a vehicle. Simple large-scale production and low host immunogenicity are their main advantages over viral methods. There are several methods for non-viral gene therapy, including the injection of naked DNA, the use of oligonucleotides, lipoplexes (micelles and liposomes are lipids which can fuse with the cell membrane releasing the nucleic acid into the cytoplasm of the cell) and polyplexes, which use a polymer to condense the nucleic acid and a lipid coat to aid entry to the cell. Practically, lipids, polymers and other naturally occurring compounds have proven to be extremely effective for *in vitro* gene delivery. However, all of the systems have failed or been unimpressive in clinical trials because of low delivery efficiency and toxicity. The low *in vivo* transfection efficiency appears to be related to the cationic nature of the gene carrier. While effective in protecting DNA from DNA degradation, the polycations in

either lipoplexes or polyplexes have the intrinsic property of causing significant aggregation in biological matrices full of negatively charged molecules, and of preventing effective release of DNA once inside the cells (Gao et al., 2007).

Cell based delivery systems

The success of gene therapy relies largely on an effective targeted gene delivery system and as described so far, various issues have limited the clinical applications of both viral and non-viral delivery systems. Cell-based delivery systems, where genetic manipulation is performed *ex vivo* on cells such as leukocytes, are emerging as an alternative for the targeted delivery system. Various groups have shown successful HO-1 cell based delivery in various disease models as summarised in Table 3.

Table 3: Cell based HO-1 delivery systems in various diseases models.

Model (Species)	**Cell used**	**Method**	**Effects**	**References**
Renal IRI (mouse)	Bone marrow derived Macrophages	Adenoviral transduction	↓Serum creatinine No effect on ATN ↓Platelet deposition	(Ferenbach et al., 2010)
Liver transplant IRI (rat)	Bone marrow derived Macrophages	Adenoviral transduction	↑Survival rate ↓Serum alanine aminotransferase ↓Hepatocellular damage ↓TNFα, IL-1β and MCP1 ↑IL-10	(Shen et al., 2011)
Myocardial ischemia	Bone marrow derived MSC	Lipofection	↓Apoptosis ↑VEGF ↑Capillary density ↓Infarction size	(Tsubokawa et al., 2010)
MSC infusion	Bone marrow derived MSC	Adenoviral transduction	Localisation of HO-1+ cells in healthy lungs	(Zhou et al., 2006)

1.3.3 Kidney gene therapy

Delivering genes to the kidney may offer new strategies to treat diseases of both native and transplanted kidneys. The choice of vector for the delivery as well as the administration route determines the site of transduction. The challenge with the kidney is that the organ is well differentiated with a variety of specialised compartments (*i.e.* glomerular, tubular, interstitial and vascular compartments) physically separated by membranes and associated cells. This compartmentalisation, as well as factors such as cell turnover rate, blood and urine flow may affect the delivery, specificity and efficacy of gene therapy in the kidney because the vectors may not pass easily through the anatomical and physiological barriers (Imai et al., 2004). On the other hand, the kidney has a major advantage over other solid organs since it is accessible by many routes including the renal parenchyma, the renal artery, the renal vein and the urinary tract as well as via the systemic circulation (Figure 6).

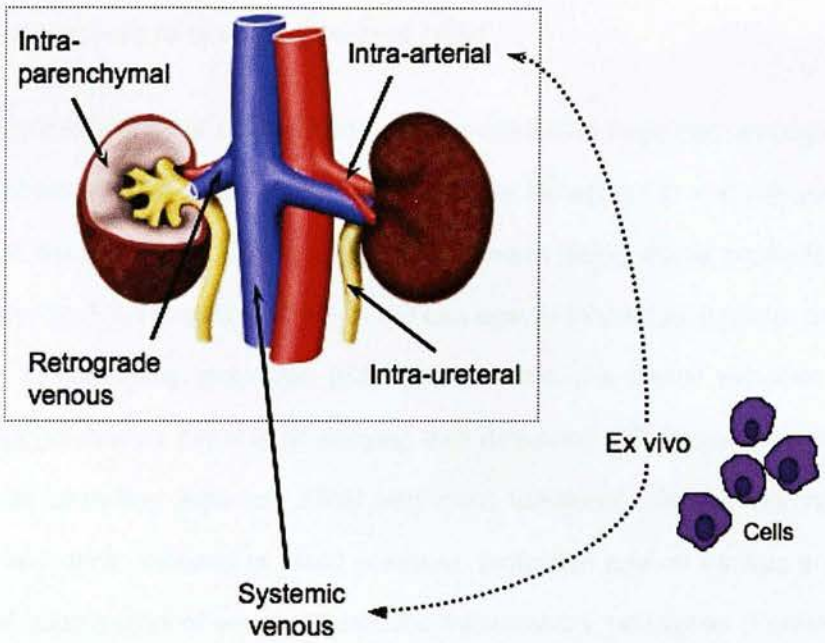

Figure 6: Potential routes of gene delivery to the kidney.

The kidney is accessible by many routes including the renal parenchyma (intra-parenchymal), the renal artery (intra-arterial), the renal vein (retrograde venous) and the urinary tract (retro-ureteral) as well as via the systemic circulation.

1.3.4 Alternatives to direct targeting of HO-1

The beneficial effects of HO-1 induction are mediated, in large part, through one or more products of the heme degradation pathway including CO and bile pigments. The last decade has seen an increase in studies using these products as an alternative to direct targeting of HO-1. CO can now be inhaled as a gas or delivered through CO-releasing molecules (CORMs). CORMs are mostly transition metal-containing carbonyls capable of carrying and delivering CO to biological systems (Hill-Kapturczak and Agarwal, 2006) and exert functional effects including blood vessel relaxation, lowering of blood pressure, protection against cardiac and renal IRI, and suppression of endotoxin-induced inflammatory responses (Foresti et al., 2005; Guo et al., 2004; Sawle et al., 2005; Vera et al., 2005).

Delivery of biliverdin alone also conferred protection against vascular disease. Interestingly, combination of biliverdin and CO resulted in increased protection compared to either agent alone in models of heart and kidney transplant associated IRI (Nakao et al., 2005).

1.4 Macrophages

Macrophages (Mφ) are key sentinel cells of the innate immune system. Mφ are versatile and play a crucial role in the initiation, progression and resolution of inflammation (Jaguin et al., 2013). As host primary defence cells, Mφ are present in all normal tissues but can also be derived from circulating monocytes that are recruited to inflamed tissues. Mφ have various roles including phagocytosis, antigen presentation as well as cytokine and pro-inflammatory mediator production (Siamon, 2007). The Mφ capacity to acquire diverse cellular phenotypes and effector functions according to their microenvironment has been revealed by *in vitro* studies. The various Mφ phenotypes described below (Figure 7) have been classified based on their fundamental functions that are involved in maintaining homeostasis, i.e.: host defence, wound-healing and immune regulation. However it should be noted that *in vivo*, macrophages can evolve to exhibit characteristics that are shared by more than one macrophage population described below.

Classical macrophage activation (M1 phenotype)

Mφ adopt a classically activated phenotype following stimulation with IFN-γ and microbial products such as LPS that engage Toll like receptors (TLR). This classical or 'M1' phenotype is also induced by innate cells such as natural killer cells (NK) or adaptive immune cells such as T helper cells 1(T_H1) and results in a Mφ population with high microbicidal activity. Indeed, M1 polarised Mφ show enhanced pro-inflammatory cytokine production (TNF-α) as well as iNOS expression and ROS production (Martinez, 2011; Mosser and Edwards, 2008).

Wound-healing or alternative macrophage activation (M2 phenotype)

The alternative activation of Mφ (M2 phenotype) is also a response to the innate and adaptive immune systems. Granulocytes are early sources of innate IL-4 and T_H2 cells also produce IL-4 and IL-13. IL-4 and IL-13 stimulated Mφ fail to present antigen to T cells, produce limited amounts of pro-inflammatory mediators and are considered to play a role in tissue repair by producing increased levels of collagen precursors (Hesse et al., 2001; Mosser and Edwards, 2008; Stein et al., 1992).

Regulatory Macrophage or Deactivation

The regulatory Mφ phenotype is attained by the presence of IL-10, TGF-β and glucocorticoids in the milieu and by the ingestion of apoptotic cells. These Mφ develop anti-inflammatory properties through the production of IL-10, TGF-β and PGE_2 as well as a reduced expression of MHC Class II molecules. Their generation towards the latter stage of the adaptive immune response suggests an important role for Mφ in the resolution of inflammation (Mosser, 2008; Gordon, 2005; Erwig, 2007; Siamon, 2007).

Taking into account that Mφ will adapt to the local environment by developing properties that may either cause further injury or alternatively evolve into cells that promote resolution of inflammation and promote tissue repair, different groups have focused on the modulation of Mφ phenotype and function and taken an interest in harnessing their anti-inflammatory and wound-healing properties for therapeutic gain in inflammatory disease.

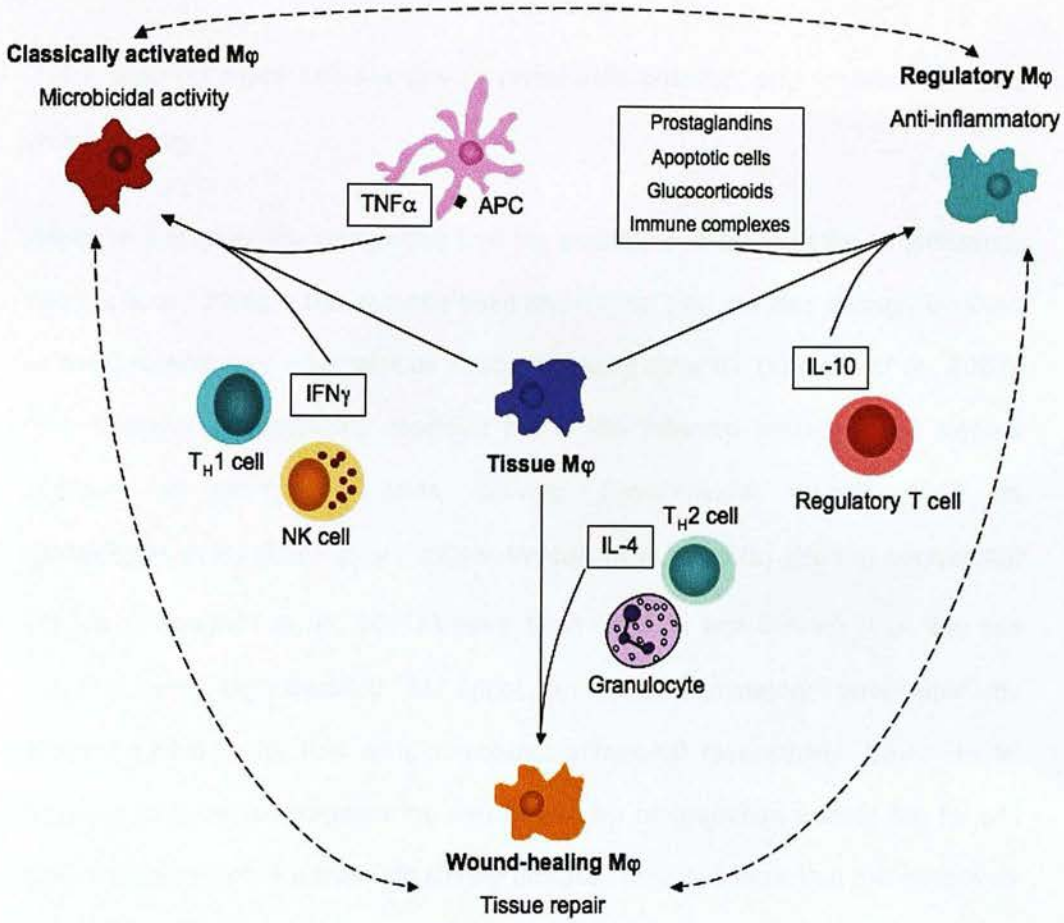

Figure 7: Cytokines produced by immune cells can give rise to distinct murine Mφ populations.

Classically activated M1 Mφ arise in response to IFNγ and TNFα produced by T_H1, natural killer (NK) cells and antigen presenting cells (APC) during immune responses. They have a potent microbicidal activity. Regulatory Mφ are generated in response to various stimuli including prostaglandins, apoptotic cells, glucocorticoids, immune complexes and IL-10. They have an anti-inflammatory activity. Wound-healing M2 Mφ arise in response to IL-4 produced by T_H2 cells and granulocytes and are involved in tissue repair.

1.4.1 Macrophages cell therapy in renal inflammation and ischaemic acute kidney injury

Although it is generally recognised that Mφ contribute to the initiation of ischaemic AKI (Jo et al., 2006), it has recently been shown that they are also strongly involved in renal regeneration after various insults including renal IRI (Vinuesa et al., 2008). The 'trapping' of genetically modified Mφ in the inflamed kidneys is an elegant method for site-specific gene delivery. Experimental models such as glomerulonephritis (Kluth et al., 2001b; Wilson et al., 2002a) and tubulointerstitial fibrosis (Yamagishi et al., 2001a) have been used to test the effect of 'Mφ cell therapy' with Mφ modified to adopt an 'anti-inflammatory phenotype' by overexpressing IL-10, IL-4 or IL-1 receptor antagonist respectively. David Harris' group extensively investigated the role of *ex vivo* programmed splenic Mφ for cell therapy in a model of proteinuric kidney disease. Data indicates that the adoptively transferred Mφ localise to the inflamed kidney and ameliorate disease (Table 4).

Table 4: Macrophage Cell therapy in experimental renal disease

Model	Cell used	Modification	Route of delivery	Results	Study
Rat NTN	NR8383 cell line	Ad-IL4 transduction	Renal Artery injection	Localisation at d 7. Reduced injury and proteinuria injury	(Kluth et al., 2001b)
	BMDM	Ad-IL10 transduction	Renal Artery injection	Reduced proteinuria and histological injury	(Wilson et al., 2002a)
Adriamycin nephropathy in SCID mice	Splenic Mϕ	IL-25 activation	IV injection	Reduced renal injury by induction of Th2 immune response	(Cao et al., 2011)
	Splenic Mϕ	IL-4/IL-13 activation	IV injection	Localisation at 28d and reduced functional injury	(Wang et al., 2007)
	Splenic Mϕ	IL-10/TGF-β activation	IV injection	Decreased renal inflammation, structural and functional injury	(Cao et al., 2010)
UUO (murine)	BMDM	Ad-IL-1ra transduction	IV injection post irradiation	Decreased Mϕ infiltration and fibrosis	(Yamagishi et al., 2001)
Murine IRI	BMDM	Ad-HO-1 transduction	IV injection	Unchanged ATN Improved renal function, reduced CD41+ platelet deposition	(Ferenbach et al., 2010)

1.4.2 Macrophages as vector for HO-1 therapy in renal inflammation and ischaemic acute kidney injury

Recent work shows that HO-1 influences Mφ to adopt their regulatory (i.e. anti-inflammatory) phenotype (Weis et al., 2009). Bone marrow-derived macrophages (BMDM) induced to overexpress HO-1 by adenoviral transduction exhibited an anti-inflammatory phenotype with increased IL-10 production, and reduced TNF-α and NO production following LPS stimulation. In addition, they exhibited increased phagocytosis of apoptotic cells *in vitro*. Furthermore, administration of these HO-1 overexpressing BMDM ameliorates AKI in a model of renal IRI (Ferenbach et al., 2010).

1.5 Embryonic Stem Cells

Embryonic stem cells (ESC) are derived from blastocysts that are structures formed in the early development of vertebrates and consist of two primary cell types:

(i) The inner cell mass (ICM) which is the source of ESC and

(ii) The trophoblast, which will give rise to the placenta.

ESC possess two distinctive properties that make them interesting candidates for regenerative medicine:

(i) They are pluripotent and are thus able to give rise to cell types of all three germ layers (*i.e.* mesoderm, ectoderm and endoderm) and thus eventually to all of an animal's tissues and organs.

(ii) They are able to self-renew indefinitely thus dividing and perpetuating the stem cell pool whilst maintaining an undifferentiated state (He et al., 2009).

Today, mouse and human ESC can be expanded indefinitely in culture and differentiated *in vitro* into mature cells including blood cells, cardiac muscle and neural cells (Figure 8).

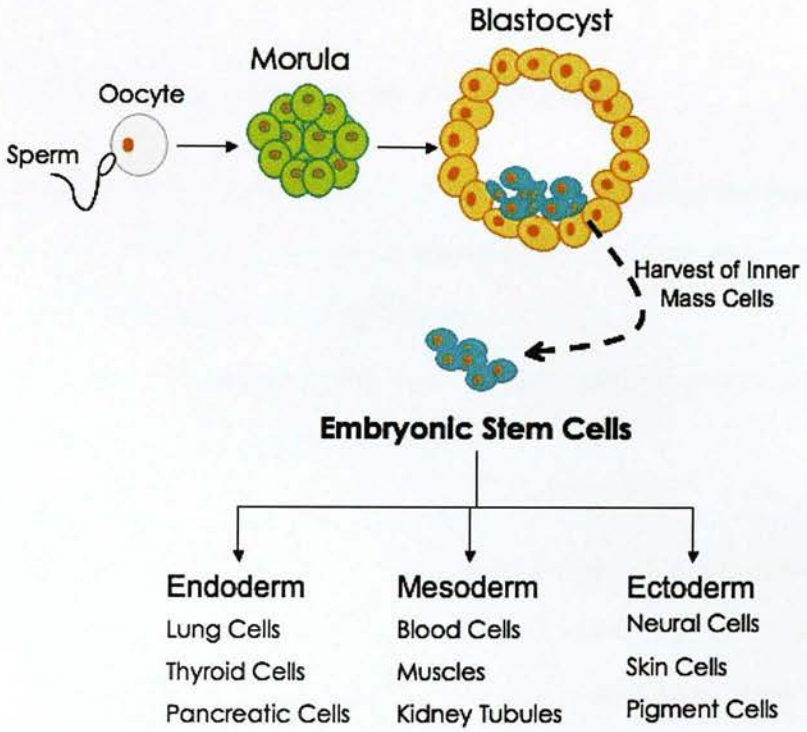

Figure 8: Embryonic stem cells originate as inner mass cells within a blastocyst.

ESC can be differentiated *in vitro* into mature cell types of all three germ layers (i.e. endoderm, mesoderm and ectoderm) such as blood cells, cardiac muscle and neural cells.

1.5.1 Embryonic stem cell derived macrophages

To a certain extent, our current knowledge of Mφ biology has been generated from *in vitro* examination of isolated macrophages and their precursors. The two main approaches used to study Mφ include:

(i) The isolation of primary Mφ or their precursors followed by culture or

(ii) The culture of Mφ cell lines.

Each of these approaches has obvious advantages and disadvantages. Acquisition of primary cells requires access to living organisms, invasive isolation procedures and engenders issues over purity of cell populations and limitation in cell number. In addition, primary cells are inherently difficult to manipulate genetically which limits their use for studying the molecular mechanisms associated with their function. By contrast Mφ cell lines provide supplies of limitless numbers of pure cell populations that can readily be manipulated but as they are transformed cells they are far removed from the normal state. They do however retain certain features of normal Mφ and their precursors are consequently widely used in Mφ research.

Today, a new source of Mφ is available as it has been showed that both mouse and human ESC can be differentiated *in vitro* into mature Mφ (Karlsson et al., 2008; Odegaard et al., 2007; Zhuang et al., 2012) as well as dendritic cells (Fairchild et al., 2000) and monocytes (Karlsson et al., 2008). Derivation of Mφ from ESC combines both the advantages of tumour cell lines by avoiding *in vivo* access and isolation problems and primary Mφ by essentially studying normal cells. ESC can be expanded in large numbers *in vitro* and are highly amenable to sophisticated genetic manipulations (Evans and Kaufman, 1981; Thomson et al., 1998) so they have the

potential to provide highly pure populations of wild-type or genetically manipulated Mφ. This ability to genetically manipulate ESC prior to differentiation makes ESDM an attractive source of therapeutic cell types. Mφ cell therapy has great potential to improve human disease, such as AKI. Various groups have already reported investigating the general physiology of ESDM and their implication in various disease models (Table 5).

For example, murine ESC-derived macrophages (ESDM) have been applied to the investigation of macrophage activities in atherosclerotic lesions (Moore et al., 1998) and microglial cells (Napoli et al., 2009) as well as general macrophage physiology (Odegaard et al., 2007). Similarly, human ESC have been used as productive sources of human Mφ for mechanistic studies (Karlsson et al., 2008; Subramanian, 2009).

Table 5: ESDM General Physiology Studies

ESDM type	Control Cell	Phenotyping	Phagocytosis	Inflammatory Response	Chemotaxis	Reference
Murine ESDM (P388D1 ESC line)	RAW 264.7 cell line	F4/80, CD11b, FcγRII, CD36, CD68, MMP-3, MMP-9	0.8 μm Latex beads	TNF-α, IL-6		(Moore et al., 1998)
Murine Microglia	BV2 cell line	IBa1, CD11b, CD45, F4/80, CD49d, CD29 CX3CR1	Microsphere beads	NO, IL-1β, TNF-α	CX3CL1	(Napoli et al., 2009)
Murine ESDM (E14 ESC line)	BMDM	F4/80, CD11b, CD64	Apoptotic cells		CCL5, VEGF, C5a	(Zhuang et al., 2012)
Murine ESDM (J1-HoxA9-ER ESC line)		F4/80, CD11b, CD16/32, CD80	2 μm Latex beads	TNF-α, NO		(Odegaard et al., 2007)

1.6 Hypothesis

This thesis will examine the hypothesis that ***anti-inflammatory HO-1 overexpressing macrophages can be generated from embryonic stem cells in vitro and that the administration of these embryonic stem cell-derived macrophages overexpressing HO-1 will protect mice from renal IRI in vivo.***

1.7 Aims

Our aim is to undertake 'proof of principle' studies to determine whether HO-1 overexpressing ESDM are anti-inflammatory *in vitro* and renoprotective *in vivo* following renal IRI. For this purpose, we will address the following issues:

1. ESDM will be phenotyped using a panel of cell surface markers and compared to BMDM.
2. ESC will be genetically manipulated to overexpress HO-1. The effect of genetic manipulations undertaken pre-differentiation will be examined to determine any deleterious effect upon the ESDM differentiation process.
3. The phenotype of control and manipulated ESDM in response to inflammatory stimuli will be assessed.
4. A model of murine IRI will be established in the 129/P2 mouse strain to provide clinically significant renal injury and dysfunction
5. Control and ESDM overexpressing HO-1 will be administered to mice with renal IRI.

Chapter 2. Material and Methods

2.1 Materials and reagents

Tissue culture reagents were ordered from Life Technologies (Paisley, UK). Unless stated, all other reagents were obtained from Sigma-Aldrich (Poole, UK). Tissue culture plates, dishes and tubes were purchased from Costar (Loughborough, UK) and Falcon (Runcorn, UK). Antibodies employed for flow cytometry, monocyte purification, Western blotting and immunohistochemistry were purchased from various suppliers and are summarised in Tables 6 to 9.

2.2 Embryonic stem cells

Depending on the genetic manipulation required for a given experiment, the following murine male embryonic stem cell (ESC) lines were used.

2.2.1 E14 IV cell line

E14 IV cells are embryonic stem cells generated from male 129/P2 mice (formerly designated 129/OlaHsd) at the Institute for Stem Cell Research, University of Edinburgh.

2.2.2. A2lox.cre cell line

The A2lox.cre ESC line was kindly donated by Dr M. Kyba (University of Minnesota). A2lox.cre cells constitutively express a reverse tetracycline transactivator (rtTA) from the Rosa26 locus located on chromosome 6. Upstream from the HPRT locus on the X chromosome, this cell line harbours an Inducible

Cassette Exchange (ICE) driven by a tetracycline responsive element (TRE) to which the gene of interest can be targeted and stably integrated via loxP, loxM and Cre-mediated recombination. In the presence of tetracycline, the rtTA is able to bind the TRE and activate expression of the integrated gene of interest. Figure 9 is a schematic representation of the engineered cell line.

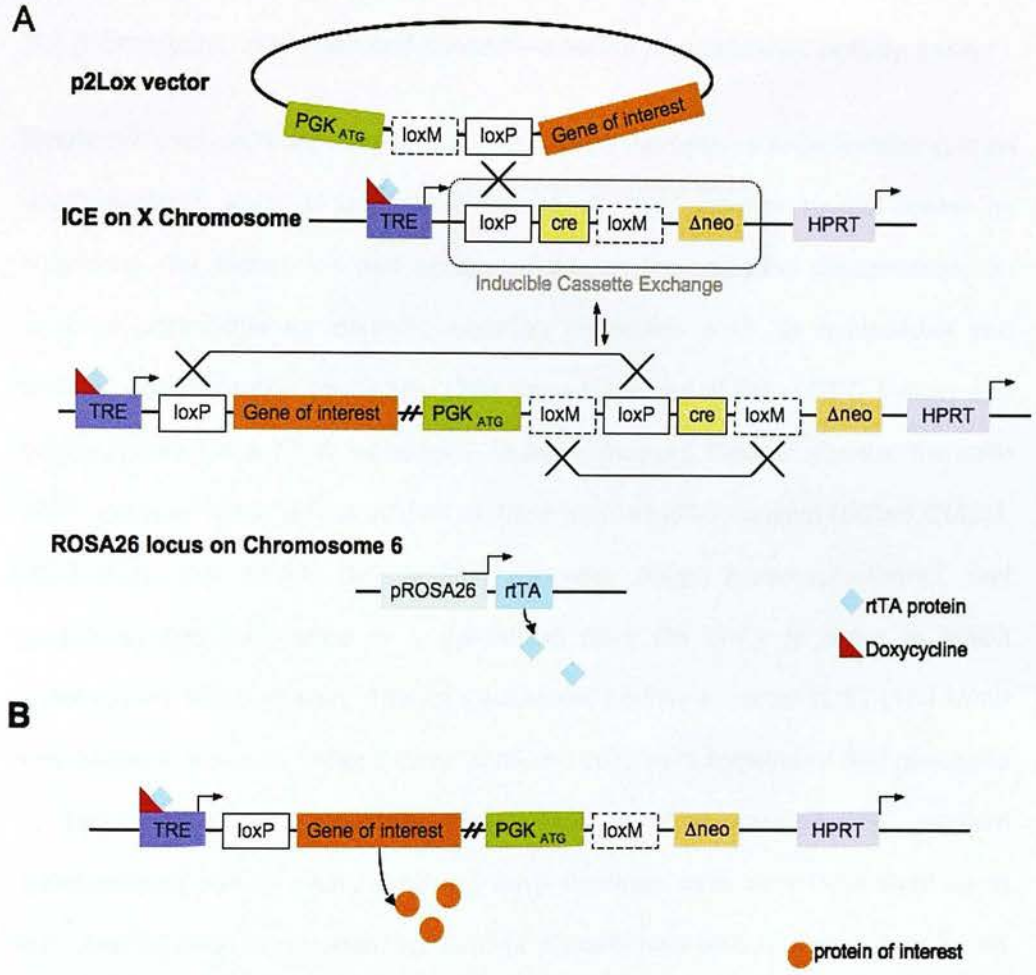

Figure 9: The A2lox.cre embryonic stem cell line.

A: An inducible cassette exchange (ICE) has been targeted to the HPRT locus on the X chromosome. The cDNA for cre recombinase has been inserted behind a tetracycline response element (TRE) and between loxP and loxM sites. In the presence of rtTA protein produced by the ROSA26 locus on chromosome 6 and doxycycline, the cells express cre and the ICE is self excised and exchanged for an incoming plasmid containing the gene of interest cDNA. **B:** stable new inducible cell line expressing the gene of interest protein upon the addition of doxycycline.

2.2.3 Embryonic stem cell self-renewal–alkaline phosphatase activity assay

Embryonic stem cells are able to divide and renew themselves while remaining in an undifferentiated state. It is possible to assess their potential to self renew by monitoring the expression and activity of the enzyme alkaline phosphatase, an enzyme responsible for dephosphorylating molecules such as nucleotides and proteins under alkaline conditions. Cells were taken out of the -140°C freezer and quickly thawed in a 37°C water-bath. Using a plugged Pasteur pipette, the cells were resuspended in a final volume of 10ml warmed ESC medium (500ml GMEM, 50ml FCS, 5ml NEAA, 5ml sodium pyruvate, 500µl 2-mercaptoethanol, 5ml glutamine) and transferred to a gelatinised flask (25 cm^2). In order to inhibit spontaneous differentiation, 10µl of Leukaemia Inhibitory Factor (LIF) (100 U/ml) was added to the cells. After 2 days, confluent cells were trypsinised and passaged at $1.5x10^6$ cells per gelatinised $25cm^2$ flask in 10ml warmed ESC medium supplemented with LIF. After another 2 days, confluent cells were trypsinised again and counted prior to commencing alkaline phosphatase activity assay. $1x10^3$ cells were plated per well in 6-well plates and cultured for 6 days in ESC medium in triplicate. The propagation of ESC in an undifferentiated pluripotent state is dependent on the presence of LIF. Consequently, cells were either grown in the presence or absence of LIF (100 U/ml). On day 6, colonies were stained for alkaline phosphatase (AP) activity using the Leukocyte AP staining kit (Sigma Diagnostics). AP Staining Kits are histochemical assays that use a solution containing a substrate and colour dye as the colorimetric read-out for the enzymatic activity. The entire experiment was performed at room temperature and the staining was carried according as directed by the manufacturer. Demonstration of AP activity can be done by simultaneous capture using substituted naphtols and diazonium salts as

substrate. To prepare the substrate (made up and stored in the dark), 1ml of sodium nitrite solution was added to 1ml of Fast Red Violet-Alkaline solution and allowed to stand for 2min (*i.e.* coloured diazonium salt). This mixture was then added to 45ml of de-ionised water followed by addition of 1ml Naphthol AS-BI Alkaline solution.

Media was removed from the wells and colonies were fixed by addition of citrate-formaldehyde-acetone fixative (25ml citrate solution, 65ml acetone and 8ml formaldehyde) for 30 seconds then washed off carefully with water (1ml/well) for 45 seconds. Colonies were then incubated with 1ml substrate per well for 15 minutes in the dark. Wells were carefully rinsed with water, counterstained with hematoxylin solution for 2min and air-dried. Active AP expressed by ESC can be visualised by the generation of a pink colour following incubation with the substrate. Differentiated cells that do not express the enzyme remain unstained and appear white. Subsequently, the number of colonies of stem cells (pink), unstained differentiated cells (white) and mixed stem cell and differentiated cells were scored by microscopic examination. Figure 10 depicts representative examples of the 3 different types of colonies discernible during microscopic analysis of cell cultures following staining for active alkaline phosphatase.

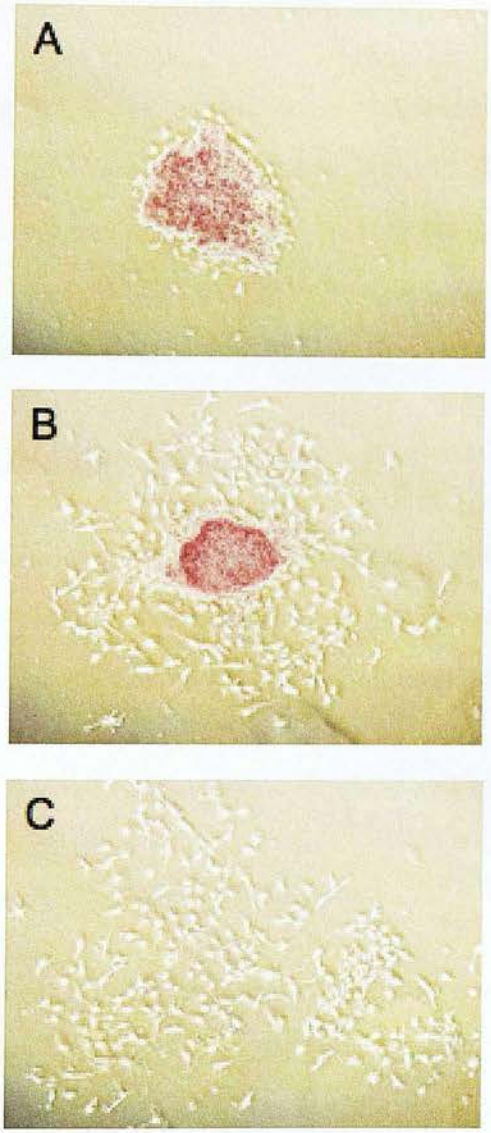

Figure 10: Microscopic examination of alkaline phosphatase activity assay.

$1x10^3$ cells were plated per well in 6-well plates and cultured for 6 days in ESC medium. On day 6, colonies were stained for alkaline phosphatase activity using the Leukocyte AP staining kit. **A:** A stem cell colony stains pink indicating expression of alkaline phosphatase. **B:** A mixed colony of stem cells (pink) and differentiated cells (white). **C:** A fully differentiated colony does not express alkaline phosphatase and appears white with no pink staining evident.

2.2.4 Retinoic acid – embryonic stem cell differentiation assay

Stem cells were induced to differentiate using retinoic acid (RA) treatment as previously described (Forrester et al., 1996). $1.5x10^5$ cells were plated on gelatinised TC dishes and incubated at 37°C in 10 ml GMEM medium supplemented by 5% FCS for 24h. The medium was then complemented with RA at a final concentration of 10^{-6}M for a further 48h.

2.2.5 Embryonic stem cell cryopreservation

Embryonic stem cells were resuspended in a 1 in 10 dilution of DMSO in GMEM medium and stored in 1ml cryovials (2 cryovials per 25 cm^2 flask). They were kept overnight at -80°C then stored in a -140°C freezer until next use.

2.3 Preparation of macrophages, dendritic cells and monocytes

2.3.1 Preparation of L929-Conditioned Medium

L929 conditioned medium, a source of murine macrophage colony-stimulating factor (M-CSF), was prepared by maintaining L929 cells in 50ml DMEM F/12 medium supplemented with 10% FCS and 1% P/S, in a T-162 filter cap flask. After a week, the supernatant, further referred to as "L929-conditioned medium", was removed from the T-162 flask, collected in 0.22µm filter units, aliquoted in 50ml Falcon tubes then frozen at -20°C until further use.

L929 cells still plated in the T-162 flask were gently washed with 50ml of warmed PBS -/- to remove all trace of FCS. The PBS was removed and the cells trypsinised with 10ml of Trypsin EDTA (TE) for 3-5mins at 37°C until detached from the flask, then rinsed with 20ml of fresh DMEM F/12 medium to deactivate the TE and

transferred to 50ml Falcon tubes. Cells were pelleted by centrifugation at 300g for 5 min and excess medium discarded. The cells were then thoroughly resuspended in 50ml fresh DMEM F/12 medium supplemented with 10% FCS and 1% P/S. The single cell suspension was transferred to a new T-162 filter cap flask and cultured for another week.

2.3.2 Preparation of embryonic stem cell-derived macrophages

Stem cells were taken out of the -140°C freezer and quickly thawed out in a 37°C water-bath. Using a plugged Pasteur pipette, the cells were resuspended in a final volume of 10ml warmed ESC medium and transferred to a gelatinised flask (25 cm^2). In order to inhibit spontaneous differentiation, 10µl of LIF (100 U/ml) was added to the cells. After 2 days, confluent cells were trypsinised and passaged at $1.5x10^6$ cells per gelatinised $25cm^2$ flask in 10ml warmed ES medium supplemented with LIF. After another 2 days, confluent cells were trypsinised again and counted prior to commencing the preparation of embryoid bodies (EB) and the generation of embryonic stem cell-derived macrophages (ESDM). A drop of $6x10^5$ ESC in suspension was added to each bacteriological dish in the presence of 17ml ESC medium, 3ml L929 conditioned medium (15% final concentration) and 2µl IL-3 (1 ng/ml final concentration). The medium was refreshed on day 4 and day 6 and after 8 days, the cells spontaneously formed mature EB that were plated down onto gelatinised TC dishes with 17ml ESC medium, 3ml L929 conditioned medium, 2µl IL-3 and 200µl of 100 U/ml penicillin and 100 µg/ml streptomycin (P/S). Every second day from day 10 to day 30, non-adherent cells in the supernatant were collected and subsequently re-plated onto bacteriological dishes (100x15mm) in the presence of 17ml ES medium, 3ml L929 and 200µl P/S to produce ESDM (Figure 11). Medium was replaced in the gelatinised dishes to enable further cell production.

This whole protocol was based on work done in the CIR by Dr Lihui Zhuang (Zhuang et al., 2012). Figure 12 depicts representative pictures of EB in suspension, plated EB and the adherent cells generated by the protocol.

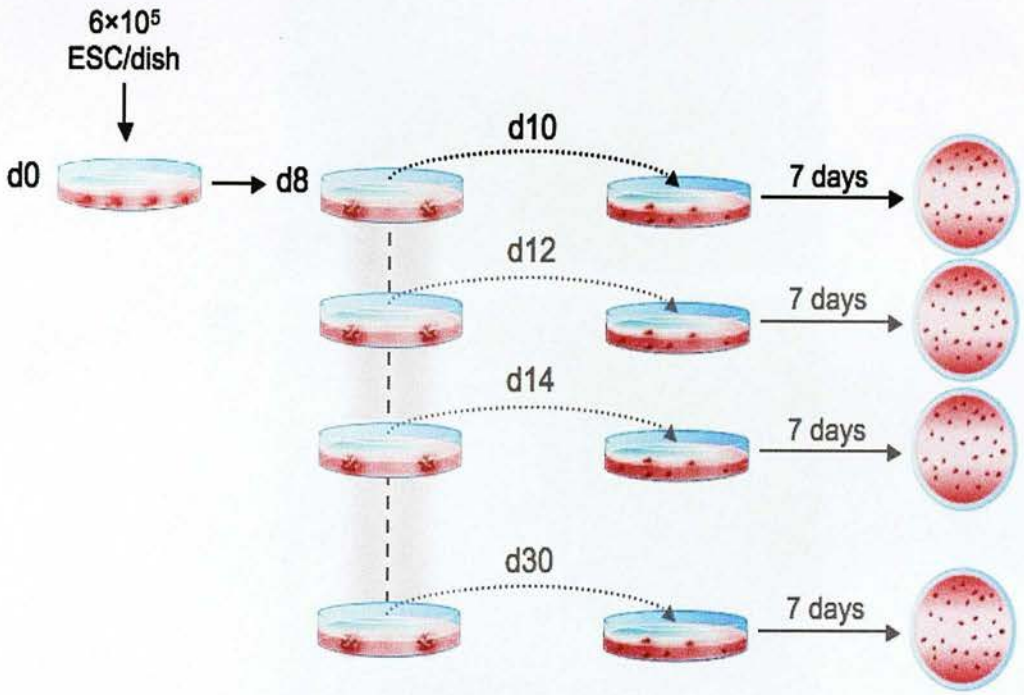

Figure 11: Method for the differentiation of embryonic stem cells into macrophages.

On day 0, a drop of $6x10^5$ ESC in suspension is added per bacteriological dish (100x15mm) and cultured for 8 days. During these 8 days, ESC spontaneously form embryoid bodies (EB) in suspension. On day 8, EB are plated down onto a gelatinised TC dish. While plated, EB start releasing non-adherent cells into their culture supernatant. We call these cells macrophage progenitor cells (MPC). On day 10, the first harvest of MPC is plated onto a bacteriological dish and after 7 days of maturation, adherent cells are produced. The media in the plated EB dish is refreshed to enable subsequent harvests every 2 days until day 30.

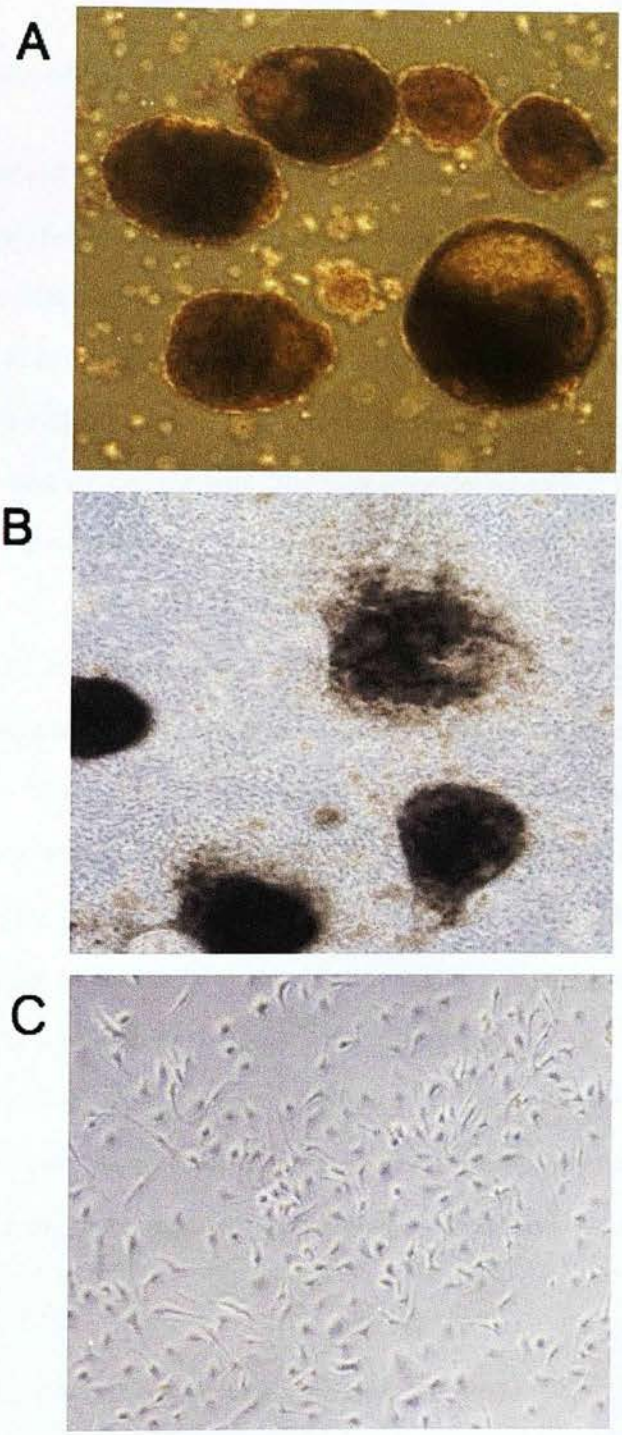

Figure 12: Representative pictures of cells generated during the embryonic stem cell-derived macrophage differentiation.

A: Embryoid bodies (EB) in suspension **B:** EB plated down onto a gelatinised TC dish. **C:** Adherent cells produced from plated macrophage progenitor cells (MPC) generated by plated EB (x100 magnification).

2.3.3 Preparation of bone marrow derived macrophages

Bone marrow derived macrophages (BMDM) were derived from femurs and tibias of 129/P2 mice aged 6-8 weeks old obtained commercially or from in-house colonies. The mouse was killed by cervical dislocation and its coat was washed with 70% ethanol (EtOH) to limit contamination by fur. Autoclaved instruments were used to incise the skin laterally about midway down the abdomen and the skin was removed from the lower abdomen and the legs. The legs were detached and tissue debrided. The intact femurs and tibias were then harvested, rinsed with 70% EtOH and placed directly on ice in DMEM/F12 containing 100 U/ml penicillin and 100µg/ml streptomycin (P/S) and transported to a sterile pre-cleaned tissue culture hood. In the hood, the residual muscle and tissue was removed with a sterile scalpel and bones cleaned in 70% EtOH. Bone extremities were severed and the bone marrow of 1 femur and tibia was flushed into a universal container with 10ml of macrophage (Mφ) medium that consisted of DMEM/F12 supplemented with 20% L929 conditioned medium (a source of murine macrophage colony-stimulating factor [M-CSF]), 10% FCS and 1% P/S). Cells were resuspended and counted with a haemocytometer. Bone marrow cells from 1 femur and tibia were then plated down onto three 55cm^2 petri dishes in a total volume of 20ml Mφ medium. Cells were matured for seven days with medium being entirely renewed every second day.

2.3.4 Preparation of bone marrow derived dendritic cells

Femurs and tibias of 129/P2 mice aged 6-8 weeks old were obtained as described for the preparation of BMDM. However, bone marrow cells were cultured for 7 days in dendritic cell medium that comprised RPMI 1640 supplemented with 10% FCS,

1% P/S and 20 ng/ml of granulocyte macrophage colony-stimulating factor (GM-CSF). Fresh GM-CSF was added every third day.

2.3.5 Purification of bone marrow monocytes

Femurs and tibias of 129/P2 mice aged 6-8 weeks old were obtained as described for the preparation of BMDM. The extremities of the bones were severed to allow flushing of the bone marrow into a 50ml Falcon tube with sterile HBSS-Prep (Ca^{2+}/Mg^{2+} free HBSS supplemented with 20mM Na-HEPES [pH 7.4] and 0.5% FCS) using a 25G needle and a 20ml syringe. Bone marrow from different bones was pooled into the same tube and disaggregated through a 19G needle prior to centrifugation at 400g for 5 min. The pellet was resuspended in 5ml 0.2% NaCl for 45 seconds to lyse red blood cells and osmolarity was restored by adding an equal volume of ice cold 1.6% NaCl. The suspension was filtered through a 100µm cell strainer in order to remove residual blood clot and bone remnants. Cells were pelleted again by centrifugation at 400g for 5 min. A 90% Percoll solution (3ml 10x PBS in 27ml Percoll Stock) and a 62% Percoll solution (3.2ml of 90% Percoll solution in 1.8 ml HBSS-Prep) in a 15ml Falcon tube were prepared. The bone marrow was then resuspended in 5ml HBSS-Prep and carefully layered on top of the 62% Percoll gradient prior to a 30 min centrifugation at 1000g on acceleration 5 with no brake. At the end of the gradient centrifugation, a sharp interface formed on top of the 62% Percoll containing immature cells of the non-granulocyte lineages. In contrast, the cloudy pellet at the bottom contains granulocytes. The interface containing the non-granulocyte cells was carefully harvested into another 15ml Falcon tube (approximately 3ml) and washed twice at 400g for 5 min with HBSS-Prep made up to 15ml. The cells were counted and resuspended in 200µl FACS

buffer (PBS-/- with 10% mouse serum) for 5 min. In order to deplete the T cells, B cells and NK cells, 2μl of biotinylated anti-CD3ε, anti-B220 and anti-NK1.1 antibodies were added and left for 30 min on ice. After a PBS wash, cells were resuspended in 200μl MACS buffer (PBS, 2mM EDTA, 0.5% BSA) and 15μl magnetic beads and left in the fridge for 15 min. In order to remove any unbound beads, cells were washed in 5ml MACS buffer then resuspended in a volume of 500μl. Magnetic selection columns were rinsed with MACS buffer prior to running the sample. Cells that run through the column are negatively selected monocytes.

2.4 Characterisation of macrophages

2.4.1 Cytospin followed by Diff-quick staining

The morphology of BMDM and ESDM was assessed by the cytospin and Diff-quick staining method. 200μl of a suspension of BMDM or ESDM was added to the well of a 'cytospin holder' and the cells were cytocentrifuged at 300g for 3 min in a Shandon Cytospin II (Shandon, UK). The cells were then fixed with 100% methanol (MeOH) for 2 min, followed by staining in the Diff-quick Red solution for 1 min followed by staining in the Diff-quick Blue solution for 1 min (Gaminor Ltd, UK). All steps were performed at room temperature (RT). The slides were rinsed with distilled water, left to air dry and finally coverslipped and mounted.

2.4.2 Immunohistochemistry analysis of cells

An indirect 3,3'-Diaminobenzidine (DAB) based detection system was used to detect the stem cell marker Oct4 and the mononuclear phagocyte markers F4/80 and CD11b. Cytospin preparations of ESDM and supernatant cells were fixed with 3%

paraformaldehyde for 20 minutes and stored in PBS at 4°C. BMDM and ES cells were also fixed as positive and negative controls for F4/80/CD11b and Oct4 respectively. The slides were transferred to a sequenza rack (Shandon, Inc.) and washed with PBS. Non-specific avidin, biotin and protein interactions were then blocked for 10 min each using an Avidin/Biotin Blocking Kit (Vector Labs SP-2001) and a Protein Block (DAKO Cat X0909) respectively. Slides were incubated at 4°C overnight with 125µl primary antibody or 125µl ISO-rat IgG2a isotype antibody. To stain for the intracellular transcription factor Oct4, cells were further permeabilised with 0.2% triton x100 in PBS (10 minutes). After washing 3 times with PBS, cells were incubated with a biotinylated secondary antibody at room temperature (RT) for 30 minutes, washed 3 times with PBS. Three drops of Vectastain RTU elite solution (Vector labs) were then added per slides for 30 minutes. Cells were washed 3 times with PBS prior to addition of 125µl DAB solution (Dako, North America Inc) and incubation for 5 min (1 drop of stock DAB solution per ml buffer). The slides were then placed in a PBS bath prior to being counterstained with haematoxylin for 20 seconds, rinsed with running tap water and dehydrated through baths of increasing ethanol concentration (70%, 80%, 90%, 100%) for 1 min each prior to immersion in xylene for 5 min followed by mounting and coverslipping. Cells that were positive for Oct 4, F4/80 or CD11b were identified by the presence of brown staining under a Leica Zeiss Axiovert light microscope.

2.4.3 Flow cytometry

Mature BMDM and ESDM were also characterised by flow cytometric analysis of surface expression of several Mφ and dendritic cell markers including F4/80, CD11b, CD11c and MHC class II (Table 6).

Mφ were harvested from Petri dishes using detachment buffer (HBSS, 5mM EDTA, 0.2% BSA) and gently scrapped off with a cell lifter prior to being transferred to chilled polystyrene FACS tubes ($2.5x10^5$ cells/tube) and centrifuged at 300g for 5min at 4°C. The supernatant was carefully discarded and the cells were washed by adding 2ml of cold PBS, followed by centrifugation at 300g for 5 min at 4°C. After discarding the supernatant, cells were resuspended in 100µl blocking solution (PBS -/- containing 10% mouse serum) and incubated for 5 min on ice. Fluorochrome conjugated antibodies of interest or their respective isotype control diluted 1/100 in blocking solution were then added. The cells were mixed gently and incubated on ice for 30 min in the dark. Before undergoing flow cytometric analysis, 1ml PBS -/- was added and the tubes centrifuged once more at 300g for 5 min at 4°C. The supernatant was discarded and the reaction was completely stopped by adding 100µl of 10% formalin. Analyses were performed using a FACScalibur instrument and the results were analysed with FlowJo software (Treestar, USA).

Table 6: Conjugated primary antibodies used for flow cytometric analysis of cells derived from bone marrow or embryonic stem cells

Antigen	Target Cell	Fluorochrome	Supplier	Reference	Isotype
F4/80	Macrophage & dendritic cell	PE	Caltag Laboratories	MF48004	Rat IgG2b
F4/80	Macrophage & dendritic cell	APC	eBioscience	17-4801-82	Rat IgG2a,κ
CD11b	Monocyte Macrophage Neutrophil	PerCP-Cy5.5	eBioscience	45-0112	Rat IgG2b
CD11c	Macrophage Dendritic Cell	APC	Invitrogen	MCD11c05	Hamster IgG
MHC Class II	Antigen Presenting Cell	FITC	eBioscience	11-5321-82	Rat IgG2b,κ
Ly6C	Neutrophil Ly6c$^+$ Monocyte	FITC	BD Biosciences	553104	Rat IgG2b,κ
CD3ε	T lymphocytes, NK-T cells, thymocytes	Biotin	BD Biosciences	553239	N/A
B220	B lymphocytes	Biotin	BD Biosciences	553085	N/A
NK1.1	NK cells	Biotin	BD Biosciences	553163	N/A
HO-1	Various cells	PE	Stressgen	OSA-111PED	IgG2b

2.4.4 Phagocytosis assay

2.4.4.1 Flow cytometry analysis of phagocytosis of fluorescent latex beads

BMDM and ESDM were seeded into 12-well plates ($5x10^5$ cells/well) and left to adhere for 3h in 0.5ml of Mφ media at 37°C. After washing non-adherent Mφ away with media, 3μm fluorescent green latex beads (Polysciences Inc, Germany) were added to each Mφ well at a ratio of 10 beads per Mφ and the plates gently agitated manually to ensure an even 'carpet' of beads (i.e the availability of beads for ingestion was not limiting). Plates were then placed in a dark incubator for 1h at 37°C. One experimental plate was kept on ice in order to prevent phagocytosis and was used as a control to assess non-specific binding of beads to Mφ. Wells containing Mφ alone were used to assess the intrinsic autofluorescence of Mφ alone. On completion of the incubation period, all plates were placed on ice and the wells washed vigorously 3 times with ice-cold PBS to remove any non-ingested or unbound beads. Mφ were lifted off the plastic using detachment buffer (HBSS, 5mM EDTA, 0.2% BSA) and gently scrapped off with a cell lifter. The cells were then transferred into chilled polystyrene FACS tubes and stained for F4/80 as outlined previously. Analyses were performed using a FACScalibur instrument and the results were analysed with FlowJo software (Treestar, USA).

2.4.4.2 Preparation of apoptotic thymocytes

Thymi from 4-8 week old female mice were stored in ice-cold RPMI 1640 media containing 1% P/S. In a sterile hood, the thymus was dissociated to single cells by grinding and washing with media. 10µl CM green fluorescent dye was added and the tubes were incubated at 37°C for 30 min. 1ml of 1% FCS was then added to quench any free CM green dye and the suspension was transferred to a $75cm^2$ tissue culture flask. The volume was made up to 100ml and dexamethasone was added at a final concentration of 1µM to facilitate the induction of apoptosis. The flask was incubated in an upright position to increase cell density for 20 hours. Cells were then resuspended and transferred to falcon tubes. After centrifuging at 300g for 5 min, the cells were pooled and centrifuged again at 300g for 5 min before counting with a haemocytometer.

2.4.4.3 Fluorescent microscopy analysis of phagocytosis of apoptotic thymocytes

Mφ were seeded onto glass coverslips in 12-well plates ($5x10^5$ cells/well) and left to adhere for 3h in 0.5ml of Mφ media at 37°C. After washing non-adherent Mφ away with media, apoptotic thymocytes were added to each Mφ well at a ratio of 10 particles per Mφ and the plates gently agitated to ensure that an even 'carpet' of apoptotic cells overlay the Mφ. Plates were then placed in a dark incubator for 1h at 37°C. One experimental plate was kept on ice in order to prevent phagocytosis and was used to assess non-specific binding. On completion of the incubation period, all plates were placed on ice and the wells washed vigorously 3 times with ice-cold PBS to remove excess non-ingested or unbound apoptotic thymocytes. Mφ were then stained with Cell Tracker Orange (Life Technologies Invitrogen, UK) in serum

free medium and the plates were incubated for 30min. Wells were washed with 10% FCS containing media to quench any remaining dye and cells fixed with 10% formalin. Images of the phagocytic macrophages were taken with a fluorescent microscope (Fluorescent Axiovert 200, Zeiss). When assessing phagocytosis of particles by Mφ, the main issue is distinguishing actual ingestion from cell surface binding. We visually defined phagocytosis on a case-by-case analysis of the Mφ. Cell tracker orange labelling of the cytoplasm helped define the contour of the Mφ and once ingested, green apoptotic cells would appear yellow. In contrast, non-ingested apoptotic cells bound to the Mφ cell surface remained green (Figure 13). We visually quantified two phagocytosis parameters:

(i) **The percentage phagocytosis**: the number of Mφ that have ingested particles divided by the total number of Mφ multiplied by a hundred.

(ii) **The phagocytic index**: the mean number of particles ingested by Mφ

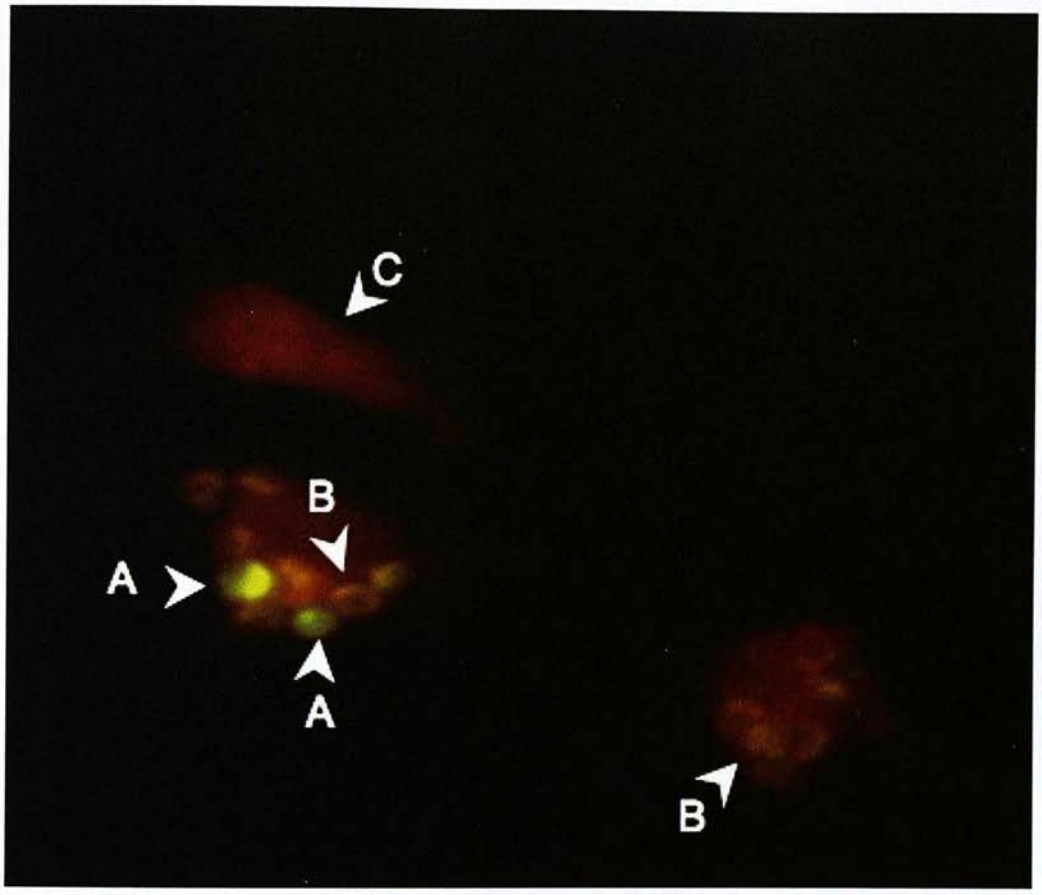

Figure 13: Visual assessment of macrophage phagocytosis of apoptotic thymocytes under fluorescent microscope.

Representative fields of bone marrow derived macrophages (BMDM) cultured on glass coverslips that were exposed to fluorescent green apoptotic cells for 1h. BMDM were then labelled with cell tracker orange and fixed with 10% formalin prior to fluorescent microscopy. **A:** fluorescent green apoptotic cells bound to the surface of a BMDM remain green whilst **B:** ingested fluorescent green apoptotic cells appear yellow following phagocytosis by a cell tracker orange labelled macrophage. **C:** Cell tracker orange labelling of the cytoplasm of a non-phagocytic BMDM (x320 magnification).

2.4.5 Macrophage activation: LPS and IFNγ stimulation

$1x10^6$ cells were plated in 6-well plates and left to adhere for 3h. Unbound cells were washed off with PBS and adherent cells were activated by incubation with LPS (1µg/ml) and IFNγ (100U/ml). Control non-activated cells were exposed to culture medium alone. Every condition was prepared in triplicate and the plates were incubated for 24h at 37°C.

2.4.5.1 Nitric oxide measurement

Nitric oxide (NO) released from cells is rapidly oxidised to nitrite (NO_2^-) in culture medium so that nitrite concentrations were used as an indirect measurement of NO production. The Griess method of measuring nitrite concentration consists of a two-step reaction where nitrite molecules react with sulfanilamide to generate a transient diazonium derivative. This intermediate further interacts with N-(1-naphthyl)ethylene diamine to yield a coloured diazo end product that strongly absorbs at 540nm as showed on Figure 14. Briefly, 50µl of cell culture supernatants derived from control or LPS/IFNγ activated Mφ were mixed with 50µl of Griess reagent (1% sulphanilamide, 0.1% N-(1-naphthyl) ethylene diamine) in triplicate in 96-well plates. After 15 min incubation at RT, absorbance was read at 540 nm and the level of NO was calculated using a standard curve generated by known sodium nitrite concentrations.

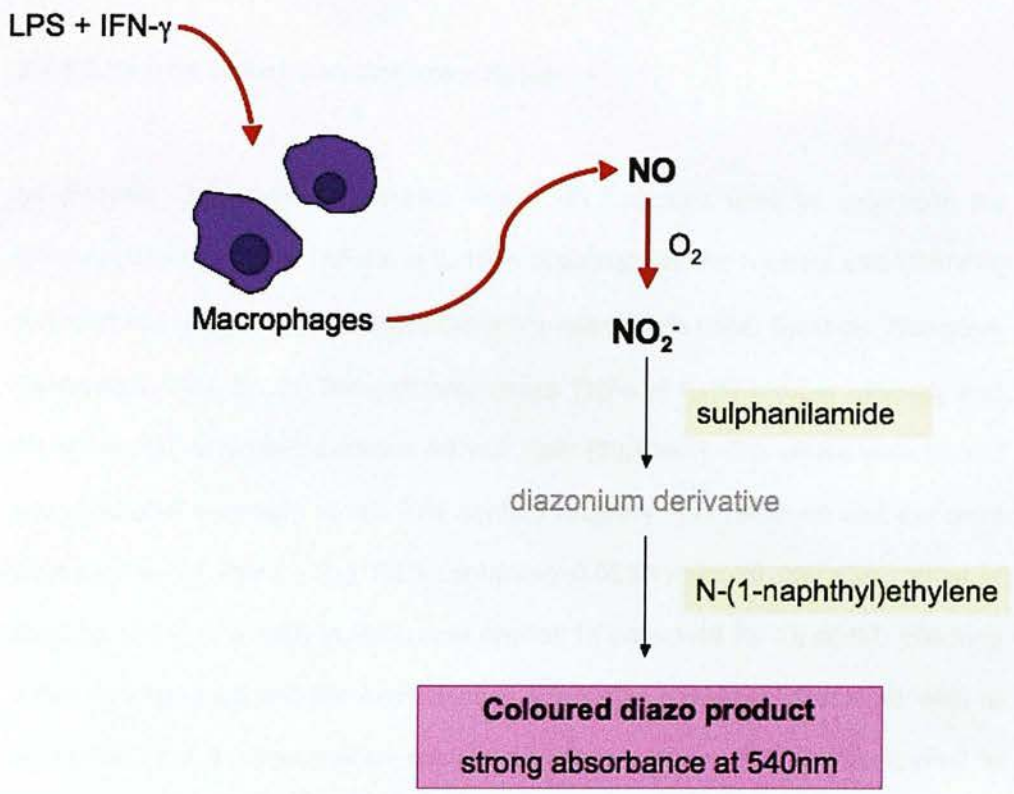

Figure 14: Griess reaction assay following LPS and IFN-γ activation of macrophages.

Nitric oxide (NO) released in the supernatant of LPS/IFN-γ activated macrophages was assessed by the Griess assay. NO is rapidly oxidized to nitrite (NO_2^-) that subsequently reacts with sulfanilamide to generate a transient diazonium derivative. This intermediate product further interacts with N-(1-naphthyl)ethylene diamine to yield a coloured diazo end product that absorbs strongly at 540nm. The level of NO was then calculated using a standard curve generated by known sodium nitrite concentrations.

2.4.5.2 Enzyme Linked Immunosorbent Assay

An Enzyme Linked Immunosorbent Assay (ELISA) was used to determine the concentration of murine TNFα and IL-10 in supernatants from control and LPS/IFNγ activated Mφ according to the manufacturer's instructions (R&D Systems, Abingdon, Oxfordshire, UK). Briefly, the goat anti-mouse TNFα or IL-10 capture antibody was diluted in PBS and used to coat a 96 well plate (50µl/well). The plates were sealed and incubated overnight at RT. The capture antibody was removed and the wells were washed 3 times using PBS containing 0.05%Tween-20 (pH 7.4). 300µl of blocking buffer (1% BSA in PBS) was applied to each well for 1h at RT. Blocking buffer was removed and the wells washed 3 times as previously described. 50µl of either standard or experimental sample diluted in reagent diluent was applied to each well. Both standards and experimental samples were run in duplicate. The plates were sealed and incubated at RT for 2h. Wells were washed 3 times as described and 50µl of biotinylated goat anti-mouse TNFα or IL-10 detection antibody diluted in reagent diluent was added to each well. Following 2h incubation, the detection antibody was removed and the wells washed 3 times again. 50µl of streptavidin-horseradish peroxidase (HRP) was applied to each well. The plate was covered and incubated for 20 min at RT. Further washing was followed by the addition of 50µl of substrate solution to each well and the plates were incubated for a further 20 min with protection from light. The reaction was then stopped by the addition of 50µl of stop solution (2N H_2SO_4) to each well. The optical density of each well was evaluated using a microplate reader (Dynatech Laboratories, USA) set to a wavelength of 450nm with the wavelength correction set to 570nm.

2.5 Induction of hemeoxygenase-1 expression

2.5.1 Pharmacological induction of hemeoxygenase-1 expression

The pharmacological induction of hemeoxygenase-1 (HO-1) expression was achieved by incubation of cells with heme arginate (HA) (Orphan Europe, Paris, France). Cells were plated in 12-well plates ($5x10^5$ cells/well) and exposed to 10μM HA (dissolved in Mφ medium) for 24h.

2.5.2 Genetically engineered induction of hemeoxygenase-1 expression

Generation of HO-1 overexpressing ESC was performed by Dr Richard Axton from the MRC Centre for Regenerative Medicine at the University of Edinburgh. Genetic engineering was employed to generate ESC cell lines with either:

(i) Constitutive overexpression of HO-1 or,

(ii) Inducible overexpression of HO-1.

In both cases, amplified murine HO-1 cDNA (Reverse: 5'-GCGGCCGCTTACATGGCATAAATTCCCACTGCCACTGTT-3'; Forward: 5'CTCGAGAATTCGGTACCACCATGGAGCGTCCACAGCCCGACAGCATGC-3') was subcloned into a TA Cloning® vector using a TOPO® cloning kit (Invitrogen, Paisley, UK).

2.5.2.1 Constitutive overexpression of hemeoxygenase-1 under the pCAG promoter

The HO-1/TA cloning® vector was subsequently cloned into a mammalian expression vector pCAG containing an internal ribosome entry site (IRES) and puromycin. Integration of the expression vector into the cell genome via

electroporation then produced stable HO-1 expressing ESC lines selected by their puromycin resistance.

2.5.2.2 Tetracycline inducible system: using the A2lox.cre embryonic stem cell line

The HO-1/TA cloning® vector was subsequently cloned into a p2Lox targeting vector. Cre/Lox recombination was used to insert p2Lox into the inducible cassette exchange (ICE) behind a tetracycline responsive element as previously described (Iacovino et al., 2011). In the tetracycline inducible system, doxycycline (Dox - a broad-spectrum antibiotic of the tetracycline family) is required in conjunction with rtTA to drive the Cre/Lox recombination as well as TRE and HO-1 expression (Figure 9). Inducible cells were exposed to 5µg/ml Dox and incubated at 37°C for 24h.

2.6 Detection of Hemeoxygenase-1 Protein

2.6.1 Western blotting

The protein content of Mφ was assessed with a Bio-Rad Protein Assay Kit, based on the Bradford method prior to performing Western blotting. 20µg of protein samples were subjected to 10% SDS-polyacrylamide gel electrophoresis (SDS-PAGE) in 1mm slab gels according to the procedure of Laemmli (Laemmli, 1970) and the separated polypeptides were then transferred electrophoretically from the gel to a pure nitrocellulose membrane using transfer buffer (0.25M Tris base, 1.92M glycine, and 1% SDS). Following electroblotting, the nitrocellulose membrane was stained with Ponceau Red for protein detection. Destaining was performed with distilled water and the membrane blocked with skimmed milk powder (5% in Tris

Buffered Saline [TBS]) for 30min at RT. The nitrocellulose blot was then incubated overnight on a shaker at 4°C with a rabbit anti-mouse HO-1 antibody (diluted 1/5000 in 1% BSA made up in TBS-0.05% Tween 20). The membrane was then washed 3x with TBS-Tween and exposed to a secondary goat anti-rabbit IgG-HRP antibody for 35 min on a shaker at RT. The membrane was washed repeatedly with TBS-Tween with the final wash being with TBS without Tween as this can interfere with the developing agent. The blots were developed using the chemiluminescence reagent SuperSignal West Femto Trial Kit (Thermo Scientific) and visualised in a VersaDoc Molecular Imager (VersaDoc MP 4000 Imaging System, PC/Mac from Bio-Rad). Other antibodies used for Western blotting can be found in Table 7.

Table 7: Antibodies used for Western blotting

Antigen	Primary antibody (Dilution)	Supplier & Reference	Secondary antibody (Dilution)	Supplier & Reference
HO-1	Polyclonal rabbit anti-mouse (1:5000)	Enzo Life Sciences ADI-SPA-896	Goat anti-rabbit IgG-HRP (1:5000)	Abcam ab6721-1
Oct 4	Mouse monoclonal IgG_{2b} (1:500)	Santa Cruz Biotechnology Sc-5279	Polyclonal goat anti-mouse HRP (1:5000)	Dako P0447-DAKO
VP16	Mouse monoclonal IgG_{2a} (1:200)	Santa Cruz Biotechnology sc-7546	Sheep anti-mouse IgG-HRP (1:5000)	GE Healthcare Life Sciences NA9310
tetR	Polyclonal rabbit anti-mouse (1:2000)	Abcam ab25845	Goat anti-rabbit IgG-HRP (1:5000)	Abcam ab6721-1

2.6.2 Flow cytometry analysis of intracellular hemeoxygenase-1 expression

As previously described, Mφ were stained for the cell surface marker F4/80 with an APC-conjugated anti-mouse F4/80 antibody prior to intracellular staining of HO-1, performed using a monoclonal PE-conjugated HO-1 antibody. Cells were permeabilised using the Fixation/Permeabilisation Concentrate and Diluent kit and 10x Permeabilisation Buffer (eBioscience, UK) according to the manufacturer's instructions. Analyses were performed using a FACScalibur instrument and the results were analysed with FlowJo software (Treestar, USA).

2.7 Detection of Hemeoxygenase-1 gene expression

2.7.1 RNA extraction

RNA was extracted from cells using the Trizol method (Chomczynski and Sacchi, 1987). Briefly, cells grown in Petri dishes were lysed directly by adding 1ml of Trizol Reagent and homogenised by passing the cell lysate several times through a pipette. The homogenised samples were transferred to autoclaved eppendorf tubes and were either frozen at -80°C until further use, or incubated for 5 min at room temperature (RT) to permit the complete dissociation of nucleoprotein complexes. 200µl of chloroform was then added to the samples. The eppendorf tubes were vigorously shaken and incubated for 3 min at RT prior to 15 min centrifugation at 12,000g at 4°C. Following centrifugation, the RNA remains in the colourless upper aqueous phase and was transferred to fresh eppendorf tubes. The RNA was precipitated by adding 500µl isopropyl alcohol and samples incubated for 10 min at RT prior to 10 min centrifugation at 12,000g at 4°C. The supernatant was carefully

removed and the RNA pellet washed once with 75% ethanol (in RNase-free water) by vortexing then centrifuging the samples for 5 min at 7500g at 4°C. The RNA pellet was air-dried for 10 min and then dissolved in 30µl RNase-free water and incubated for 10min at 55°C.

2.7.2 DNase treatment

To exclude genomic DNA contamination, RNA samples were treated with DNase I using a TURBO DNA-free™ kit (Applied Biosystems/Ambion, Ref. AM1907). Briefly, RNA samples were incubated with DNase I at 37°C for 30 min. Controls samples were incubated with TURBO Buffer instead. The reaction was stopped using DNase inactivation reagent for 5 min. Samples were centrifuged at 10,000g for 1.5 min and RNA transferred to fresh eppendorfs.

2.7.3 Reverse transcriptase PCR

The RNA concentration of the samples was determined using a NanoDrop spectrophotometer (Thermo Fisher Scientific Inc.). For the Reverse Transcriptase assay, 1µg RNA was mixed with 3.5µl RNase-free water, 2µl 10x MMuLV Reverse Transcriptase Buffer (Stratagene, Ref. 600083-52), 2µl of 40mM dNTP Mix (Stratagene, Ref. 200415-51), 0.5µl RNasin® RNase Inhibitor (Promega, Ref. N211A), 1µl MMuLV Reverse Transcriptase (Stratagene, Ref. 600084-51) and 1µl Oligo (dT) 15 Primer (Promega, Ref. C110A). In order to allow the reverse transcription of RNA into cDNA to take place, samples were incubated for 10 min at 20°C followed by 60 min at 37°C and 5 min at 95°C in a Bio-Rad iCycler. At the end of the cycle, samples were kept at 4°C then kept at -20°C until further use.

2.7.4 Quantitative real time PCR

Quantitative real time PCR (qPCR) was used to detect the expression levels of various genes (Table 8). Samples were dispensed in triplicates in MicroAmp® Optical 96-well reaction plates (Applied Biosystems®, Life Technologies Ltd, Paisley, UK) and analysed using an Applied Biosystems 7500 Fast-Real PCR System with the following thermal cycle conditions:

(i) 20 seconds at 95°C followed by

(ii) 40 repetitions of 3 seconds at 95°C and 30 seconds at 60°C

Relative quantitation was calculated using the deltaCT method in ABI SDS1.4 software using 18s or GAPDH as the endogenous control. Data are presented as the fold change in gene expression relative to an internal calibrator.

Table 8: qPCR primers

All primers with SYBR® green detection were designed by Dr A. Czopek, the University of Edinburgh. Professor L. Forrester's team designed the HPRT primers (Gordon-Keylock et al., 2010). Ready-made primers were purchased from Applied Biosystems®, LifeTechnologies Ltd (Paisley, UK).

Gene	Primers	Detection
TNFα	Forward: CACAAGATGCTGGGACAGTGA Reverse: TCCTTGATGGTGGTGCATGA	SYBR® green
GAPDH	Forward: ACTGGCATGGCCTTCCG Reverse: CAGGCGGCACGTCAGATC	
HO-1	Forward: CAGCCCCACCAAGTTCAAA Reverse: TCAGGTGTCATCTCCAGAGTGTTC	
iNOS	Forward: GGCAGCCTGTGAGACCTTTG Reverse: TGAAGCGTTTCGGGATCTG	
IL-1β	Forward: AGTTGACGGACCCCAAAAGAT Reverse: GGACAGCCCAGGTCAAAGG	
IL-6	Forward: CCACGGCCTTCCCTACTTC Reverse: TTGGGAGTGGTATCCTCTGTGA	
IL-10	Forward: CCCAGAAATCAAGGAGCATTTG Reverse: CGCATCCTGAGGGTCTTCA	
IL-12	Forward: GGAATGTCTGCGTGCAAGCT Reverse: ACATGCCCACTTGCTGCAT	
HPRT	Forward: GCTCGAGATGTCATGAAGGAGA Reverse: AAAGAACTTATAGCCCCCCTTGA	TaqMan®

Applied Biosystems®, LifeTechnologies Ltd primers

Gene	Assay ID	Cat#	Detection
18s	Mm03928990_g1	4331182	TaqMan®
NANOG	Mm02019550_s1	4331182	
ROSA26	Mn03456292_m1	4426961	

2.8 Murine Model of Renal Ischaemia/Reperfusion Injury

Female and male 129-P2 mice aged 6-8 weeks old were obtained commercially or from in-house colonies. Anaesthesia was induced by injection of 250µl of ketamine and metatomidine mix (4.14ml normal saline, 0.36ml ketamine, 0.5ml metatomidine) via the intraperitoneal route. Via a midline laparotomy a right nephrectomy was performed and the kidney fixed in methyl-Carnoy's solution (60% methanol, 30% chloroform and 10% acetic acid) for histological analysis as baseline normal tissue. The left renal pedicle was then clamped using an atraumatic clamp (Teleflex Medical, UK) for 20, 25 or 30 minutes and the kidney was observed to ensure that it became pale. During the ischaemic period the body temperature was maintained at 37°C using a heating blanket with a homeostatic control via a rectal temperature probe (Harvard Apparatus, Boston MA). The clamp was then removed and the kidney was observed to ensure a complete restoration of blood flow. The peritoneum was closed with 5/0 silk suture and the skin was closed with metal clips. Anaesthesia was reversed using 200µl atipamezole diluted 1:10 in normal saline and 50µl buprenorphine (0.04ml made up to 1ml with normal saline) injected subcutaneously to provide post-operative analgesia. To ensure adequate hydration, 1ml of sterile saline was administered subcutaneously both prior to and following surgery. The animals were maintained in a 28°C incubator overnight. Mice were culled 24 hrs following ischaemia/reperfusion injury (IRI) and the left kidney was removed, cut longitudinally and either snap frozen in liquid nitrogen or fixed in methyl-Carnoy's solution prior to embedding in paraffin. Blood samples were collected at 24h post surgery under terminal anaesthesia. Procedures were performed under Home Office licences 60/3317 (Project license - Renal Inflammation and Repair Licence held by Dr David Kluth) and 60/12064 (Personal Licence held by Miss Noémie Nkejabega).

2.8.1 Characterisation of ischaemic injury

2.8.1.1 Assessment of renal histology

Paraffin embedded kidneys sections were cut into 4µm tissue slices and stained with haematoxylin and eosin by members of the QMRI Histology Laboratory (University of Edinburgh). All sections were then assessed using a Leica light microscope. Acute tubular necrosis (ATN) scores were obtained by taking 5 non-overlapping pictures (x100 magnification) of the outer stripe of the outer medulla (OSOM) region of the kidney (Figure 15) and tubules counted as either viable or necrotic based on nuclear morphology and integrity of the epithelial cell layer using ImageJ software (NIH). The percentage of necrotic tubules was calculated using the formula:

$$\textit{Percentage Necrosis} = \frac{\textit{Number of necrotic tubules}}{\textit{Number of total tubules}} \times 100$$

Average percentage necrosis of the 5 fields was used for statistical analyses.

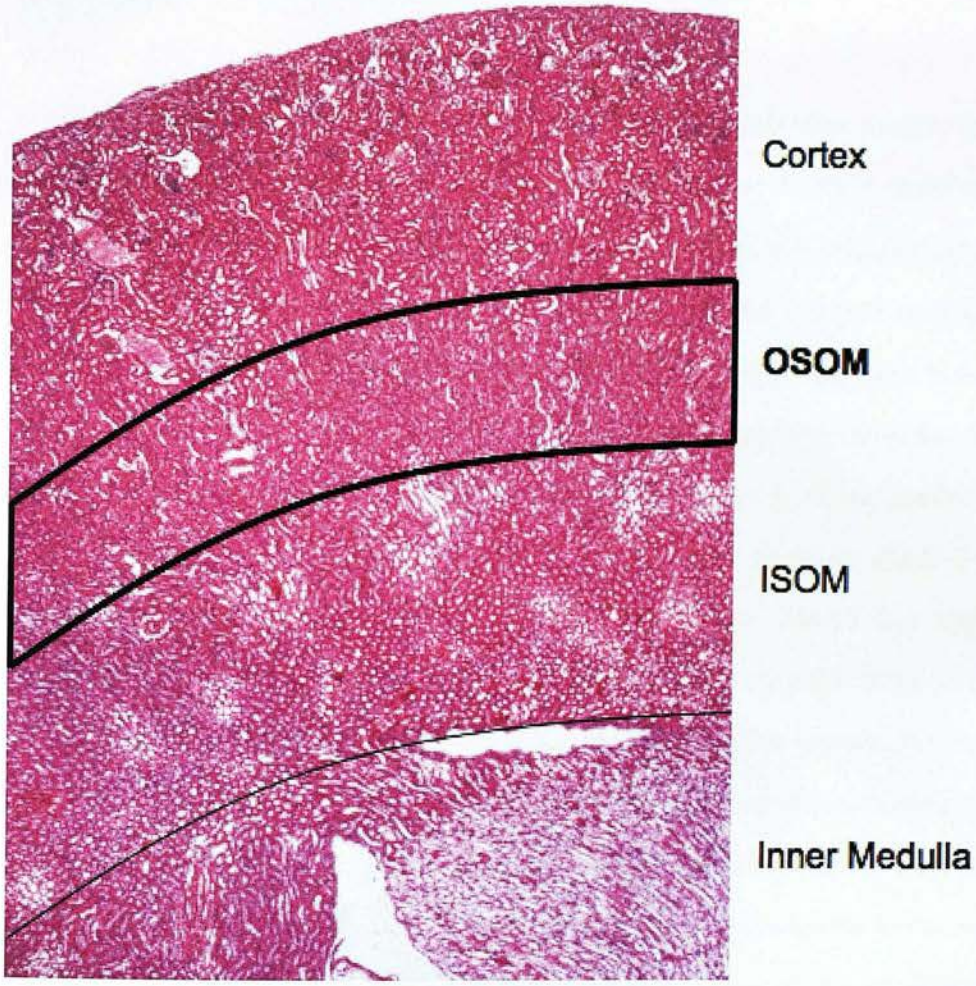

Figure 15: The outer stripe of the outer medulla (OSOM) is one of four kidney regions.

Representative 4µm slice of paraffin embedded kidney section stained with haematoxylin and eosin. The outer stripe of the outer medulla (OSOM) is the region of the renal medulla adjacent to the cortex. It is mainly constituted of the S3 segments of the proximal tubules and distal nephron tubules. Acute tubular necrosis scores were determined following analysis of the OSOM as this area is the most severely injured kidney region following renal ischaemia-reperfusion injury.

2.8.1.2 Immunohistochemistry of tissue sections

An indirect 3,3'-diaminobenzidine (DAB) based detection system was used to detect expression of HO-1 and the Mφ and dendritic cell marker F4/80 in renal cells. Paraffin embedded kidneys were cut into 4µm tissue sections and mounted on glass slides then dewaxed in xylene for 10 min and rehydrated through decreasing ethanol concentration baths (100%, 90%, 80%, 70%) for 1 min each prior to being immersed in PBS. The slides were transferred to a sequenza rack (Shandon, Inc.) and then washed with PBS. Potential non-specific interaction of the tissue with avidin, biotin and protein were blocked for 10 min each using an Avidin/Biotin Blocking Kit (Vectro Labs SP-2001) and a Protein Block (DAKO Cat X0909) respectively. Tissue sections were incubated at 4°C overnight with 125µl primary antibody or the corresponding isotype (Table 9). After 3 PBS washes, the tissue sections were incubated with a biotinylated secondary antibody at room temperature (RT) for 30 min and then washed 3 times with PBS and incubated in Vectastain RTU elite (Vector labs) for 30 min. Tissue sections were then washed 3 times with PBS prior to the addition of 125µl DAB solution (5 min, 1 drop of DAB stock per ml buffer) (Dako, North America Inc). The slides were counterstained with haematoxylin for 20 seconds, rinsed then dehydrated through baths of increasing ethanol concentration (70%, 80%, 90%, 100%) for 1 min each prior to being immersed in xylene. The slides were coverslipped to avoid degradation. Positive immunoreactive cells were identified by the presence of brown staining under a light microscope. Cell counts were expressed as mean cell number per microscope field (x400 magnification) with 5 fields being assessed per tissue section.

Table 9: Antibodies used for immunohistochemistry

This table summarises the various antibodies (Ab) used to analyse both cytospins of cell preparations and paraffin embedded tissue sections.

Primary Ab Supplier Catalog Number	**Target Cell**	**Secondary Ab** Supplier Catalog Number	**Dilution**	**Isotype**
F4/80 Invitrogen MF48000	Macrophage Dendritic Cell	**Biotinylated Rabbit anti Rat** Vector Labs BA-4000	1:100	**Rat IgG2a** Biolegend Cat 400621
CD11b AbD Serotec MCA711G	Macrophage Monocytes	**Biotinylated Rabbit anti Rat** Vector Labs BA-4000	1:100	**Rat IgG2a** Biolegend Cat 400621
HO-1 Enzo LifeSciences Ltd SPA-896F	Various cells	**Biotinylated Goat anti Rabbit** Abcam ab64256	1:300	**Polyclonal Rabbit IgG**
Oct 4 Santa Cruz sc-5279	Stem Cells	**Polyclonal Goat anti-mouse IgG/biotinylated** Dako E0433	1:60	N/A

2.8.1.3 Assessment of renal function

Blood collected pre- and post-injury was centrifuged at 1000g for 5 min. Serum was aliquoted and subsequently analysed for creatinine and urea concentration. Dr Forbes Howie of the Department of Clinical Chemistry, the University of Edinburgh performed the creatinase assay (enzymatic colorimetric Trinder kit, Sentinel CH., Italy) and the Infinity™ Urea Liquid Stable Reagent (Thermo Electron, USA) on a Cobas Fara Centrifugal Analyser (Roche Diagnostics Ltd., Welwyn Garden City, UK) according to the manufacturer's instructions.

2.9 In vivo localisation of embryonic stem cell-derived macrophages

2.9.1 PKH26 dye labelling of macrophages

In order to track ESDM *in vivo*, they were labelled prior to injection using the PKH26 red fluorescent cell linker kit for phagocytic cells (PKH26PCL) according to manufacturer's instructions. The labelling occurs through the formation of dye aggregates, which significantly limits the uptake of dye by non-phagocytic cells, but facilitates ingestion by phagocytic cells. Figure 16 shows PKH26-labelled macrophages. Following staining, ESDM were counted and kept on ice until being intravenously administered to mice via the tail vein after the induction of renal IRI.

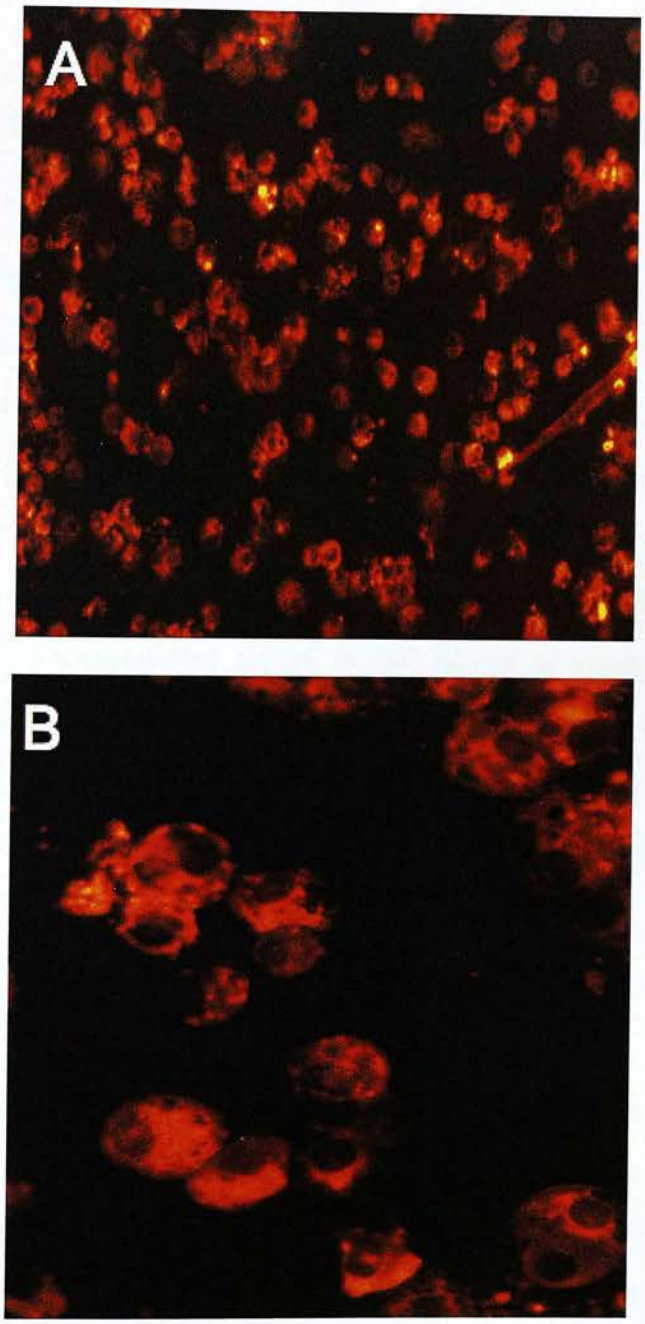

Figure 16: PKH26 labelled embryonic stem cell-derived macrophages.

Cytospin preparations of PKH26 positive embryonic stem cell-derived macrophages. **A**: photomicrograph (50x magnification) showing that the majority of cells are strongly labelled. **B**: photomicrograph (320x magnification) showing the nature of the labelling, which localises to the phagolysosomes within the macrophage.

2.9.2 Localisation of macrophages following renal ischaemia/reperfusion injury

The model of IRI was adapted to facilitate a direct comparison of the localisation of ESDM to either injured or normal kidney tissue. The right kidney was left *in situ* while the left kidney pedicle was clamped for 25 min as described previously. After restoration of the renal blood supply, $5x10^6$ PKH26-labelled ESDM were injected via the tail vein. The left and right kidneys, liver, spleen and lungs were harvested 1h post cell injection under terminal anaesthesia and snap frozen in liquid nitrogen. The localisation of PKH26-labelled ESDM to the normal or injured kidney was determined by counting PKH26-labelled cells by fluorescence microscopy on 5µm frozen sections mounted on glass slides with DAPI mounting medium. The results were expressed as mean cell number per high power field (x400 magnification) with 5 fields being counted per organ.

2.10 Statistical analysis

All statistical analysis was performed using GraphPad Prism version 4.0c for Macintosh (GraphPad Software, USA). All data, unless otherwise stated, are expressed as mean ± standard deviation (SD). The Student's Unpaired t-test was employed to compare two groups whereas multiple conditions were compared using one-way ANOVA coupled with Tukey's *post hoc* test for multiple comparisons. Two-way ANOVA was used to compare the effects of 2 or more factors on different groups. When populations were not normally distributed, samples were compared using the non-parametric Mann-Whitney U test. P values of less than 0.05 ($p<0.05$) were deemed to be statistically significant. N values stand for experiment repeats (i.e. when cells are involved, n values are for number of cell preparations).

Chapter 3. Deriving and phenotyping embryonic stem cell-derived macrophages

3.1 Introduction

In recent years, data from various groups has shown that macrophage 'cell therapy' has significant potential to improve human disease. In nephrology more specifically, experimental models of renal inflammation such as ischaemic acute kidney injury (Ferenbach 2010), immune-mediated glomerulonephritis (Kluth 2001, Wilson 2002) and progressive tubulointerstitial fibrosis (Yamagishi 2001) have been used to test the effect of cell therapy with bone marrow derived macrophages (BMDM) modified to adopt an 'anti-inflammatory phenotype' by overexpression of HO-1, IL-10, IL-4 or IL-1RA respectively. These studies indicate that adoptively transferred modified BMDM can localise to the inflamed kidney and ameliorate disease. However, the relative complexity of genetically manipulating primary macrophage cultures represents a considerable problem. To overcome this difficulty, scientists have turned to embryonic stem cells (ESC) that are highly amenable to genetic manipulation. Recent work has shown that both mouse and human ESC can be differentiated *in vitro* into mature macrophages, monocytes (Odegaard 2007, Karlsson 2008, Zhuang, 2012) as well as dendritic cells (Fairchild 2000). Embryonic stem cell-derived macrophages (ESDM) are an attractive source of potentially therapeutic cells to use to ameliorate the progression of disease because of their ability to be genetically manipulated prior to being differentiated into macrophages. This chapter outlines the derivation, phenotyping and functional characterisation of ESDM in comparison to primary BMDM.

3.2 Phenotyping embryonic stem cell-derived macrophages

Macrophages are key sentinel cells of the innate immune system and exhibit various key functions including phagocytosis as well as cytokine and pro-inflammatory mediator production. To assess whether ESDM possess these crucial properties, we studied their morphology, the expression of cell surface markers, phagocytic capacity and the response to Toll-like receptor stimulation.

3.2.1 Embryonic stem cell-derived macrophages exhibit a macrophage-like morphology

Macrophages possess morphological features that distinguish them from other leukocytes and reflect their scavenger function. They are the largest of the white blood cells, have a small round nucleus with abundant cytoplasm and are vacuolated. Macrophage morphology was primarily assessed by examining Diff Quick stained cytospin preparations of both ESDM and BMDM. Microscopic analysis of the slides demonstrates the similar features of mature ESDM and BMDM (Figure 17).

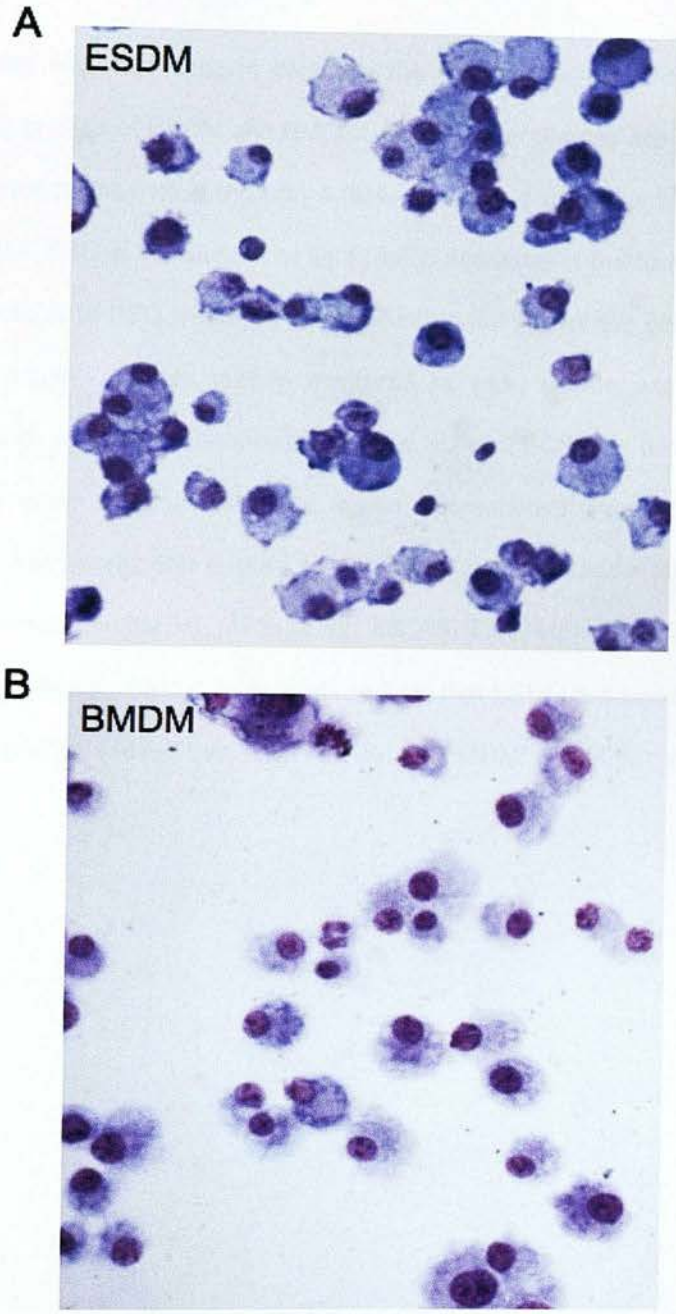

Figure 17: Embryonic stem cell-derived macrophages exhibit a macrophage-like morphology.

Cytospin preparations of macrophages were prepared and stained using the Diff Quick Method. Cells were photographed using a Leica Zeiss Axiovert light microscope. Representative photomicrographs demonstrating similar morphology between mature **A:** ESDM and **B:** BMDM (x100 magnification).

Flow cytometry was also used to compare the Forward Scatter (FSC) and Side Scatter (SSC) profiles of ESDM and BMDM. As the macrophages are aspirated into the flow cytometer, they pass through a laser beam and refract or scatter light at different angles. FSC is the amount of light that is scattered in the forward direction and the magnitude of FSC is roughly proportional to the size of the cell. In contrast, SSC is the amount of light that is scattered at wide angles and reflects the granularity and structural complexity of the cell. FSC/SSC profiles of the macrophages were analysed and the mean fluorescence intensity (MFI) was calculated for each parameter (Figure 18). Our FSC results indicate that ESDM are of comparable size to BMDM (483±32 vs. 536±38 FSC MFI; ESDM vs. BMDM; p=0.32, n=4). However, SSC data analysis reveals that ESDM are significantly more granular than BMDM (147±11 vs. 99±2; ESDM vs. BMDM; p=0.006, n=4)

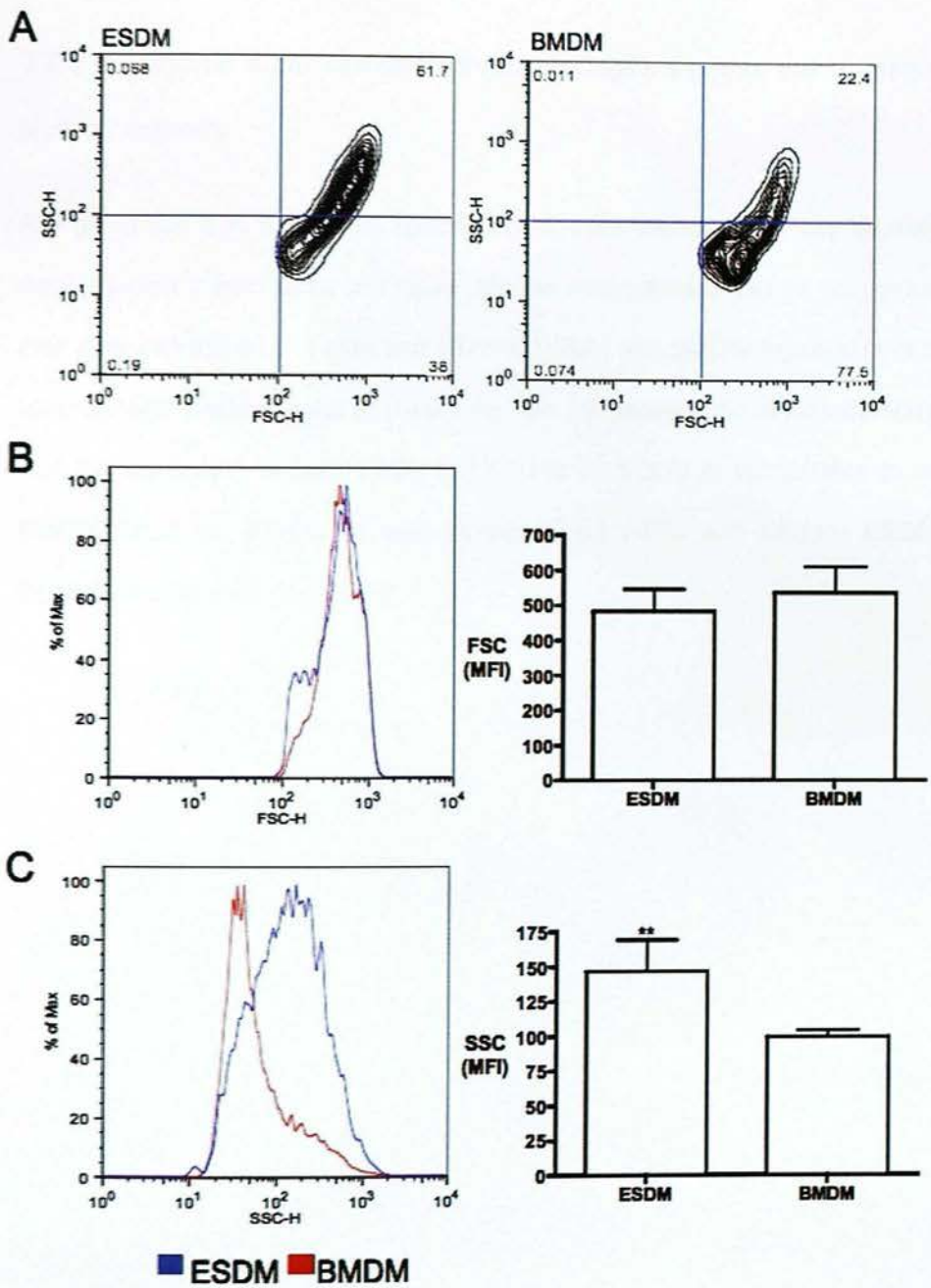

Figure 18: Embryonic stem cell-derived macrophages exhibit similar size but higher granularity than bone marrow derived macrophages.

Flow cytometry analysis of the SSC/FSC parameters of macrophages. **A:** Representative SSC/FSC contour plots of ESDM and BMDM. **B:** ESDM and BMDM FSC parameter analysis revealed both cell types have the same size. **C:** Study of ESDM and BMDM SSC parameter revealed that ESDM are more granular than BMDM ($p=0.006$, $n=4$). ** $p<0.01$

3.2.2 Embryonic stem cell-derived macrophages express macrophage cell surface markers

Any given cell type possesses specific cell surface markers that may be useful in distinguishing it from other cell types. Murine macrophages can be recognised by their dual expression of F4/80 and CD11b. ESDM and BMDM expression of these 'macrophage markers' was assessed by flow cytometry. Our results demonstrate that the expression of both F4/80 and CD11b by ESDM is comparable to that of BMDM (91±4 vs. 87±6% of cells co-expressing F4/80 and CD11b; ESDM vs. BMDM; p=0.16, n=3) (Figure 19).

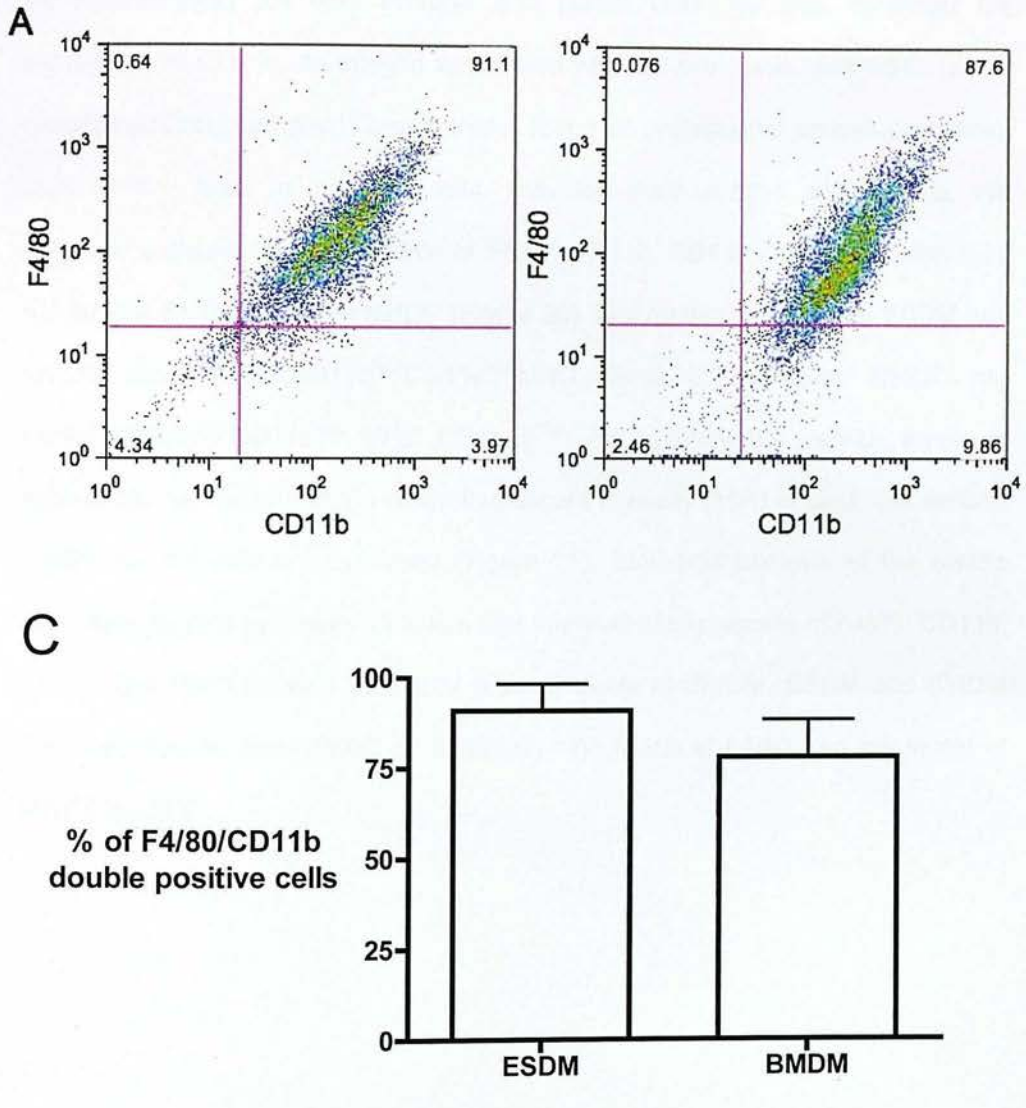

Figure 19: Day 7 embryonic stem cell-derived and bone marrow derived macrophages exhibit comparable expression of F4/80 and CD11b by flow cytometry.

ESDM and BMDM were dual labelled with antibodies for F4/80 and CD11b and analysed by flow cytometry. **A**: Representative dot plot showing an ESDM population with 91% cells being F4/80+ and CD11b+. **B**: Representative BMDM dot plot showing 88% of cells being F4/80+ and CD11b+. **C**: Percentage of double positive cells for F4/80 and CD11b (n=3).

As macrophages are very versatile and plastic cells, we also assessed the expression of CD11c, an integrin associated with dendritic cells, and MHC (major histocompatibility complex) Class II that is found on professional antigen-presenting cells (APCs) such as dendritic cells, activated macrophages and B cells. We therefore compared the expression of F4/80, CD11b, CD11c and MHC Class II by ESDM and BMDM to that of BMDC (Figure 20). Our results indicate that ESDM and BMDM are $F4/80^{high}CD11b^{high}CD11c^{high}$MHC Class II^{low} whereas BMDC are $F4/80^{low}CD11b^{high}CD11c^{high}$ MHC Class II^{high}. To quantify the various levels of expression, we measured the mean fluorescent intensity (MFI) of each cell surface marker for the different cell types (Figure 21). Statistical analysis of the results generated by flow cytometry indicates that the level of expression of F4/80, CD11b, CD11c and MHC Class II by ESDM is comparable to BMDM. ESDM and BMDM differ significantly from BMDC by exhibiting high levels of F4/80 and low levels of MHC class II^{lhigh}.

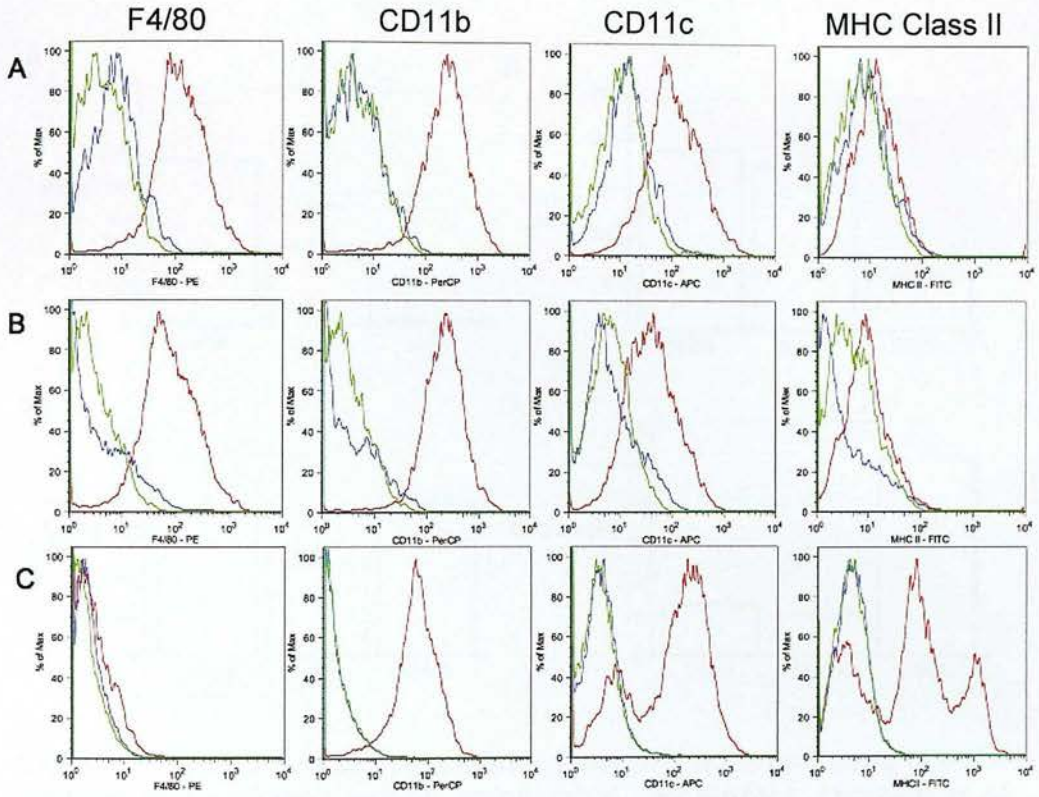

Figure 20: Flow cytometric analysis of F4/80, CD11b, CD11c and MHC class II expression of day 7 ESDM, BMDM and BMDC.

Representative histograms of F4/80, CD11b, CD11c and MHC class II expression of ESDM (**A**), BMDM (**B**) and BMDC (**C**). The green and blue lines represent unstained cells and staining with an isotype control antibody respectively whilst the red line depicts the cell surface expression of the relevant cell surface marker.

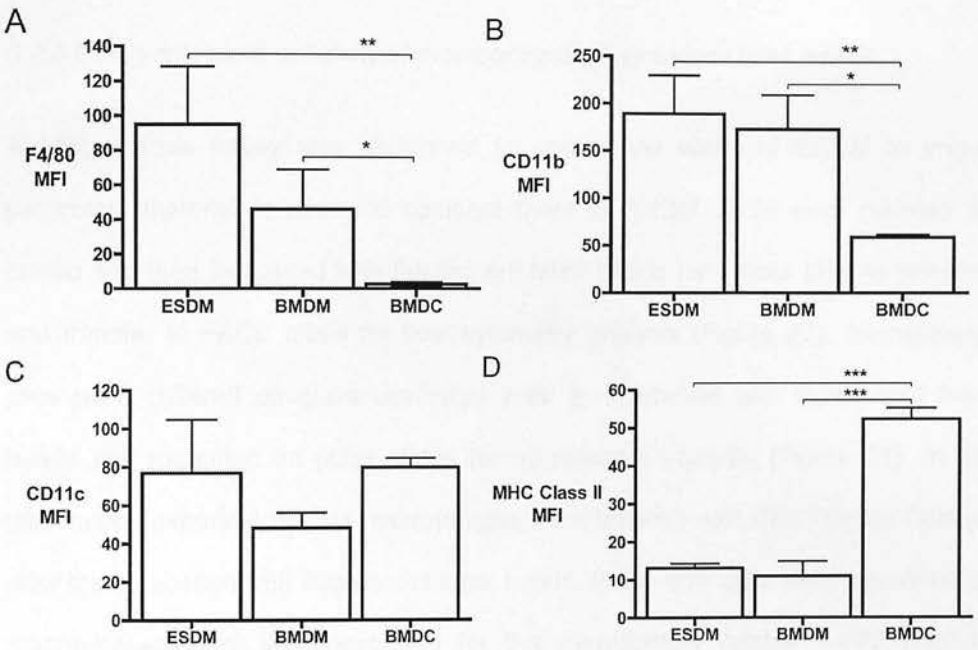

Figure 21: Embryonic stem cell-derived macrophages and bone marrow derived macrophages exhibit comparable cell surface expression of F4/80, CD11b, CD11c and MHC II.

Comparison of ESDM, BMDM and BMDC cell surface marker expression by flow cytometry. ESDM are comparable to BMDM and are F4/80^{high} CD11b^{high} CD11c^{high} MHC Class II^{low} whereas BMDC are F4/80^{low} CD11b^{low} CD11c^{high} MHC Class II^{high}. * $p<0.05$, ** $p<0.01$ and *** $p<0.001$ vs BMDC; n=3.

3.2.3 Embryonic stem cell-derived macrophages phagocytose latex beads

A phagocytosis assay was performed to assess the ability of ESDM to engulf particulate material *in vitro* and compare them to BMDM. Cells were cultured on plastic and then incubated with fluorescent latex beads for 1 hour prior to washing and transfer to FACS tubes for flow cytometry analysis (Figure 22). Alternatively, cells were cultured on glass coverslips prior to incubation with fluorescent latex beads and mounting on glass slides for microscopic analysis (Figure 24). In the microscopy experiments, the macrophages were labelled with Cell Tracker Orange after the incubation with fluorescent latex beads. In the flow cytometry experiments, macrophages were immunostained for the macrophage marker F4/80 prior to analysis.

We analysed the phagocytic capacity of cells by determining the percentage of cells that ingested fluorescent latex beads (% phagocytosis). Flow cytometric analysis was used to determine the percentage of F4/80 positive cells that were also positive for fluorescent green latex beads. These data indicated that both ESDM and BMDM were phagocytic with no significant difference evident between the cell types (32±2 vs. 28±2 % phagocytosis; ESDM vs. BMDM; p=0.11, n=3, Figure 23). Similarly, no significant difference in the phagocytic capacity of ESDM and BMDM was evident when phagocytosis was analysed by fluorescent microscopy (67±6 vs. 79±5 % macrophages exhibiting phagocytosis of beads; ESDM vs. BMDM; p=0.20, n=4). In addition, we calculated the macrophage phagocytic index, which is the mean number of beads ingested by each macrophage that exhibits phagocytosis. The macrophage phagocytic index of ESDM was also comparable to that of BMDM (3.0±0.44 vs. 3.3±0.35 beads per macrophage; ESDM vs. BMDM; p=0.60, n=4)

(Figure 25). Additional control experiments included the incubation of beads with macrophages at 4^0C prior to flow cytometry or microscopy. Macrophages would be metabolically inactive and unable to actively ingest particles at this low temperature and this 4^0C interaction could be used to assess any non-specific binding between the beads and the macrophages. Analysis indicated very limited interaction between beads and the macrophages at this low temperature.

Flow cytometry and microscopy analysis are qualitatively similar in that there is no difference in phagocytosis between ESDM and BMDM. However, the different methodologies did generate markedly different levels of phagocytosis with flow cytometry demonstrating ~30% phagocytosis compared with ~70% phagocytosis for the microscopy analysis. In other words, the microscopy assay appeared to overestimate the phagocytic signal. This may reflect several aspects that differed between the assays. First, although all macrophages were washed extensively, flow cytometric analysis required macrophages to be physically removed from the plate for processing and this manoeuvre might act to remove any adherent beads to the macrophage cell surface. Also, the very strong brightness of the green fluorescent latex beads and the comparatively weak cytoplasmic staining of macrophages with Cell Tracker Orange made it difficult to discern actual phagocytosis of beads from non-specific cell surface binding.

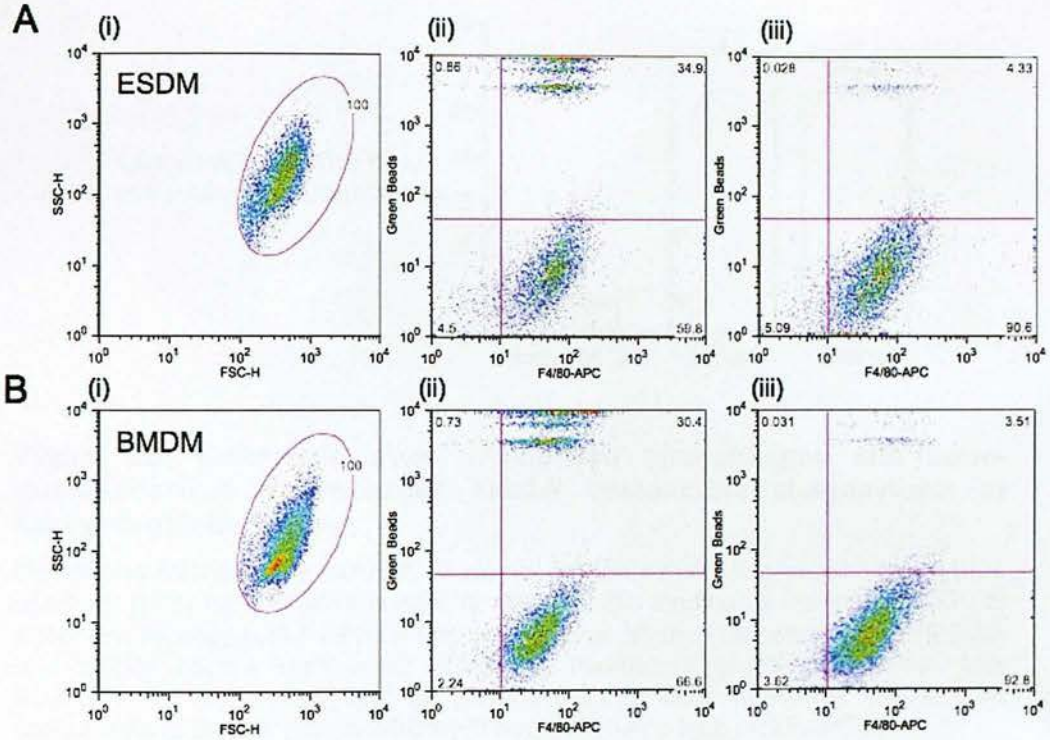

Figure 22: Flow cytometric analysis of the phagocytosis of fluorescent green latex beads by F4/80 positive macrophages.

ESDM and BMDM were cultured on plastic, incubated with fluorescent green latex beads, transferred to FACS tubes and labelled with F4/80 for flow cytometry analysis. SSC/FSC profile of **A (i):** ESDM and **B (i)**: BMDM populations were subsequently analysed for the expression of F4/80 and uptake of fluorescent green latex beads. **A (ii):** Flow cytometric analysis of the ESDM population showing that 34.9% of ESDM ingested beads at 37°C. **A (iii):** 4.3% of ESDM ingested beads at 4°C. **B (ii):** 30.4% of BMDM phagocytosed beads at 37°C. **B (iii):** 3.5% BMDM ingested beads at 4°C.

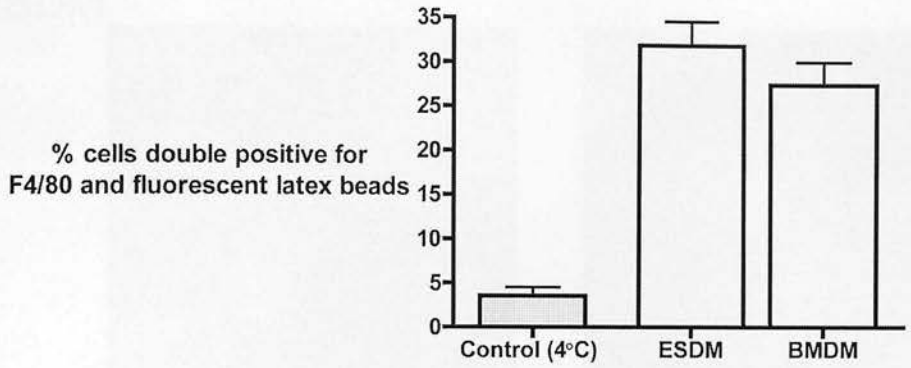

Figure 23: Embryonic stem cell-derived macrophages and bone-marrow-derived macrophages exhibit comparable phagocytosis of fluorescent latex beads.

ESDM and BMDM were cultured on plastic, incubated with fluorescent green latex beads at 37°C (or 4°C as a control for non-specific binding), transferred to FACS tubes and labelled with F4/80 for flow cytometry analysis. The percentage of ESDM and BMDM double positive for F4/80 and fluorescent green latex beads was assessed by flow cytometry. The phagocytosis of latex beads by ESDM was comparable to BMDM (Mann-Whitney U non parametric test; p=0.2, n=3).

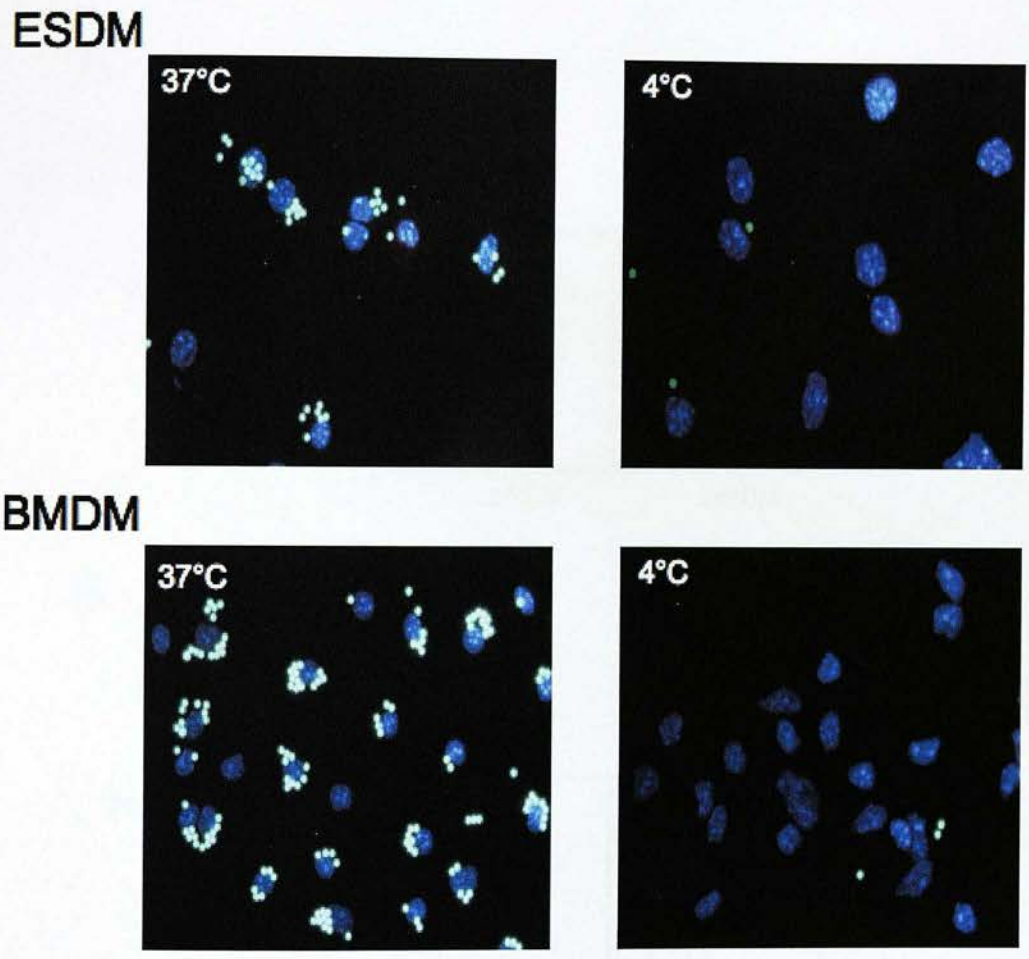

Figure 24: Microscopic analysis of fluorescent green latex bead phagocytosis by Cell Tracker Orange labelled embryonic stem cell-derived and bone marrow derived macrophages.

Macrophages were cultured on glass coverslips, incubated with fluorescent green latex beads then labelled with Cell Tracker Orange and mounted on glass slides for microscopic analysis. Representative fields of ESDM and BMDM phagocytosis of latex beads at 37°C (Left panels) and 4°C (Right panels). The brightness of the green fluorescent latex beads and relatively weak cytoplasmic stain of macrophages makes it difficult to discern actual phagocytosis from non-specific cell surface binding.

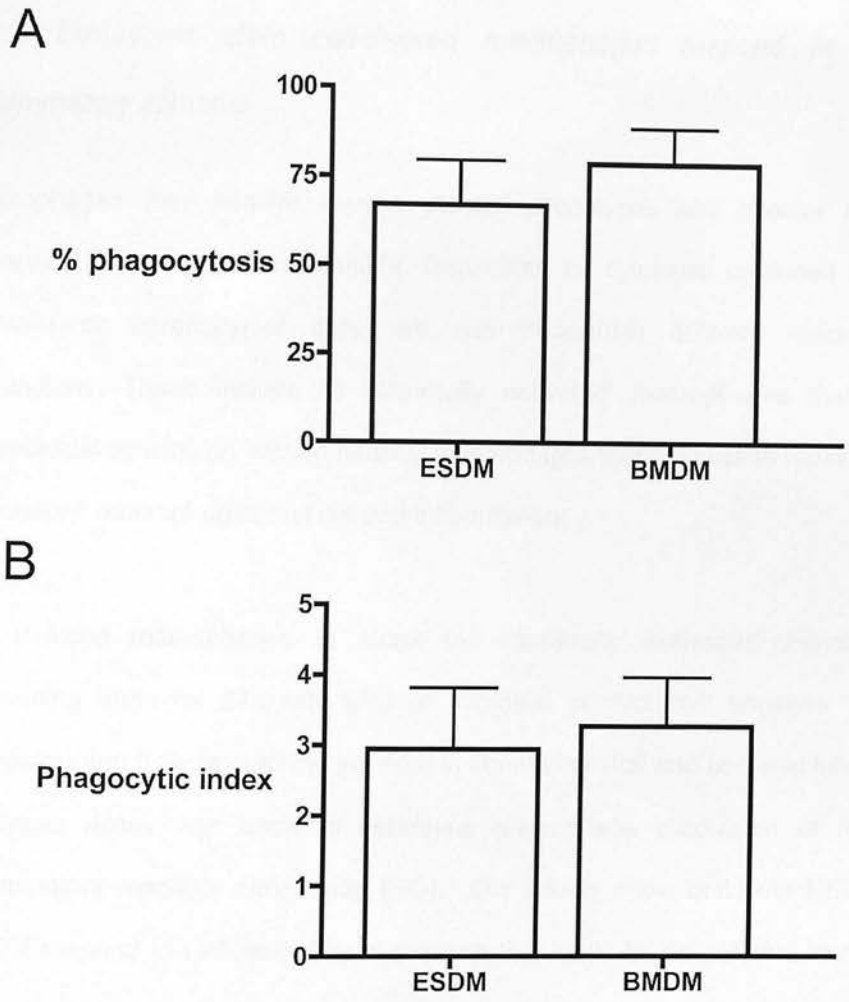

Figure 25: Percentage phagocytosis and phagocytic index of embryonic stem cell-derived and bone marrow derived macrophages following incubation with fluorescent latex beads.

ESDM and BMDM were cultured on glass coverslips, incubated with fluorescent latex beads then labelled with Cell Tracker Orange and mounted on glass slides for microscopic analysis. The percentage of cells exhibiting phagocytosis and the macrophage phagocytic index (expressed as the mean number of beads phagocytosed per macrophage) were visually assessed. No significant differences were evident between ESDM and BMDM in either **A:** the percentage of cells exhibiting phagocytosis (Mann-Whitney U non-parametric test; p=0.3; n=4) or **B**: the macrophage phagocytic index (p=0.6; n=4).

3.2.4 Embryonic stem cell-derived macrophages respond to a pro-inflammatory stimulus

Macrophages may acquire diverse cellular phenotypes and effector functions according to their microenvironment. Depending on cytokines produced by other immune or parenchymal cells, we can distinguish different macrophages populations. These include (i) 'classically activated' macrophages that exhibit microbicidal activity, (ii) 'wound healing' macrophages that help tissue repair and (iii) 'regulatory' macrophages that are anti-inflammatory.

We induced macrophages to adopt the 'classically' activated phenotype by stimulating them for 24h with LPS (a microbial product that engages Toll like receptors) and IFNγ (a cytokine involved in combating viral and bacterial infections). A Griess assay was used to determine macrophage production of the pro-inflammatory mediator nitric oxide (NO). Our results show that both ESDM and BMDM respond to LPS and IFNγ stimulation that leads to a significant increase in NO production with no difference evident between ESDM and BMDM ($p=0.44$; $n=4$) (Figure 26).

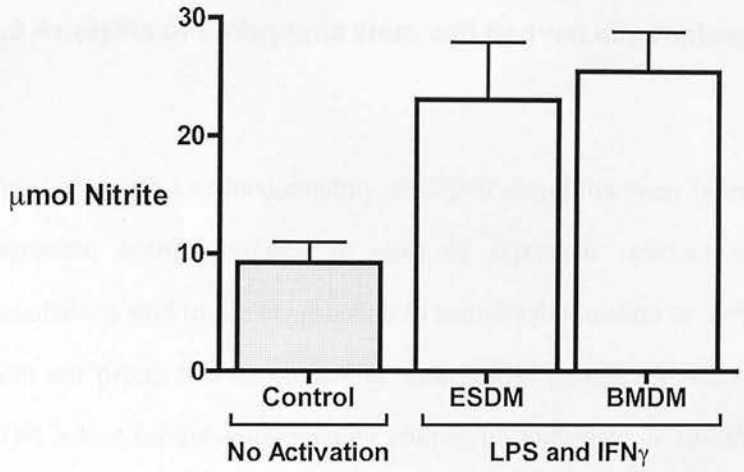

Figure 26: Embryonic stem cell-derived macrophages are activated by LPS/IFNγ stimulation and release nitric oxide.

ESDM and BMDM were activated for 24h by incubation with LPS (1 μg/ml) and IFNγ (100 U/ml). Control cells were exposed to medium alone. ESDM and BMDM responded to the LPS and IFNγ stimulation and increased production of NO measured as nitrite. However, there was no difference between the levels of NO released by ESDM compared to BMDM ($p=0.44$; $n=4$).

3.3 Analysis of embryonic stem cell-derived macrophage differentiation

Monocytes are key inflammatory cells that patrol the body in the bloodstream and represent both a source of cells to replenish resident tissue macrophage populations and to rapidly respond to tissue inflammation and injury. Previous work from our group has demonstrated that BMDM genetically modified to overexpress HO-1 adopt an anti-inflammatory phenotype and result in reduced functional injury when administered to mice following renal ischaemia/reperfusion injury (IRI). However, the macrophages do not circulate in the blood and also localise to a range of non-inflamed tissues including spleen, liver and lungs (Ferenbach, Ramdas et al. 2010).

Our method for generating ESDM involved the 'harvesting' of non-adherent cells in the supernatant of embryoid body cultures. These cells are then plated and cultured for a further 7 days to produce ESDM. Since macrophages differentiate from monocytes *in vivo*, we hypothesised that the supernatant cells (termed 'Macrophage progenitor cells' or MPC) may be monocytes. If this was the case, MPC may actually represent a more useful reagent for cell therapy as monocytes circulate in the blood until recruited to inflamed sites.

3.3.1 Phenotyping the embryonic stem cell-derived macrophage progenitor cells isolated from embryoid body culture supernatants.

MPC were isolated from the supernatant of EB tissue culture plates. To phenotype these MPC, we studied their morphology, expression of monocyte/macrophage cell

surface markers and their phagocytic capacity. MPC were compared to ESC, ESDM, BMDM and bone marrow monocytes (BMM).

3.3.1.1 Embryonic stem cell-derived macrophage progenitor cells acquire a macrophage-like morphology with maturity

Morphology was assessed by light microscopy analysis of cytospin preparations of the different cell types following Diff Quick staining. As previously described, both ESDM and BMDM form a homogenous population and exhibit standard macrophage morphology. They are mononuclear cells, vacuolated with a small nucleus to cytoplasm ratio and do not resemble ESC, which form a heterogeneous population of small cells with the nucleus filling almost the entire cytoplasm (Figure 27). As stem cells have the capacity to give rise to all embryonal tissues, it was important for further experiments to confirm that the MPC population was homogeneous. We examined the morphology of MPC at different time points following setting up the EB cultures (d10, d12, d14, d16, d18 MPC harvests and ESDM) (Figure 28). Early MPC (d10) formed a highly heterogeneous population. However, as the EB culture matures the MPC were noted to increase in size and their nucleus to cytoplasm ratio increased. By day 14, the ESC formed a more homogeneous population of large, vacuolated, mononuclear cells that were similar to ESDM and BMDM.

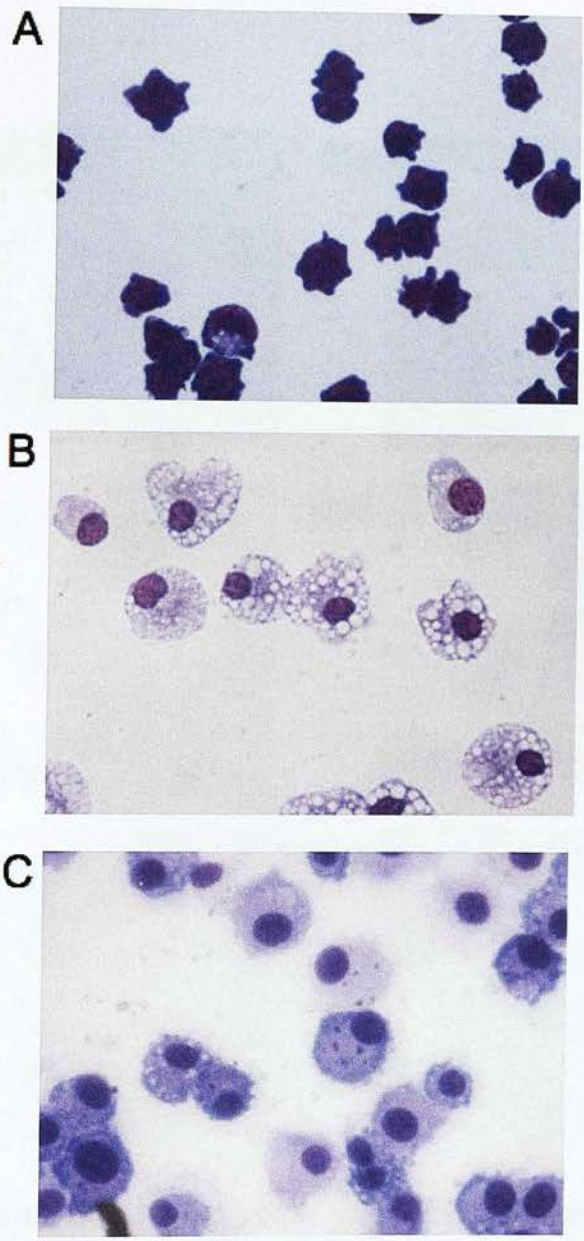

Figure 27: Qualitative assessment of cell morphology by light microscopy.

Representative pictures of Diff Quick stained cytospin preparations of **A**: ESC, **B**: ESDM and **C**: BMDM (x100 magnification).

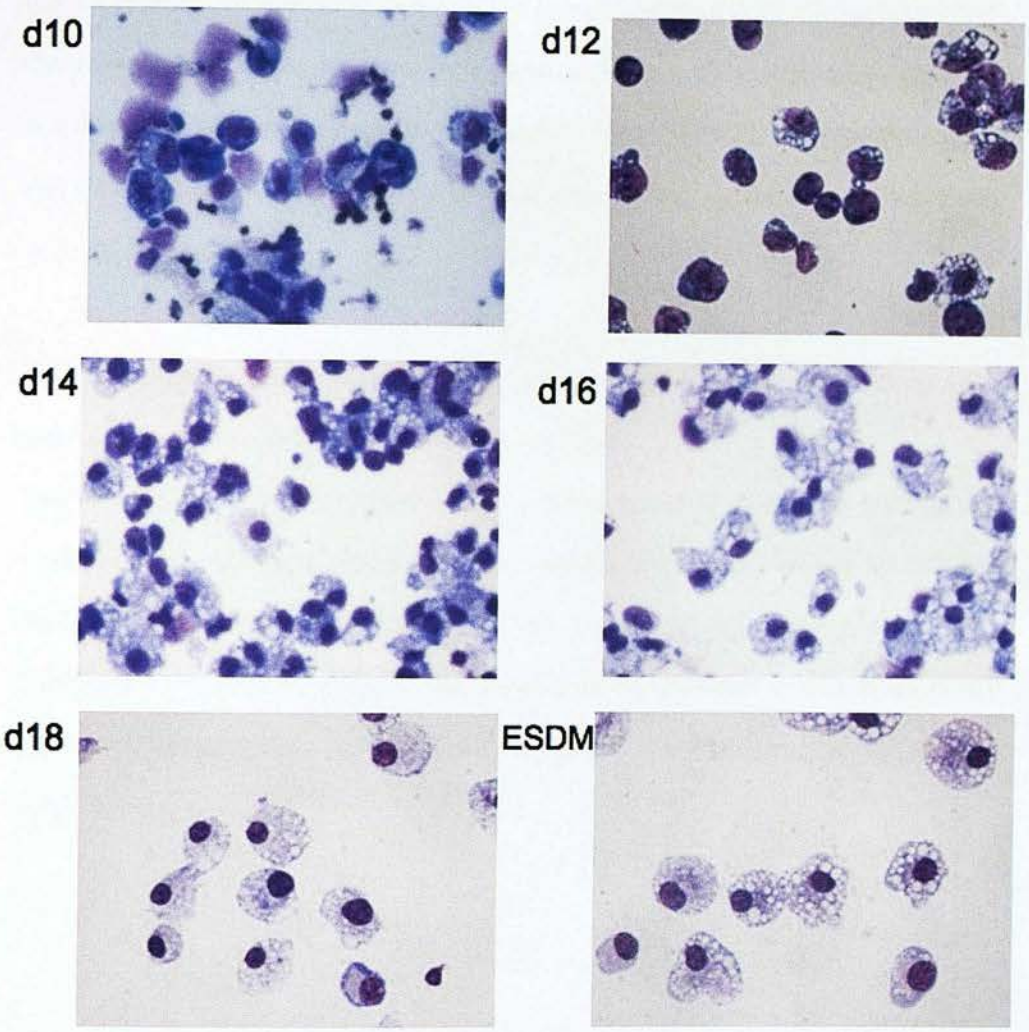

Figure 28: Maturation of embryonic stem cell-derived macrophage progenitor cells.

Cytospin cell preparations were stained by Diff-quick. Representative pictures illustrating the macrophage progenitor cells (MPC) morphological changes as the embryoid body cultures mature. At d10, the MPC exhibit variable morphology with cellular debris and ghosts present. However, as the maturity of the EB culture increases, the MPC develop an increasing similarity to ESDM (x100 magnification).

3.3.1.2 Embryonic stem cell-derived macrophage progenitor cells do not express the stem cell marker Oct4

Oct4 is a stem cell marker and involved in the self-renewal of undifferentiated ESC. We assessed the expression of Oct4 protein in different MPC populations (d12, d14 and d18 MPC harvests) as well as ESC and ESDM (Figure 29). The results suggest that the harvested MPC are no longer stem cells as they have lost Oct4 expression by d12.

3.3.1.3 Embryonic stem cell-derived macrophage progenitor cells express the macrophage cell surface markers F4/80 and CD11b

The expression of the macrophage cell surface markers F4/80 and CD11b was evaluated by immunohistochemistry. Our results show that, as for ESDM and BMDM, the MPC are positive for both F4/80 (Figure 30) and CD11b (Figure 31). The number of positively stained cells appears to increase as the maturity of the EB culture increases thereby reflecting the changes in morphology seen with the diff-quick staining.

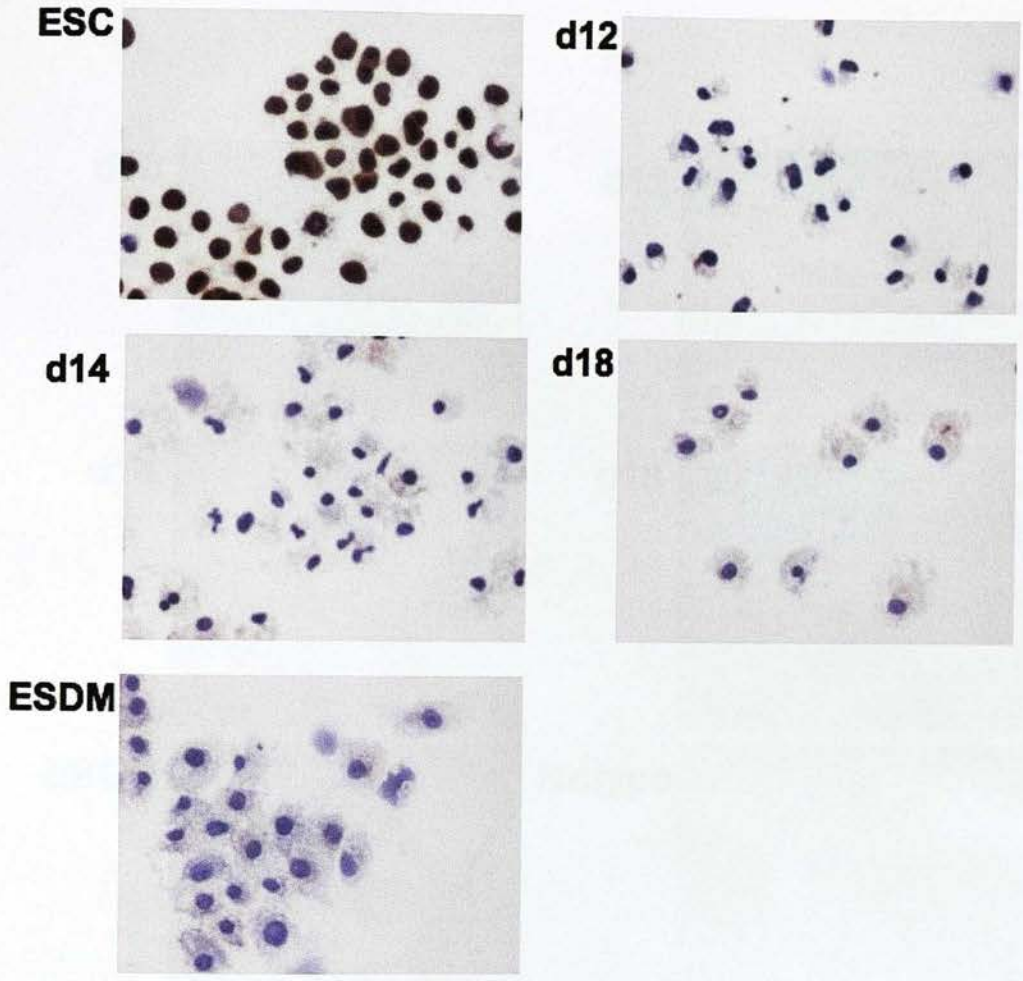

Figure 29: Embryonic stem cell-derived macrophage progenitor cells and embryonic stem cell-derived macrophages do not express the stem cell marker Oct4.

Oct4 immunohistochemistry was undertaken on cytospin cell preparations of embryonic stem cells (ESC), macrophage progenitor cells (MPC) and ESDM. The complete absence of staining for the transcription factor Oct4 in the MPC and ESDM confirms the cellular differentiation of these cells from the Oct4 positive ESC population (x100 magnification).

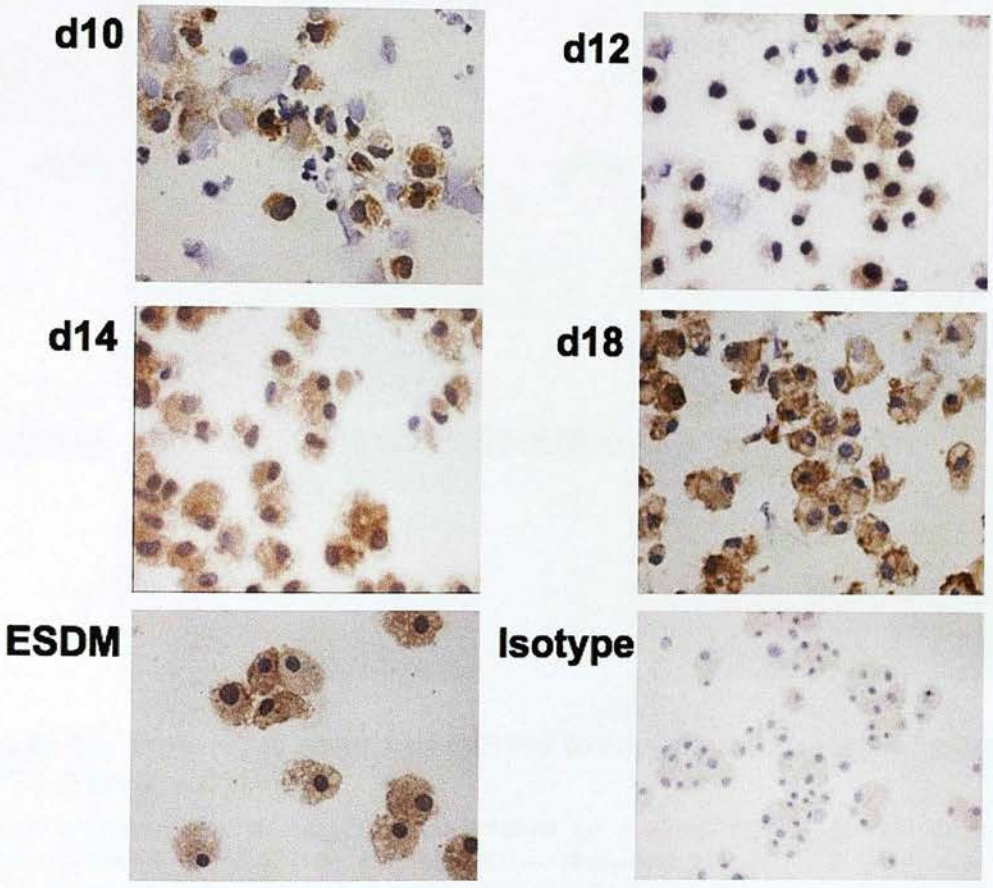

Figure 30: Embryonic stem cell-derived macrophage progenitor cells express F4/80.

F4/80 immunohistochemistry was undertaken on macrophage progenitor cells (MPC) cytospin preparations. Representative photomicrographs illustrating that MPC are positive for the macrophage marker F4/80. At d10, the MPC exhibit limited F4/80 immunostaining. However, as the maturity of the embryoid body culture increases, MPC show generalised high F4/80 expression comparable to ESDM. No significant staining is evident on ESDM with the control isotype antibody (x100 magnification).

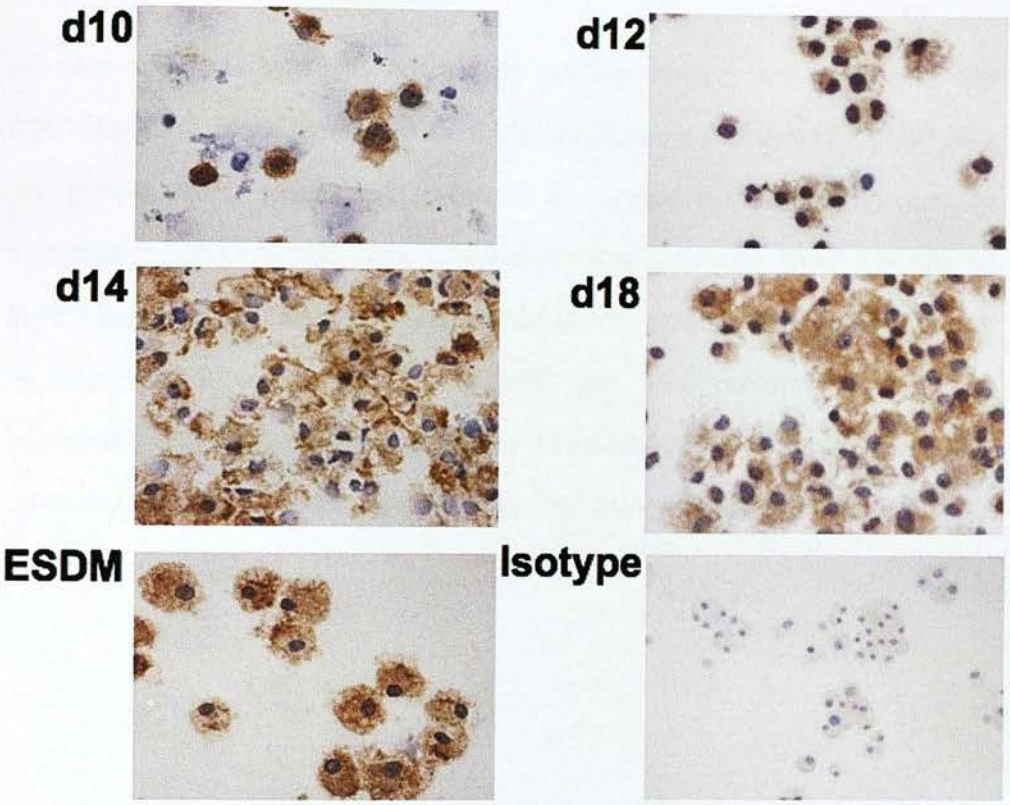

Figure 31: Embryonic stem cell-derived macrophage progenitor cells (EPC) express CD11b.

CD11b immunohistochemistry was undertaken on macrophage progenitor cells (MPC) cytospin preparations. Representative photomicrographs illustrating that MPC are positive for the macrophage marker CD11b. At d10, the MPC exhibit limited immunostaining for CD11b with occasional cells being CD11b positive. However, as the maturity of the embryoid body culture increases, MPC show generalised high CD11b expression comparable to ESDM. No significant staining is evident on ESDM with the control isotype antibody (x100 magnification).

We also used flow cytometry analysis to examine the expression of F4/80 and CD11b by MPC. Since flow cytometry analysis requires a minimum of $1.5x10^6$ cells per sample, MPC yields were recorded throughout the various harvests to determine if sufficient cells were available for flow cytometry. From the original $6x10^5$ ESC cultured, the optimum yields of MPC were obtained from day 14 and day 16 supernatants with a mean of $3.2x10^6$ and $3x10^6$ cells being produced respectively (Figure 32). Subsequently, day 14 and day 16 MPC were used for flow cytometry analysis as the harvests on these days gave sufficient cell numbers.

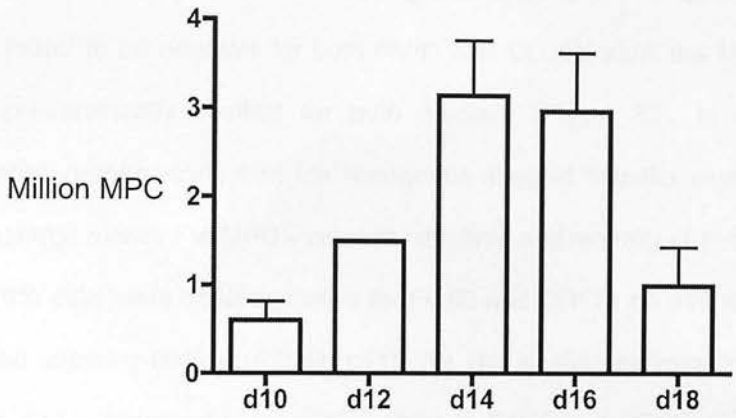

Figure 32: Day 14 and Day 16 embryonic stem cell-derived macrophage progenitor cells harvests produce the highest cell yields.

Embryoid bodies cultures were established and the number of macrophage progenitor cells (MPC) quantified at time points between day 10 and day 18. The highest yield of MPC was obtained at days 14 and 16 (n=3, except d12 n=1).

The dual expression of the cell surface markers F4/80 and CD11b was then assessed in a quantitative manner using flow cytometry. The ESC population was again found to be negative for both F4/80 and CD11b while the MPC and ESDM were predominantly positive for both markers (Figure 33). In addition, these population graphs along with the histograms suggest that the expression level of macrophage markers in MPC increases with time and maturity of the EB cultures as only 79% cells were double positive for F4/80 and CD11b on d14 rising to 88% on d16 and reaching 90% as ESDM (n=1). We also studied expression of the integrin CD11c and it increased in a similar fashion to F4/80 and CD11b. This is illustrated by both the shift in cell populations towards the double positive F4/80 and CD11c quadrant in the flow cytometry dot plot diagrams and by the right shift in the histograms representing the level of marker expression (Figure 34).

The expression of F4/80, CD11b, CD11c and MHC class II by d14 and d16 MPC was also compared to bone marrow monocytes (BMM), expected to be $F4/80^{low}$ and $CD11b^{low}$, and ESDM. BMM were obtained from femur and tibia bone marrow of 129/P2 mice aged 6-8 weeks old and isolated as described in Material and Methods. As predicted, BMM were $F4/80^{low}$ $CD11b^{low}$ $CD11c^{low}$ MHC Class II^{low}. In contrast, ESDM were $F4/80^{high}$ $CD11b^{high}$ $CD11c^{high}$ MHC class II^{low}. Interestingly, the d14 and d16 MPC appear to adopt a somewhat intermediate phenotype (Figure 35).

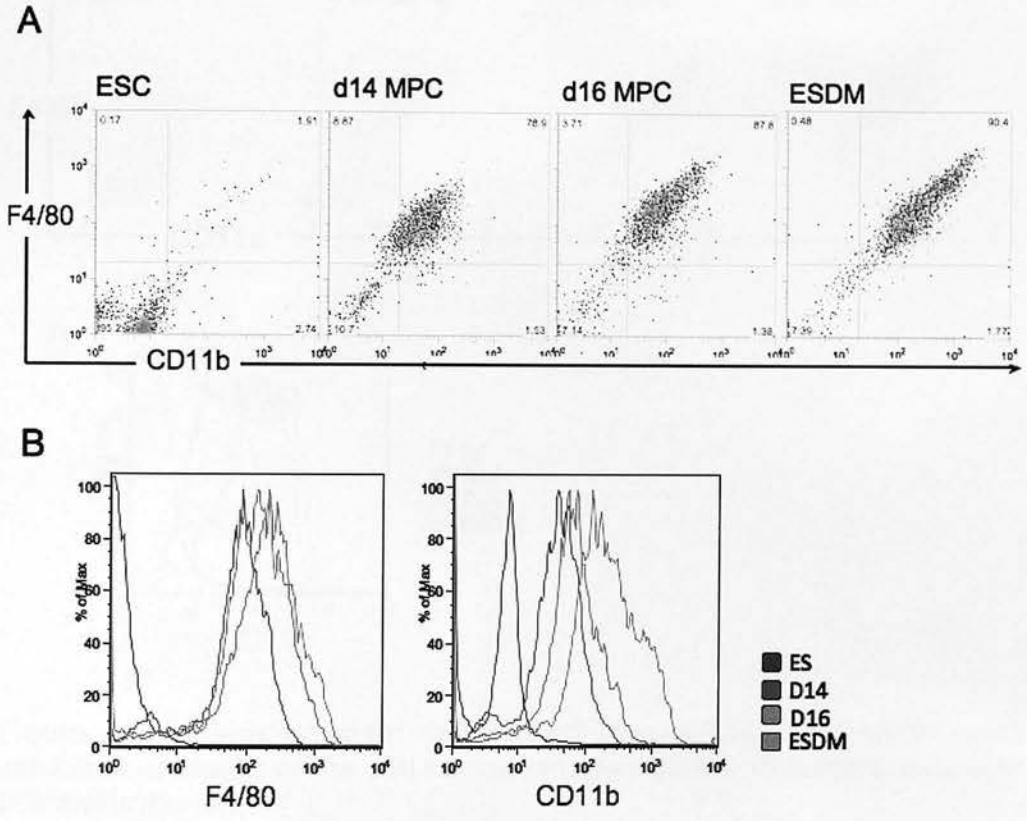

Figure 33: Embryonic stem cell-derived macrophage progenitor cells exhibit dual expression of the macrophage cell surface markers F4/80 and CD11b that increases with cell maturity.

Flow cytometry of macrophage progenitor cells (MPC) harvested at d14 and d16 for macrophage markers F4/80 and CD11b. MPC expression of F4/80 and CD11b increases as the embryoid body cultures mature though it is more evident for CD11b. **A:** Flow cytometry dot plots show a double negative ESC population for F4/80 and CD11b while d14 and d16 MPC populations and the ESDM population are positive for both F4/80 and CD11b. **B:** Histograms representing the increase in F4/80 and CD11b expression in d14 and d16 MPC and ESDM compared with ESC.

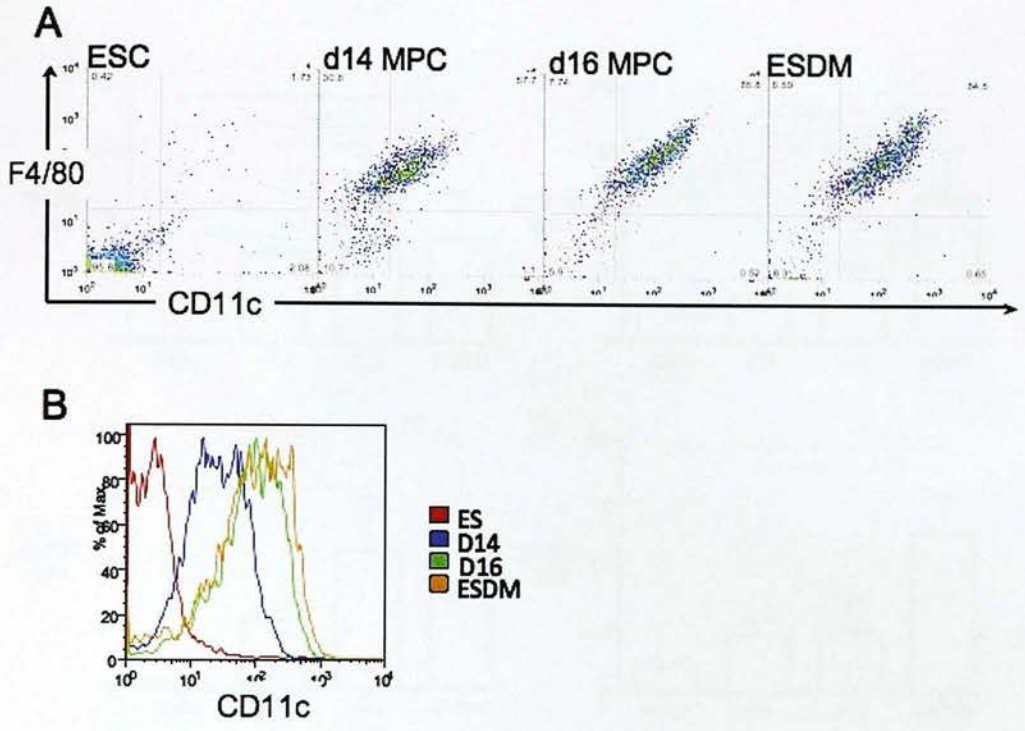

Figure 34: Embryonic stem cell-derived macrophage progenitor cells exhibit expression of the cell surface marker CD11c that increases with cell maturity.

Flow cytometry of macrophage progenitor cells (MPC) harvested at d14 and d16 for F4/80 and CD11c. MPC expression of CD11c increases as the embryoid body cultures mature. **A:** Flow cytometry dot plots show the ES cell population is negative for F4/80 and CD11c while day 14 and day 16 MPC and the ESDM population are predominantly within the double positive quadrant. **B:** Histogram representing the increase in CD11c expression in d14 and d16 MPC and ESDM compared with ESC.

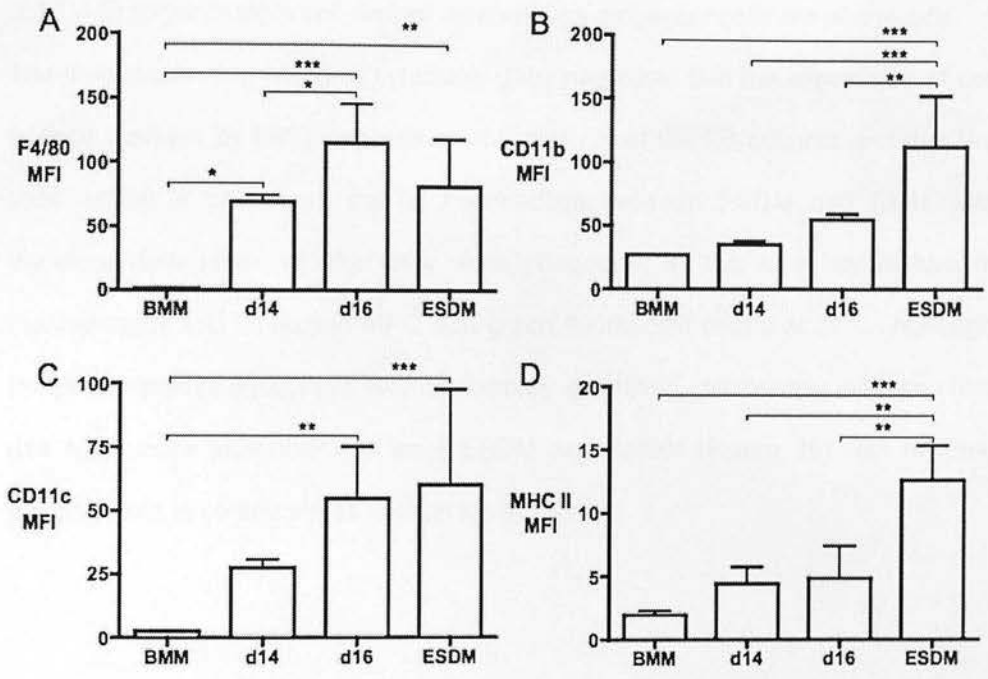

Figure 35: Comparison of the cell surface expression of F4/80, CD11b, CD11c and MHC class II by bone marrow monocytes, d14 and d16 embryonic stem cell-derived macrophage progenitor cells and embryonic stem cell-derived macrophages.

Comparison of BMM, d14 and d16 MPC and ESDM F4/80, CD11b, CD11c and MHC class II expression by flow cytometry. Our results indicate that BMM are $F4/80^{low}$ $CD11b^{low}$ $CD11c^{low}$ MHC Class II^{low}. In contrast, ESDM are $F4/80^{high}$ $CD11b^{high}$ $CD11c^{high}$ MHC Class II^{low}. Day 14 and d16 MPC exhibit a somewhat intermediate phenotype. Although MPC are F4/80 positive, the expression of CD11b, CD11c and MHC Class II increases as the embryoid body cultures mature though this is only significant for CD11c (n=3, * $p<0.05$, ** $p<0.01$ and *** $p<0.001$).

3.3.1.4 Embryonic stem cell-derived macrophage progenitor cells are phagocytic

The immunostaining and flow cytometry data suggested that the expression of cell surface markers by MPC depends on the maturity of the EB cultures and that the cells exhibit a phenotype that is intermediate between ESDM and BMM. We therefore determined whether they were phagocytic as this is a key feature of macrophages and incubated MPC with green fluorescent beads at 37°C. Although the percentage phagocytosis was not formally quantified, microscopy indicated that d14 MPC were phagocytic as were ESDM and BMDM (Figure 36) with minimal phagocytosis in control plates kept on ice (4°C).

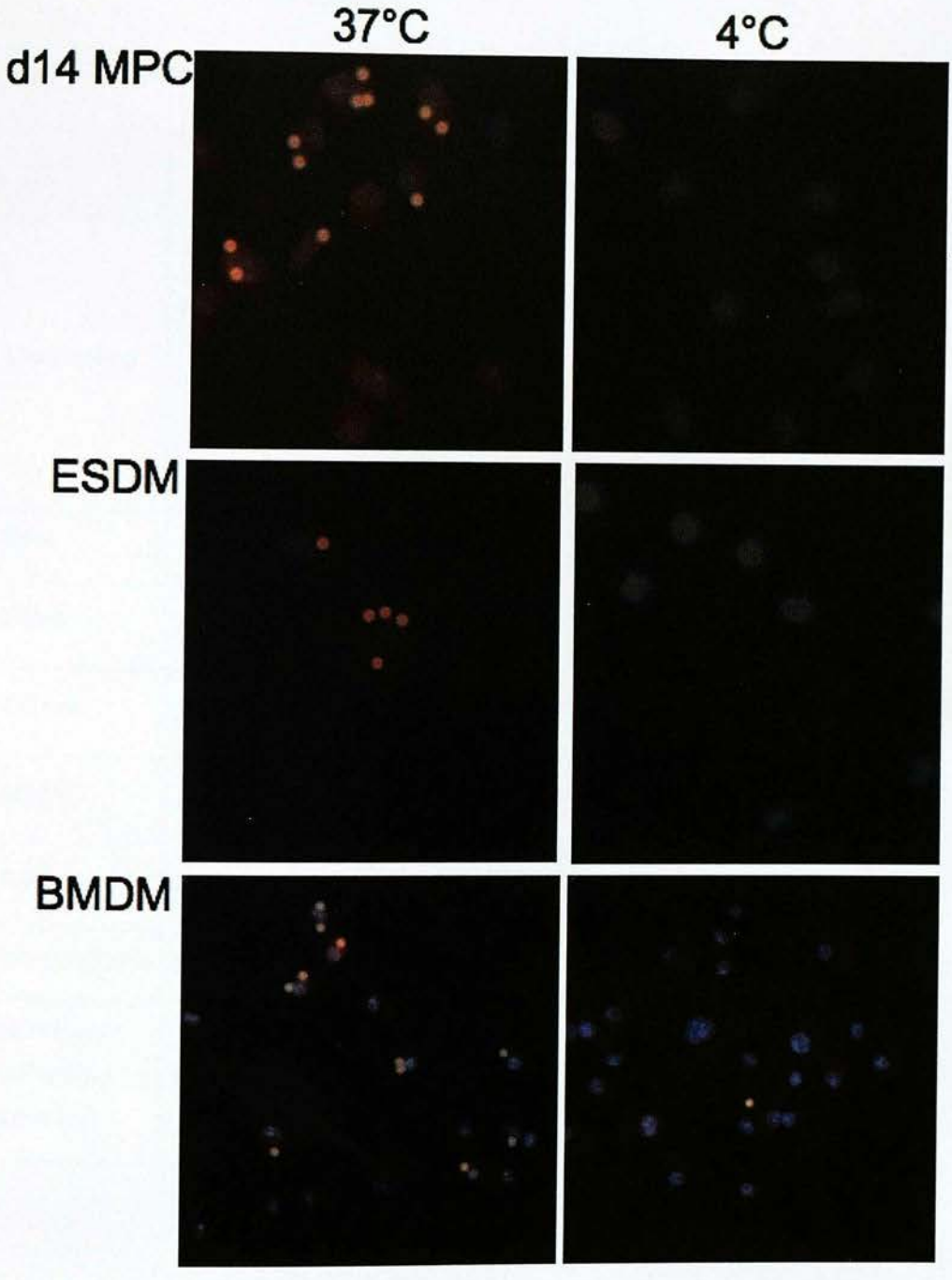

Figure 36: Embryonic stem cell-derived macrophage progenitor cells are able to phagocytose green fluorescent beads.

Cells were incubated with green fluorescent beads for 30 minutes in the dark at 37°C or on ice (4°C). Microscopic assessment of the cells reveals that d14 MPC are able to phagocytose green fluorescent beads at 37°C like ESDM and BMDM whilst little or no phagocytosis was evident at 4°C (n=1).

Table 10: Summary table of ESC, MPC, ESDM and BMDM properties

	ESC	MPC	ESDM	BMDM
Morphology	Heterogeneous population of small cells with big nucleus	Become homogeneous population of large vacuolated cells with small nucleus over time (d10 MPC highly heterogeneous)	Homogeneous population of large vacuolated cells with small nucleus	Homogeneous population of large vacuolated cells with small nucleus
Oct4	Yes	No	No	No
F4/80	No	Yes - increases over time	Yes	Yes
CD11b	No	Yes - increases over time	Yes	Yes
CD11c	No	Yes - increases over time	Yes	Yes
MHC II	N/A	Yes - increases over time	Yes	Yes
Phagocytosis	N/A	Yes	Yes	Yes
NO release (LPS/IFNγ stimulus)	N/A	N/A	Yes	Yes

3.4 Summary

In this chapter, we demonstrated that ESDM are highly comparable to BMDM using various cell surface markers and multiple functional assays. We report that ESDM:

- Exhibit a large mononuclear cell morphology,
- Are F4/80^{high}CD11b^{high}CD11c^{high}MHC class II^{low} by flow cytometry,
- Actively phagocytose beads,
- Produce significant levels of NO when classically activated by LPS and IFNγ.

Further analysis of ESDM differentiation showed that ESC can be used to produce a substantial number of MPC. Our data suggests that MPC:

- Develop into a homogeneous population of large, vacuolated cells that resemble ESDM as EB cultures mature,
- Do not express the stem cell marker Oct4 and express high levels of the macrophage cell surface marker F4/80,
- Phagocytose beads,
- Express increasing levels of CD11b and CD11c as the EB cultures mature and, depending upon the EB culture maturation stage, have a phenotype that is somewhat intermediary between BMM (F4/80^{low} CD11b^{low} CD11c^{low} MHC Class II^{low}) and ESDM (F4/80^{high} CD11b^{high} CD11c^{high} MHC Class II^{low}).

Chapter 4. Constitutive and inducible overexpression of hemeoxygenase-1 in embryonic stem cells and embryonic stem cell-derived macrophages

4.1 Introduction

As previously outlined, macrophages (Mφ) have the ability to exhibit considerable anti-inflammatory and pro-reparative properties and there is growing interest in harnessing these properties for therapeutic gain in inflammatory disease. A body of work indicates that 'cell therapy' with Mφ modified to adopt an anti-inflammatory phenotype results in amelioration of disease in various experimental models of kidney inflammation including renal ischaemia reperfusion injury, immune-mediated glomerulonephritis, ureteric obstruction, adriamycin induced nepropathy and streptozotocin-induced diabetic nephropathy (Ferenbach et al., 2010; Kluth et al., 2001; Wang et al., 2007; Wilson et al., 2002; Yamagishi et al., 2001; Zheng et al., 2011). However, these previous studies were either using modified bone marrow derived or splenic Mφ.

In Chapter 3, we demonstrated our capacity to generate functional embryonic stem cell derived Mφ (ESDM). We now plan to extend work done in the field of 'Mφ cell therapy' by developing and using genetically manipulated ESDM to ameliorate disease. Our aims include: (i) the production of a genetically modified HO-1 expressing embryonic stem cell line and (ii) the subsequent derivation of functional HO-1 expressing ESDM for *in vivo* studies. We hypothesise that HO-1 expressing ESDM will exhibit an anti-inflammatory phenotype *in vitro* and be renoprotective in experimental ischaemic AKI *in vivo*. Genetic engineering was employed to generate ESC cell lines with either constitutive or inducible overexpression of HO-1.

4.2 Constitutive over expression of hemeoxygenase-1: the pCAG system

4.2.1 Embryonic stem cells constitutively overexpress hemeoxygenase-1 under the exogenous pCAG promoter

Dr Richard Axton at the University of Edinburgh generated stable ESC lines that constitutively overexpressed HO-1 under the exogenous pCAG promoter. The HO-1 cDNA was cloned into a pCAG vector containing an internal ribosome entry site (IRES) and the puromycin resistance gene. The pCAG-HO-1 plasmid was then randomly integrated into the ESC genome via electroporation and stable HO-1 expressing ESC lines were selected by their puromycin resistance.

The HO-1 expression level of seven different ESC lines was determined by Western blot analysis (Figure 37) and this suggested that the generated clones exhibited various levels of HO-1 overexpression. In order to determine any potential deleterious effects that the genetic manipulation might have upon the stem cells, four HO-1 over-expressing ESC clones were selected for further analysis:

(i) HO-1/2 and HO-1/3 represented "low HO-1 expressing ESC"

(ii) HO-1/5 and HO-1/6 representing "high HO-1 expressing ESC".

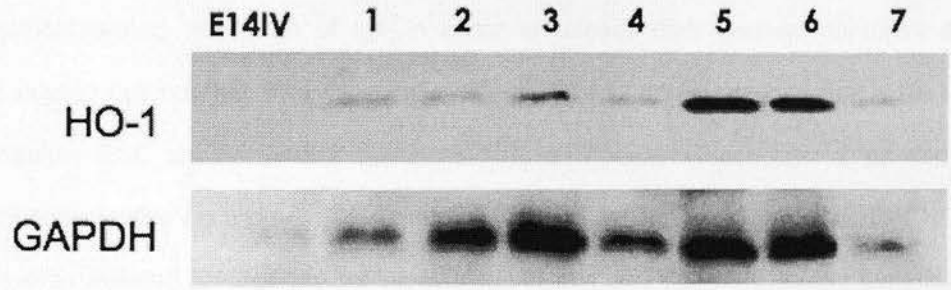

Figure 37: Stable embryonic stem cell lines overexpressing hemeoxygenase-1 under the constitutive pCAG promoter.

Representative HO-1 Western blot of seven stable HO-1 overexpressing ESC lines (1 to 7). Variable expression of HO-1 is evident. Low HO-1 expressing ESC line 2 (HO-1/2) and 3 (HO-1/3) and high HO-1 expressing ESC line 5 (HO-1/5), and 6 (HO-1/6) were selected in order to assess whether the genetic manipulation had any deleterious effects upon the stem cells.

4.2.2 Random integration of pCAG-HO-1 adversely affects the ability of embryonic stem cells to self-renew

When ESC are thawed from their cryopreservation state, they are generally passaged twice at a concentration of $1.5x10^6$ cells/$25cm^2$ flask in 10ml ESC medium supplemented with 10µl of LIF in order to assess their general condition and increase cell number. Previous work with the E14 IV line suggested that a flask of healthy ESC should yield a minimum of $5.5x10^5$ cells/ml/flask after 2 passages. Subsequently, we assessed the general condition of the genetically modified HO-1 overexpressing ESC clones by quantifying cell number. Cell yields of the genetically modified clones were compared to that of unmodified parental E14 IV cells (Figure 38). The cell number data indicated a significant reduction in the cell yields of ESC lines HO-1/3 ($p<0.001$), HO-1/5 ($p<0.01$) and HO-1/6 ($p<0.001$) whereas clone HO-1/2 yielded similar amounts of cells compared to the unmodified parental E14 IV line ($p>0.05$).

We then explored these findings further by analysing the ability of the pCAG-HO-1 ESC clones to engage in cell division while remaining in a pluripotent, undifferentiated state using a self-renewal assay. For this experiment, the expression and activity of the enzyme alkaline phosphatase, an ESC marker, was determined after the cells have been cultured for 6 days. Usually, three different types of colonies are then discernible: (i) alkaline phosphatase positive ESC colonies that self renew and are pluripotent, (ii) mixed colonies containing both ESC and differentiated cells and (iii) fully differentiated alkaline phosphatase negative colonies that have lost their pluripotency. The colonies of the various pCAG-HO-1 clones were compared to the control unmodified parental E14 IV ESC line (Figure

39). The percentage of mixed colonies containing both stem cells and differentiated cells as well as totally differentiated colonies is significantly higher in all of the pCAG-HO-1 clones. This suggests an impairment of pCAG-HO-1 clone self-renewal and a potentially detrimental effect of the genetic modification.

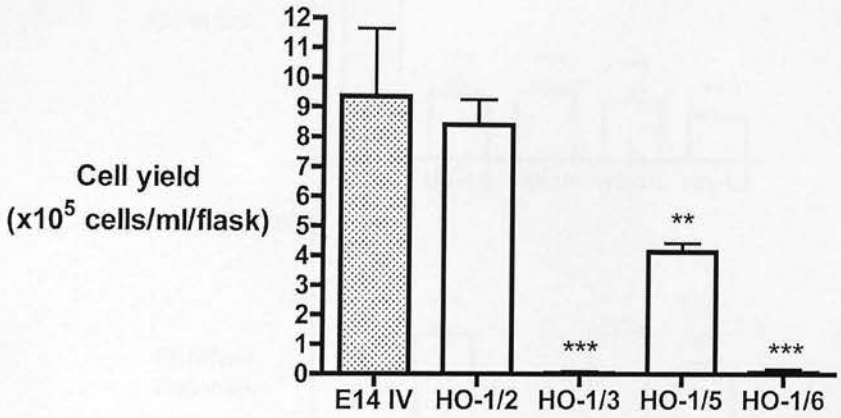

Figure 38: General stem cell condition is impaired following insertion of a pCAG-HO-1 vector into the genome of the cells.

The different stem cell lines were taken out of the -140°C freezer and quickly thawed out in a 37°C water-bath. The cells were cultured in a gelatinised 25cm^2 flask in a total volume of 10ml ESC medium supplemented with 10µl of LIF. After 2 days, cells were trypsinised and passaged at 1.5x10^6 cells per gelatinised 25cm^2 flask in 10ml of warm ES medium supplemented with LIF. After another 2 days, cells were trypsinised again and counted with a haemocytometer. Our results indicate significantly reduced cell number of genetically modified ESC lines HO-1/3, HO-1/5 and HO-1/6 whereas clone HO-1/2 yielded a comparable cell number to the control E14 IV line (n=3).

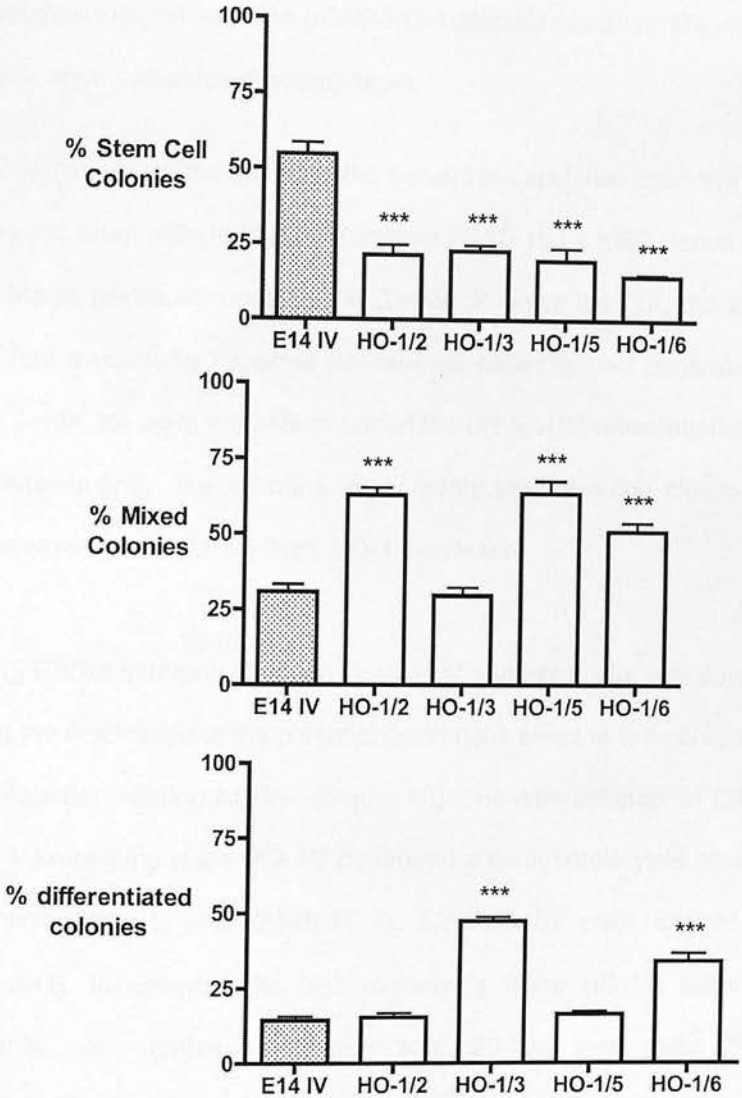

Figure 39: The random integration of pCAG-HO-1 reduces embryonic stem cell self-renewal ability and promotes cell differentiation.

ESC were plated in 6-well plates ($1x10^3$ cells per well) and cultured for 6 days in ESC medium. On day 6, colonies were stained for alkaline phosphatase activity – an ESC marker. Expression of the enzyme by the pCAG-HO-1 clones was compared to the control E14 IV ESC line. Depending on the pCAG clone observed, the percentage of either mixed stem cell and differentiated colonies and totally differentiated colonies is significantly higher than the E14 IV control, suggesting impaired ESC self-renewal and a potentially detrimental effect of the genetic modification (n=3).

4.2.3 Random integration of the pCAG-HO-1 plasmid can affect the differentiation of embryonic stem cell-derived macrophages

In order to investigate the impact of the genetic manipulation upon the differentiation of embryonic stem cells to Mφ, the modified pCAG-HO-1 ESC clones were cultured to form Mφ as previously described in Chapter 2. Since the ESC clones HO-1/3 and HO-1/6 had a markedly impaired self-renewal capacity, and generated particularly low cell yields, we were not able to undertake the ESDM differentiation studies with them. Subsequently, the following experiments only describe clones HO-1/2 (low HO-1 expresser) and HO-1/5 (high HO-1 expresser).

Following ESDM differentiation, the number of adherent cells was counted and this provided the first insight of the potential deleterious effect of the genetic modification on the Mφ differentiation process (Figure 40). The differentiation of ESDM from the low HO-1 expressing clone HO-1/2 generated a comparable yield of adherent cells to the control E14 IV line (2.9 ± 0.17 vs. $3.2\pm0.23\times10^6$ cells; E14 IV vs. HO-1/2; $p=0.28$, $n=3$). In contrast, the high expressing clone HO-1/5 failed to produce respectable cell numbers and generated 20-fold less cells (2.9 ± 0.17 vs. $0.14\pm0.03\times10^6$ cells; E14 IV vs. HO-1/5; $p<0.001$, $n=3$).

Diff Quick stained cytospin preparations of adherent cells generated by the ESDM differentiation protocol reinforced the cell count findings. Cells derived from E14 IV cells and the low HO-1 expressing clone HO-1/2 exhibited a comparable phenotype with similar Mφ-like features. In contrast, the cells derived from the high HO-1 expressing clone HO-1/5 were few in number and highly abnormal with variable cell size (Figure 41). Since the high HO-1 expresser HO-1/5 clone did not generate

sufficient Mφ for flow cytometry experiments, it was not included in further experiments.

In order to confirm the generation of Mφ from the modified pCAG-HO-1/2 clone, we assessed the expression of Mφ cell surface markers by flow cytometry. Results indicate that low HO-1 expresser HO-1/2 ESC were able to differentiate into Mφ as the cells generated are F4/80^{high} CD11b^{high} CD11c^{low} MHC class II^{low} (Figure 42).

Rather than studying gene expression to confirm that the pCAG-HO-1/2 clone still overexpressed HO-1, and trying to dissect the mechanisms responsible for the clonal variability outlined in this chapter, we attempted to overcome this problem by developing and testing a more precise, targeted tetracycline inducible system (p165).

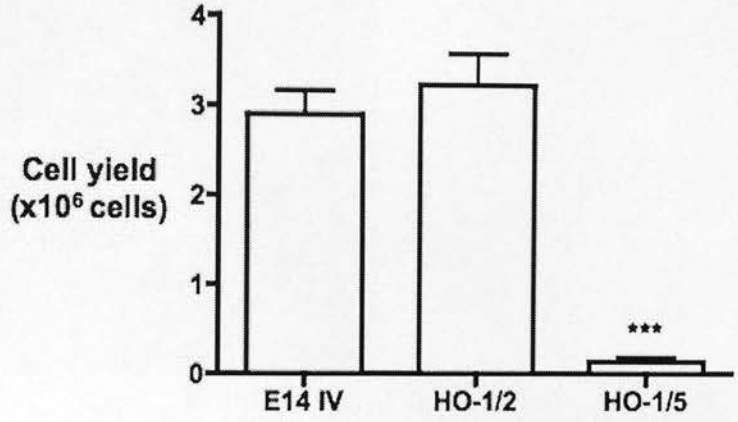

Figure 40: A variable number of adherent cells are generated by the embryonic stem cell-derived macrophage protocol following genetic modification of embryonic stem cells.

$6.5x10^5$ embryonic stem cells were plated per dish and the cells were induced to differentiate into macrophages. At the end of 17 days in culture, the number of adherent cells produced per dish was counted with a haemocytometer. The high HO-1 expresser clone HO-1/5 generates significantly less cells than the control E14 IV cell line and the low HO-1 expresser clone HO-1/2 ($p<0.001$ vs. control E14 IV cell and the HO-1/2 clone) (n=3).

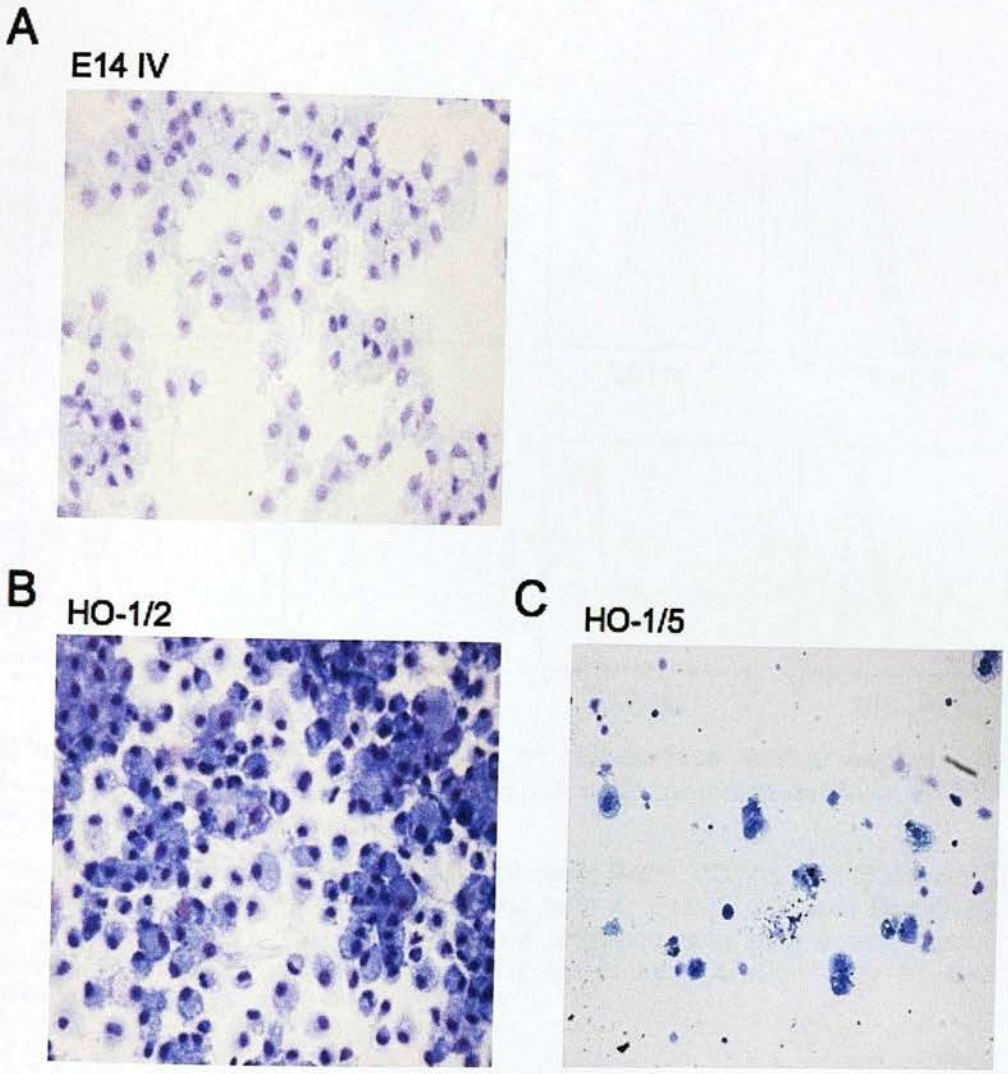

Figure 41: Cell morphology of day 7 E14IV, HO-1/2 and HO-1/5 embryonic stem cell-derived macrophages.

Diff Quick staining of cytospin preparations indicating the morphology of cells derived from **A:** E14IV, **B:** HO-1/2 and **C:** HO-1/5 stem cells (x100 magnification) following the ESDM differentiation protocol. Cells generated from E14IV cells and HO-1/2 clones exhibit macrophage-like features with abundant cytoplasm. In contrast, the limited number of cells derived from clone HO-1/5 were heterogeneous and displayed variable morphology.

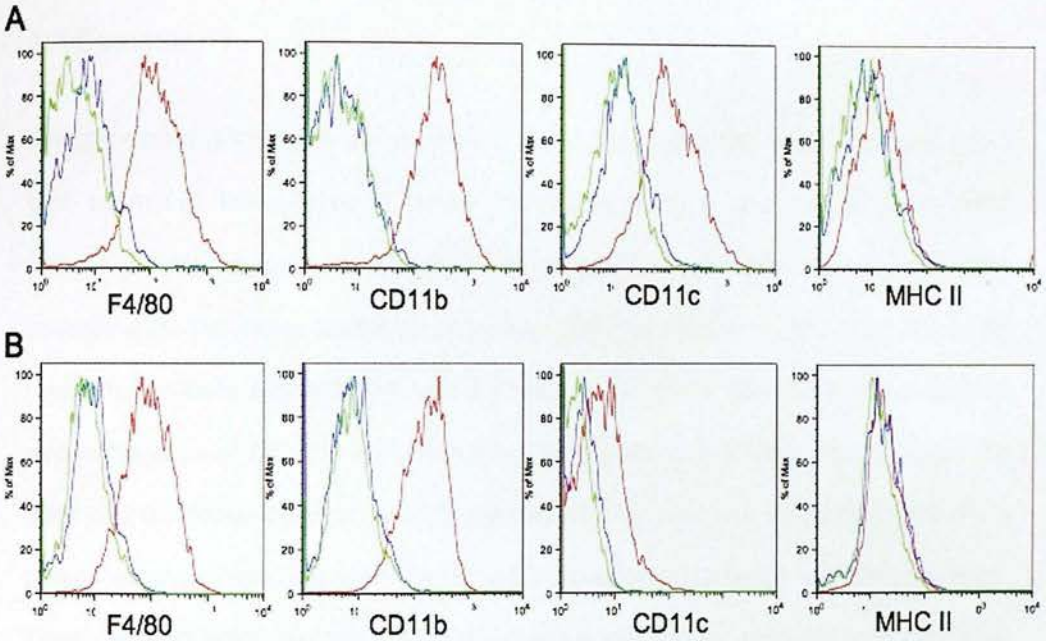

Figure 42: Flow cytometric analysis of cell surface marker expression of day 7 embryonic stem cell-derived macrophages derived from E14 IV and HO-1/2 cell lines.

Representative flow cytometry histograms showing F4/80, CD11b, CD11c and MHC Class II expression of day 7 ESDM derived from **A:** E14 IV ESC and **B:** HO-1/2 ESC. The green and blue lines represent unstained cells and isotype control antibody respectively and the red line corresponds to the expression of the indicated cell surface marker.

4.3 Summary 1

We generated genetically manipulated ESC that constitutively overexpressed HO-1 and examined the effects of these manipulations upon the behaviour of ESC including their capacity to undergo differentiation to ESDM. Our results differ according to the clone analysed indicating that the genetic modification does not result in uniform alteration of cell behaviour. In some clones, the constitutive overexpression of HO-1 in ESC with the pCAG system adversely impacts upon the yield of ESC following routine ESC culture (HO-1/3 and HO-1/6 clones). All HO-1 clones exhibited reduced self-renewal associated with increased cell differentiation. Lastly, HO-1/2 ESC (low HO-1 expresser) generated comparable Mφ to control E14 IV ESC following ESDM differentiation both in cell number and cell surface marker expression whilst the HO-1/5 ESC (high HO-1 expresser) generated a minimal number of Mφ.

The HO-1 cDNA is cloned into a pCAG vector that is then *randomly* integrated into the genome of ES cells. This random insertion increases the risk of inadvertently disrupting key genes such as those involved in ESC self-renewal and/or Mφ differentiation. Rather than trying to dissect the mechanisms responsible for the clonal variability outlined in this chapter, we attempted to overcome this problem by developing and testing a more precise, targeted tetracycline inducible system. There are numerous potential advantages of this approach. First, we will target a specific site in the genome of the ESC in order to avoid silencing of any other genes. Secondly, the use of an inducible system will provide tight control over the cellular expression of HO-1. This will allow us to study the effect of HO-1 overexpression upon either ESC biology or Mφ differentiation by inducing HO-1 expression at different time points.

4.4 Tetracycline inducible over-expression of hemeoxygenase-1: the A2lox.cre cell line inducible system.

The genetically modified A2lox.cre embryonic stem cell line ($Ctrl^{ind}$ ESC) used by Dr Richard Axton from the University of Edinburgh to generate HO-1 inducible ESC ($HO\text{-}1^{ind}ESC$) was kindly donated by Dr Michael Kyba from the University of Minnesota (Iacovino et al., 2011) (Figure 43).

4.4.1 Hemeoxygenase-1 inducible embryonic stem cells overexpress hemeoxygenase-1 following doxycycline treatment

$Ctrl^{ind}$ and $HO\text{-}1^{ind}$ ESC were subjected to either 5μg/ml Dox for 24h or cultured in Dox-free medium. The inducibility of HO-1 overexpression in $HO\text{-}1^{ind}$ ESC following exposure to Dox was then verified by Western blot analysis. Our results illustrate that $HO\text{-}1^{ind}$ ESC exhibit increased HO-1 expression when treated with Dox compared to cells cultured in normal medium with $Ctrl^{ind}$ ESC not expressing HO-1 at all (Figure 44). These findings indicated the successful generation of a genetically modified embryonic stem cell line with tetracycline inducible HO-1 overexpression.

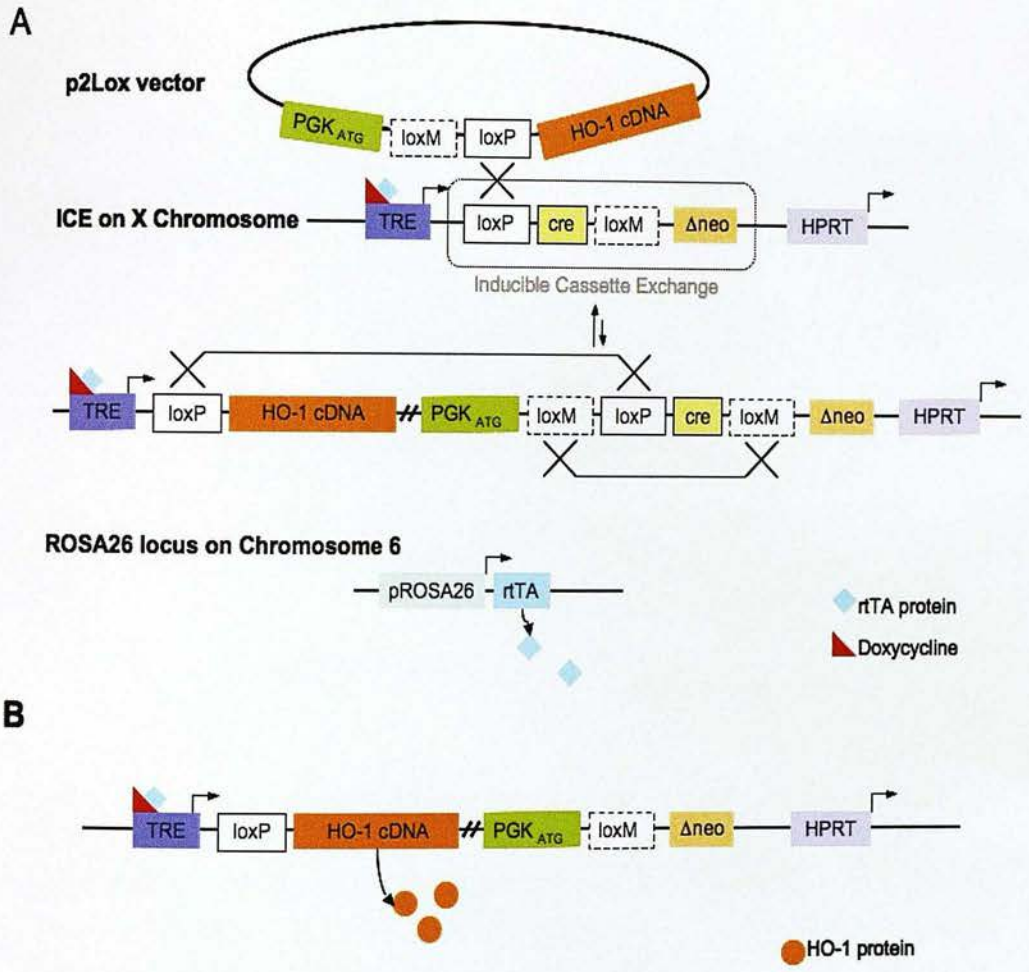

Figure 43: Use of the A2lox.cre embryonic stem cell line to generate HO-1^{ind} embryonic stem cells.

In order to overcome any adverse effects of the random insertion of genes into the genome, we developed an inducible HO-1 expression system. **A:** An inducible cassette exchange (ICE) has been targeted to the HPRT locus on the X chromosome. The cDNA for cre has been inserted behind a tetracycline response element (TRE) and between loxP and loxM sites. Only in the presence of both the rtTA protein produced by the ROSA26 locus on chromosome 6 and doxycycline, can the cells express cre and the ICE is self excised and exchanged for an incoming plasmid containing HO-1 cDNA. **B:** stable new inducible cell line expressing HO-1 protein upon the addition of doxycycline to the culture medium.

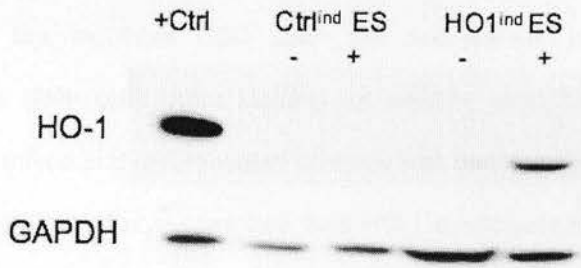

Figure 44: Doxycycline induces hemeoxygenase-1 overexpression in the inducible embryonic stem cells.

Representative Western blot of Ctrl^{ind} and HO-1^{ind} ESC treated with 5µg/ml Dox for 24h (+) or cultured in Dox-free medium (-). The HO-1 positive control is a HO-1 expressing COS-7 clone. Ctrl^{ind} ESC do not express HO-1 in the absence or presence of Dox stimulation. In contrast, HO-1^{ind} ESC do not express HO-1 under basal conditions but do upregulate HO-1 expression following treatment with Dox.

4.4.2 Inducible Hemeoxygenase-1 expression has no effect on the self-renewal properties of the inducible embryonic stem cells

Self-renewal assays were performed on the HO-1^{ind} ESC and the colonies were stained for alkaline phosphatase activity (ESC marker). This experiment was key in order to identify any possible adverse effects of the doxycycline treatment and HO-1 upregulation in the inducible ESC upon the self-renewal and differentiation properties of the stem cells. After staining for alkaline phosphatase activity, the number of ESC, mixed and differentiated colonies was counted by light microscopy. Our results confirm that doxycycline and thus HO-1 overexpression, has no effect on the self-renewal properties of ESC (Figure 45).

4.4.3 The generation of hemeoxygenase-1 inducible embryonic stem cell-derived macrophages from the genetically modified stem cell line

The genetically engineered HO-1^{ind} ESC were cultured to form ESDM as previously described in Chapter 3. However, 24h before their final harvest, the cells were exposed to 5μg/ml Dox to induce expression of HO-1 or treated with control medium. In this section we investigated (i) the impact of the genetic manipulation upon ESDM differentiation, (ii) the effect of Dox treatment upon ESDM morphology and cell surface marker expression and more importantly, (iii) the 'inducibility' of the HO-1^{ind} ESDM following doxycycline exposure.

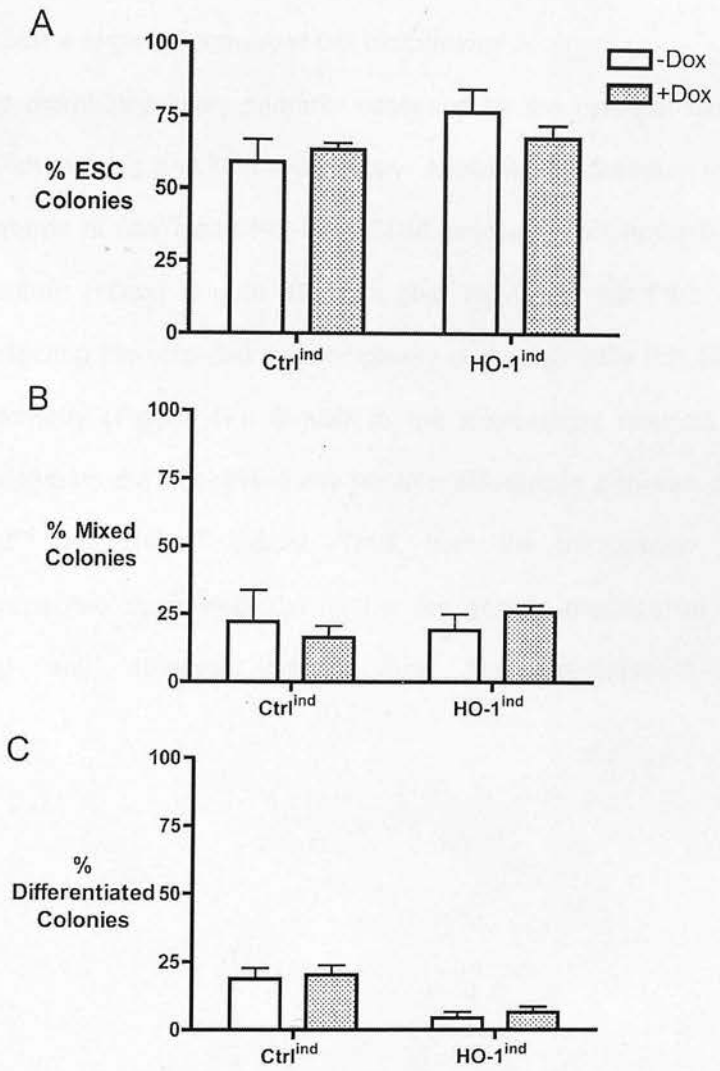

Figure 45: Inducible Hemeoxygenase-1 expression has no effect on the self-renewal properties of the inducible embryonic stem cells.

ESC were plated in 6-well plates ($1x10^3$ ESC per well) and cultured for 6 days in ESC medium. 5µg/ml Dox was added on day 5 for 24h and on day 6, colonies were stained for alkaline phosphatase activity. **A**: $Ctrl^{ind}$ ESC and $HO\text{-}1^{ind}$ ESC colonies, **B**: Percentage of mixed colonies and **C**: Percentage of differentiated colonies are not affected by inducible HO-1 expression following Dox treatment (n=3).

4.4.3.1 Hemeoxygenase-1 inducible embryonic stem cell-derived macrophages exhibit a large mononuclear cell morphology

Mφ morphology was primarily assessed by the cytospin method followed by Diff Quick staining and light microscopy. Analysis demonstrates the Mφ-like and similar features of $Ctrl^{ind}$ and $HO\text{-}1^{ind}$ ESDM exposed to control (-Dox) or Dox-containing medium (+Dox) (Figure 46). We also examined the FSC and SSC parameters (reflecting the size and the complexity of the inducible ESDM respectively) by flow cytometry (Figure 47). Similar to the microscopic analysis, the FSC and SSC histograms did not reveal any notable differences between control or Dox-treated $Ctrl^{ind}$ and $HO\text{-}1^{ind}$ ESDM. Thus, both the microscopic and flow cytometric approaches suggested that neither the genetic modification nor exposure to Dox had any adverse impact upon Mφ development and differentiation.

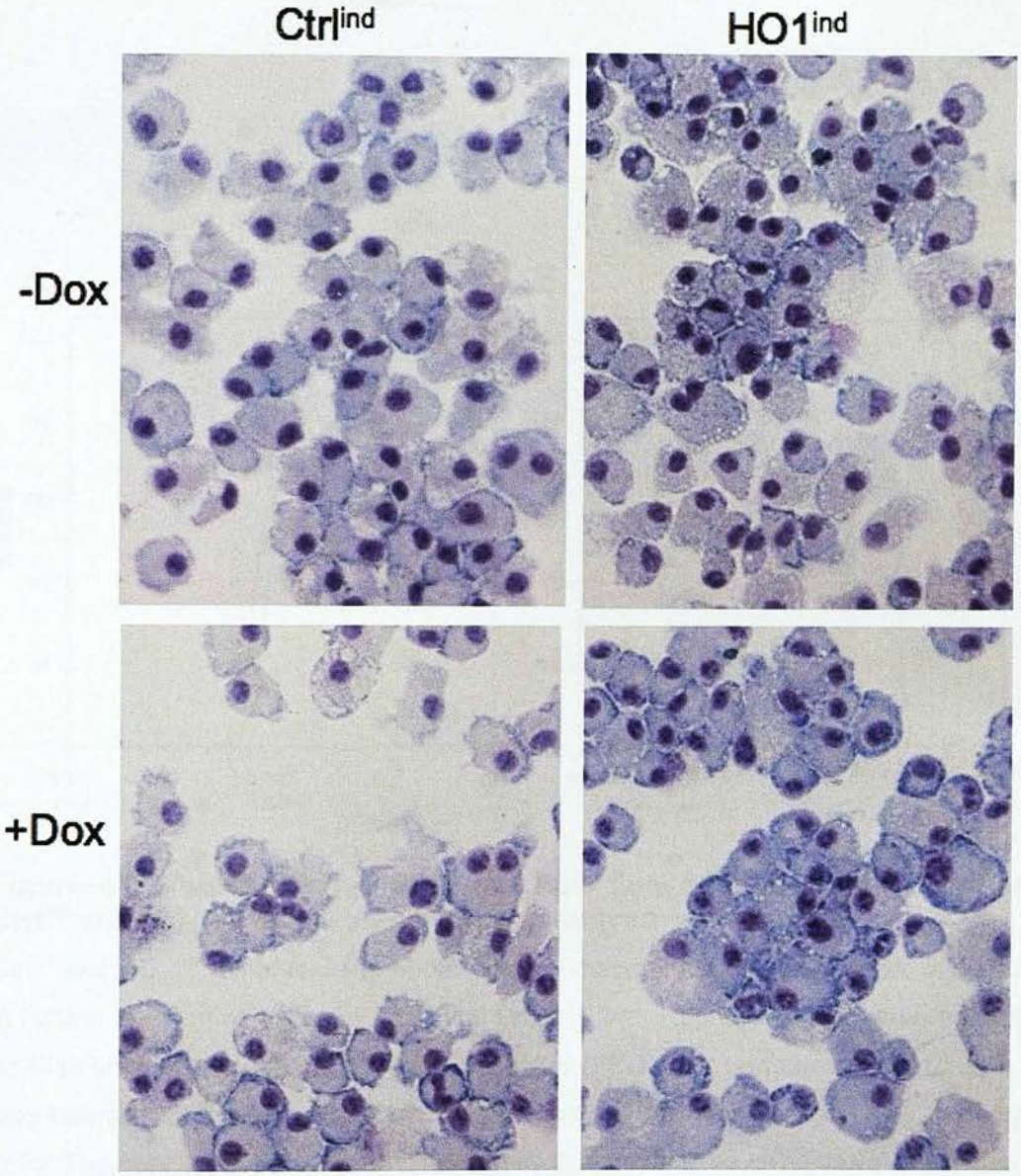

Figure 46: Control inducible and hemeoxygenase-1 inducible embryonic stem cell-derived macrophages exhibit a macrophage-like morphology.

HO-1^{ind} embryonic stem cell-derived macrophages (ESDM) were generated as described in the text. 24h before harvest, the cells were exposed to 5μg/ml Dox. Cell cytospins were stained using the Diff Quick Method. Light microscopy analysis indicates a comparable large mononuclear cellular morphology of all ESDM preparations with no discernible difference between Ctrl^{ind} and HO-1^{ind} ESDM in the presence or absence of Dox (x100 magnification).

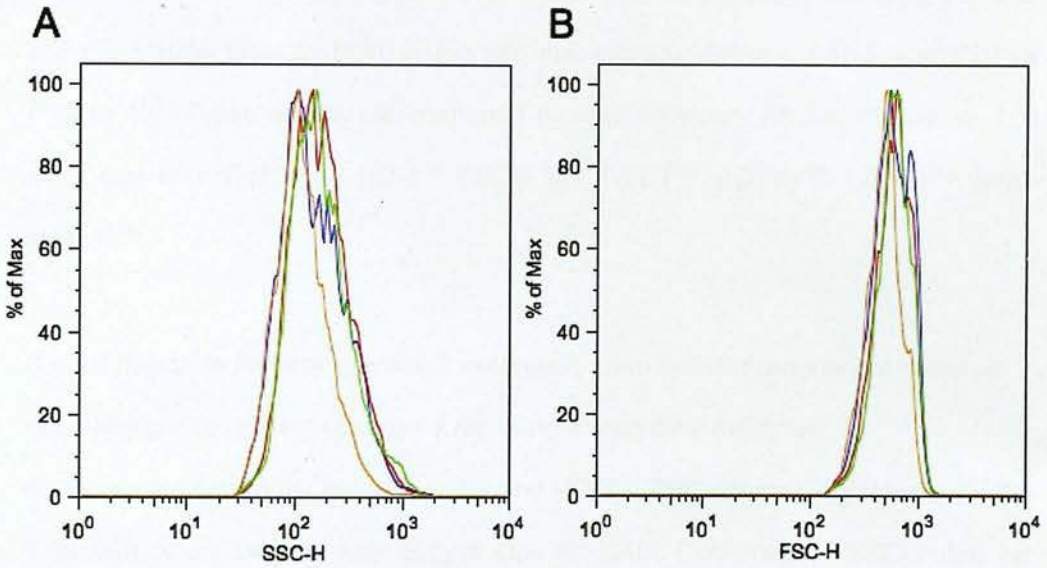

Figure 47: Representative SSC and FSC flow analysis histograms of Ctrl^{ind} and HO-1^{ind} embryonic stem cell-derived macrophages.

Ctrl^{ind} and HO-1^{ind} embryonic stem cell-derived macrophages (ESDM) were cultured in control medium or exposed to 5μg/ml Dox for 24h. Representative histograms of **A:** Side scatter (SSC-H) and **B:** forward scatter (FSC-H) of untreated Ctrl^{ind} (green), Dox treated Ctrl^{ind} (red), untreated HO-1^{ind} (orange) and Dox treated HO-1^{ind} (blue) cells. The overlapping histogram lines signify that neither the HO-1 cDNA insert nor the Dox treatment have an impact on the side scatter or forward scatter of ESDM.

4.4.3.2 Hemeoxygenase-1 inducible embryonic stem cell-derived macrophages express macrophage cell surface markers

To confirm that the cells generated from the modified inducible ESC line were Mφ, we assessed the expression of various cell surface markers by fluorescent immunohistochemistry (FIHC) and flow cytometry. FIHC pictures demonstrate that HO-1^{ind} ESDM express both of the Mφ cell surface markers F4/80 and CD11b (Figure 48). These results are confirmed by flow cytometry (Figure 49) where it is clear that both Ctrl^{ind} and HO-1^{ind} ESDM are F4/80^{high} CD11b^{high} CD11c^{med} MHC class II^{low}.

4.4.3.3 Inducible hemeoxygenase-1 embryonic stem cell-derived macrophages do not overexpress hemeoxygenase-1 following doxycycline treatment

As demonstrated earlier in this chapter, the HO-1^{ind} ESC express high levels of HO-1 protein when treated with 5μg/ml Dox for 24h. Furthermore, ESDM can be successfully derived from HO-1^{ind} ESC and exhibit a comparable morphology and cell surface marker profile to Ctrl^{ind} ESC. However, it was important to determine that the ability of Dox to induce the expression of HO-1 was not impaired following the Mφ differentiation process such that the genetically modified ESDM are still able to induce HO-1 upon the addition of doxycycline. Therefore, the lysates of Ctrl^{ind} and HO-1^{ind} ESDM treated with 5μg/ml Dox or control medium were analysed by Western blot (Figure 50). Surprisingly, the results indicated that Dox treated HO-1^{ind} ESDM do not significantly upregulate HO-1 as there was no significant difference between the level of HO-1 expression of Ctrl^{ind} and HO-1^{ind} irrespective of whether the cells were exposed to Dox.

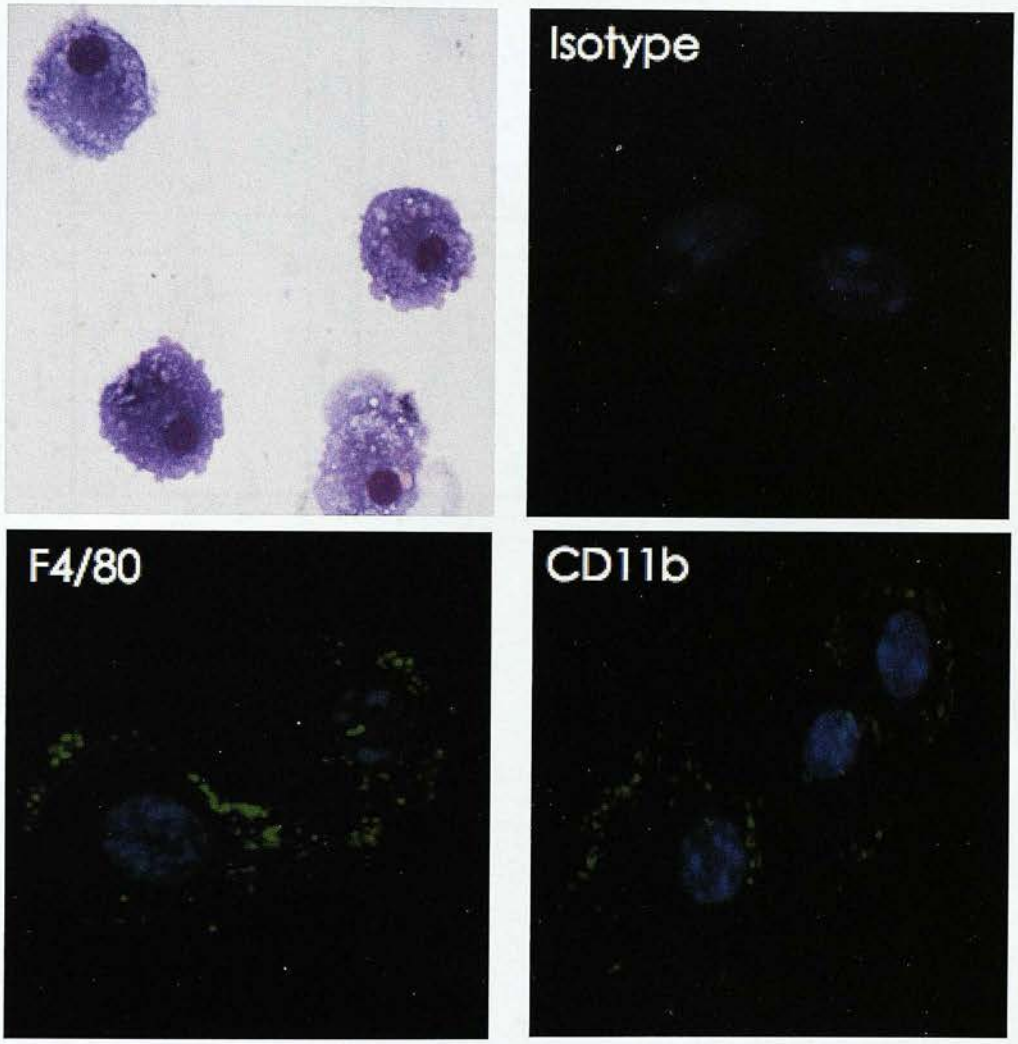

Figure 48: Hemeoxygenase-1 inducible embryonic stem cell-derived macrophages express cell surface markers F4/80 and CD11b.

Cytospin preparations of embryonic stem cell-derived macrophages (ESDM) derived from HO-1^{ind} ESC were fixed in acetone and exposed to rat anti-mouse F4/80 or CD11b primary antibodies followed by biotinylated goat anti-rat secondary antibodies. Positive staining was revealed by Alexa Fluor-488 streptavidin dye and fluorescence microscopy. **A:** Diff Quick staining indicating that the mononuclear cell morphology of HO-1^{ind} ESDM. **B:** Isotype antibody treatment revealed no significant staining, **C:** HO-1^{ind} ESDM express F4/80 and **D:** HO-1^{ind} ESDM express CD11b.

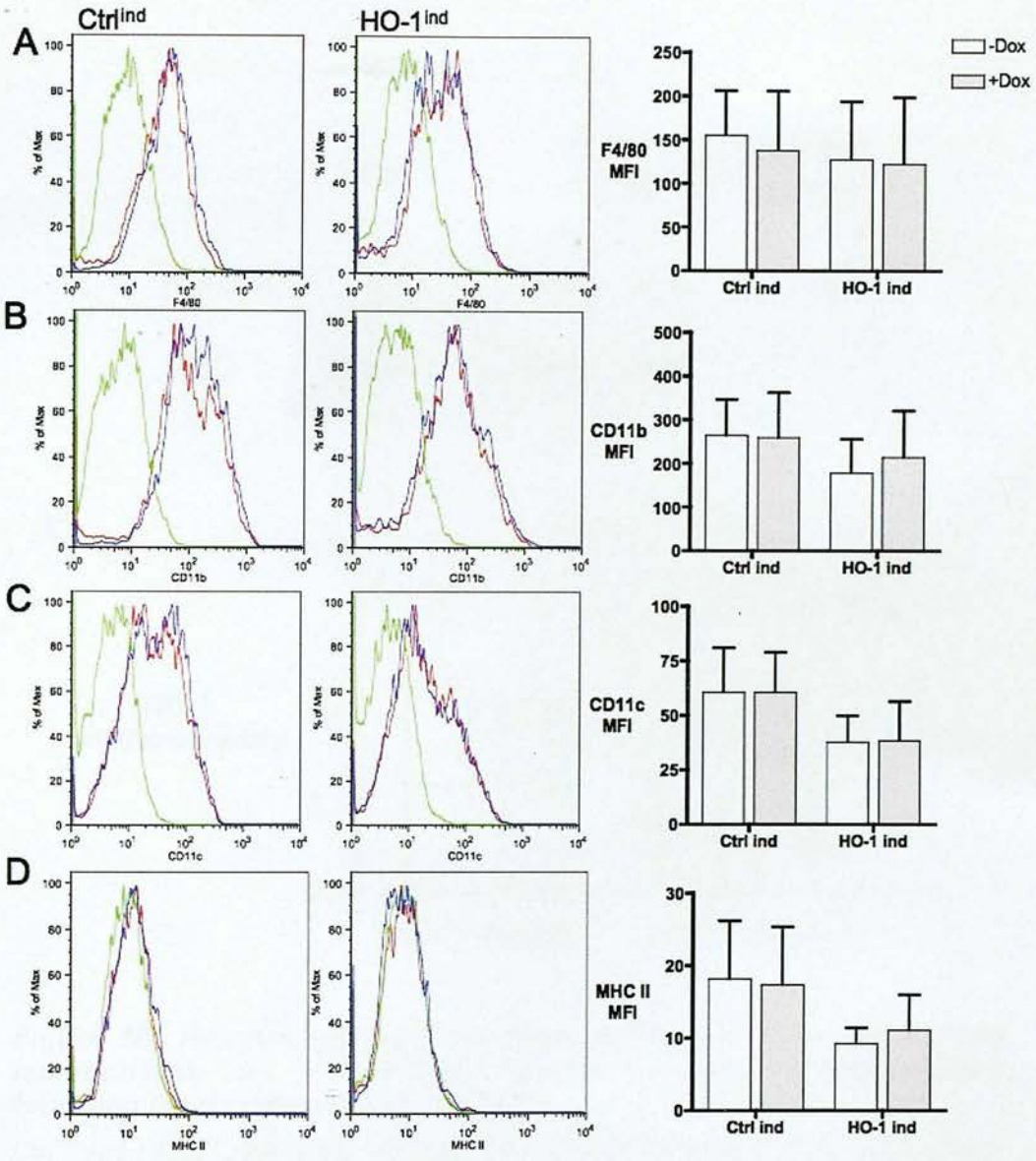

Figure 49: Inducible embryonic stem cell-derived macrophages are F4/80^{high} CD11b^{high} CD11c^{med} MHC class II^{low}.

Embryonic stem cell-derived macrophages (ESDM) derived from Ctrl^{ind} and HO-1^{ind} ESC underwent antibody staining for F4/80, CD11b, CD11c and MHC class II followed by flow cytometry. Representative flow cytometry histograms and mean fluorescence intensity graphs representing **A:** F4/80, **B**: CD11b, **C**: CD11c and **D:** MHC Class II expression. Ctrl^{ind} and HO-1^{ind} ESDM express similar levels of markers irrespective of Dox treatment as confirmed by the MFI graphs (green: unstained, blue: -Dox and red: +Dox) (n=3).

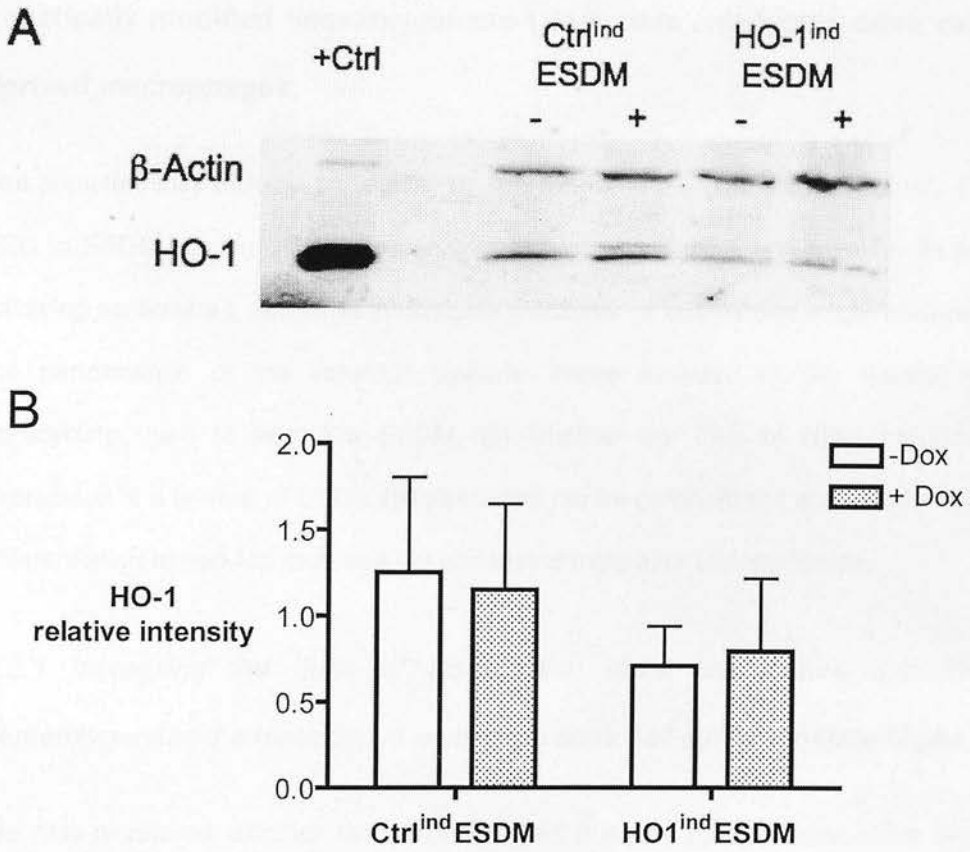

Figure 50: Hemeoxygenase-1 inducible embryonic stem cell-derived macrophages do not induce hemeoxygenase-1 overexpression following Doxycycline treatment.

Ctrl^{ind} and HO-1^{ind} embryonic stem cell-derived macrophages (ESDM) lysates were analysed by Western blot following 24h treatment with Dox (+) or control medium without Dox (-). **A:** Western blot illustrating a low level of HO-1 expression with no upregulation of HO-1 expression by HO-1^{ind} ESDM following Dox treatment (HO-1 positive control is an HO-1 pCAG ESC clone). **B:** Densitometry analysis of the Western blot band analysis where HO-1 relative intensity represents the HO-1 band intensity corrected by the intensity of the β-actin band (n=3).

4.5 Investigating the loss of hemeoxygenase-1 inducibility in genetically modified hemeoxygenase-1 inducible embryonic stem cell-derived macrophages.

The complete loss of HO-1 inducibility by Dox following the differentiation of HO-1^{ind} ESC to ESDM was an unexpected finding and required further investigation. In the following sections we set out to investigate a number of factors that might influence the performance of the inducible system. These included (i) the dosage of tetracycline used to treat the ESDM, (ii) whether the loss of HO-1 inducible expression is a feature of ESDM differentiation *per se* or whether it occurs following differentiation to non-Mφ cells and (iii) underlying molecular biology issues.

4.5.1 Increasing the dose of Doxycycline does not restore inducible hemeoxygenase-1 expression in embryonic stem cell derived macrophages

We first wondered whether the recommended dose of 5μg/ml doxycycline was sufficient to induce HO-1 in the genetically modified ESDM. Therefore, ESDM derived from HO-1^{ind} ESC were treated with increasing doses of tetracycline for 24h (0μg/ml, 5μg/ml, 10μg/ml and 20μg/ml Dox). Western blot analysis shows similar levels of HO-1 expression in HO-1^{ind} ESDM across the various doses of Dox with no evidence of HO-1 overexpression compared to $Ctrl^{ind}$ ESDM (Figure 51). These results raise the possibility that there is a genuine loss of tetracycline inducible HO-1 expression that occurs at some stage along the pathway of Mφ differentiation from the genetically modified ESC.

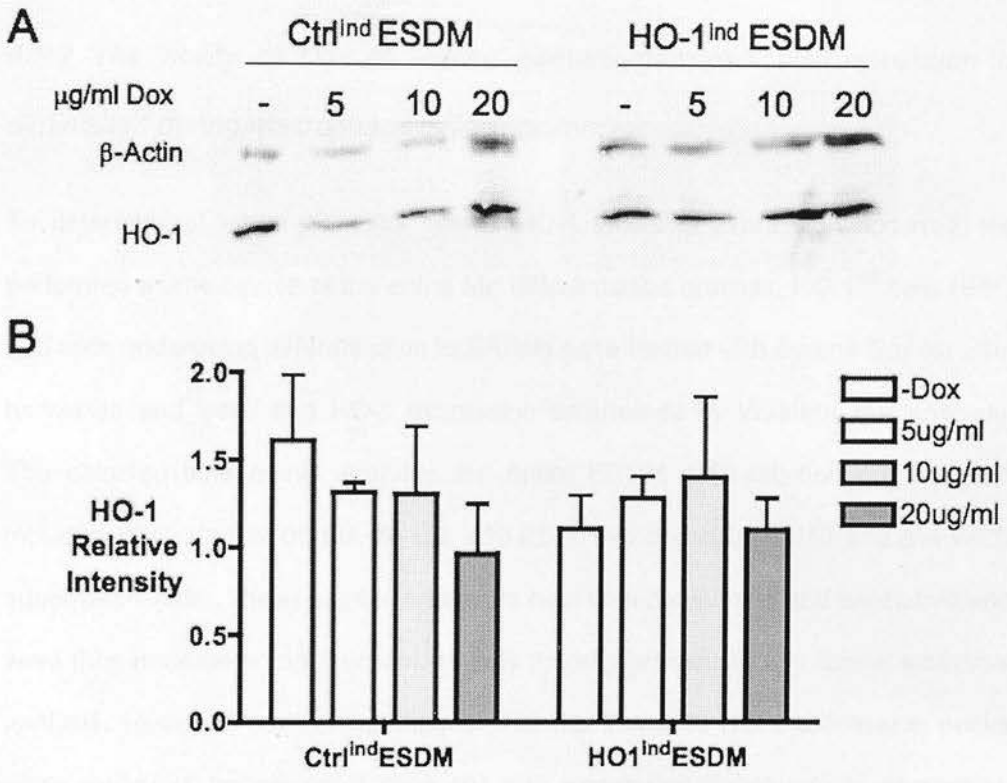

Figure 51: Increasing the dose of Doxycycline does not restore inducible hemeoxygenase-1 expression in genetically modified embryonic stem cell-derived macrophages.

HO-1^{ind} embryonic stem cell-derived macrophages (ESDM) were treated with 0µg/ml, 5µg/ml, 10µg/ml and 20µg/ml of Dox for 24h, harvested and ESDM cell lysates analysed by Western blot analysis. **A:** Representative HO-1 Western blot of HO-1 expression following treatment with increasing doses of Dox. **B:** Densitometry analysis of HO-1 relative intensity based on the HO-1 band analysis corrected for the intensity of the band of the control housekeeping protein β-actin (n=3).

4.5.2 The ability of Dox to induce hemeoxygenase-1 overexpression is diminished during macrophage differentiation

To determine at which point the loss of HO-1 inducible expression occurred, we performed a time course of the entire Mφ differentiation process. HO-1^{ind} cells (ESC and cells undergoing differentiation to ESDM) were treated with 5μg/ml Dox for 24h, harvested and lysed and HO-1 expression determined by Western blot analysis. The selected time points spanned the entire ESDM differentiation process and included ESC, d4 EB, d6 EB, d8 EB, d10 EB, d14 EB and both d10 and d14 MPC supernatant cells. These experiments were both time consuming and expensive and were thus undertaken on 2 occasions only thereby preventing any formal statistical analysis. However, our results suggest that the inducible HO-1 expression peaks when embryoid bodies are 4 days old with expression subsequently decreasing below the induction level of HO-1^{ind} ESC by day 6. By day 10, the inducible Dox-treated cells express low levels of HO-1 that were comparable to the HO-1 expression evident in control cells that were not treated with Dox (Figure 52).

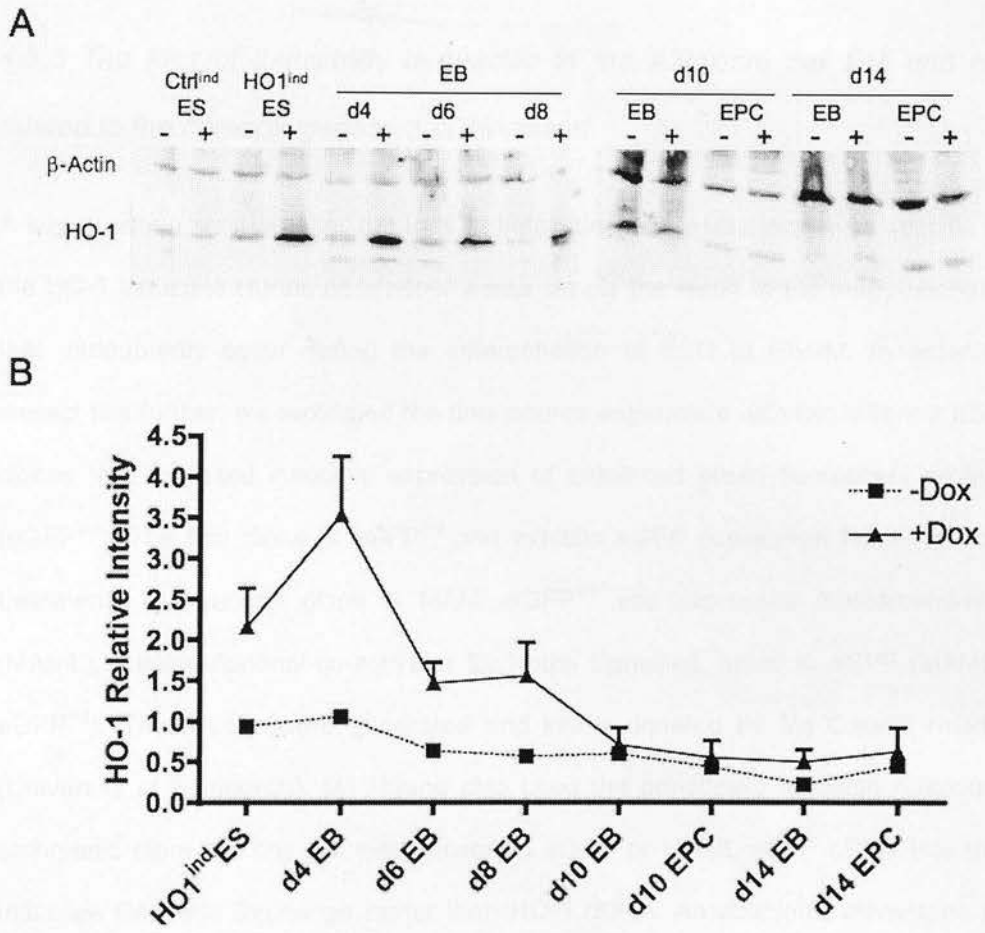

Figure 52: Inducible hemeoxygenase-1 expression decreases from day 4 of embryoid body formation and disappears by day 10.

HO-1^{ind} ESC, d4 embryoid bodies (EB), d6 EB, d8 EB, d10 EB, d14 EB and both d10 and d14 macrophage progenitor supernatant cells (MPC) were treated with 5µg/ml Dox or control media for 24h before being lysed for Western blot analysis of HO-1 expression. **A:** Western blot of the various cells (no Dox (-), 5µg/ml Dox (+)). **B:** Densitometry analysis of HO-1 band with respect to β-actin control (n=2).

4.5.3 The loss of inducibility is specific to the A2lox.cre cell line and not related to the hemeoxygenase-1 cDNA insert.

A key question was whether the loss of inducible gene expression was specific to the HO-1 inducible clones or whether it was simply the result of the many changes that undoubtedly occur during the differentiation of ESC to ESDM. In order to dissect this further, we replicated the time course experiment with two different ESC clones that exhibited inducible expression of enhanced green fluorescent protein ($eGFP^{ind}$). The first clone is $eGFP^{ind}$ and exhibits eGFP expression following Dox treatment. The second clone is MAML-$eGFP^{ind}$ and expresses mastermind-like (MAML), a transcriptional co-activator for Notch signalling, fused to eGFP (MAML-$eGFP^{ind}$). These cells were generated and kindly donated by Ms Caoxin Huang (University of Edinburgh). Ms Huang also used the genetically modified A2lox.cre embryonic stem cell line but either inserted eGFP or MAML-eGFP cDNA into the Inducible Cassette Exchange rather than HO-1 cDNA. An additional advantage of working with eGFP expressing cells is that the induced green fluorescence enables the tracking of any changes in eGFP expression levels by flow cytometry. As previously described, $eGFP^{ind}$ and MAML-$eGFP^{ind}$ cells were treated with 5µg/ml Dox for 24h, harvested and transferred to FACS tubes for flow cytometry analysis. Selected time points covering the whole period of ESC to ESDM differentiation included ESC (d0), d4 EB, d6 EB, d8 EB, d10 and d12 MPC supernatant cells as well as d12 ESDM. We examined our results by two different approaches. Firstly, we plotted the percentage of eGFP positive (% eGFP+) $eGFP^{ind}$ and MAML-$eGFP^{ind}$ cells (Figure 53 and Figure 54). It is striking for both clones that the percentage of eGFP+ cells steadily decreases as soon as the cells start differentiating. 87% $eGFP^{ind}$ ESC exhibited induce expression of eGFP at baseline but this fell to 71.9%

by d4 of the ESDM differentiation process and to below 50% by d6. ESDM differentiated from eGFP^{ind} ESC were predominantly eGFP negative with only 12.7% being eGFP positive. The results from MAML-eGFP^{ind} cells were similar with 86.2% of MAML-eGFP^{ind} ESC cells being eGFP positive at baseline. eGFP positivity gradually fell during the differentiation time course with 26.1% of ESDM being eGFP positive. Thus, the majority of ESDM differentiated from 2 different ESC clones that exhibited strong baseline induction of eGFP expression with Dox treatment do not exhibit induction of eGFP^{ind} following Dox treatment.

Secondly, as the percentage of eGFP+ cells does not indicate the intensity of fluorescence, we also determined the change in eGFP mean fluorescence intensity (MFI) over time (Figure 55). The MFI results for eGFP^{ind} and MAML-eGFP^{ind} cells during the differentiation time course mirrored the previous data. By day 6 of EB formation, the induced eGFP protein expression was drastically reduced compared to that expressed by ESC. Day 12 exhibited a slight augmentation of the eGFP MFI but this was an artefact due to the auto-fluorescence of the ESDM after a total 19 days in culture as it was also seen in HO-1^{ind} cells that do not express eGFP (Figure 56).

Overall, although multiple separate time course experiments were not undertaken, the combined results confirm that the loss of Dox inducibility over time is linked to the differentiation of the genetically modified cell line rather than to the nature of the cDNA insert.

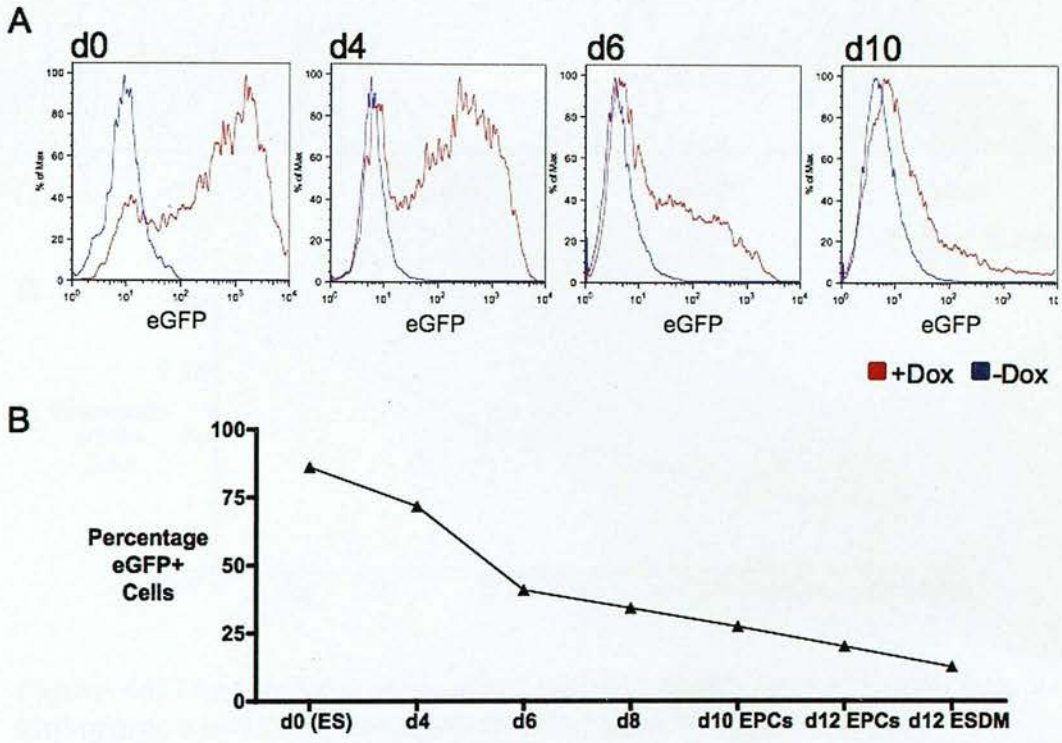

Figure 53: The percentage of eGFP positive eGFP^{ind} cells decreases as embryonic stem cells undergo differentiation to macrophages.

eGFP^{ind} ESC were induced to undergo differentiation to macrophages (ESDM) and cells from different time points of the differentiation process were treated with 5µg/ml Dox for 24h prior to flow cytometry analysis to determine the percentage of eGFP positive cells. **A:** Representative eGFP histograms indicating that eGFP^{ind} cells lose eGFP expression during ESDM differentiation as the shift between Dox treated cells (red line) and control untreated cells (blue line) is progressively reduced from baseline d0 eGFP^{ind} ESC cells to d10 embryoid body (EB) cells. **B:** time course representation of eGFP^{ind} ESDM differentiation shows a gradual fall in the percentage of eGFP positive cells during ESDM differentiation (87% ESC at d0 falling to 12.7% of ESDM) (n=1).

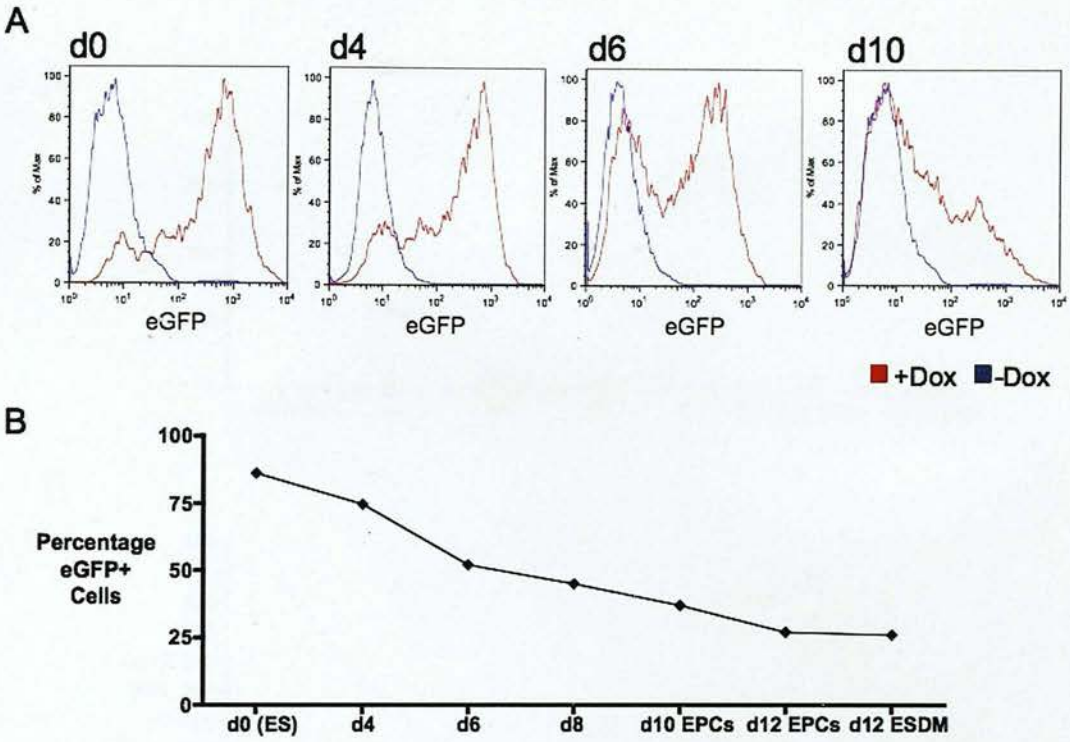

Figure 54: The percentage of eGFP positive MAML-eGFP^{ind} cells falls as embryonic stem cells undergo differentiation to macrophages.

MAML-eGFP^{ind} ESC were induced to undergo differentiation to macrophages (ESDM) and cells from different time points of the differentiation process were treated with 5µg/ml Dox for 24h prior to flow cytometry analysis to determine the percentage of eGFP positive cells. **A:** Representative eGFP histograms indicating that MAML-eGFP^{ind} cells lose eGFP expression during ESDM differentiation as the shift between Dox treated cells (red line) and control (blue line) is progressively reduced from d0 to d10. **B:** time course representation of MAML-eGFP^{ind} ESDM differentiation shows a gradual fall in the percentage of eGFP positive cells (86.2% ESC at d0 falling to 26.1% of ESDM) (n=1).

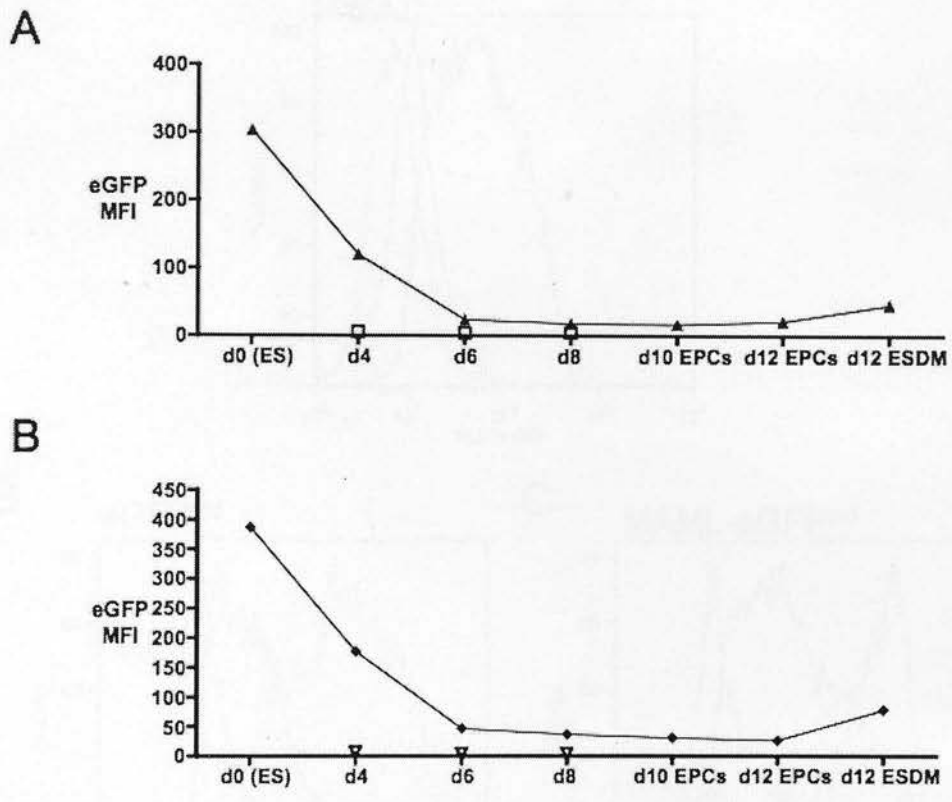

Figure 55: The mean fluorescence intensity of eGFP decreases early during cell differentiation.

eGFP^{ind} ESC or MAML-eGFP^{ind} ESC were induced to undergo differentiation to macrophages (ESDM) and cells from different time points of the differentiation process were treated with 5µg/ml Dox for 24h prior to flow cytometry analysis to determine the mean fluorescence intensity of eGFP expression. **A:** time course of eGFP^{ind} ESDM differentiation indicates that eGFP MFI falls early during the differentiation process and is at a low level by d6. **B:** time course of MAML-eGFP^{ind} ESDM differentiation shows a similar finding with an early decline in eGFP MFI.

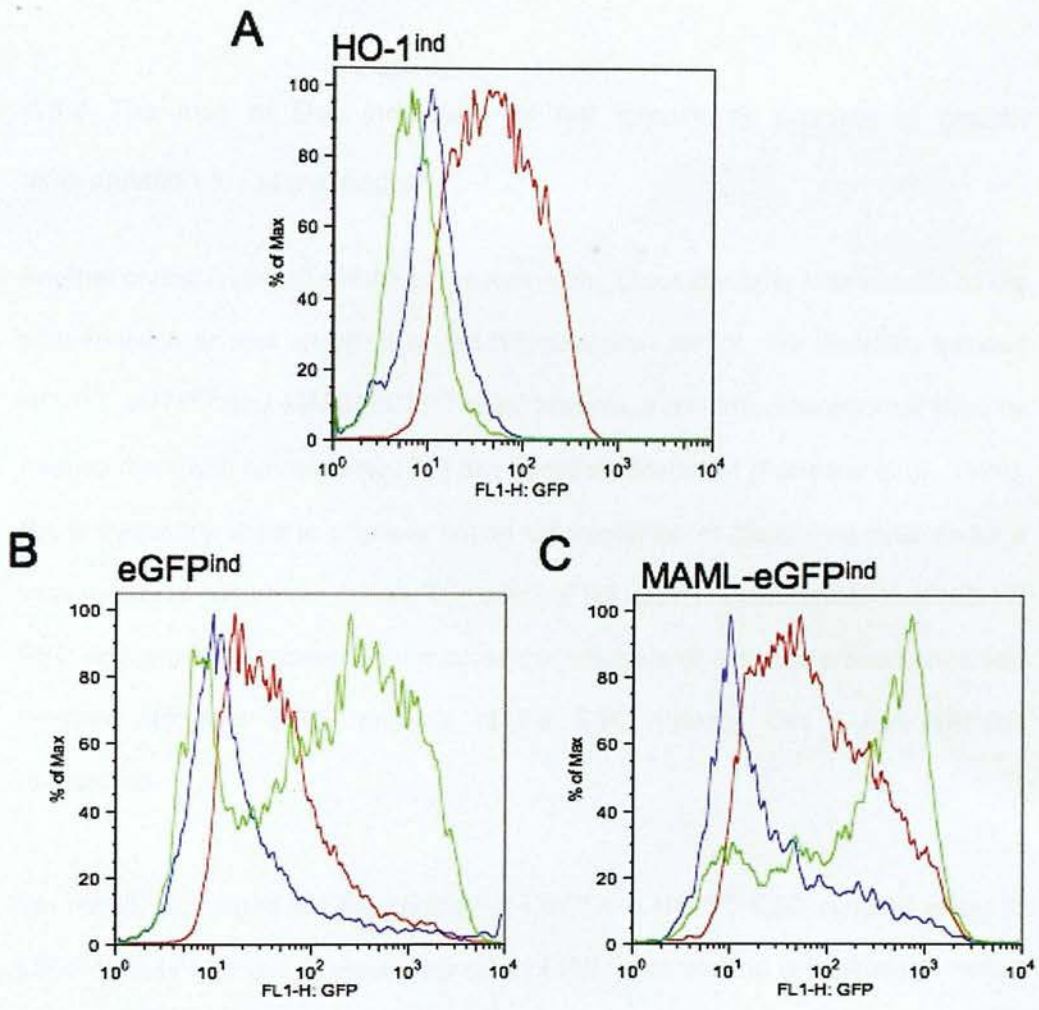

Figure 56: Embryonic stem cell-derived macrophages are autofluorescent.

Flow cytometry histograms of d4 embryoid body (EB) (green), d12 macrophage progenitor cells (MPC) (blue) and d12 embryonic stem cell-derived macrophages (ESDM) (red) following 24 hour treatment with Dox **A:** HO-1^{ind} d12 ESDM (red) exhibit a positive shift in fluorescence but these cells do not express inducible eGFP. The shift is therefore secondary to the intrinsic autofluorescence of d12 ESDM. **B & C:** eGFP^{ind} and MAML-eGFP^{ind} respectively. The eGFP inducible clones express green eGFP protein by d4 EB (green) but not by d12 MPC (blue). The slight shift to the right by the d12 ESDM (red) is similar to the change seen in the HO-1^{ind} cells and so can be attributed to autofluorescence.

4.5.4 The loss of Dox inducibility is not specific to process of cellular differentiation to macrophages

Another crucial issue was whether the loss of the Dox inducibility was specific to Mφ differentiation or was an effect of cell differentiation *per se*. We therefore induced HO-1^{ind}, eGFP^{ind} and MAML-eGFP^{ind} ESC towards a non-Mφ differentiated state by treating them with retinoic acid (RA) as previously described (Forrester et al., 1996). RA is frequently used to promote neural differentiation of pluripotent cells under a wide variety of culture conditions. The effect of RA upon the differentiation of HO-1^{ind} ESC was primarily assessed by microscopic analysis of cytospin preparations and Western blot and qPCR analysis of the ESC markers Oct 4 and NANOG respectively.

We initially compared the morphology of Ctrl^{ind} and HO-1^{ind} ESC cultured either in LIF or treated with RA. Photomicrographs of Diff Quick stained cell cytospins reveal the drastic change in shape and size of the RA treated HO-1^{ind} cells, indicating cell differentiation compared to ESC cultured in LIF (Figure 57).

We then determined the expression of the stem cell transcription factor Oct4 following RA treatment by Western blot analysis. Ctrl^{ind} ESC and HO-1^{ind} ESC were either cultured in LIF or treated with 10^{-6}M RA for 48h to induce cell differentiation. Cells were then lysed and the expression of Oct 4 was determined by Western blot analysis. LIF treated Ctrl^{ind} ESC and HO-1^{ind} ESC exhibited prominent expression of the stem cell marker Oct4. In contrast, Ctrl^{ind} ESC and HO-1^{ind} ESC exposed to RA for 48hrs exhibited a dramatic loss of Oct4 expression indicating the effective induction of cell differentiation by RA (Figure 58).

We also studied the profile of NANOG gene expression levels by real-time quantitative polymerase chain reaction (qPCR) (Figure 59). NANOG gene encodes the NANOG protein that is another transcription factor critically involved with self-renewal of undifferentiated embryonic stem cells. Control E14 IV ESC together with $Ctrl^{ind}$ ESC or HO-1^{ind} ESC were either cultured in LIF or treated with 10^{-6}M RA for 48h to induce cell differentiation. NANOG mRNA expression was determined by qPCR. NANOG mRNA was expressed by all ESC cultured in LIF but expression was completely lost in cells treated with RA. The loss of NANOG expression indicates a loss of the ESC phenotype secondary to RA-induced cell differentiation.

These experiments indicate that RA treated cells adopt a distinct morphology and lose the expression of the ESC markers Oct4 and NANOG indicating that the cells have undergone cell differentiation and are no longer ESC.

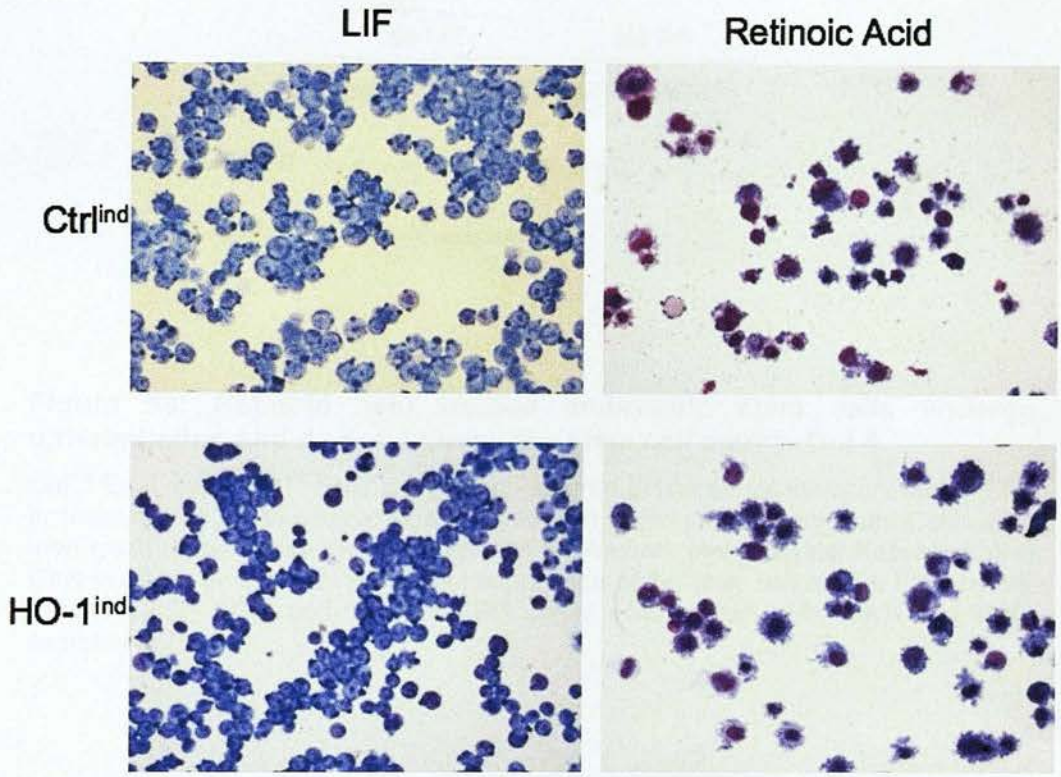

Figure 57: The morphology of retinoic acid treated embryonic stem cells is different to embryonic stem cells cultured in leukaemia inhibitory factor.

$1.5x10^5$ $Ctrl^{ind}$ ESC or HO-1^{ind} ESC were plated in 5% FCS medium for 24h and then treated with 10^{-6}M retinoic acid (RA) for 48h. Control cells were cultured in leukaemia inhibitory factor (LIF) medium alone. Cell cytospins were stained by the Diff Quick method and pictures captured on a Zeiss Axiovert light microscope (200x magnification). A change in the shape and size of the RA treated $Ctrl^{ind}$ ESC and HO-1^{ind} ESC is evident indicating cell differentiation compared to control ESC cultured in LIF.

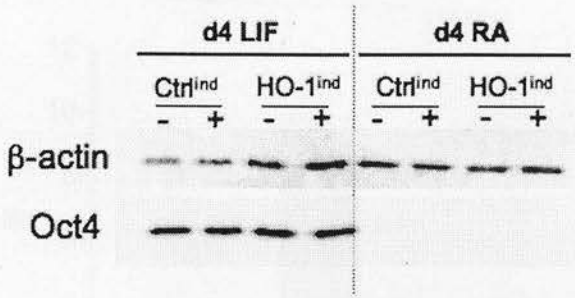

Figure 58: Retinoic acid treated embryonic stem cells undergo differentiation and do not express the stem cell marker Oct 4.

$Ctrl^{ind}$ ESC and HO-1^{ind} ESC were either cultured in leukaemia inhibitory factor (LIF) or treated with 10^{-6}M retinoic acid (RA) for 48h to induce differentiation. Cells were then lysed to determine Oct 4 expression by Western blot analysis. Representative Oct4 Western blot reveals prominent expression of the stem cell marker Oct4 by LIF treated $Ctrl^{ind}$ ESC and HO-1^{ind} ESC whilst RA treated cells have lost Oct4 expression.

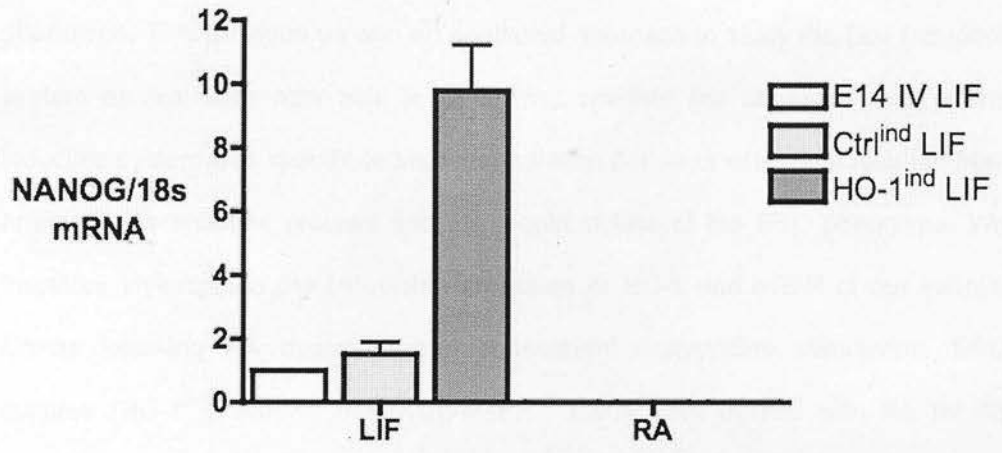

Figure 59: Gene expression of NANOG gene is silenced following retinoic acid treatment of genetically modified embryonic stem cells.

E14 IV ESC, $Ctrl^{ind}$ ESC or HO-1^{ind} ESC were either cultured in leukaemia inhibitory factor (LIF) or treated with 10^{-6}M retinoic acid (RA) for 48h to induce differentiation. The level of NANOG mRNA expression was then determined by qPCR. NANOG mRNA is expressed by all ESC cultured in LIF but is completely silenced following RA treatment indicating a loss of the ESC phenotype secondary to RA-induced cell differentiation (n=1, in triplicate).

The previous experiments indicated that RA treated ESC rapidly lose their stem cell phenotype. This provided us with an additional approach to study the Dox inducible system as we were now able to determine whether the observed loss of the inducible system was specific to Mφ differentiation *per se* or whether it resulted from any cell differentiation process and the resultant loss of the ESC phenotype. We therefore investigated the inducible expression of HO-1 and eGFP of our various clones following RA treatment and subsequent doxycycline stimulation. ESC cultures (HO-1^{ind}, $eGFP^{ind}$ or MAML-$eGFP^{ind}$ ESC) were treated with RA for 48 hours (days 1-3) with cells being exposed to Dox either at day 3 or day 5. After 24 hours of Dox treatment cells were analysed at day 4 or day 6 by flow cytometry (eGFP), Western blotting (HO-1) and qPCR (Figure 60).

Western blot analysis and HO-1 relative intensity graph indicated that HO-1^{ind} embryonic stem cells express stable and relatively high levels of inducible HO-1 when they are maintained in an undifferentiated state by LIF. However, analysis of day 4 and day 6 cells following sequential treatment with both RA and Dox indicated that the level of inducible HO-1 expression falls drastically (Figure 61).

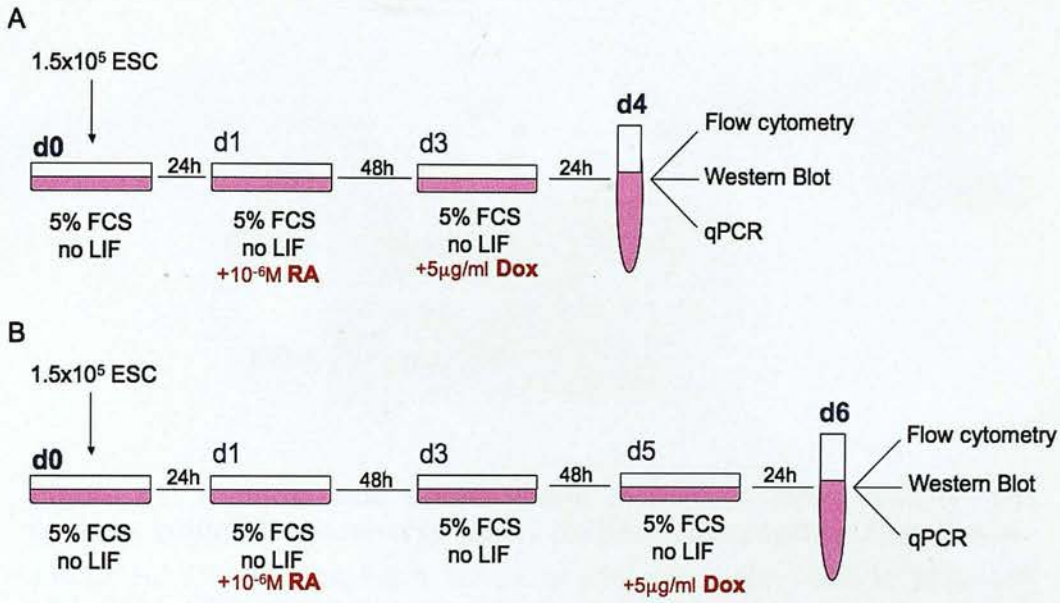

Figure 60: Method for the assessment of inducible expression of HO-1 and eGFP of our various ESC clones following retinoic acid treatment and doxycycline stimulation.

On d0, $1.5x10^5$ ESC were plated on gelatinised tissue culture dishes and incubated at 37°C in 10ml 5% FCS medium for 24h. The medium was then supplemented with Retinoic Acid (RA) at a final concentration of 10^{-6}M for a further 48h. Retinoic acid supplemented medium was subsequently removed and either **A:** replaced by medium containing 5µg/ml Dox for 24h. Following 24h incubation with Dox the medium was removed and the cells harvested at d4; or **B:** RA medium was replaced by Dox-free medium until d5. On d5, medium was supplemented with 5µg/ml Dox with cells being harvested 24 hours later on d6.

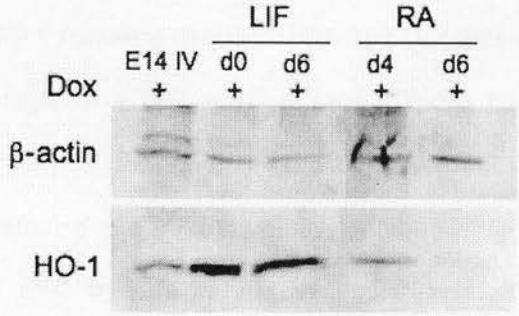

Figure 61: Retinoic acid differentiated embryonic stem cells do not express inducible hemeoxygenase-1 following doxycycline stimulation.

$1.5x10^5$ HO-1^{ind} ESC were left to adhere for 24h, differentiated with 10^{-6}M retinoic acid (RA) for 48h and treated with 5µg/ml Dox for 24h. D0 represents untreated, undifferentiated ESC. HO-1 Western blot: ESC cultured in LIF and treated with 5µg/ml Dox for 24h maintain the capacity to induce HO-1 whilst this is lost following RA-induced cell differentiation (n=1).

Analysis of eGFP expression by flow cytometry was undertaken in a series of experiments with the eGFP^{ind} and MAML-eGFP^{ind} cells. The induction of eGFP^{ind} and MAML-eGFP^{ind} following sequential RA and Dox differentiation, was determined by the percentage of eGFP positive cells (Figure 62) as well as the mean fluorescent intensity of the eGFP (Figure 63). For both clones, the percentage of eGFP+ cells remains stable and relatively high when they are maintained as undifferentiated ESC by LIF. Indeed, around 80% of eGFP^{ind} ESC and MAML-eGFP^{ind} ESC express eGFP with expression being maintained between day 4 and day 6. However, following RA treatment of eGFP^{ind} ESC, the number of eGFP+ cells falls from around 80% to 40% by day 4 and to 20% by day 6. Comparable results were found following RA treatment of MAML-eGFP^{ind} cells with the percentage of eGFP+ cells falling from about 90% to 70% on day 4 and 50% on day 6. Similarly, the eGFP mean fluorescent intensity of RA treated eGFP^{ind} and MAML-eGFP^{ind} ESC decreased following the induction of cell differentiation by RA (Figure 63).

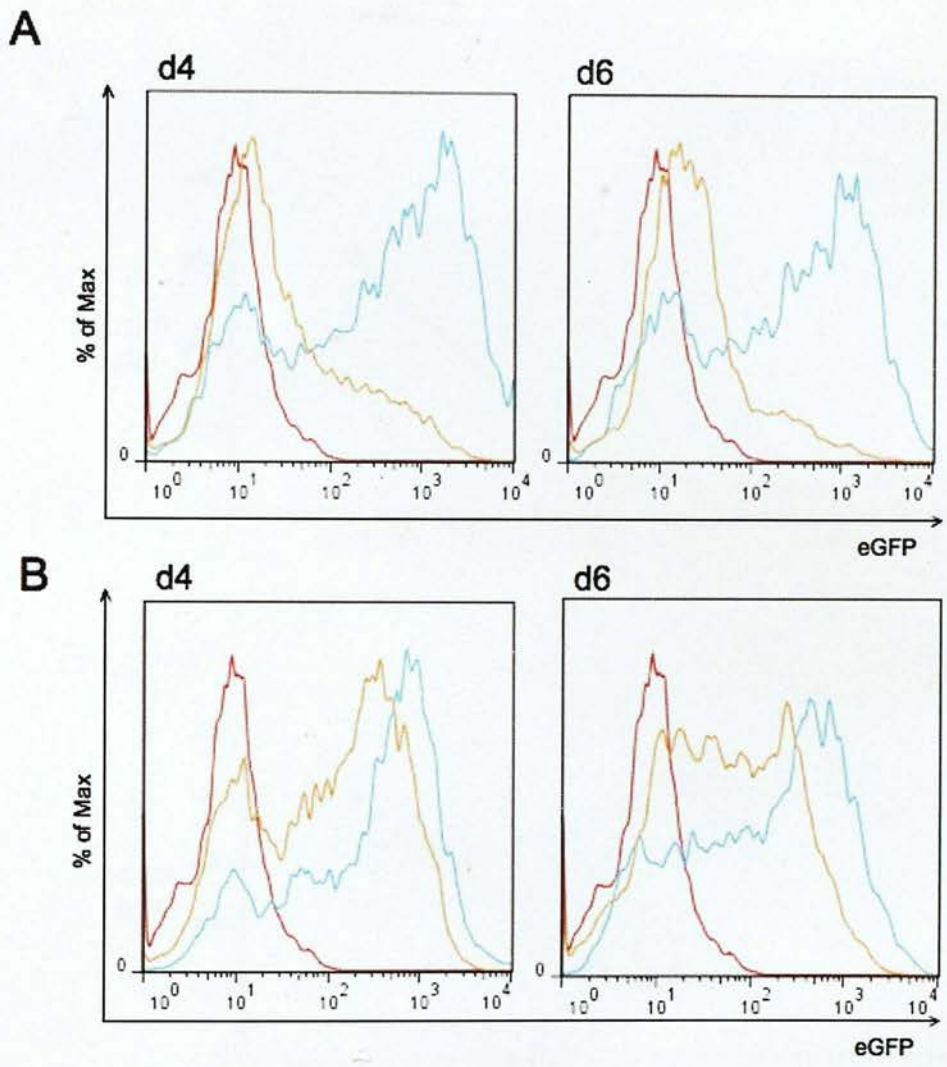

Figure 62: The percentage of eGFP positive cells decreases following retinoic acid differentiation of eGFP^{ind} ESC and MAMI-eGFP^{ind} ESC.

Flow cytometry analysis of the percentage of eGFP positive cells. $1.5x10^5$ eGFP^{ind} ESC and MAMI-eGFP^{ind} ESC were left to adhere for 24h, differentiated with 10^{-6}M retinoic acid (RA) for 48h and treated with 5µg/ml Dox for 24h. The percentage of eGFP+ cells was determined for flow cytometry **A:** eGFP^{ind} ESC **B:** MAML-eGFP^{ind} ESC. Red histograms: ESC not exposed to Dox are eGFP negative. Blue histograms: Dox treatment of LIF treated ESC induced eGFP expression by the majority of cells. Orange histograms: RA treatment of ESC resulted in reduced proportion of cells being eGFP positive with this effect being more evident following RA treatment of eGFP^{ind} ESC. (n=1).

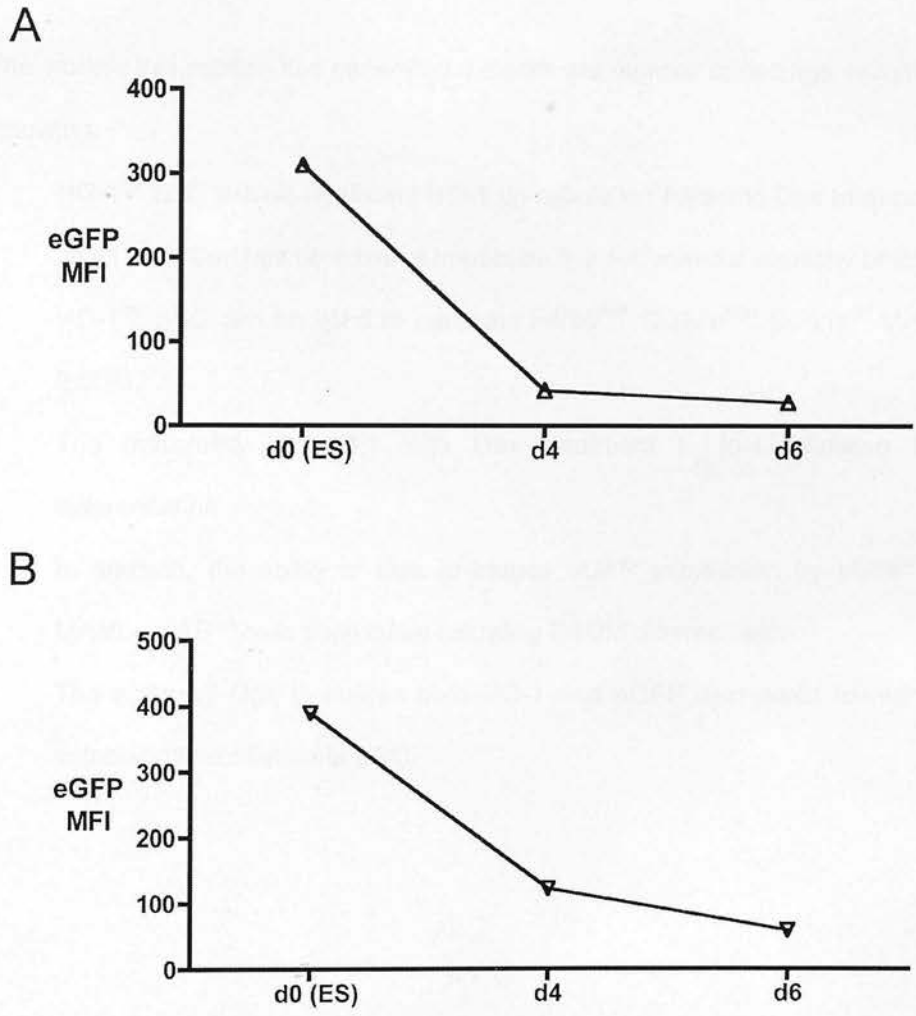

Figure 63: Mean fluorescence intensity of eGFP decreases following retinoic acid differentiation.

Flow cytometry analysis was used to determine the level of expression of eGFP with expression being expressed as mean fluorescence intensity (MFI). Embryonic stem cells (ESC) are differentiated in the presence or absence of 10^{-6}M retinoic acid (RA) for 48h and treated with 5µg/ml Dox for 24h. d0 represents untreated, undifferentiated ESC. **A:** time course of eGFP^{ind} RA differentiated ESC indicates a marked fall in eGFP MFI with RA treatment. **B:** time course of MAML-eGFP^{ind} RA differentiated cells show a similar fall in eGFP MFI with RA treatment. (n=1).

4.6 Summary

The work is this section has generated a significant number of findings including the following:

- HO-1^{ind} ESC exhibit significant HO-1 up-regulation following Dox treatment.
- HO-1 induction has no adverse impact on the self-renewal capacity of ESC.
- HO-1^{ind} ESC can be used to generate F4/80^{high} CD11b^{high} CD11c^{int} MHC II^{low} ESDM.
- The inducibility of HO-1 with Dox treatment is lost following ESDM differentiation.
- In addition, the ability of Dox to induce eGFP expression by eGFP^{ind} and MAML-eGFP^{ind} cells diminishes following ESDM differentiation.
- The ability of Dox to induce both HO-1 and eGFP decreases following RA induced differentiation of ESC.

Chapter 5. Pharmacological induction of hemeoxygenase-1: heme arginate treatment of ESDM.

5.1 Introduction

Heme Arginate (HA) is a stable heme compound (Tenhunen et al., 1987) and approved by the FDA[3] for use in humans. HA (Normosang® trade name) is currently used in the treatment of acute porphyria (Diot et al., 2007). Various studies have shown that HA is a potent inducer of HO-1 expression in rats (Kubulus et al., 2008), mice (Ferenbach et al., 2011) and humans (Doberer et al., 2010) and may exert an anti-inflammatory effect. In this chapter, we examined the effect of HA upon HO-1 expression of both embryonic stem cells (ESC) and embryonic stem cell-derived macrophages (ESDM) and the subsequent modulation of cell phenotype. We hypothesise that HA treatment will result in ESDM adopting an anti-inflammatory phenotype.

5.2 Heme arginate modulates the potential of embryonic stem cells to undergo self-renewal

One unique feature of ESC is their ability to self-renew i.e. engage in cell division while remaining in a pluripotent, undifferentiated state. In a standard ESC self-

---

[3] List of Orphan Products Designation and Approvals. Source: http://www.fda.gov/ohrms/dockets/dailys/00/mar00/030100/lst0094.pdf

renewal assay (see Material and Methods for details), three different types of colonies are discernible: (i) ESC colonies that self-renew and are pluripotent, (ii) mixed colonies comprising of both ESC and differentiated cells and (iii) fully differentiated colonies that have lost pluripotency and contain no ESC. To our knowledge, there are no previous studies of the impact of HA on ESC self-renewal. $1x10^3$ ESC were plated in 6-well plates and cultured for 6 days in ESC medium. On day 5, HA (final concentration 10μM) was added for 24h and the colonies were stained for alkaline phosphatase activity on day 6. The proportion of each type of colony (ESC, mixed or differentiated) was determined (Figure 64). The presence of HA resulted in a small but significant increase in the percentage of ESC colonies (58±2.6 vs. 68±2.3 % ESC colonies; ES vs. ES+HA; p=0.0499, n=3). However, no differences were evident in the proportion of either mixed (p=0.14) or differentiated colonies (p=0.49).

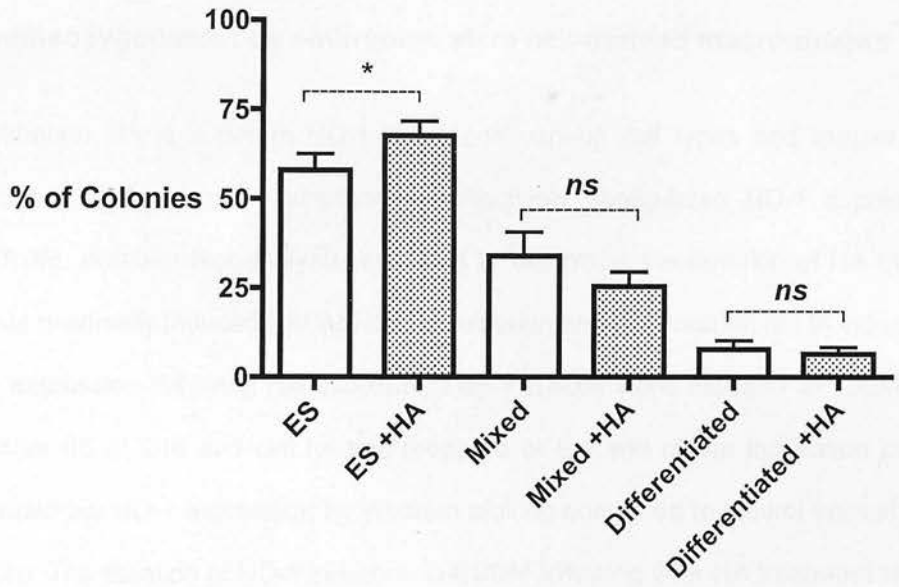

Figure 64: Heme arginate modulates the potential of embryonic stem cell to self-renew.

An embryonic stem cell (ESC) self-renewal assay was performed in the absence or presence of 10mM heme arginate (HA). The percentage of alkaline phosphatase positive ESC colonies was significantly higher when treated with HA for 24h (58±2.6 vs. 68±2.3 % ESC colonies; ES vs. ES+HA; p=0.0499, n=3). No effect upon the percentage of mixed (p=0.1356) or differentiated colonies (p=0.486) was evident (n=3).

5.3 Heme arginate significantly upregulates the expression of hemeoxygenase-1 by embryonic stem cell-derived macrophages

Although HA is a potent HO-1 inducer in various cell types and tissues, it was important to determine whether HA effectively upregulated HO-1 expression in ESDM. Western blot analysis was used to determine the duration of HA treatment that maximally induced ESDM HO-1 expression and the duration of HA induced HO-1 expression following HA exposure. Day 7 ESDM were exposed to 10μM HA for either 6h or 24h and cell lysates prepared at the end of the incubation period to determine HO-1 expression by Western blotting compared to control untreated cells (0h). The duration of HO-1 induction in ESDM following 24hr HA treatment was then determined. Cells were washed after 24h of HA treatment and cell lysates prepared after a further 24h or 48h (Figure 65). Densitometry analysis of the Western blots indicates that HA strongly increases HO-1 expression with the strongest signal evident after 24h HA treatment. Furthermore, HO-1 is still expressed by ESDM 48h following the removal of HA though expression is evidently starting to fall.

A

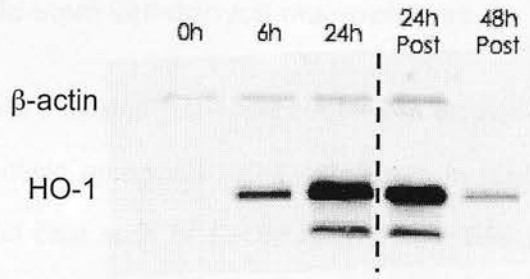

B

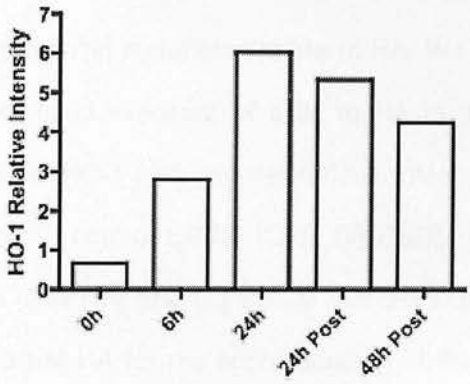

Figure 65: Heme arginate increases expression of hemeoxygenase-1 by embryonic stem cell-derived macrophage.

$0.5x10^6$ embryonic stem cell-derived macrophages (ESDM) were plated down in 6-well plates and treated with 10μM HA for either 6h or 24h with control ESDM not being exposed to HA (0h). In a parallel experiment, ESDM were treated with HA for 24h before washing to remove HA before further culture for 24h and 48h (24 post and 48h post). **A:** HO-1 and β-actin Western blot and **B:** densitometry graph of the relative intensity of HO-1 compared to β-actin. HA increases ESDM HO-1 expression and the ESDM still express HO-1 48h post removal of HA (n=1).

5.4 Study of the effect of heme arginate exposure upon the phenotype of embryonic stem cell-derived macrophages

Previous results indicated that 10μM HA for 24h did not adversely affect ESC self-renewal and could upregulate HO-1 expression by ESDM. The pharmacological manipulation of cells such as ESDM derived from ESC could either include short periods of treatments with HA or other drugs or the inclusion of HA/drug for the entire differentiation period. Also, the administration of several doses of HA over a period of time to experimental mice (or humans) would expose monocytes, mature Mφ and monocytes undergoing maturation to Mφ to HA. We therefore explored the effects of short or prolonged exposure of cells to HA to determine whether the prolonged upregulation of HO-1 had any deleterious effect on ESDM. We set up experiments comprising (i) control ESDM (Ctrl), (ii) ESDM that had been treated with 10μM HA for 24h (24h HA) and (iii) ESDM that were differentiated from ESC cultures exposed to 10 μM HA for the entire duration of the ESDM differentiation process (later referred to as 'HA differentiation')(Figure 66). In this section, we investigated the impact of HA treatment on the phenotype of ESDM and their inflammatory response following stimulation with LPS and IFNγ. The experimental design is depicted in Figure 67.

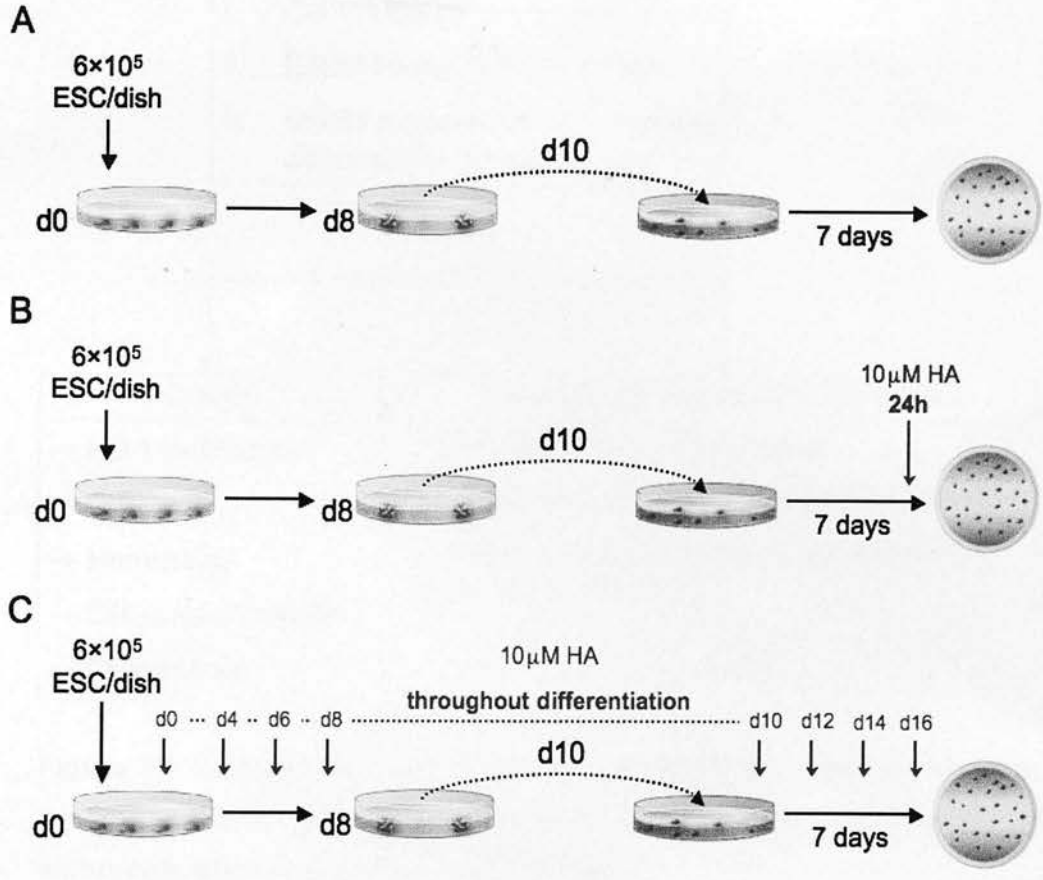

Figure 66: Heme arginate treatment protocols

Embryonic stem cell-derived macrophages (ESDM) were generated as described in the text. **A:** Cells were not exposed to heme arginate (HA) in the 'Control ESDM' differentiation, **B:** '24h HA ESDM' were treated with 10μM HA for 24h on the last day of their differentiation process and **C:** 'HA differentiation ESDM' were cultured in medium supplemented with 10μM HA throughout their differentiation. HA medium was entirely refreshed every second day. (Note: control medium was also refreshed every second day for 'Control' and '24h HA' ESDM).

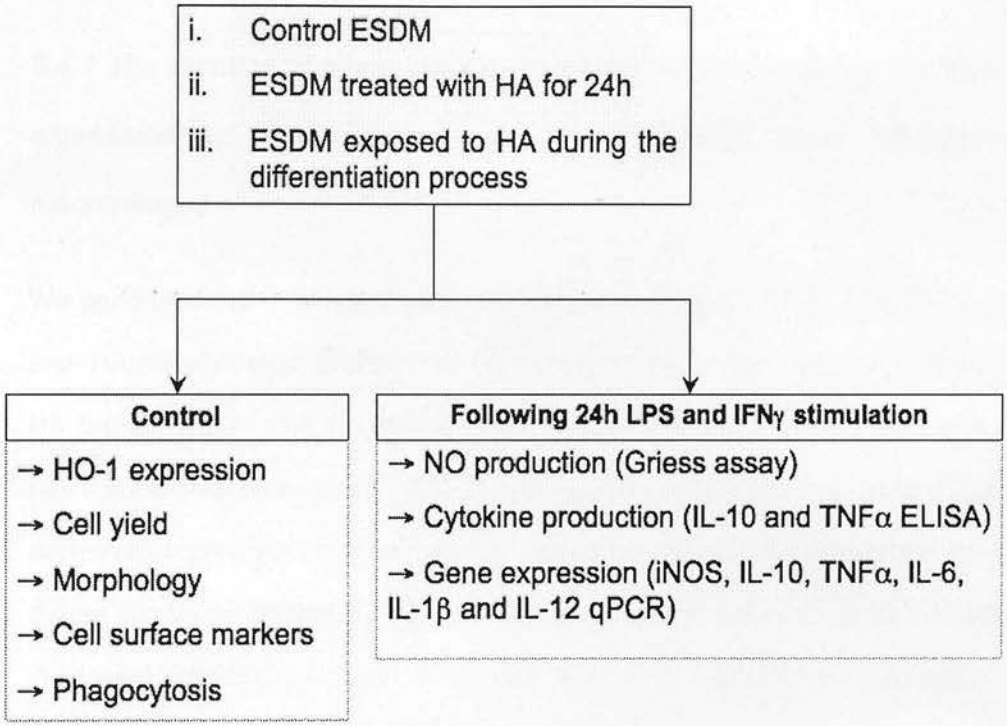

Figure 67: Experimental design for the study of the effect of short or prolonged heme arginate treatment upon the phenotype and function of embryonic stem cell-derived macrophages

5.4.1 The duration of heme arginate exposure has an impact on the level of expression of hemeoxygenase-1 by Embryonic Stem Cell-Derived Macrophages

We performed HO-1 Western blots and qPCR of Control ESDM, '24h HA' ESDM and 'HA differentiation' ESDM. The Western blot shows that cell lysates from 24h HA treated ESDM and HA differentiation ESDM exhibited strong upregulation of HO-1 compared to control ESDM (Figure 68 A). Importantly, the control ESDM expressed a low baseline level of HO-1 expression thereby indicating that the cell culture conditions did lead to HO-1 upregulation via hypoxia or cell stress pathways. In contrast, ESDM treated with HA for only 24h exhibit a striking HO-1 upregulation. ESDM differentiated in the presence of HA also strongly upregulated HO-1 though this is to a lesser extent than that exhibited by 24h HA treated ESDM.

Densitometry was used to analyse the relative intensity of HO-1 expression of 24h HA ESDM and HA differentiation ESDM compared to control ESDM. This analysis indicated that both short and prolonged HA treatment significantly upregulated HO-1 (Control ESDM vs. 24h HA ESDM; $p<0.001$, $n=3$ and Control ESDM vs. HA differentiation ESDM; $p<0.05$, $n=3$) (Figure 68 B). However, these results also underline the fact that HO-1 upregulation is significantly higher when ESDM are treated for 24h compared to ESDM that have undergone the entire differentiation process in the presence of HA (24h HA ESDM vs. HA differentiation ESDM; $p<0.01$, $n=3$).

Finally, HO-1 gene expression analysis indicated a low level of HO-1 mRNA expression in Control ESDM that was in accordance with the Western blot result. Both 24h HA treated ESDM and ESDM differentiated in HA exhibited strong and comparable upregulation of HO-1 mRNA expression (Figure 68 C).

A

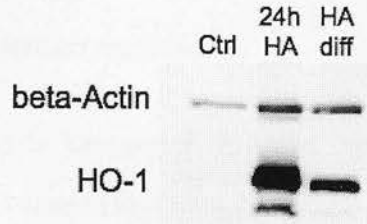

B

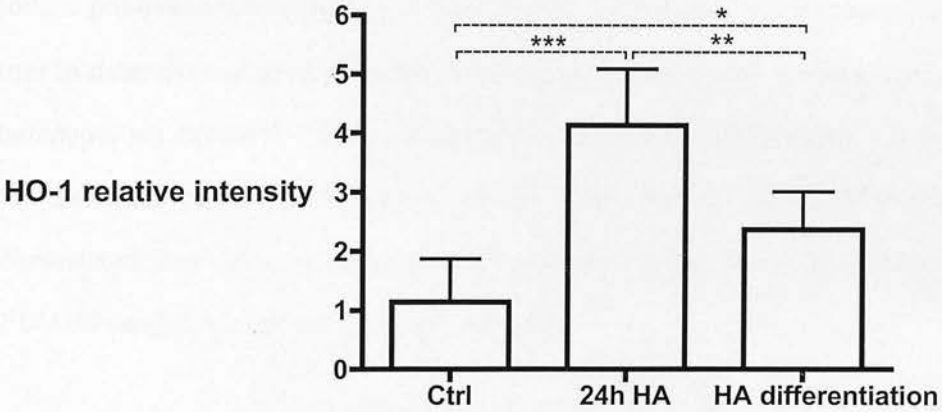

C

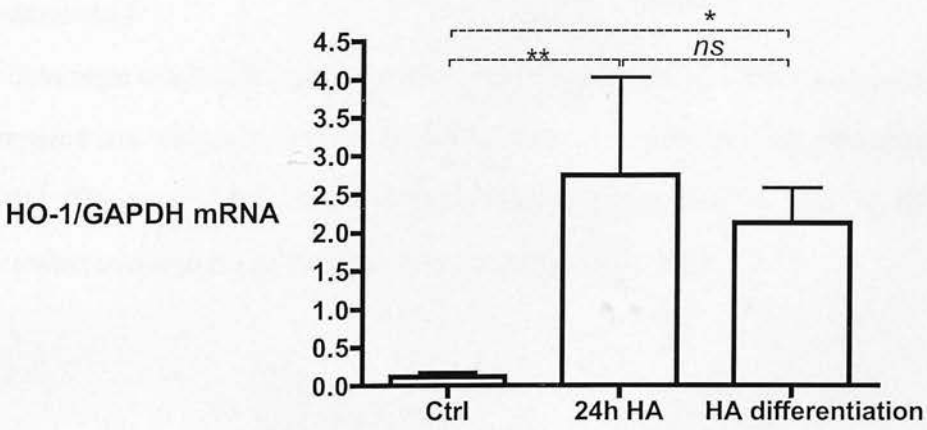

Figure 68: Short or prolonged exposure to heme arginate significantly upregulates hemeoxygenase-1 expression.

A: HO-1 Western blot of untreated control ESDM (Ctrl), ESDM exposed to 10µM HA for 24h (24h HA) and ESDM that were exposed continuously to 10µM HA during their differentiation (HA differentiation). **B:** HO-1 Western blot band intensity analysis corrected for β-actin (n=3). **C:** qPCR results of HO-1 mRNA levels (n=3).

5.4.2 The effect of heme arginate treatment upon the phenotype of embryonic stem cell-derived macrophages

Previous work outlined in Chapter 3 indicated that ESDM are phenotypically comparable to BMDM. ESDM exhibit a Mφ-like morphology, express the classic Mφ cell surface markers F4/80 and CD11b and phagocytose beads. ESDM also produce pro-inflammatory mediators when classically activated by LPS and IFN-γ. In order to determine whether treatment with HA modulates ESDM differentiation and phenotype, we repeated these experiments on (i) control ESDM (Ctrl), (ii) ESDM that have been treated with 10μM HA for 24h (24h HA) and (iii) ESDM that were differentiated from cultures exposed to 10 μM HA for the entire duration of the ESDM differentiation process (HA differentiation).

5.4.1.1 Heme arginate does not influence the yield of embryonic stem cell-derived macrophages

To determine whether HA had any effect upon the number of ESDM generated, we compared the cell yields of control ESDM, 24h HA ESDM and HA differentiation ESDM (Figure 69). No difference was evident in the final number of ESDM generated between the three culture conditions ($p=0.234$, $n=4$).

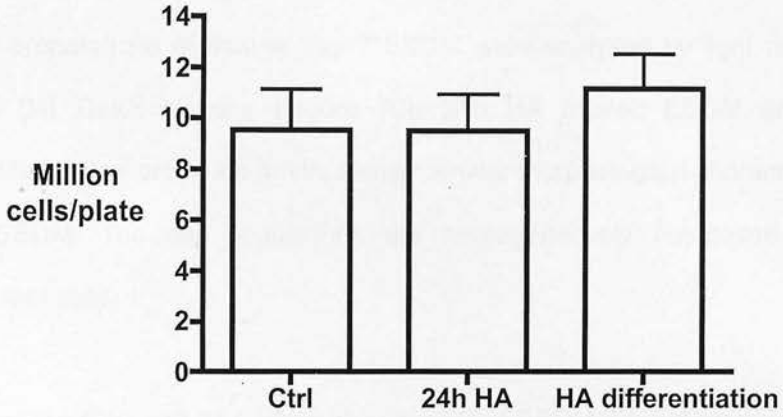

Figure 69: Short or prolonged exposure to heme arginate does not influence the yield of embryonic stem cell-derived macrophages.

The final number of embryonic stem cell-derived macrophages (ESDM) was determined in untreated control ESDM (Ctrl), ESDM exposed to 10μM HA for 24h prior to analysis (24h HA) and ESDM that were exposed continuously to 10μM HA during their differentiation (HA differentiation). The numbers of ESDM generated were comparable under all cell culture conditions. ($p=0.234$, $n=4$).

5.4.1.2 Heme arginate treated embryonic stem cell-derived macrophages exhibit a macrophage-like morphology

Cytospin preparations of mature day 7 ESDM were analysed by light microscopy following Diff Quick staining (Figure 70). 24h HA treated ESDM and ESDM differentiated in the presence of HA display similar morphological characteristics to control ESDM. The cell populations are homogeneously composed of large mononuclear cells.

In addition, the FSC and SSC characteristics of the ESDM were determined by flow cytometry as these reflect cell size and cell granularity respectively. No difference was evident between ESDM preparations neither in FSC nor is SSC analysis ($p=0.135$ and $p=0.051$ respectively, $n=4$) (Figure 71).

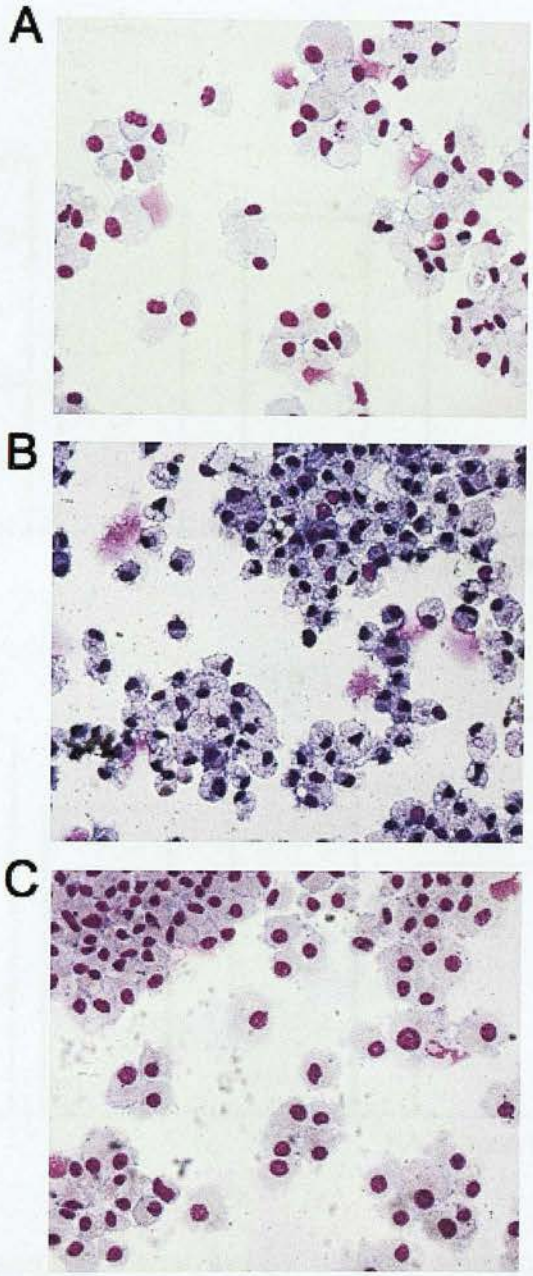

Figure 70: Heme arginate treated embryonic stem cell-derived macrophages exhibit a macrophage-like morphology.

Diff Quick stained cytospin preparations of **A**: control embryonic stem cell-derived macrophages (ESDM), **B**: ESDM treated with heme arginate for 24h and **C**: ESDM differentiated in the presence of heme arginate.

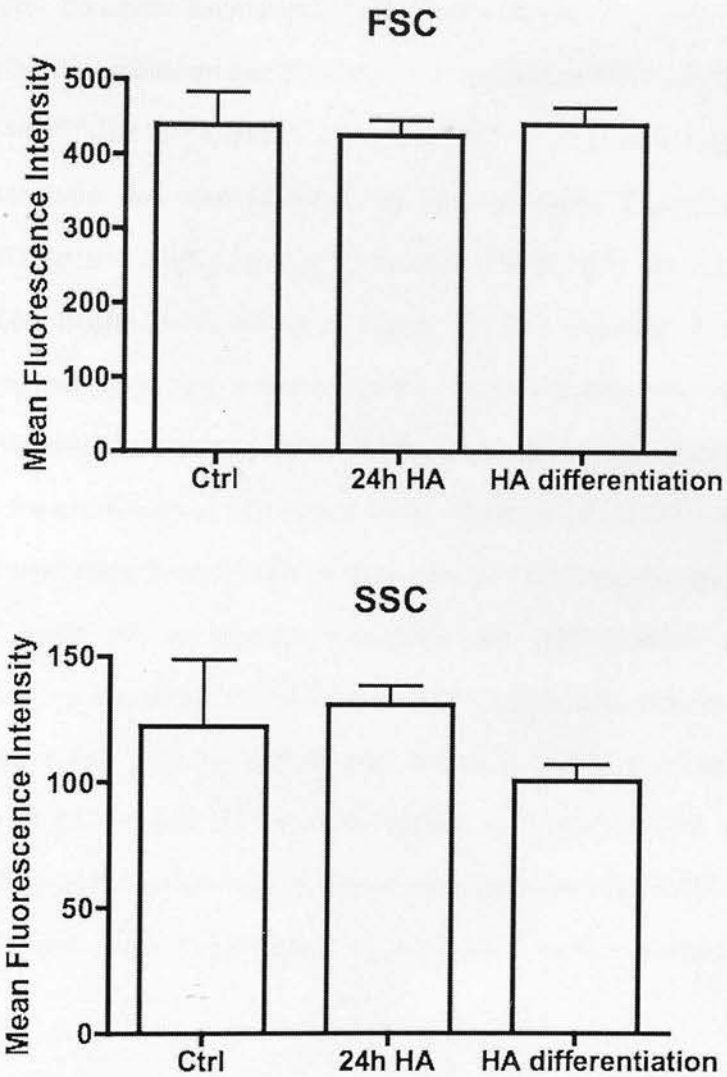

Figure 71: FSC and SSC analysis by flow cytometry: heme arginate does not influence embryonic stem cell-derived macrophage size or granularity.

Control embryonic stem cell-derived macrophages (ESDM), ESDM treated with heme arginate for 24h and ESDM differentiated in the presence of heme arginate underwent flow cytometry analysis. Analysis of the FSC and SSC parameters, which respectively reflect cell size and cell granularity, revealed no significant differences between the groups ($p=0.135$ and $p=0.051$, $n=4$).

5.4.1.3 Exposure to heme arginate during embryonic stem cell-derived macrophage differentiation modulates expression of CD11b and CD11c

In chapter 3, we established that ESDM are comparable to BMDM by flow cytometry and are F4/80^{high}CD11b^{high}CD11c^{high}MHC class II^{low}. The potential impact of HA on ESDM phenotype was also assessed by flow cytometry. Expression of F4/80, CD11b, CD11c and MHC class II for control ESDM, 24h HA ESDM and HA differentiation ESDM is illustrated in Figure 72. The intensity of expression is indicated by the mean fluorescence intensity with all ESDM expressing Mφ cell surface markers. Interestingly, the exposure to HA during ESDM maturation modulates the expression of CD11b and CD11c (both $p<0.0001$) with no effect upon F4/80 and MHC class II expression ($p=0.094$ and $p=0.094$ respectively). The ESDM generated when HA is present throughout the differentiation process are characterised by increased expression of CD11b (HA differentiation ESDM vs. Control ESDM and 24h HA ESDM, both $p<0.001$) and a significantly reduced expression of CD11c (HA differentiation ESDM vs. Control ESDM and 24h HA ESDM, both $p<0.001$). In contrast, the short-term exposure of d7 ESDM to HA for a 24h period exerts no effect upon any of the cell surface markers studied.

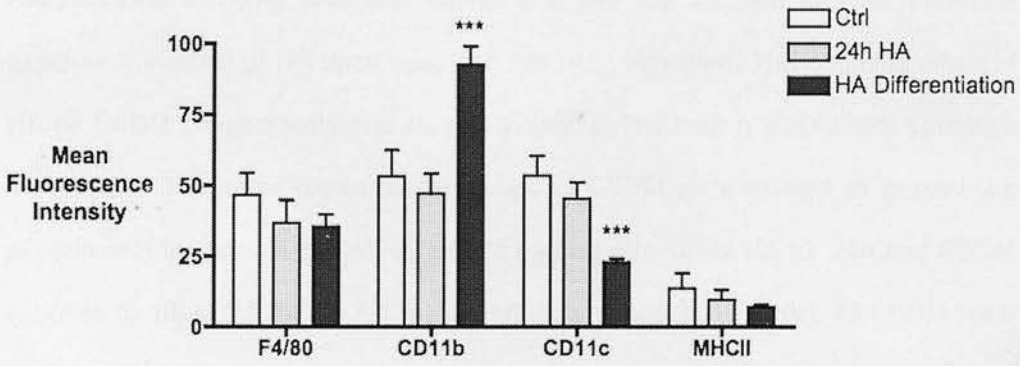

Figure 72: Exposure to heme arginate during embryonic stem cell-derived macrophage differentiation modulates expression of CD11b and CD11c.

The following cells were analysed by flow cytometry to assess the expression of cell surface markers F4/80, CD11b, CD11c and MHC class II: (i) control embryonic stem cell-derived macrophages (ESDM), (ii) d7 ESDM treated with 10μM HA for 24h HA and (iii) ESDM exposed to 10μM HA for the entire differentiation process (17 days). Significant effects are only evident in ESDM exposed to HA during differentiation with significantly increased CD11b expression and decreased CD11c expression (n=4).

5.4.1.4.Heme arginate treated macrophages are significantly more phagocytic

Phagocytosis of dying cells and debris is a key Mφ function and we therefore explored the effect of HA upon apoptotic cell (AC) ingestion. The potential effect of HA on ESDM phagocytosis was studied *in vitro* by incubating ESDM with apoptotic thymocytes. The same experimental groups of ESDM were studied as in previous experiments i.e. control ESDM, d7 ESDM treated with 10μM HA for 24h and ESDM exposed to 10μM HA for the entire differentiation process (17 days). All ESDM were grown on glass coverslips and cultured with fluorescent Cell Tracker green labelled AC for 1h at a ratio of 10 AC per Mφ in order to ensure that the availability of AC was not limiting. ESDM were then labelled with Cell Tracker orange, fixed *in situ* and representative fields captured by a fluorescent microscope. Depending on the colour of the cells i.e. non-ingested AC are green, ingested AC are yellow and non-phagocytic ESDM are orange (Figure 73). Two parameters of phagocytosis were determined: (i) the percentage of ESDM that exhibited phagocytosis and (ii) the mean number of AC ingested by each phagocytic Mφ (the phagocytic index).

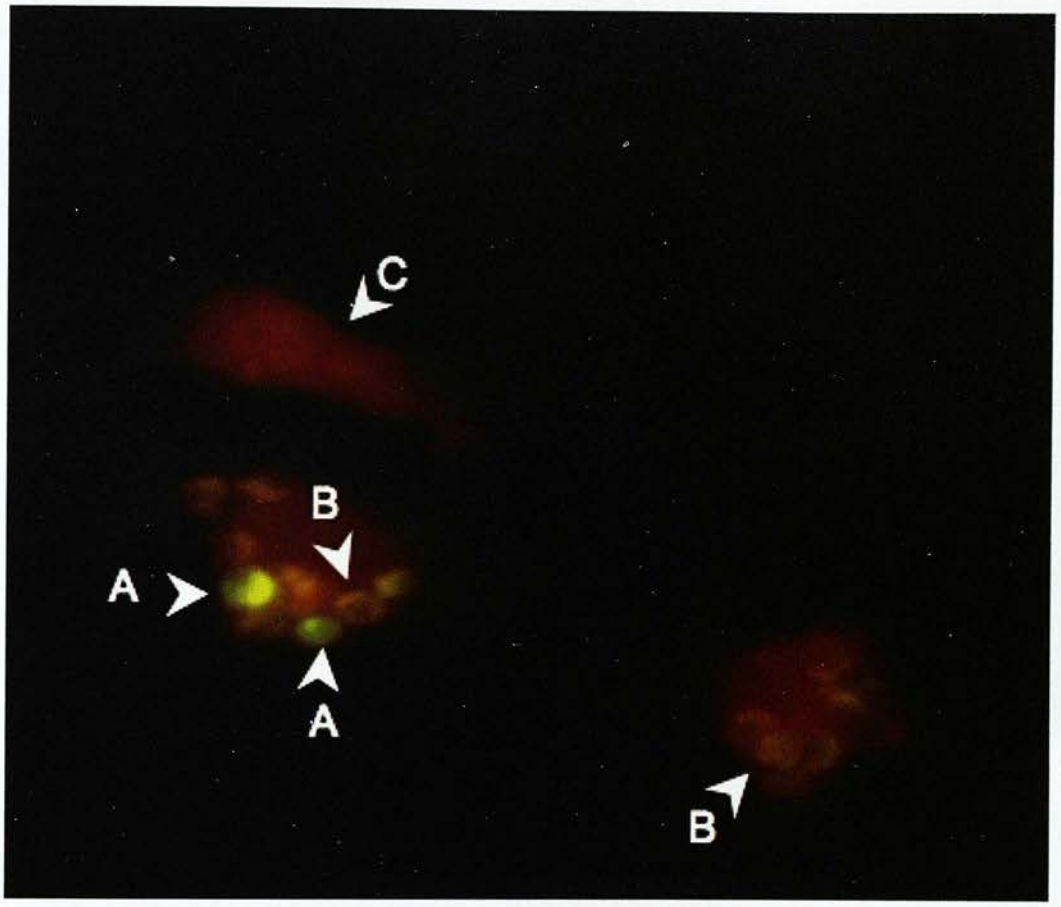

Figure 73: Assessment of macrophage phagocytosis of apoptotic thymocytes by fluorescent microscopy.

Representative fields of bone marrow-derived macrophages (BMDM) cultured on glass coverslips that were exposed to fluorescent green AC for 1h. Macrophages were then labelled with cell tracker orange and fixed *in situ* prior to fluorescent microscopy. **A:** fluorescent green AC bound to the surface of a macrophage remain green whilst **B:** ingested fluorescent green AC appear yellow following phagocytosis by a cell tracker orange labelled macrophage. **C:** Cell tracker orange labelling of the cytoplasm of a non-phagocytic macrophage.

Microscopic analysis indicated that control and HA treated ESDM are notably phagocytic. Control experiments undertaken with metabolically inactive ESDM cultured at 4^0C revealed a minimal interaction between AC and ESDM thereby suggesting that there was very limited non-specific adhesion between the cells (Figure 74). Interestingly, quantification of phagocytosis shows that the proportion of ESDM exhibiting active AC phagocytosis was significantly increased by short 24h HA exposure or long-term HA exposure during the entire period of ESDM differentiation (Control ESDM vs. 24h HA ESDM % phagocytosis; $p<0.05$ and Control ESDM vs. HA differentiation ESDM % phagocytosis; $p<0.001$, $n=4$) (Figure 75). However, there was no significant difference in the percentage of phagocytic cells in 24h treated ESDM compared to HA differentiation ESDM cultures ($p>0.05$). These data indicate that exposure of ESDM to HA results in a greater proportion of ESDM exhibiting the ability to recognise, bind and ingest AC and is in accord with previous data from our group indicating that murine BMDM adenovirally transduced to overexpress HO-1 exhibited increased phagocytosis (Ferenbach et al., 2010).

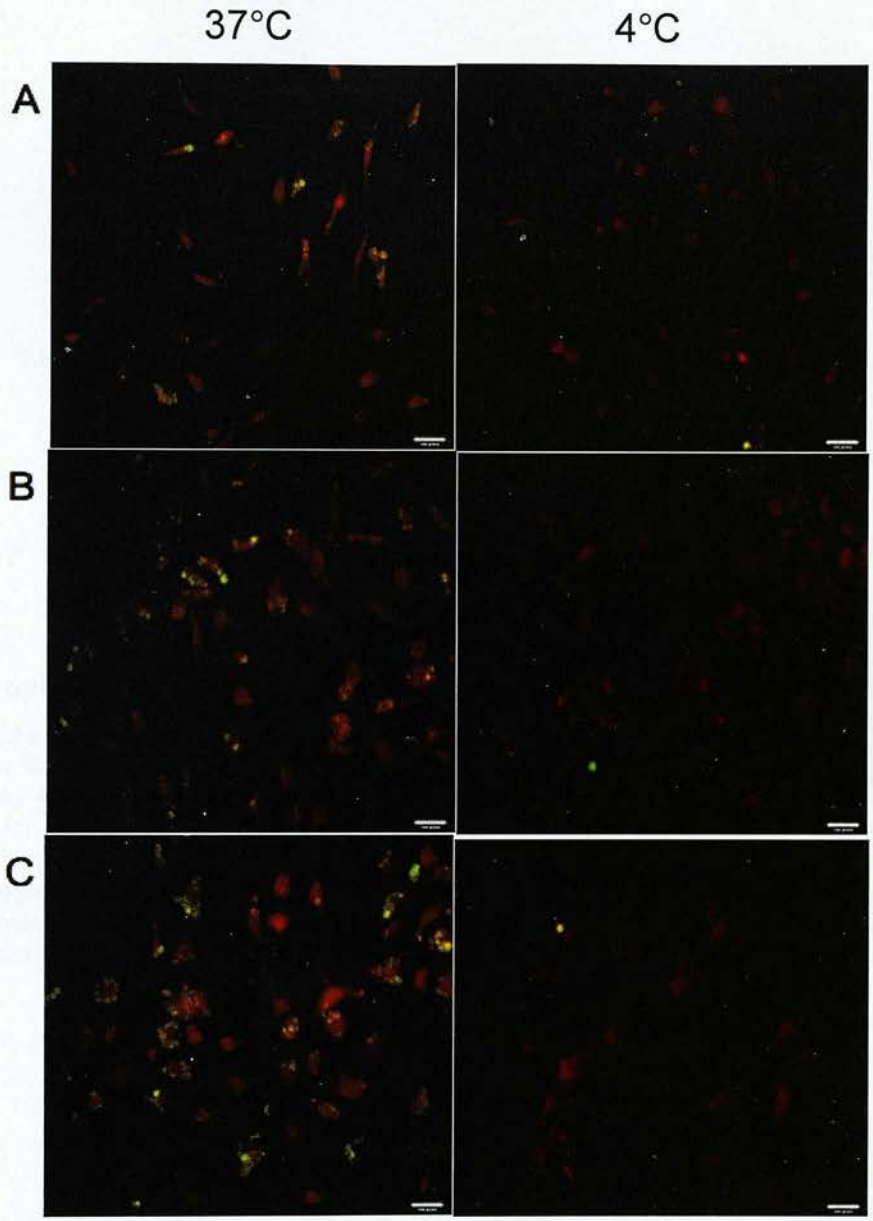

Figure 74: Control and heme arginate treated embryonic stem cell-derived macrophages phagocytose apoptotic thymocytes.

Embryonic stem cell-derived macrophages (ESDM) were cultured on glass coverslips and incubated with fluorescent green apoptotic cells for 1h at 37^0C or 4^0C, labelled with cell tracker orange then fixed *in situ* for further analysis by fluorescent microscopy. **A:** Control ESDM **B:** ESDM exposed to HA for 24h **C:** ESDM exposed to HA during the entire differentiation process. All ESDM populations ingest AC at 37^0C whilst minimal AC ingestion is evident at 4^0C.

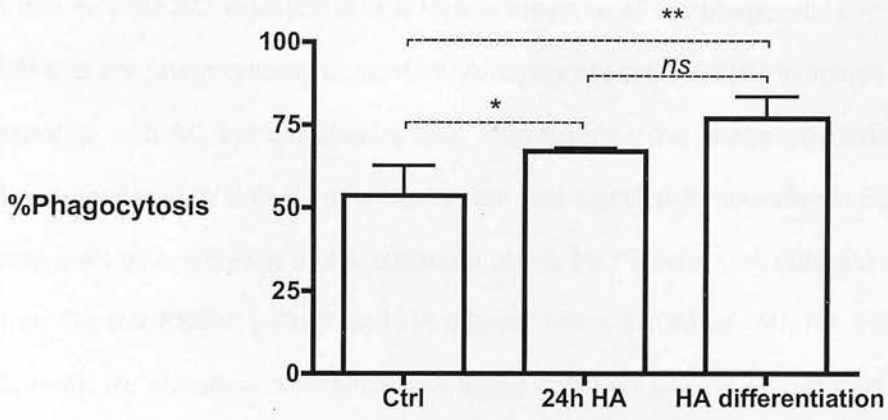

Figure 75: Heme arginate treated embryonic stem cell-derived macrophages exhibit increased phagocytosis of apoptotic thymocytes.

Control embryonic stem cell-derived macrophages (ESDM) (Ctrl), ESDM exposed to HA for 24h (24hr HA) and ESDM exposed to HA during the entire differentiation process (HA differentiation) were incubated with fluorescent green apoptotic cells (AC) for 1h at 37^0C and the proportion of ESDM exhibiting AC phagocytosis quantified by fluorescent microscopy. Short-term or long-term exposure of ESDM to HA significantly increased ESDM phagocytosis compared to control ESDM. However, there was no statistical difference in the percentage of phagocytic cells between 24h HA exposure and exposure to HA during the ESDM differentiation.

The phagocytic index is a measure of the mean number of AC ingested by each ESDM that exhibits AC ingestion and is thus a measure of the phagocytic capacity of ESDM that are phagocytically competent. Analysis of control ESDM indicated that they ingested ~2.5 AC per cell (Figure 76). Interestingly, the phagocytic index of ESDM was unaltered by 24h exposure to HA but was significantly elevated in ESDM that underwent differentiation in the presence of HA for 17 days (HA differentiation ESDM vs. Control ESDM; $p<0.01$ and HA differentiation ESDM vs. 24h HA ESDM; $p<0.05$, $n=4$). No statistical difference was noted between Control ESDM and 24h HA ESDM ($p>0.05$). Thus, although short-term exposure to HA increases the proportion of ESDM able to recognise and ingest AC, the phagocytic index is only increased by exposure of cells to HA during the ESDM differentiation process.

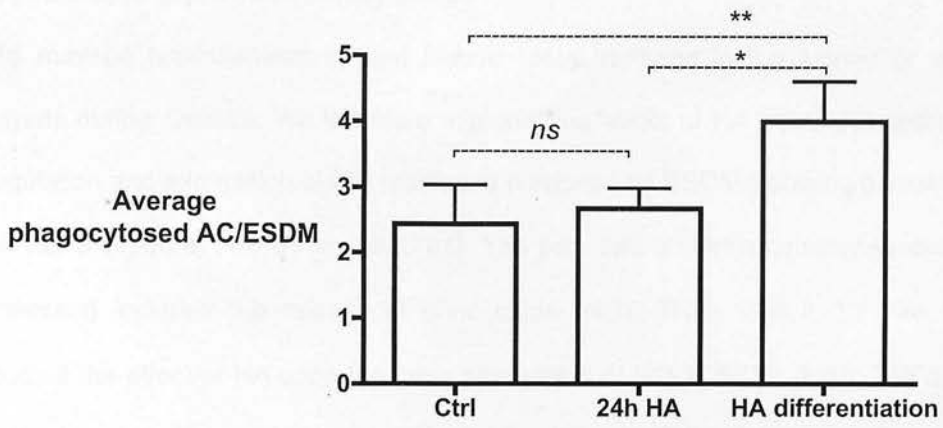

Figure 76: Exposure to heme arginate during embryonic stem cell-derived macrophage differentiation increases the phagocytic index for apoptotic thymocytes.

Control embryonic stem cell-derived macrophages (ESDM) (Ctrl), ESDM exposed to HA for 24h (24hr HA) and ESDM exposed to HA during the entire differentiation process (HA differentiation) were incubated with fluorescent green apoptotic cells (AC) for 1h at 37^0C and the mean number of AC ingested per phagocytic ESDM was quantified by fluorescent microscopy. Short-term exposure of ESDM to HA had no effect upon the phagocytic index compared to control ESDM. In contrast, exposure to HA during the ESDM differentiation process significantly increased the phagocytic index of ESDM compared to control ESDM ($p<0.01$) and 24h HA ESDM ($p<0.05$).

5.4.1.5 Heme arginate modulates the response of embryonic stem cell-derived macrophages to pro-inflammatory stimuli

Mφ may be pro-inflammatory and induce tissue damage in the kidney or other organs during disease. We therefore explored the effect of HA treatment upon the regulation and expression of key mediators produced by ESDM following stimulation with LPS (1μg/ml) and IFN-γ (100U/ml). The pro- and anti-inflammatory mediators assessed included the release of nitric oxide (NO), TNFα and IL-10. We also studied the effect of HA upon the gene expression of HO-1, iNOS, IL-10, TNFα, IL-6, IL-1β and IL-12 following the treatment with LPS and IFN-γ.

5.4.1.5.1 Heme arginate treated embryonic stem cell-derived macrophages produce less nitric oxide following treatment with LPS and IFNγ

Control ESDM (Ctrl), ESDM exposed to HA for 24h (24hr HA) and ESDM exposed to HA during the entire differentiation process (HA differentiation) were exposed to LPS (1μg/ml) and IFNγ (100U/ml) for 24h and then the cell culture supernatants were collected and nitrite quantified by the Griess method. Treatment with LPS and IFNγ induced significant NO production from control ESDM. However, exposure of ESDM to HA for 24h or during the entire differentiation period resulted in a significant reduction in NO production (Control ESDM vs. 24h HA ESDM; $p<0.05$ and Control ESDM vs. HA differentiation ESDM; $p<0.01$, $n=4$) (Figure 77). The duration of exposure to HA had no significant effect upon NO production with comparable NO production by ESDM exposed to HA for 24 hr or during the differentiation period. These results indicate that HA exposure significantly reduces ESDM production of NO and exerts an anti-inflammatory effect of HA that may well be secondary to the upregulation of HO-1.

5.4.1.5.2 Prolonged HA exposure significantly downregulates iNOS gene expression following stimulation with LPS and IFNγ

We then explored the effect of HA upon the expression of iNOS mRNA. Interestingly, our results reveal differing effects of the HA treatment protocol upon the mRNA expression of iNOS. Prolonged exposure of ESDM to HA during the differentiation process modulates the iNOS gene expression with significant downregulation of iNOS mRNA expression evident following LPS and IFNγ stimulation ($p<0.05$, $n=4$) (Figure 78). In contrast, 24h treatment of ESDM with HA had no effect upon iNOS mRNA expression despite the reduction in NO production detected by the Griess assay. Thus, the more prolonged exposure of cells to HA resulted in downregulation of iNOS gene. Interestingly, despite the differential effect of short or long-term HA exposure upon the expression of iNOS mRNA, there was no significant difference evident in the nitrite generated by '24 hour' ESDM and 'HA differentiation' ESDM.

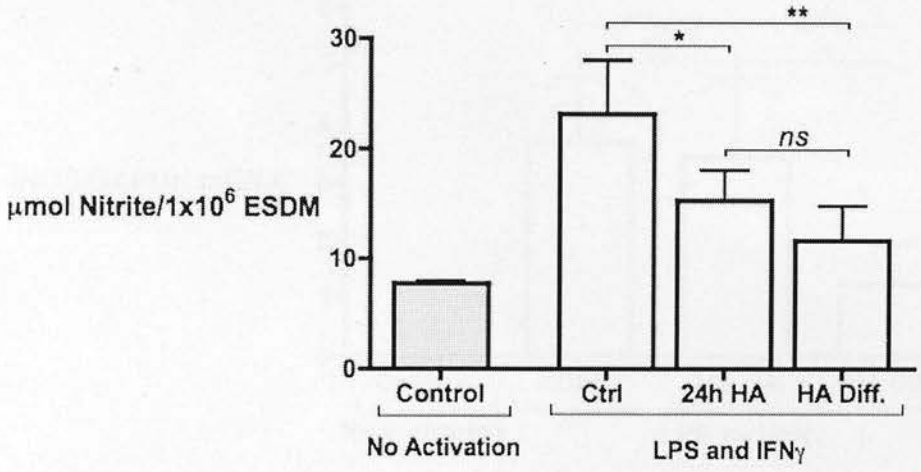

Figure 77: Heme arginate treated embryonic stem cell-derived macrophages produce significantly less nitric oxide following LPS and IFNγ activation.

Control embryonic stem cell-derived macrophages (ESDM) (Ctrl), ESDM exposed to HA for 24h (24hr HA) and ESDM exposed to HA during the entire differentiation process (HA differentiation) were exposed to LPS (1μg/ml) and IFNγ (100U/ml) for 24h. Nitric oxide generation was measured by a Griess assay of ESDM cell culture supernatants. Non-stimulated ESDM do not generate significant NO. HA treated ESDM released significantly less NO than untreated control ESDM. The duration of HA exposure did not affect the NO produced (n=4 in each group).

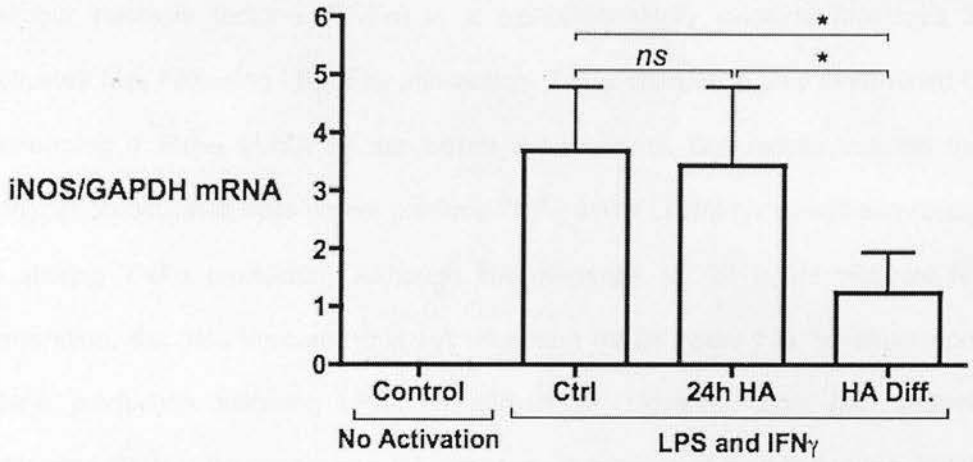

Figure 78: Prolonged heme arginate exposure of embryonic stem cell-derived macrophages significantly downregulates iNOS gene expression following LPS and IFNγ stimulation.

Control embryonic stem cell-derived macrophages (ESDM) (Ctrl), ESDM exposed to HA for 24h (24hr HA) and ESDM exposed to HA during the entire differentiation process (HA differentiation) were exposed to LPS (1µg/ml) and IFNγ (100U/ml) for 24h at which time the expression of iNOS mRNA was determined. Non-stimulated ESDM do not express iNOS mRNA. LPS/IFNγ markedly increased iNOS mRNA expression with 24 hour HA treatment having no inhibitory effect. However, ESDM exposed to HA during differentiation exhibit significantly reduced iNOS gene expression compared to both Control ESDM and 24h HA ESDM (both $p<0.05$, $n=4$).

5.4.1.5.3 Prolonged heme arginate exposure significantly downregulates TNFα production by embryonic stem cell-derived macrophages following LPS and IFNγ stimulation

Tumour necrosis factor-α (TNFα) is a pro-inflammatory cytokine produced by activated Mφ. Following LPS/IFNγ stimulation, TNFα production was determined by performing a TNFα ELISA on the ESDM supernatants. Our results indicate that control non-activated cells do not produce TNFα whilst LPS/IFNγ stimulation results in striking TNFα production. Although HA treatment for 24 hours reduces NO generation, the data indicated that HA treatment for 24 hours has no effect upon TNFα production following LPS/IFNγ stimulation. However, *post hoc* analysis highlights the fact that prolonged HA exposure is capable of modulating the ESDM phenotype regarding TNFα production with reduced TNFα release observed in ESDM exposed to HA during differentiation ($p=0.0155$, $n=4$) (Figure 79).

5.4.1.5.4 Heme arginate has no impact on TNFα gene expression by embryonic stem cell-derived macrophages following LPS and IFNγ stimulation

In addition to measuring release of TNFα we also examined TNFα mRNA expression by the various ESDM. LPS/IFNγ stimulation induced marked upregulation of TNFα mRNA. However, statistical analysis of the relative TNFα mRNA levels did not reveal any difference between control ESDM, ESDM exposed to HA for 24h and ESDM exposed to HA during the entire differentiation process ($p=0.8049$) (Figure 80). These data suggested that the prolonged exposure of ESDM to HA might modulate TNFα production at a post-translational level.

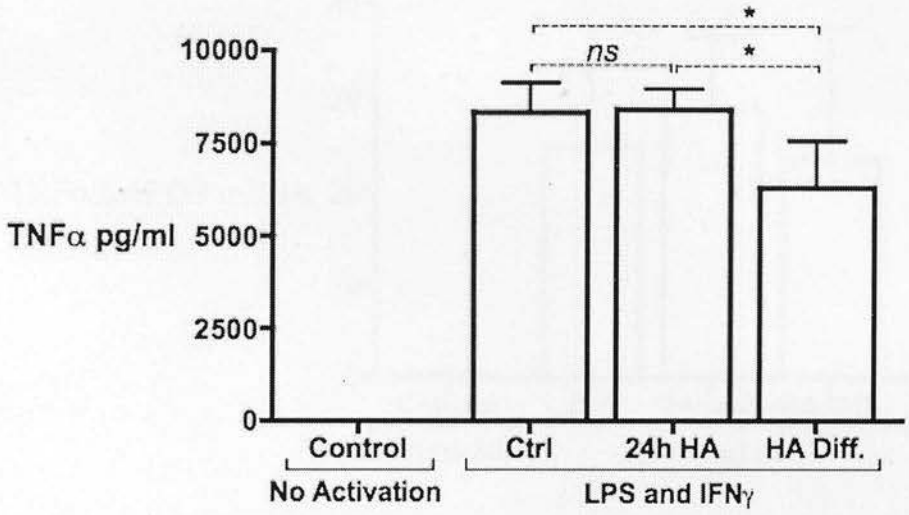

Figure 79: Prolonged heme arginate exposure of embryonic stem cell-derived macrophages significantly downregulates TNFα production following LPS and IFNγ stimulation.

Control embryonic stem cell-derived macrophages (ESDM) (Ctrl), ESDM exposed to HA for 24h (24hr HA) and ESDM exposed to HA during the entire differentiation process (HA differentiation) were exposed to LPS (1µg/ml) and IFNγ (100U/ml) for 24h at which time the production of TNFα was determined by ELISA of cell culture supernatants. Non-stimulated ESDM do not produce TNFα. LPS/IFNγ markedly increased TNFα production with 24 hour HA treatment having no effect ($p>0.05$, $n=4$). ESDM exposed to HA during differentiation exhibit significantly reduced TNFα production compared to both Control ESDM and 24h HA ESDM ($n=4$).

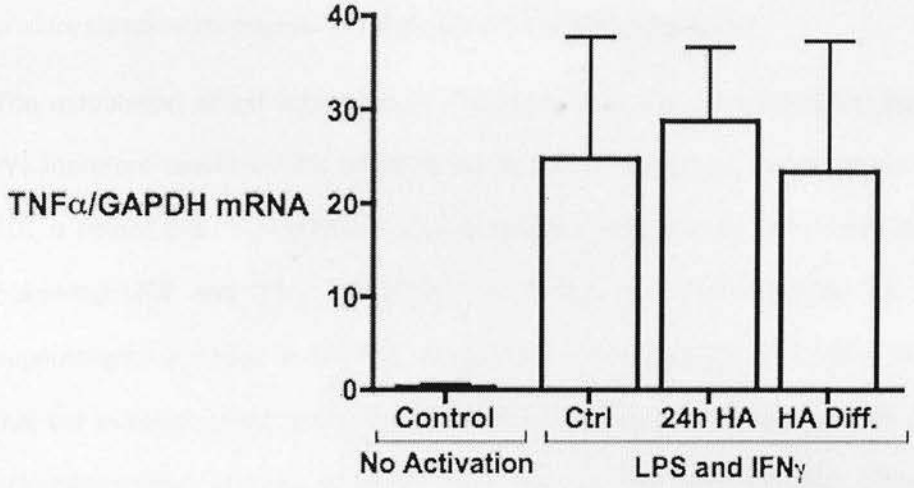

Figure 80: Heme arginate treatment of embryonic stem cell-derived macrophages has no significant impact on TNFα gene expression following LPS and IFNγ stimulation.

Control embryonic stem cell-derived macrophages (ESDM) (Ctrl), ESDM exposed to HA for 24h (24hr HA) and ESDM exposed to HA during the entire differentiation process (HA differentiation) were exposed to LPS (1µg/ml) and IFNγ (100U/ml) for 24h at which time the expression of TNFα mRNA was determined. Non-stimulated ESDM do not express TNFα mRNA. One-way ANOVA revealed that HA has no impact on TNFα gene expression as all the groups have statistically comparable means (p=0.8049)

5.4.1.5.5 Embryonic stem cell-derived macrophages treated with heme arginate for 24h produce significantly more IL-10 following LPS and IFNγ stimulation

The modulation of anti-inflammatory mediators may also be biologically important. We therefore examined the effect of HA upon the production of interleukin-10 (IL-10), a potent anti-inflammatory cytokine released primarily by monocytes and Mφ. Following LPS and IFNγ stimulation, an ELISA was performed on the ESDM supernatants to detect IL-10. The previous data regarding NO and TNFα indicated that the inclusion of HA during ESDM differentiation exerted a comparable or more anti-inflammatory marked effect compared to 24h treatment with HA. Intriguingly, this was not the case for IL-10 as only the 24h HA treatment resulted in a significant increase in IL-10 production (both Control ESDM vs. 24h HA ESDM and 24h HA ESDM vs. HA differentiation ESDM: $p<0.001$, $n=4$) (Figure 81).

5.4.1.5.6 Prolonged heme arginate exposure significantly downregulates IL-10 gene expression by embryonic stem cell-derived macrophages following LPS and IFNγ stimulation

In addition to measuring release of IL-10 we also examined IL-10 mRNA expression by the various ESDM. LPS/IFNγ stimulation induced marked upregulation of IL-10 mRNA (Figure 82). Interestingly, despite increasing IL-10 release into the supernatant, 24 hour treatment with HA had no significant effect upon IL-10 mRNA expression. Furthermore, prolonged exposure to HA during the ESDM differentiation process significantly reduced IL-10 gene expression following LPS and IFNγ stimulation compared to control ESDM ($p<0.05$, $n=4$) despite that fact that comparable levels of immunoreactive IL-10 were secreted into the cell culture supernatant.

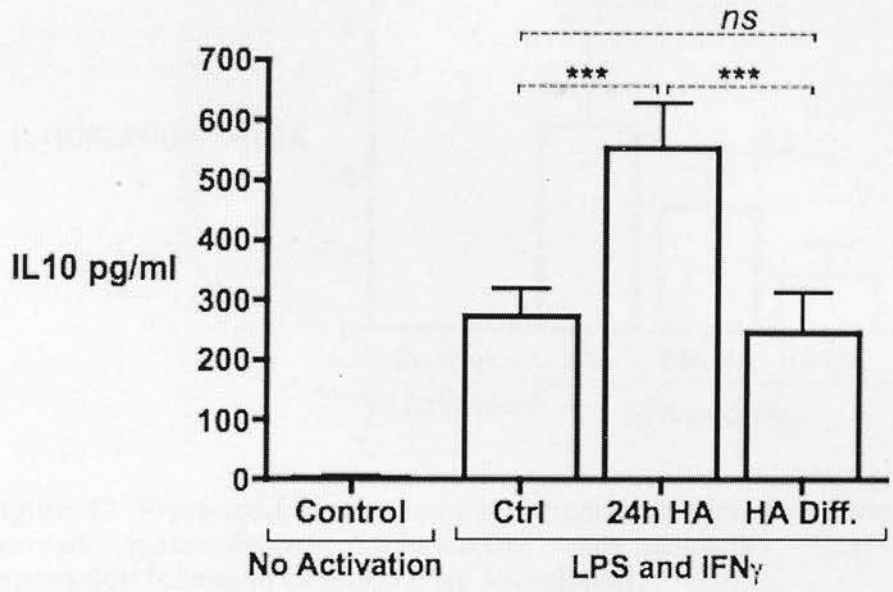

Figure 81: Embryonic stem cell-derived macrophages treated with heme arginate for 24h produce significantly more IL-10 following LPS and IFNγ stimulation.

Control embryonic stem cell-derived macrophages (ESDM) (Ctrl), ESDM exposed to HA for 24h (24hr HA) and ESDM exposed to HA during the entire differentiation process (HA differentiation) were exposed to LPS (1µg/ml) and IFNγ (100U/ml) for 24h at which time the production of IL-10 was determined by ELISA of cell culture supernatants. Non-stimulated ESDM do not produce IL-10. 24h HA treated ESDM release significantly more IL-10 than both Control ESDM and HA differentiation ESDM ($p<0.001$, $n=4$). There is no statistical difference in IL10 production from Ctrl vs. HA differentiation ESDM ($p>0.05$, $n=4$).

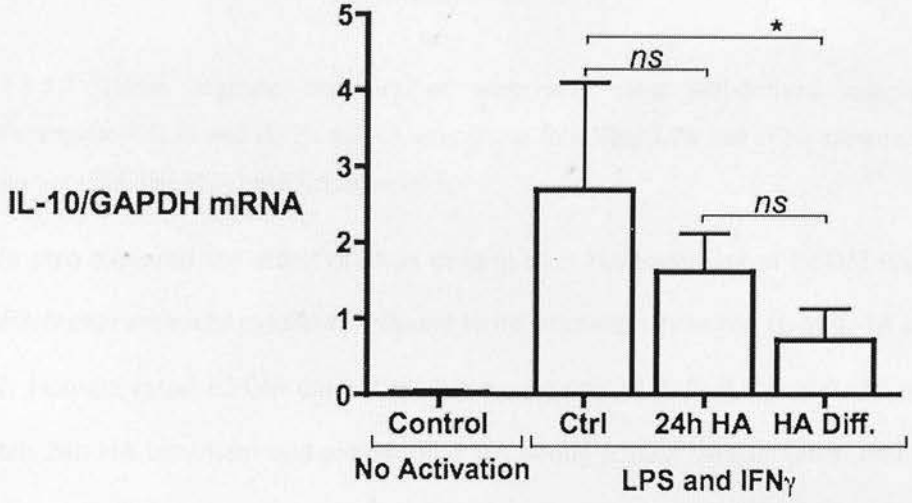

Figure 82: Prolonged heme arginate exposure of embryonic stem cell-derived macrophages significantly downregulates IL-10 gene expression following LPS and IFNγ stimulation.

Control embryonic stem cell-derived macrophages (ESDM) (Ctrl), ESDM exposed to HA for 24h (24hr HA) and ESDM exposed to HA during the entire differentiation process (HA differentiation) were exposed to LPS (1µg/ml) and IFNγ (100U/ml) for 24h at which time the expression of IL-10 mRNA was determined. Non-stimulated ESDM do not express IL-10 mRNA. HA differentiated ESDM exhibited a significantly decrease in IL-10 gene expression following LPS and IFNγ stimulation compared to Control ESDM ($p<0.05$, $n=4$). No statistical differences were noted between Control ESDM and 24h HA ESDM or between 24h HA ESDM and HA differentiation ESDM (all $p>0.05$, $n=4$).

5.4.1.5.7 Heme arginate exposure of embryonic stem cell-derived macrophages downregulates IL-6 and IL-1β mRNA expression following LPS and IFNγ stimulation but does not modulate IL-12 mRNA expression

We also explored the effect of short or long-term HA treatment of ESDM upon the mRNA expression of cytokines relevant to inflammation including IL-6, IL-1β and IL-12. Non-activated ESDM did not exhibit expression of IL-6, IL-1β or IL-12 mRNA. Both 24h HA treatment and exposure to HA during ESDM differentiation resulted in a very significant downregulation of both IL-6 (both $p<0.01$, $n=4$) and IL-1β mRNA expression ($p<0.05$, $n=4$) following LPS and IFNγ stimulation compared to Control ESDM. No statistically significant differences in IL-6 or IL-1β mRNA levels were noted between 24h HA ESDM and HA differentiation ESDM ($p>0.05$, $n=4$) indicating that HA exposure alone is enough to have an impact on the expression of these cytokine genes. In contrast, HA treatment has no impact on IL-12 gene expression as all the groups have statistically comparable means ($p=0.4921$) (Figure 83).

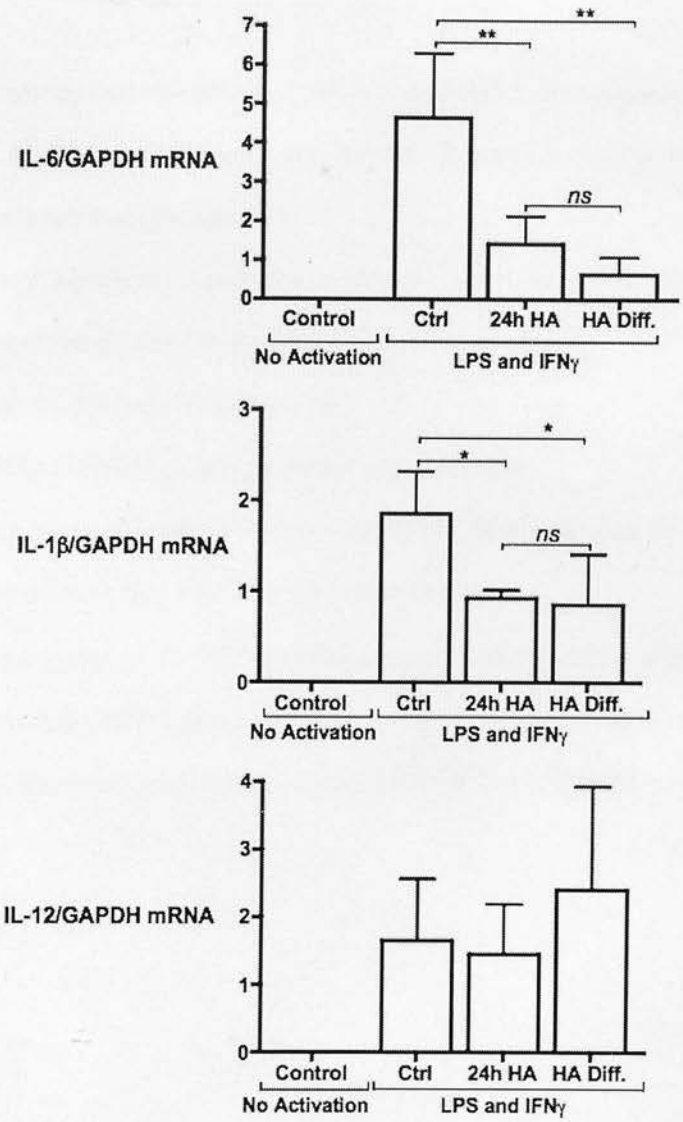

Figure 83: Heme arginate exposure downregulates IL-6 and IL-1β gene expression following LPS+IFNγ stimulation but has no effect on IL-12.

Control embryonic stem cell-derived macrophages (ESDM) (Ctrl), ESDM exposed to HA for 24h (24hr HA) and ESDM exposed to HA during the entire differentiation process (HA differentiation) were exposed to LPS (1µg/ml) and IFNγ (100U/ml) for 24h at which time the mRNA expression for IL-6, IL-1β and IL-12 was determined. Non-stimulated ESDM do not express IL-6, IL-1β and IL-12 mRNA. HA treatment significantly downregulated both IL-6 and IL-1β gene expression following LPS and IFNγ stimulation but has no effect on IL-12 gene expression.

5.5 Summary

In this chapter, we investigated the effect of HA induced HO-1 upregulation upon both the behaviour of ESC and subsequent ESDM phenotype. Using various techniques, we have shown that HA treatment:

- Exerts a mild though significant effect upon embryonic stem cell self renewal
- Significantly upregulates ESDM HO-1 protein and gene expression
- Does not influence ESDM yield or morphology
- Enhances the ability of ESDM to phagocytose apoptotic cells
- Modulates the pro- and anti-inflammatory response of ESDM following LPS and IFNγ stimulation regarding NO, TNFα and IL-10 production
- Modulates the expression of pro-inflammatory and anti-inflammatory genes by significantly upregulating HO-1 gene expression and downregulating iNOS, IL-10, IL-6 and IL-1β gene expression following LPS and IFNγ stimulation.

Chapter 6. Development of a model of acute kidney injury in 129/P2 mice and the localisation of embryonic stem cell derived macrophages *in vivo*

6.1 Introduction

One of our aims was to administer control and HO-1 over-expressing ESDM to mice with acute kidney injury (AKI) in order to determine their effect upon renal injury and dysfunction. The embryonic stem cells used for our experiments have been generated using the 129/P2 mouse strain. Previous work in the group had used the FVB/NJ mouse strain for experiments involving AKI and this raised the issue of whether it was possible to administer 129/P2 ESDM to FVB/NJ mice without detrimental effects upon the administered cells that would be discerned as 'foreign'. Rather then exploring whether this strain mismatch was possible in the relatively short time frame of the proposed experiments, we decided to avoid the possibility of inducing an inflammatory and immunological response and cellular rejection by establishing the model of renal ischaemia/reperfusion injury (IRI) in 129/P2 mice. It was thus necessary to determine the period of ischaemia that resulted in the appropriate level of AKI in 129/P2 mice.

In this chapter, we outline the initial development and validation of an *in vivo* model of renal IRI in the 129/P2 mouse strain. This model will enable us to study the potential anti-inflammatory properties of control and HO-1 over-expressing ESDM in AKI.

6.2 The severity of acute kidney injury in 129/P2 mice is influenced by gender and duration of ischaemia.

Initial experiments determined the effect of gender and duration of ischaemia upon the severity of AKI in 129/P2 mice aged 6 to 8 weeks. The ideal model would exhibit clear and reproducible injury with demonstrable acute tubular necrosis (ATN) and significant elevation of the serum creatinine. However, the level of injury would be important as the induction of very severe injury might make it difficult to see the beneficial impact of the administered cells. The unilateral surgical model of IRI was adopted. This includes performing a right nephrectomy at the time of the operation such that the mouse develops an elevated serum creatinine that is used to quantify the severity of acute renal failure. Following a right nephrectomy, the left renal pedicle that contains the renal artery and vein is clamped for varying periods of time. The clamp is removed and the kidney reperfused for 24h. 24 hours following reperfusion, the kidney was harvested to determine the extent of tissue injury by determining the ATN score and blood was collected to determine the serum creatinine to assess renal function (Figure 84). This model of renal injury is temperature sensitive with increased body temperature of the mouse being associated with increased injury. Therefore the temperature of the mouse was maintained at 37°C throughout the procedure using a rectal probe and a homeothermic blanket system.

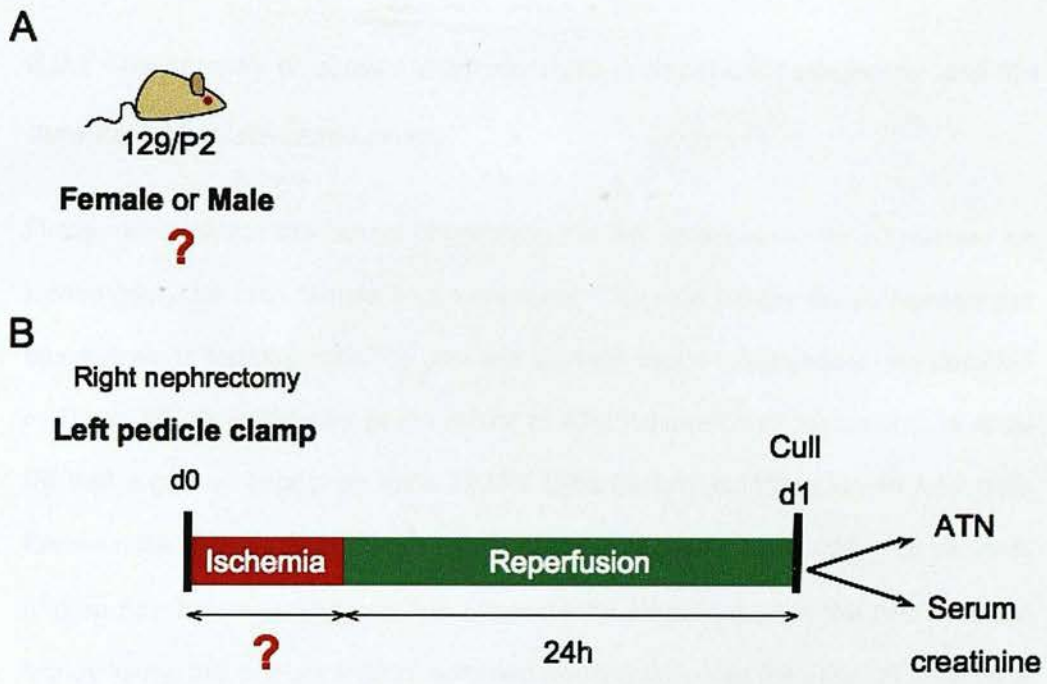

Figure 84: The Ischaemia/reperfusion injury model in the 129/P2 strain: determining the effects of gender and the duration of ischaemia.

The surgical model of renal ischaemia reperfusion injury (IRI) consisted of a right nephrectomy followed by clamping of the left renal pedicle. **A:** male or female mice were used and **B:** the duration of ischaemia was varied (i.e. how long the left renal pedicle is clamped). Following renal ischaemia, the left kidney was reperfused for 24h and harvested to determine the severity of acute tubular necrosis. Blood was collected for the measurement of serum creatinine as an indicator of the severity of renal failure. Temperature was maintained at 37°C throughout the procedure using a rectal probe and a homeothermic blanket system.

6.2.1 The severity of acute tubular necrosis is dependent on gender and the duration of the ischaemic period

Firstly, we analysed the impact of clamping the left renal pedicle for 20 minutes on kidney injury for both female and male mice. The right kidney tissue represented baseline renal histology and the pre- and post-IRI tissue appearances are depicted in Figure 85. Quantification of the extent of ATN indicated that 20 minutes of renal IRI had a greater impact on male 129/P2 mice as they exhibited worse ATN than female mice (7.8±6.2% vs. 39±7% ATN; females vs. males; $p=0.025$, $n=6$ vs. $n=4$) (Figure 86). However, compared to experimental models used in the field of acute kidney injury, this is a low level of ATN and insufficient to see the effect of potentially renoprotective interventions such as the administration of HO-1 over-expressing ESDM. We therefore increased the ischaemic period to 30 minutes for female mice and 25 minutes for male mice (Figure 87). This resulted in a significant 8-fold increase in the extent of ATN in female mice (7.8±6.2% vs. 67.4±3.6% ATN; 20 min vs. 30 min; $p<0.001$, $n=6$/group vs. $n=4$/group). The ATN score of male mice was also aggravated following an increase in the duration of the ischaemic period but, as expected, it was less pronounced than that evident in female mice with a 1.5-fold increase in ATN score (39±7% vs. 68.1±2.94% ATN; 20 min vs. 25 min; $p=0.02$, $n=4$ per group). There was no difference in the severity of structural kidney injury between female mice and male mice subjected to 30 minutes or 25 minutes of IRI respectively.

A

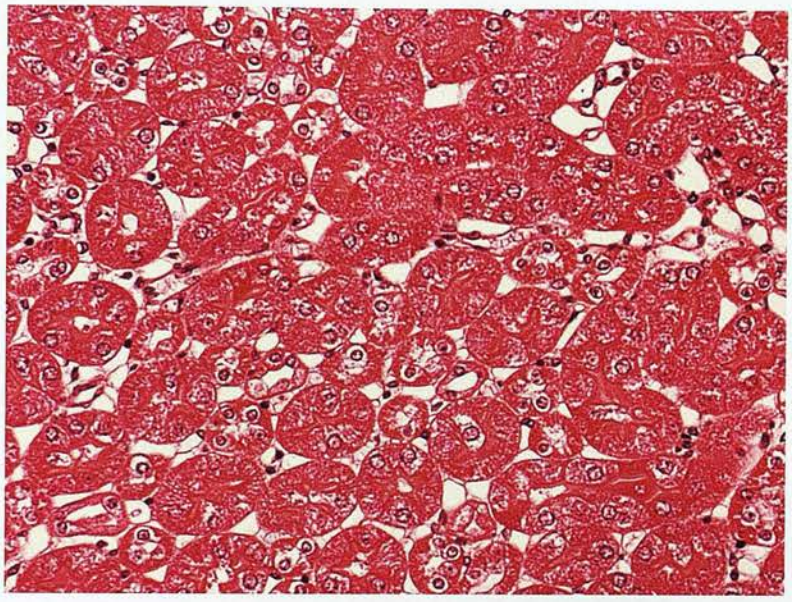

B

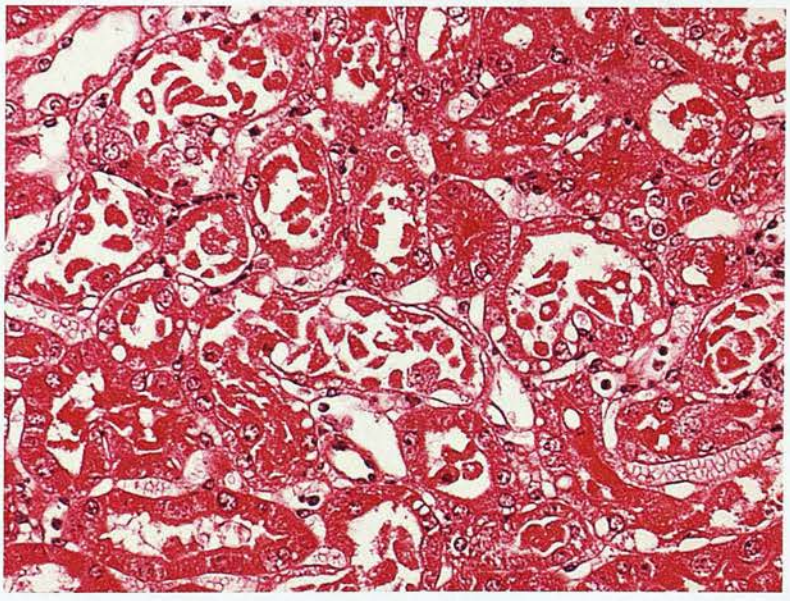

Figure 85: Representative renal histology of normal kidneys and kidneys 24 hours following renal ischaemia reperfusion injury.

H&E staining of kidney sections from 129/P2 male mice showing the outer stripe of the outer medulla (OSOM) region of the kidney before and 24 hours following renal ischaemia reperfusion injury (IRI). **A:** pre-IRI the intact renal tubules exhibit a healthy simple cuboidal epithelium. **B:** post-IRI (25 min ischaemia followed by 24h reperfusion) many the tubules are necrotic with abnormal nuclear morphology, loss of integrity of the epithelial cell layer and the presence of cast material in their lumen (x200 magnification).

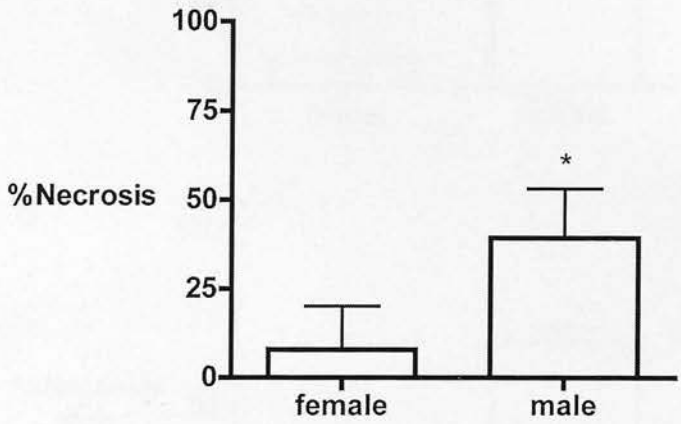

Figure 86: The severity of kidney injury following 20 minutes of renal ischaemia reperfusion injury is dependent on gender.

At the time of the operation, the 6-8 week old mice underwent a right nephrectomy. The left kidney was subsequently clamped for 20 minutes and reperfused for 24h prior to being harvested. The ATN score was used to determine the severity of tissue injury. Male mice exhibit worse kidney injury than the female mice (females vs. males, n=6 vs. n=4).

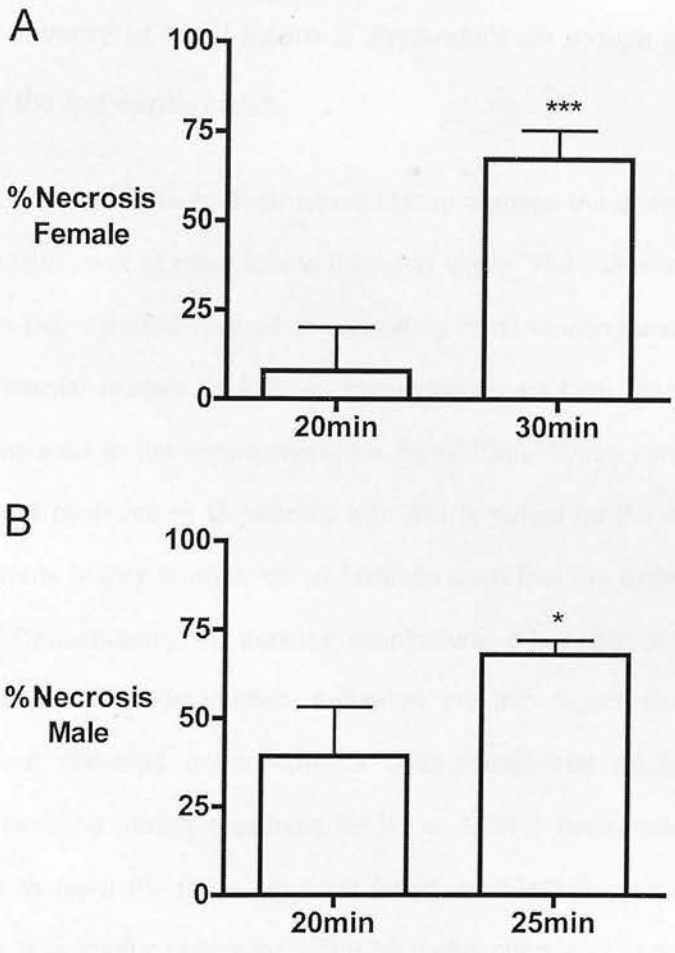

Figure 87: Acute tubular necrosis increases with the duration of renal ischaemia reperfusion injury

At the time of the operation, mice underwent a right nephrectomy and the left kidney was clamped for the designated period. Kidneys were harvested after 24h reperfusion and the ATN score determined. **A:** Increasing the ischaemic period from 20min to 30min resulted in a highly significant 8-fold increase in the ATN score in female mice ($p<0.001$, $n=6$). **B:** The ATN score in male mice was modestly augmented with a 1.5-fold increase in ATN score ($p=0.0192$, $n=4$) following an increase of the ischaemic period from 20min to 25min. There was no difference in kidney injury between females following the 30min IRI and males following 25min IRI.

6.2.2 The severity of renal failure is dependent on mouse gender and the duration of the ischaemic insult.

The ATN score is a measure of structural kidney damage but does not provide any indication of the level of renal failure following injury. The measurement of serum creatinine is the standard method of assessing renal function and ischaemic and toxic experimental models of AKI are characterised by both marked ATN and a significant increase in the serum creatinine. In addition, from a clinical perspective, the severity of renal failure in patients with AKI is based on the serum creatinine level, as a renal biopsy is often not undertaken such that the extent of ATN is not determined. Consequently, the serum creatinine was a key read-out in the renal IRI model employed in these studies. Following the 24h reperfusion phase, blood samples were collected under terminal anaesthesia and analysed for serum creatinine. Baseline serum creatinine levels in 129/P2 mice were determined 2 weeks prior to renal IRI following a tail bleed. Interestingly, the baseline serum creatinine is significantly higher for 129/P2 females compared to males (21.5±2.28 vs. 9.5±3.01 µmol/l serum creatinine; females vs. males; p=0.0114, n=8 vs. n=4) (Figure 88). Initial experiments using 20 minutes of renal ischaemia followed by 24h reperfusion revealed a trend towards an increased serum creatinine in males and females (Figure 89) but this was not statistically significant despite the fact that tissue injury was induced as reflected in the ATN scores (Figure 87). However, when the ischaemic period was increased to 30 minutes for female mice, serum creatinine levels increased significantly (21.5±2.3 vs. 46.8±5.6 µmol/l serum creatinine; baseline vs. 30min IRI females; p=0.0006, n=8 vs. n=6). Also, an increase in the ischaemic period to 25 minutes for male mice resulted in a significant increase in serum creatinine levels (10.3±4.1 vs. 71.5±8.3 µmol/l serum creatinine;

baseline vs. 25min IRI males; p=0.002, n=4). Our results reveal that male mice are more vulnerable to IRI compared to female mice as they exhibit worse renal function following a shorter period of ischaemia, (46.8±5.6 vs. 71.5±8.3 µmol/l serum creatinine; 30min IRI females vs. 25min IRI males; p=0.033, n=6 vs. n=4).

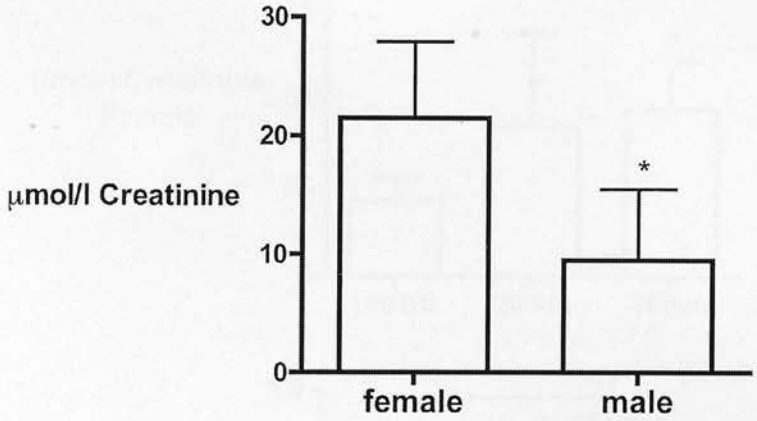

Figure 88: 129/P2 females exhibit higher baseline serum creatinine levels than male mice.

Blood samples were collected via tail vein 2 weeks prior to renal ischaemia reperfusion injury and analysed for baseline serum creatinine levels. Results indicate that 129/P2 females exhibit higher serum creatinine levels than the males at baseline (females vs. males; p=0.0114, n=8 vs. n=4)

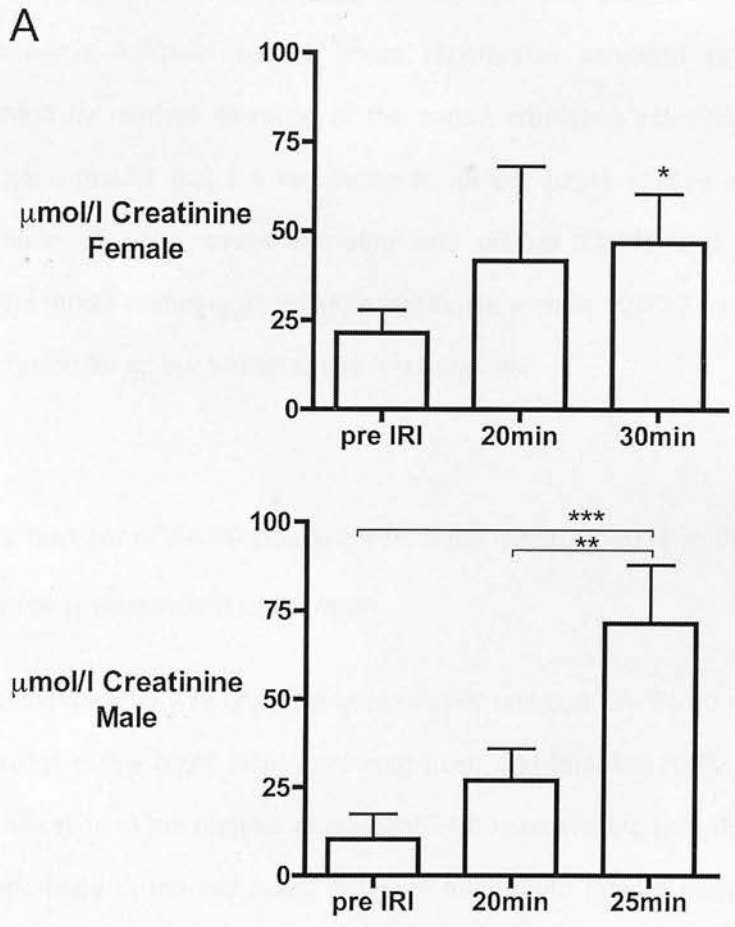

Figure 89: Severity of renal function impairment is dependent on the duration of the ischaemic insult.

Blood samples were collected via tail vein either 2 weeks prior (pre IRI) or 24h following IRI (20, 25 or 30 min ischaemia) and analysed for serum creatinine levels. Results indicate that an increase in the ischaemic period results in an increase of serum creatinine for both 129/P2 females and males.

The above studies indicated that 129/P2 male mice that underwent 25 minutes of renal ischaemia followed by 24 hours reperfusion exhibited significant ATN accompanied by marked elevation of the serum creatinine indicating acute renal failure. These results met the requirements for our future studies employing the administration of HO-1 over-expressing and control ESDM and we therefore adopted the model featuring 25 minutes ischaemia in male 129/P2 mice followed by 24h reperfusion for all our further *in vivo* experiments.

6.2.3 The number of F4/80 positive interstitial macrophages in the medulla of 129/P2 mice is dependent on gender

Immunohistochemistry was undertaken to identify and quantify F4/80 positive Mφ in baseline renal tissue (right kidney) of both male and female 129/P2 mice (Figure 90). Quantification of the number of resident F4/80 positive Mφ (pre-IRI) indicated a striking difference in the cell count between males and female mice. Indeed, the resident Mφ population of 129/P2 males is at least 8 times more than females' (Figure 91).

6.2.4 Medullary influx of F4/80 positive macrophages is not evident in 129/P2 mice 24 hours following renal ischaemia reperfusion

Immunohistochemistry was undertaken to identify and quantify F4/80 positive Mφ in the left kidney of both male and female 129/P2 mice 24 hours after renal ischaemia reperfusion injury. There was no detectable change in number of F4/80 positive Mφ in the medulla of male or female 129/P2 mice at 24h post IRI (Figure 91).

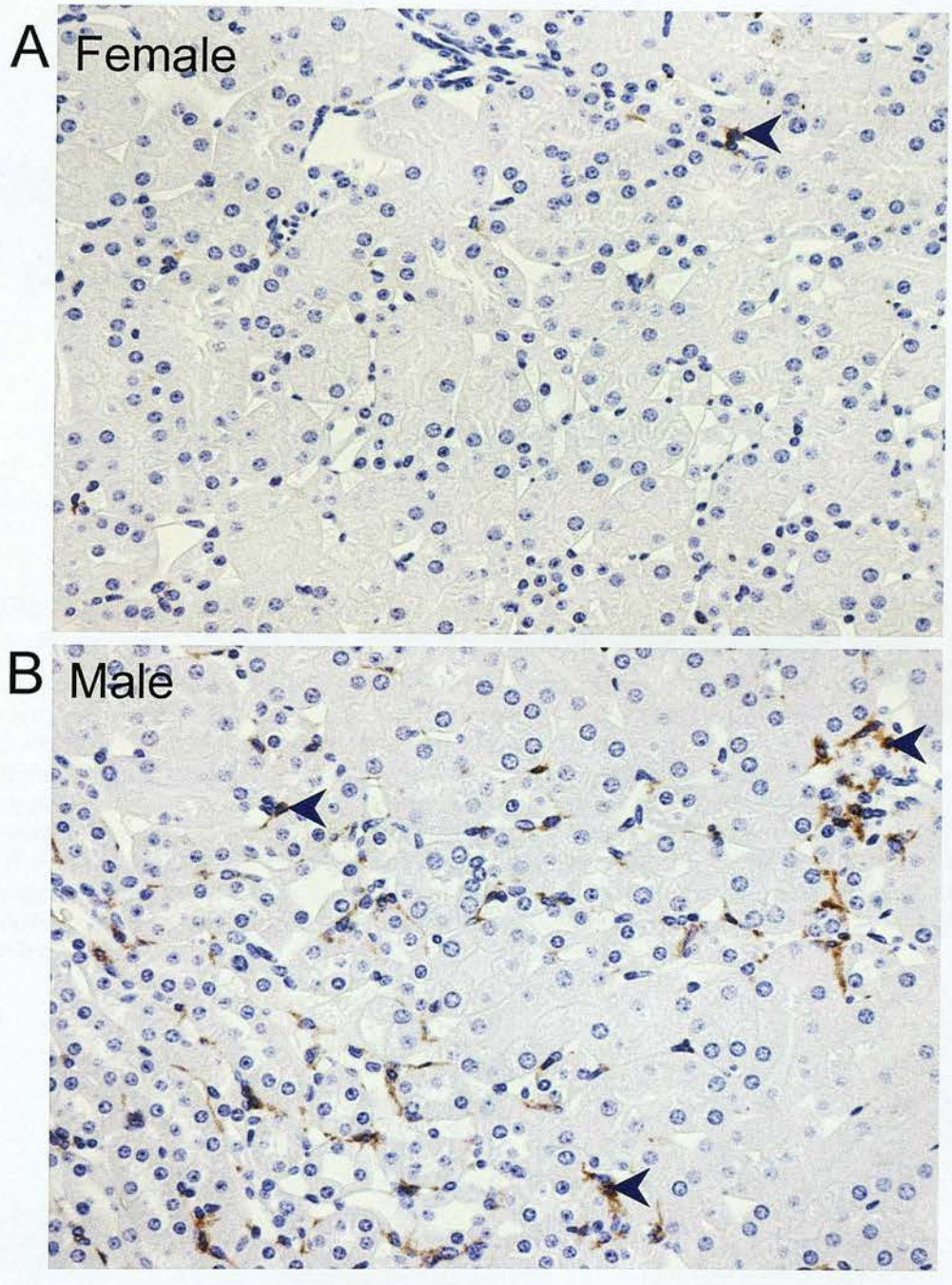

Figure 90: Immunohistochemistry staining of F4/80 positive resident macrophages in the non-injured medulla of 129/P2 mice.

Representative fields of baseline medulla immunohistochemistry for F4/80 positive resident macrophages. **A:** Female 129/P2 mice have few F4/80 positive resident macrophages in the medulla. **B:** In contrast, male 129/P2 mice exhibit relatively high numbers of F4/80 positive interstitial macrophages. Arrowheads indicate some F4/80 positive resident macrophages.

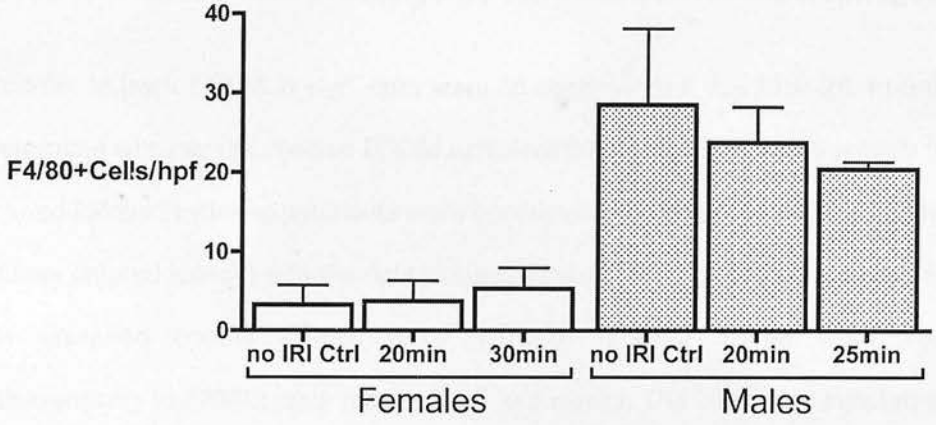

Figure 91: Medullas of 129/P2 male mice exhibit significantly higher numbers of F4/80 positive interstitial macrophages than female mice.

At the time of the operation, the right kidney was removed and served as baseline renal tissue ('no IRI control'). The left kidney was subsequently clamped for variable periods of ischaemia and the left kidney was removed 24 hours later. Immunohistochemistry was undertaken to identify and quantify F4/80 positive macrophages in baseline and injured kidney. 5 pictures of non-overlapping fields were taken per section (x200 magnification) and F4/80 positive cells were counted. The medulla of 129/P2 male mice contains significantly more F4/80 positive macrophages than female mice at baseline. There was no significant change in the number of medullary F4/80 positive macrophages at 24h post IRI in male or female mice.

6.3 In vivo localisation of embryonic stem cell derived macrophages

In order to track ESDM *in vivo*, cells were labelled with the dye PKH-26. In order to determine whether the injected ESDM exhibited the ability to home selectively to the injured kidney *in vivo*, experiments were conducted with a unilateral clamp of the left kidney (injured kidney) with the right kidney (contralateral kidney) left *in situ* to act as an uninjured control kidney. $5x10^6$ PKH-26 labelled ESDM were injected intravenously to 129/P2 male mice aged 6 to 8 weeks. The cells were injected at the time of reperfusion of the kidney. The mice were culled 1 hour following the administration of ESDM and the kidneys, spleen, liver and lungs were snap frozen in liquid nitrogen. The localisation of ESDM was assessed on frozen sections mounted with DAPI mounting medium and analysed by fluorescent microscopy.

6.3.1 Embryonic stem cell-derived macrophages localise to solid organs one hour post renal ischaemia reperfusion injury

ESDM rapidly infiltrated multiple major organs following ischaemic renal injury. Indeed, 1h post injection, PHK-26 positive ESDM were already visible in the lungs, liver, spleen and kidneys of 129/P2 male mice (Figure 92).

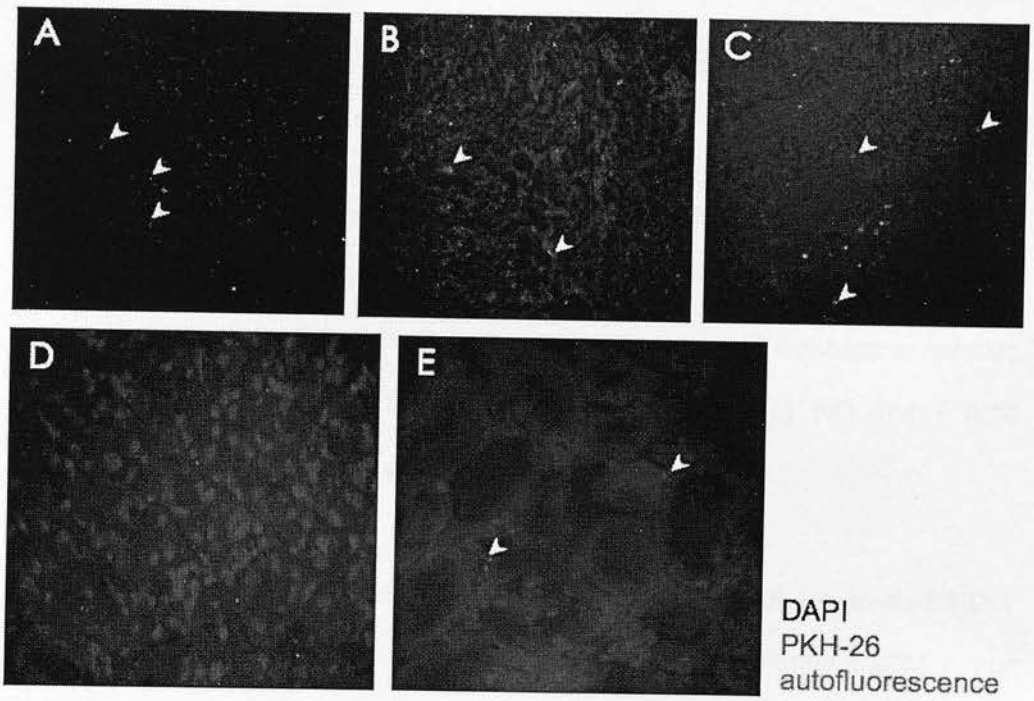

Figure 92: Embryonic stem cell derived macrophages localise to solid organs 1h post ischaemia/reperfusion injury.

Embryonic stem cell derived macrophages (ESDM) were labelled *in vitro* by PKH-26 red fluorescent dye. The left kidney of 129/P2 male mice was clamped for 25 minutes to induce a unilateral ischaemic lesion. The cells were injected via the tail vein at the time of kidney reperfusion. The mice were culled 1h post injection and organs snap frozen. Frozen sections were mounted with DAPI mounting medium and analysed by fluorescent microscopy. Representative fields of **A:** Lung **B:** Liver **C:** Spleen (x100 magnification) **D:** non-injured right kidney and **E:** injured left kidney (both x400 magnification). Blue: nuclei stained by DAPI; red: PKH-26 labelled ESDM; green: autofluorescence; white arrowheads: PKH-26 positive macrophages.

6.3.2 Control and heme arginate treated embryonic stem cell-derived macrophages preferentially home to the injured kidney one hour post renal ischaemia reperfusion injury

In chapter 5, we demonstrated that 24h incubation of ESDM with heme arginate (HA) significantly induced HO-1 expression. In addition, the *in vitro* analysis of HA treated ESDM indicated that they were more phagocytic and exhibited a reduced inflammatory response following LPS and IFNγ stimulation (↓ NO and ↑ IL10 production).

In order to study the potential anti-inflammatory properties of HA treated HO-1 expressing ESDM *in vivo*, we injected control and 24h HA treated ESDM in our model of renal ischaemia reperfusion injury in 129/P2 mice. Initial experiments explored whether HA treated ESDM exhibited a similar capacity as control ESDM to selectively localise to the injured kidney *in vivo*. Therefore, as previously, the left kidney was clamped (injured kidney) and the right kidney left *in situ* as an uninjured control (contralateral kidney). $5x10^6$ control or HA treated ESDM were injected at the time of reperfusion 25 minutes after the ischaemic insult. The mice were culled at 1h post injection and kidneys snap frozen in liquid nitrogen. Localisation was assessed on frozen sections mounted with DAPI mounting medium and analysed by fluorescent microscopy.

Greater numbers of control or HA treated PKH-26^+ ESDM were seen within the medulla of the injured kidney (IRI) compared to the contralateral control (Control ESDM: 0.48±0.07 vs. 0.73±0.03 PKH+ ESDM/hpf; contralateral kidney vs. IRI kidney; p=0.023, n=3 and HA ESDM: 0.33±0.07 vs. 0.8±0.06 PKH+ ESDM/hpf;

contralateral kidney vs. IRI kidney; p=0.0061, n=3) (Figure 93). These results suggest that ESDM have the ability to sense the injury *in vivo* and home preferentially towards an inflamed site. In addition, the induction of HO-1 expression in ESDM by 24h treatment with HA does not modulate the ability to localise to the injured kidney.

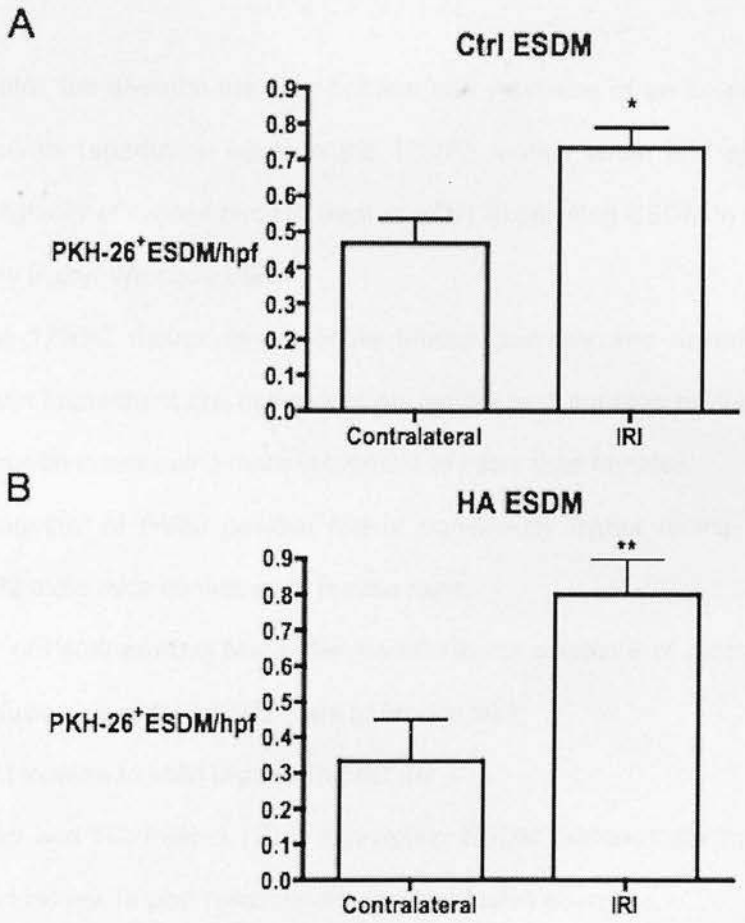

Figure 93: Control and hemeoxygenase-1 overexpressing embryonic stem cell-derived macrophages home to the injured kidney 1h post renal ischaemia reperfusion injury.

Embryonic stem cell-derived macrophages (ESDM) were either exposed to 10μM heme arginate (HA) for 24h (HA ESDM) or cultured in control medium (Ctrl ESDM). ESDM were labelled *in vitro* by PKH-26 dye. On the day of surgery, 129/P2 male mice underwent left renal ischaemia reperfusion injury. The right kidney of the mice was left intact (contralateral control) whilst the left kidney was clamped for 25min (IRI). $5x10^6$ PKH-26 labelled ESDM were injected via tail vein at the time of kidney reperfusion. 1h later, the mice were culled and kidneys snap frozen in liquid nitrogen. Frozen sections were mounted with DAPI mounting medium and analysed by fluorescent microscopy. 10 pictures of non-overlapping fields were taken per section (x400 magnification) and PKH-26 positive cells were counted (n=3 animals/group).

6.4 Summary

In this chapter, we describe the development and validation of an *in vivo* model of renal ischaemia reperfusion injury in the 129/P2 mouse strain and explored the localising capacity of control and HA treated HO-1 expressing ESDM in a setting of acute kidney injury. We show that:

- In the 129/P2 mouse strain, acute tubular necrosis and severity of renal function impairment are dependent on gender and duration of the ischaemic period with males being more vulnerable to injury than females.
- The number of F4/80 positive Mφ is significantly higher in the medulla of 129/P2 male mice compared to female mice.
- Influx of F4/80 positive Mφ in the medulla is not a feature of renal ischaemia reperfusion injury for 129/P2 male or female mice
- ESDM localise to solid organs 1h post IRI
- Control and HA treated HO-1 expressing ESDM preferentially home to the injured kidney 1h post renal ischaemia reperfusion injury.

Chapter 7. Discussion & Future Work

7.1 Deriving and phenotyping embryonic stem cell-derived macrophages.

In this thesis we present data demonstrating the successful generation of murine ESDM *in vitro*. Using various parameters including cell morphology, cell surface markers and multiple functional assays, we have shown that ESDM are comparable to BMDM for all properties tested. Specifically, ESDM are large mononuclear cells that express well-established Mϕ cell surface markers (F4/80^{high} CD11b^{high} CD11c^{high} MHC class II^{low}). ESDM are readily phagocytic for apoptotic cells and beads and produce NO when activated by LPS and IFN-γ.

Our results are consistent with the available literature on murine ESDM (Table 5, Chapter 1. Introduction). However, one could argue that we did not fully investigate the stability or the plasticity of the ESDM phenotype as Mϕ are able to adapt their phenotype for microbicidal, anti-inflammatory or tissue repair activity depending on their microenvironment (M1/M2 activation). Our work only explored ESDM ability to respond to an inflammatory stimulus, namely LPS/IFN-γ, and thus become 'classically activated' (M1). It would be interesting to test ESDM ability to adopt a wound-healing (M2) or a regulatory Mϕ phenotype (Mreg) by treating them with IL-4/IL-13 and IL-10 respectively. These studies would also enable us to assess the phenotypic stability of ESDM. Also, testing different passages of ESC prior to performing the ESDM differentiation would be useful as it could potentially support the robustness of the protocol. It would also be interesting to simply follow ESDM in

culture in the absence of M-CSF and other growth factors in order to determine whether they revert to a stem cell phenotype or remain as ESDM. The stability of the ESDM phenotype *per se* represents an important safety concern, as a reversion to a stem cell phenotype would be potentially tumourigenic.

Regarding the flow cytometry and microscopy analysis of ESDM phagocytosis, our results are qualitatively similar in that there was no difference between ESDM and BMDM. However, the different methodologies did generate markedly different levels of phagocytosis with flow cytometry demonstrating ~30% phagocytosis compared with ~70% phagocytosis for the microscopy analysis. Our results highlight the fact that different methodologies do not necessarily give similar results. We suspect that cell surface binding of beads to Mϕ can confound the interpretation and therefore, that flow cytometry is more reliable than microscopy as it examines a higher number of detached cells that are less likely to have adherent beads. Several aspects that might explain the result discrepancies differed between the assays. Firstly, although all Mϕ were washed extensively, flow cytometric analysis required Mϕ to be physically removed from the plate for processing by both washing and scraping and this manoeuvre might act to remove any beads that were tightly adherent to the Mϕ cell surface. Also, the very strong brightness of the green fluorescent latex beads and the comparatively weak cytoplasmic staining of Mϕ with Cell Tracker Orange made it difficult to discern actual phagocytosis of beads from non-specific cell surface binding. It would therefore be of interest to repeat this experiment with stronger staining of the Mϕ with Cell Tracker Orange and quench the fluorescence of any beads that are bound to the cells with trypan blue. In addition, the Mϕ could undergo microscopy after they have been physically detached and removed from the plate (as for flow cytometry). Cytospins of the detached Mϕ could be made for

microscopic assessment and quantification of phagocytosis. Further phagocytosis assays should also include bacterial pathogens and cellular debris in addition to apoptotic cells as these may also require clearance by Mϕ *in vivo*.

In this thesis, we chose several well-established Mϕ functions and markers to compare and contrast ESDM and BMDM. As Mϕ and other cells are highly complex, it would be valuable to perform gene expression profiling by microarray analysis of both BMDM and ESDM in order to create a global picture of ESDM and BMDM gene expression. Indeed, this inclusive transcriptomic approach could be adopted to interrogate the gene changes of ESDM or BMDM induced to adopt particular phenotypes to see if similarities are maintained following Mϕ responses to polarising stimuli.

Recently, several groups have reported working with human ESC as sources of ESDM for mechanistic studies (Karlsson et al., 2008; Subramanian et al., 2009). In addition, Mϕ have been generated from human induced pluripotent stem (IPS) cells (Senju et al., 2011). This is an important step forward and the *in vitro* analysis of these human ESDM will indicate whether they are similar to primary human monocyte-derived Mϕ in their behaviour. The use of human cells is appealing in the clinical setting and there is no doubt that important future work will be undertaken using human ESDM. There are, however, caveats to the exclusive use of human ESDM. For example, one of the aims of this work was to determine whether the administration of HO-1 overexpressing ESDM would be of benefit in a murine model of renal IRI and such an experiment could not be undertaken with human ESDM as these are xenogeneic cells. It would be possible to test the effect of human ESDM (e.g. HO-1 overexpressing ESDM) in immunodeficient mice such as SCID mice that

lack T and B cells. However, T and B cells are involved in the pathogenesis of renal IRI and such experiments are thus less representative of the clinical condition. It is true, however, that the use of ESDM derived from IPS cells would be advantageous, as this should overcome any immune response that might be made against the administered cells.

7.2 Constitutive and Inducible overexpression of hemeoxygenase-1 in embryonic stem cells and embryonic stem cell-derived macrophages.

Genetic engineering was employed to generate ESC lines with either constitutive or inducible overexpression of HO-1 as a means to subsequently derive HO-1 overexpressing ESDM for *in vivo* studies.

First, we generated genetically manipulated ESC that constitutively overexpressed HO-1 and examined the effect upon the behaviour of ESC including their capacity to undergo self-renewal and differentiation to ESDM. We generated a panel of clones with varying degrees of HO-1 overexpression (so called 'low' and 'high' HO-1 expressers) and our results differed according to the clone analysed indicating that the genetic modification did not result in uniform alteration of cell behaviour. In some clones, the constitutive overexpression of HO-1 in ESC with the pCAG system adversely impacted upon the yield of ESC following routine ESC culture. It is possible that this adverse effect may be secondary to either low levels of ESC proliferation or excessive levels of ESC apoptosis (or both). However, some clones exhibited reduced self-renewal associated with increased cell differentiation. The problem with the ESC cell number was not obviously related to the level of HO-1

expression as poor cell yields were seen with both low and high HO-1 expressing clones. Similarly, the reduced self-renewal of ESC was also seen in both low and high HO-1 expressers and was thus unlikely to be secondary to HO-1 *per se*.

It may be that the problem lies with the technique used to constitutively overexpress HO-1 as the HO-1 cDNA was cloned into a pCAG vector that was then *randomly* integrated into the genome of the ESC. This random insertion increases the risk of inadvertently disrupting key genes such as those involved in ESC self-renewal and/or Mϕ differentiation. The interrogation of this hypothesis formed the basis of further work and it was decided not to study the mechanisms behind this clonal variability. We attempted to overcome this problem by developing and testing a more precise, targeted tetracycline inducible system to express HO-1 that offered numerous potential advantages.

First, targeting a specific ICE site in the genome of the ESC would allow us to avoid silencing of any other genes. Secondly, this system would provide us with tight control over the cellular expression of HO-1 thereby allowing us to study the effect of HO-1 overexpression upon either ESC biology or Mϕ differentiation by inducing HO-1 expression at different time points.

Our results indicated successful generation of a genetically modified ESC line with tetracycline inducible HO-1 overexpression. Furthermore, we could produce functional ESDM from this genetically modified ESC line. However, and rather surprisingly, our data indicated that the inducible HO-1 ESDM did not upregulate HO-1 following treatment with the inducing agent doxycycline (Dox). Indeed, our data indicated a loss of HO-1 inducibility over time during the differentiation process

from ESC to ESDM. These findings were somewhat unexpected given the literature in this field (Iacovino et al., 2011; Wong et al., 2005). Indeed, the A2lox.cre cell line used to generate our inducible HO-1 ESC has been specifically engineered so that (i) the ICE containing the cDNA of interest has been targeted under a TRE element in the genomic region upstream of HPRT and (ii) the ROSA26 locus contains an rtTA transgene that results in the expression of the rtTA protein that enables Dox to induce the TRE. Both the HPRT and ROSA26 loci were chosen as docking sites because of their presumed ubiquitous and constitutive transcriptional activity (Bäckman et al., 2009; Chen et al., 2011; Iacovino et al., 2011) with work showing that ROSA26 and HPRT have been identified as silence-resistant sites in transgenic mouse studies (Bronson et al., 1996; Zambrowicz et al., 1997). However, none of these groups worked with Mϕ and our findings thus required further investigation.

We explored two potential reasons why the inducible system failed to generate mature ESDM that would express HO-1 following Dox exposure. The dosage of Dox used to treat the ESDM was varied and increased but did not restore inducible HO-1 expression in genetically modified ESDM. Dox has a long duration of action and is a commonly used tetracycline (Schach von Wittenau, 1968). However, absorption of tetracycline and thus Dox has been reported to be impaired by milk products, aluminium hydroxide gels, sodium bicarbonate, calcium and magnesium salts and interestingly iron preparations due to increased chelation of the compound (Sande and Mandell, 1990). A by-product of heme catabolism by HO-1 is iron and we could investigate whether this impairs Dox absorption into the cell. This seems unlikely as the inducible ESC only express HO-1 and thus potentially release iron following Dox exposure. However, the HO-1 Western blot of inducible 'ESC without Dox' and 'Control ESDM without Dox' reveal an element of constitutive HO-1 expression by

control ESDM whilst the inducible ESC did not express constitutive HO-1 prior the Dox treatment (no HO-1 band visible on the Western blot). It is thus conceivable that the low level of constitutive HO-1 expression by inducible ESDM in the absence of Dox treatment might somehow affect the bioavailability of Dox to the ESDM. Although further studies could include the study of Dox bioavailability in our ESDM cultures over time using HPLC, biological or fluorometric assays (Fourtillan et al., 1980; Saivin and Houin, 1988; Welling et al., 1977) it is thought unlikely that this is a major confounder.

A series of informative experiments examined an alternative hypothesis and aimed to determine whether the loss of inducible HO-1 expression was a feature of ESDM differentiation *per se* (i.e. the result of a specific feature of Mϕ differentiation) or whether it occurs following differentiation of ESC to non-Mϕ cells (i.e. the result of a generic feature of differentiation to various cell types). We therefore induced HO-1 inducible ESC towards a non-Mϕ differentiated state by treating them with retinoic acid (RA). We preliminarily show that RA differentiated cells do not induce HO-1. However, the n number of experiments requires increasing to generate a robust data set.

Further work should definitely target the underlying molecular biology issues of the inducible system. It would be interesting to perform qPCR analysis of ROSA26 and HPRT gene expression, as it is possible that unforeseen and adverse silencing of one of these loci could explain the loss of HO-1 inducibility in our system. If this is the case then this would be an important methodological finding for the field. It

would also be of interest to determine whether ESDM are more prone to DNA methylation during their differentiation or if they specifically silence target transgene expression.

7.3 Pharmacological induction of hemeoxygenase-1: heme arginate treatment of ESDM.

We investigated the effect of HA induced HO-1 upregulation upon ESC and ESDM phenotype. Using various techniques, we demonstrated that HA exerts a mild though significant effect upon the potential of ESC to undergo self-renewal. Indeed, the presence of HA resulted in a small but significant increase in the percentage of pure ESC colonies ($p=0.0499$, $n=3$). However, no differences were evident in the proportion of either mixed or differentiated colonies. One should be careful when drawing conclusions from these results because, although a p-value of less than 0.05 was achieved following 3 separate and discrete experiments, it is unlikely that this effect would have major biological relevance.

We demonstrated that HA significantly upregulates ESDM HO-1 protein and mRNA expression. Interestingly, ESDM treated with HA for 24h exhibit a more striking induction of HO-1 than ESDM differentiated in the constant presence of HA. HO-1 is an acute cell stress protein expressed in response to oxidative stress, hypoxia etc and would typically rapidly return to basal expression levels. Indeed it has been reported that continuous expression of HO-1 may be harmful to the cells (Deramaudt et al., 1999). Furthermore, although transient HO-1 overexpression provides protection against oxygen toxicity in lung cells, some deleterious effects

due to iron accumulation were observed for chronic HO-1 overexpression (Dennery et al., 2003). Accordingly, further work should include cell viability and longevity experiments by culturing the cells over a prolonged period then staining them with Propidium Iodide or Trypan Blue, to determine whether prolonged HA exposure affects ESDM survival. Our results showing a lower level of HO-1 in cells exposed chronically to the inducing agent HA does suggest some form of negative feedback controlling the expression of the enzyme. However, the underlying mechanism remains unclear.

The control ESDM also expressed a low baseline level of HO-1 expression thereby indicating that the relatively standard cell culture conditions employed for our studies did lead to HO-1 upregulation via hypoxia or cell stress pathways. This should be borne in mind in the study of HO-1 and emphasises the importance of utilising appropriate controls in experiments.

ESDM differentiated in the constant presence of HA (HA differentiation ESDM) have significantly increased CD11b but reduced CD11c expression. CD11b is known to be involved in inflammatory processes by regulating leukocyte adhesion and migration and has been implicated in several immune processes such as phagocytosis, cell-mediated cytotoxicity, chemotaxis and cell activation (Solovjov et al., 2005). Interestingly, our results show that HA treatment significantly increased the ability of ESDM to phagocytose apoptotic cells and that 'HA differentiated ESDM' tended to phagocytose more apoptotic cells than ESDM treated with HA for 24 hours, though the difference was not statistically different.

The possible mechanism of increased phagocytosis following HA treatment is of significant interest as this effect has also been seen following BMDM that have undergone adenoviral transduction to overexpress HO-1 (Ferenbach et al., 2010). There are several questions that will need to be addressed. A key issue is whether HA generally modulates phagocytosis or whether the effect is limited to particular particles. Further experiments using various particles such as beads, bacterial pathogens, opsonised zymosan and necrotic cell debris would shed light on this. In addition, it would be of interest to determine whether HA treatment modulates the expression of any ESDM cell surface receptors that are involved in the recognition and ingestion of apoptotic cells such as scavenger receptors, CD36 or the $\alpha_v\beta_3$ integrin. This may be ascertained by flow cytometric analysis of the level of cell surface expression of these receptors. If an increase in receptor expression is found following HA treatment then further work such as antibody inhibition studies might suggest whether the relevant receptor is key to the increased phagocytosis. An additional possibility is that HA may modulate the intracellular phagocytic machinery of the cell. An analysis of the proteins involved in generating phagocytic cups and phagolysosomes (e.g. Rho-kinase, Myosin-II) might therefore be of interest. It would be equally be interesting to assess if HA treatment and the resultant increased phagocytosis augments ESDM phenotypic reprogramming i.e. whether it affects the ability of the ESDM to adopt an anti-inflammatory, wound-healing or a regulatory phenotype by ELISA analysis of their culture supernatant for relevant cytokines.

It is also important to note that the role of HO-1 *per se* remains unanswered by the work described in this thesis. It remains possible, albeit unlikely, that the cellular effects of HA described may be heme dependent and HO-1 independent. In order to address this issue further work would require the analysis of the effects of HA upon

BMDM from HO-1 knockout mice and ESDM derived from ESC that lack the HO-1 gene. An alternative approach would be to employ pharmacological inhibitors of HO-1 such as tin protoporphyrin with quantification of the HO-1 enzyme bioactivity to ensure effective HO-1 inhibition. A caveat here is that such inhibitors are not specific and may have other effects upon cells. A further method to inhibit HO-1 expression would be to use HO-1 siRNA (with scrambled siRNA as control) with Western blotting being employed to ensure effective inhibition of HO-1 protein expression.

If these experiments demonstrate that HO-1 is key to the effects we reported, it would be interesting to determine if these effects are secondary to the mediators generated by HO-1 activity such as bilirubin or CO. This would require experiments to be undertaken that use exogenous bilirubin or CO that can be generated from CO releasing molecules (CORMs).

Finally, we show that HA treatment modulates the pro- and anti-inflammatory response of ESDM following stimulation with LPS and IFNγ. The effects seen were somewhat variable and did depend upon whether the ESDM had been treated for 24 hours with HA or had undergone differentiation to ESDM in the presence of HA. However, some experiments did demonstrate modulation of the production of NO, TNFα and IL-10 as well as modulation of the expression of pro- and anti-inflammatory genes (⇑HO-1 gene expression and ⇓ iNOS, IL-10, IL-6 and IL-1β gene expression) following LPS/IFNγ stimulation. The overall effect of the altered ESDM phenotype induced by HA treatment remains unanswered i.e. the nature of the sum effect of all the cytokine changes. It is important to point out that gene expression analysis has only been performed 24h after stimulation, i.e. a time point when expression levels could already have returned to baseline. It would thus be

interesting to run a timecourse experiment of gene expression following LPS/IFNγ stimulation including earlier time points than 24h, such as 2h, 4h and 12h post stimulation as these could explain the discrepancies between protein and mRNA levels for TNFα and IL-10. It would equally be interesting to perform experiments involving the transfer of the various ESDM conditioned supernatants (control ESDM, LPS/IFNγ stimulated ESDM pretreated with HA or vehicle) to a control quiescent cell (a parenchymal cell such as a tubular cell or a quiescent Mϕ). The level of activation of the 'reporter cell' could be assessed by qPCR analysis of gene expression. This would provide insight into the 'totality' of the effects of HA treatment upon ESDM activation and suggest the effect that such ESDM could have on adjacent parenchymal cells.

7.4 Development of a model of acute kidney injury in 129/P2 mice and the localisation of embryonic stem cell derived macrophages in vivo

We outlined the development and validation of an *in vivo* model of unilateral renal ischaemia-reperfusion injury in the 129/P2 mouse strain and explored the capacity of control and HA treated HO-1 expressing ESDM to localise to the acutely injured kidney.

We show that in the 129/P2 mouse strain, acute tubular necrosis and the severity of renal functional impairment depend upon gender and the duration of the ischaemic period with males being more vulnerable to injury than females. This is consistent with the literature available on gender differences in ischaemic acute kidney injury for mice and rats (Fekete et al., 2004; Muller et al., 2002; Wei et al., 2005).

However, the mechanism underlying these gender differences remains unclear. Interestingly, we show that the number of F4/80 positive resident macrophages is significantly higher in the medulla of 129/P2 male mice compared to female mice. To our knowledge, no other group has described this difference. However, studies on renal macrophage and monocyte depletion by liposomal clodronate (LC) prior to experimental IRI provided functional and structural protection from the injury (Day et al., 2006; Day et al., 2005; Ferenbach et al., 2012; Jo et al., 2006). The authors suggested that resident renal macrophages contributed to the initiation and severity of injury in renal IRI, and thus their depletion led to amelioration of renal injury. It is thus interesting to speculate that the reduced number of resident macrophages in female kidneys may underlie the reduced injury found in female mice. Although we found that there was no significant influx of F4/80 positive macrophages in the medulla following renal ischemia reperfusion injury in both male and female 129/P2 mice, it would be interesting to examine whether there were any differences in the level of infiltration by F4/80^{low} monocytes.

One of the aims of this thesis was to undertake studies to determine whether HO-1 overexpressing ESDM are renoprotective *in vivo* following renal IRI. We therefore intravenously injected PKH-26 labelled control and HA treated ESDM to 129/P2 male mice and assessed their ability to localise in a setting of acute kidney injury. We left the right kidney *in situ* in these studies in order to provide a non-injured control kidney. We demonstrated that ESDM did localise to various organs including the liver and lung and that they did preferentially homed to the injured kidney 1h post IRI. However, it is interesting to note that the numbers of recruited PKH+ ESDM in the kidney 1h following IRI is relatively low compared to the number of cells injected. Previous studies using Mϕ cell therapy targeted specifically to the

kidney via renal artery injection have demonstrated significant amelioration of disease with relatively low numbers of labelled cells detectable within the diseased organ (Kluth et al., 2001; Wilson et al., 2002; Yamagishi et al., 2001). More specifically, David Harris' team showed amelioration of disease after injecting as low as 1.10^6 macrophages (Cao et al., 2010). These results raise the possibility that the administered cells could be influencing the phenotype of other resident (or 'bystander') macrophages. Further work should also include experiments on cell fate over longer periods after their injection *in vivo*. To do so, various organs should be harvested and examined at multiple time points after cell administration.

Key further work would include assessing the potential renoprotective effect of HA treated ESDM following renal IRI by looking at functional and structural markers of injury such as creatinine and ATN scores compared to control ESDM administration and control IRI (no cells injected). The administration of HO-1 overexpressing BMDM (induced by adenoviral transduction) to mice with ischaemic AKI reduced the serum creatinine but had no effect upon the ATN score (Ferenbach et al., 2010). The suggested reason for this was the restoration of microvascular patency and it would therefore be important to assess platelet and fibrin deposition within the peritubular capillaries of the medulla.

8. Conclusion

At the end of this project, we were able to generate functional Mφ from ESC in significant numbers. Our work has shown that the advantages that were envisaged for an inducible system of gene expression did not materialise in a way that the differentiation of ESC to Mφ resulted in the loss of inducible gene expression. This is an important message for the field because inducible gene expression systems are often praised for their efficacy in stem cells. It may actually well be the case that our strategy of treating ESDM with pharmacological agents, such as HA or cytokines, might be optimal. Indeed, we show that HA treated ESDM over-express HO-1, present promising anti-inflammatory properties *in vitro* and home to the injured kidney in a model of murine IRI *in vivo*. Further experiments are still needed to determine if HA treated ESDM exert anti-inflammatory properties *in vivo*. However, our findings are a strong platform for future studies of the translational potential of using modified ESDM in cell therapy.

9. Bibliography

Abraham, N. (2003). Therapeutic applications of human heme oxygenase gene transfer and gene therapy. Current Pharmaceutical Design *9*, 2513-2524.

Abraham, N.G., and Kappas, A. (2008). Pharmacological and clinical aspects of Heme Oxygenase. Pharmacological Reviews *60*, 79-127.

Akamatsu, Y., Haga, M., Tyagi, S., Yamashita, K., Graca-Souza, A.V., Ollinger, R., Czismadia, E., May, G.A., Ifedigbo, E., Otterbein, L.E., *et al.* (2004). Heme oxygenase-1-derived carbon monoxide protects hearts from transplant-associated ischemia reperfusion injury. The FASEB Journal *18*, 771-772.

Akcay, A., Nguyen, Q., and Edelstein, C.L. (2009). Mediators of Inflammation in Acute Kidney Injury. Mediators of Inflammation *2009*.

Anderson, K.E., Bonkovsky, H.L., Bloomer, J.R., and Shedlofsky, S.I. (2006). Reconstitution of Hematin for Intravenous Infusion. Annals of Internal Medicine *144*, 537-538.

Attuwaybi, B.O., Kozar, R.A., Moore-Olufemi, S.D., Sato, N., Weisbrodt, N., Hassoun, H.T., and Moore, F.A. (2003). Heme-oxygenase-1 (HO-1) induction by hemin protects against gut ischemia/reperfusion injury. Journal of Surgical Research *114*, 289.

Beri, R., and Chandra, R. (1993). Chemistry and Biology of Heme Effect of Metal Salts, Organometals, and Metalloporphyrins on Heme Synthesis and Catabolism, with Special Reference to Clinical Implications and Interactions with Cytochrome P-450. Drug Metabolism Reviews *25*, 49-152.

Blantz, R., and Singh, P. (2011). Analysis of the prerenal contributions to acute kidney injury. Contributions to Nephrology *174*, 4-11.

Bonventre, J.V., and Weinberg, J.M. (2003). Recent Advances in the Pathophysiology of Ischemic Acute Renal Failure. Journal of the American Society of Nephrology *14*, 2199-2210.

Bonventre, J.V., and Yang, L. (2011). Cellular pathophysiology of ischemic acute kidney injury. The journal of Clinical Investigation *121*, 4210-4221.

Bonventre, V., and Zuk, A. (2004). Ischemic acute renal failure: An inflammatory disease? Kidney International *66*, 480-485.

Burne, M., Daniels, F., Ghandour, A.E., Mauiyyedi, S., Colvin, R., O'Donnell, M., and Rabb, H. (2001). Identification of the CD4(+) T cell as a major pathogenic factor in ischemic acute renal failure. Journal of Clinical Investigations *108*, 1283-1290.

Burne-Taney, M., Ascon, B., Daniels, F., Racusen, L., Baldwin, W., and Rabb, H. (2003). B cell deficiency confers protection from renal ischemia reperfusion injury. Journal of Immunology *171*, 3210-3215.

Bussolati, B., Hauser, P.V., Carvalhosa, R., and Camussi, G. (2009). Contribution of Stem Cells to Kidney Repair. Current Stem Cell Research & Therapy *4*, 2-8.

Bussolati, B., Tetta, C., and Camussi, G. (2008). Contribution of Stem Cells to Kidney Repair. American Journal of Nephrology *28*, 813-822.

Chomczynski, P., and Sacchi, N. (1987). Single-step method of RNA isolation by acid guanidinium thiocyanate-phenol-chloroform extraction. Analytical Biochemistry *162*, 156-159.

Choudhury, D. (2010). Acute kidney injury: current perspectives. Postgraduate Medicine *122*, 29-40.

Chung, S.W., and Perrella, M.A. (2004). Role of HO-1 in renoprotection: Location, location, location. Kidney International *65*, 1968-1969.

Correa-Costa, M., Semedo, P., Monteiro, A., Silva, R., Pereira, R., Gonçalves, G., Marques, G., Cenedeze, M., Faleiros, A., Keller, A., *et al.* (2010). Induction of heme oxygenase-1 can halt and even reverse renal tubule-interstitial fibrosis. PLoS ONE *5*, e14298.

Da Silva, J.-L., Zand, B.A., Yang, L.M., Sabaawy, H.E., Lianos, E., and Abraham, N. (2001). Heme oxygenase isoform-specific expression and distribution in the rat kidn. Kidney International *59*, 1448-1457.

Datta, P., Koukouritaki, S., Hopp, K., and Lianos, E. (1999). Heme oxygenase-1 induction attenuates inducible nitric oxide synthase expression and proteinuria in glomerulonephritis. Journal of the American Society of Nephrology *10*, 2540-2550.

Day, Y., Huang, L., Ye, H., Li, L., Linden, J., and Okusa, M. (2006). Renal ischemia-reperfusion injury and adenosine 2a receptor-mediated tissue protection: the role of CD4+ T cells and IFN-gamma. Journal of Immunology *176*, 3108-3114.

Devarajan, P. (2006). Update on Mechanisms of Ischemic Acute Kidney Injury. Journal of the American Society of Nephrology *17*, 1503-1520.

de Vries, B., Kohl, J., Leclercq, W.K., Wolfs, T.G., van Bijnen A.A., Heeringa, P., Buurman W.A. (2003). Complement factor C5a mediates renal ischemia-reperfusion injury from neutrophils. Journal of Immunology *170*, 3883-3889.

Diot, E., Corcia, P., Zannad, N., Chauvet, M., Borie. M., and Maillot, F. (2007). Favorable outcome of acute porphyric neuropathy after treatment with heme arginate. Rev Neurol *163*, 1100-1102.

Doberer, D., Haschemi, A., Andreas, M., Zapf, T.-C., Clive, B., Jeitler, M., Heinzl, H., Wagner, O., Wolzt, M., and Bilban, M. (2010). Haem arginate infusion stimulates haem oxygenase-1 expression in healthy subjects. British Journal of Pharmacology *161*, 1476-5381.

Durante, W. (2010). Targeting heme oxygenase-1 in vascular disease. Current Drug Targets *11*, 1504-1516.

Eguchi, Y., Shimizu, S., and Tsujimoto, Y. (1997). Intracellular ATP Levels Determine Cell Death Fate by Apoptosis or Necrosis. Cancer Research *57*, 1835-1840.

Erwig, L.-P., and Henson, P. (2007). Immunological Consequences of Apoptotic Cell Phagocytosis. American Journal of Pathology *171*, 2-8.

Evans, M.J., and Kaufman, M.H. (1981). Establishment in culture of pluripotential cells from mouse embryos. Nature *292*, 154-126.

Fairchild, P.J., Brook, F.A., Gardner, R.L., GraÁa, L., Strong, V., Tone, Y., Tone, M., Nolan, K.F., and Waldmann, H. (2000). Directed differentiation of dendritic cells from mouse embryonic stem cells. Current Biology *10*, 1515-1518.

Ferenbach, D., Sheldrake, T., Dhaliwal, K., Kipari, T., Marson, L., Kluth, D., and Hughes, J. (2012). Macrophage/monocyte depletion by chlodronate, but not diphteria toxin, improves renal ischemia/reperfusion injury in mice. Kidney International *82*, 928-933.

Ferenbach, D.A., Nkejabega, N.C.J., McKay, J., Choudhary, A.K., Vernon, M.A., Beesley, M.F., Clay, S., Conway, B.C., Marson, L.P., Kluth, D.C., and Hughes, J. (2011). The induction of macrophage hemeoxygenase-1 is protective during acute kidney injury in aging mice. Kidney International *79*, 966-976.

Ferenbach, D.A., Ramdas, V., Spencer, N., Marson, L., Anegon, I., Hughes, J., and Kluth, D.C. (2010). Macrophages Expressing Heme Oxygenase-1 Improve Renal Function in Ischemia/Reperfusion Injury. Molecular Therapy *18*, 1706-1713.

Foresti, R., Shurey, C., Ansari, T., Sibbons, P., Mann, B., Johnson, T., Green, C., and Motterlini, R. (2005). Reviewing the use of carbon monoxide-releasing molecules (CO-RMs) in biology: implications in endotoxin-mediated vascular dysfunction. Cellular and Molecular Biology *51*, 409-423.

Forrester, L., Nagy, A., Sam, M., Watt, A., Stevenson, L., Bernstein, A., Joyner, A.L., and Wurst, W. (1996). An induction gene trap screen in embryonic stem cells: Identification of genes that respond to retinoic acid in vitro. Proceedings of the National Academy of Sciences *93*, 1677-1682.

Friedewald, J.J., and Rabb, H. (2004). Inflammatory cells in ischemic acute renal failure. Kidney International *66*, 486-491.

Fujisawa, N., Masatomo, Y., Hiroyoshi, S., Yuko, K., and Kamata, T. (2010). Discrepancy between cystatin C and creatinine points leading to a diagnosis of postrenal acute kidney injury and its reversibility: three case reports. Clinical and experimental nephrology *14*, 608-613.

Gaedeke, J., Noble, N.A., and A, B.W. (2005). Curcumin blocks fibrosis in anti-Thy 1 glomerulonephritis through up-regulation of heme oxygenase 1. Kidney International *68*, 2042-2049.

Gao, X., Kim, K.-S., and Liu, D. (2007). Nonviral Gene Delivery: What We Know and What Is Next. AAPS Journal *9*, E92-E104.

Golomb, B., and Evans, M. (2008). Statin adverse effects: a review of the literature and evidence for a mitochondrial mechanism. American Journal of Cardiovascular Drugs *8*, 373-418.

Gordon, S., and Philip, R.T. (2005). Monocyte and macrophage heterogeneity. Nature Reviews Immunology *5*, 953-964.

Gordon-Keylock, S.A.M., Jackson, M., Huang, C., Samuel, K., Axton, R.A., Oostendorp, R.A.J., Taylor, H., Wilson, J., and Forrester, L.M. (2010). Induction of Hematopoietic Differentiation of Mouse Embryonic Stem Cells by an AGM-Derived Stromal Cell Line is Not Further Enhanced by Overexpression of HOXB4. Stem Cells and Development *19*, 1687-1698.

Griffin, M.D. (2012). Mononuclear phagocyte depletion strategies in models of acute kidney disease: what are they trying to tell us? Kidney International *82*, 835-837.

Gueler, F., Park, J.-K., Rong, S., Kirsch, T., Lindschau, C., Zheng, W., Elger, M., Fiebeler, A., Fliser, D., Luft, F.C., and Haller, H. (2007). Statins attenuate Ischemia-Reperfusion Injury by Inducing Heme Oxygenase-1 in Infiltrating Macrophages. The American Journal of Pathology *170*, 1192-1199.

Guo, Y., Stein, A., Wu, W., Tan, W., Zhu, X., Li, Q., Dawn, B., Motterlini, R., and Bolli, R. (2004). Administration of a CO-releasing molecule at the time of reperfusion reduces infarct size in vivo. American Journal of Physiology Heart and Circulatory Physiology *286*, 1649-1653.

Hacein-Bey-Abina S., V.K.C., Schmidt M., McCormack MP., Wulffraat N., Leboulch P., Lim A, Osborne CS, Pawliuk R, Morillon E, Sorensen R, Forster A, Fraser P, Cohen JI, de Saint Basile G, Alexander I, Wintergerst U, Frebourg T, Aurias A, Stoppa-Lyonnet D, Romana S, Radford-Weiss I, Gross F, Valensi F, Delabesse E, Macintyre E, Sigaux F, Soulier J, Leiva LE, Wissler M, Prinz C, Rabbitts TH, Le Deist F, Fischer A, Cavazzana-Calvo M. (2003). LMO2-associated clonal T cell proliferation in two patients after gene therapy for SCID-X1. Science *302*, 415-419.

Hatcher, H., Planalp, R., Cho, J., Torti, F., and Torti, S. (2008). Curcumin: From ancient medicine to current clinical trials. Cellular and Molecular Life Sciences *65*, 1631-1652.

He, S., Nakada, D., and Morrison, S.J. (2009). Mechanisms of Stem Cell Self-Renewal. Annual Review of Cell and Developmental Biology *25*, 377-406.

Herzog, R., Cao, O., and Srivastava, A. (2010). Two decades of clinical gene therapy--success is finally mounting. Discovery Medicine *9*, 105-111.

Hesse, M., Modolell, M., La Flamme, A., Schiot, M., Fuentes, J., Cheever, A., Pearce, E., and Wynn, T. (2001). Differential regulation of nitric oxide synthase-2 and arginase-1 by type 1/type 2 cytokines in vivo: granulomatous pathology is shaped by the pattern of L-arginine metabolism. Journal of Immunology *167*, 6533-6544.

Hill-Kapturczak, N., and Agarwal, A. (2006). Carbon monoxide, from silent killer to potential remedy. American Journal of Physiology Renal Physiology *290*, 787-788.

Iacovino, M., Bosnakovski, D., Fey, H., Rux, D., Bajwa, G., Mahen, E., Mitanoska, A., Xu, Z., and Kyba, M. (2011). Inducible cassette exchange: a rapid and efficient system enabling conditional gene expression in embryonic stem and primary cells. Stem Cells *29*, 1580-1588.

Imai, E., Takabatake, Y., Mizui, M., and Isaka, Y. (2004). Gene therapy in renal diseases. Kidney International *65*, 1551-1555.

Inguaggiato, P., Gonzalez-Michaca, L., Croatt, A.J., Haggard, J.J., Alam, J., and Nath, K.A. (2001). Cellular overexpression of heme oxygenase-1 up-regulates p21 and confers resistance to apoptosis. Kidney International *60*, 2181-2191.

Jo, S.-K., Sung, S.-A., Cho, W.-Y., Go, K.-J., and Kim, H.-K. (2006). Macrophages contribute to the initiation of ischaemic acute renal failure in rats. Nephrology Dialysis Transplantation *21*, 1231-1239.

Jaguin, M., Houlbert, N., Fardel, O., and Lecureur, V. (2013). Macrophages (Mφ) are key sentinel cells of the innate immune system. Mφ are versatile and play a crucial role in the initiation, progression and resolution of inflammation. Cellular Immunology *281*, 51-61.

Karlsson, K.R., Cowley, S., Martinez, F.O., Shaw, M., Minger, S.L., and James, W. (2008). Homogeneous monocytes and macrophages from human embryonic stem cells following coculture-free differentiation in M-CSF and IL-3. Experimental Hematology *36*, 1167-1175.

Kawashima, A., Oda, Y., Yachie, A., and Koizumi, S. (2002a). Heme oxygenase-1 deficiency: The first autopsy case. Human Pathology *33*, 125-130.

Kawashima, A., Oda, Y., Yachie, A., Koizumi, S., and Nakanishi, I. (2002b). Heme oxygenase-1 deficiency: the first autopsy case. Human Pathology *33*, 125-130.

Kerr, J., Wyllie, A., and Currie, A. (1972). Apoptosis: a basic biological phenomenon with wide-ranging implications in tissue kinetics. British Journal of Cancer *26*, 239-257.

Khalil, P., Murty, P., and Palevsky, P.M. (2008). The Patient with Acute Kidney Injury. Primary care *35*, 239-296.

Kinderlerer, A.R., Pombo Gregoire, I., Hamdulay, S.S., Ali, F., Steinberg, R., Silva, G., Ali, N., Wang, B., Haskard, D.O., Soares, M.P., and Mason, J.C. (2009). Heme oxygenase-1 expression enhances vascular endothelial resistance to complement-mediated injury through induction of decay-accelerating factor: a role for increased bilirubin and ferritin. Blood *113*, 1598-1607.

Kinsey, G.R., Li, L., and Okusa, M.D. (2008). Inflammation in Acute Kidney Injury. Nephron Experimental Nephrology *109*, e102-e107.

Kinsey, G.R., Sharma, R., Huang, L., Li, L., Vergis, A.L., Ye, H., Ju, S.-T., and Okusa, M.D. (2009). Regulatory T Cells Suppress Innate Immunity in Kidney Ischemia-Reperfusion Injury. Journal of the American Society of Nephrology *20*, 1744-1753.

Kluth, D., Erwig, L., and Rees, A. (2004). Multiple facets of macrophages in renal injury. Kidney International *66*, 542-557.

Kluth, D.C., Ainslie, C.V., Pearce, W.P., Finlay, S., Clarke, D., Anegon, I., and Rees, A.J. (2001). Macrophages Transfected with Adenovirus to Express IL-4 Reduce

Inflammation in Experimental Glomerulonephritis. Journal of Immunology *166*, 4728-4736.

Kubulus, D., Mathes, A., Pradarutti, S., Raddatz, A., Heiser, J., Pavlidis, D., Wolf, B., Bauer, I., and Rensing, H. (2008). Hemin Arginate-Induced Heme Oxygenase 1 Expression Improves Liver Microcirculation and Mediates An Anto-Inflammatory Cytokine Response After Hemorrhagic Shock. Shock *29*, 583-590.

Laemmli, U. (1970). Cleavage of Structural Proteins during the Assembly of the Head of Bacteriophage T4. Nature *227*, 680-685.

Lieberthal, W., and Nigam, S.K. (2000). Acute renal failure. II. Experimental models of acute renal failure: imperfect but indispensable. American Journal of Physiology - Renal Physiology *278*, F1-F12.

Lin, Q., Weis, S., Yang, G., Yi-Hao., W., Helston, R., Rish, K., Smith, A., Bordner, J., Polte, T., Gaunitz, F., and Dennery, P.A. (2007). Heme Oxygenase-1 Protein Localizes to the Nucleus and Activates Transcription Factors Important in Oxidative Stress. The Journal of Biological Chemistry *282*, 20621-20633.

Maines, M.D., Trakshel, G.M., and Kutty, R.K. (1986). Characterization of two constitutive forms of rat liver microsomal heme oxygenase. Only one molecular species of the enzyme is inducible. The Journal of Biological Chemistry *261*, 411-419.

Marshall, E. (1999). Gene Therapy Death Prompts Review of Adenovirus Vector. Science *286*, 2244-2245.

Martinez, F. (2011). Regulators of macrophage activation. European Journal of Immunology *41*, 1531-1534.

McCoubrey, W.K., Huang, T.J., and Maines, M.D. (1997). Isolation and characterization of a cDNA from the rat brain that encodes hemoprotein heme oxygenase-3. European Journal of Biochemistry *247*, 725-732.

Moore, K.J., Fabunmi, R.P., Anderson, L.P., and Freeman, M.W. (1998). In vitro-differentiated embryonic stem cell macrophages: a model system for studying atherosclerosis-associated macrophage functions. Arteriosclerosis, Thrombosis, and Vascular Biology *18*, 1647-1654.

Mosser, D.M., and Edwards, J.P. (2008). Exploring the full spectrum of macrophage activation. Nature Reviews, Immunology *8*, 858-969.

Nakao, A., Neto, J., Kanno, S., Stolz, D., Kimizuka, K., Liu, F., Bach, F., Billiard, T., Choi, A., Otterbein, L., and Murase, N. (2005). Protection against ischemia/reperfusion injury in cardiac and renal transplantation with carbon monoxide, biliverdin and both. American Journal of Transplantation *5*, 282-291.

Napoli, I., Kierdorf, K., and Neumann, H. (2009). Microglial precursors derived from mouse embryonic stem cells. Glia. *57*, 1660-1671.

Nath, K.A. (2006). Heme oxygenase-1: A provenance for cytoprotective pathways in the kidney and other tissues. Kidney International *70*, 432-443.

Nimura, T., Weinstein, P.R., Massa, S.M., Panter, S., and Sharp, F.R. (1996). Heme oxygenase-1 (HO-1) protein induction in rat brain following focal ischemia. Molecular Brain Research *37*, 201-208.

Odegaard, J.I., Vats, D., Zhang, L., Ricardo-Gonzalez, R., Smith, K.L., Sykes, D.B., Kamps, M.P., and Chawla, A. (2007). Quantitative expansion of ES cell-derived myeloid progenitors capable of differentiating into macrophages. Journal of Leukocyte Biology *81*, 711-719.

Otterbein, L.E., Soares, M.P., Yamashita, K., and Bach, F.H. (2003). Heme oxygenase-1: unleashing the protective properties of heme. Trends in Immunology *24*, 449-455.

Pae, H.-O., Eun-Cheol., K., and Hun-Taeg., C. (2008). Integrative Survival Response Evoked by Heme Oxygenase-1 and Heme Metabolites. Journal of Clinical Biochemistry and Nutrition *42*, 197-203.

Poss, K.D., and Tonegawa, S. (1997). Heme oxygenase 1 is required for mammalian iron reutilization. Proceedings of the National Academy of Sciences of the United States of America *94*, 10919-10924.

Ryter, S.W., Alam, J., and Choi, M.K. (2006). Heme Oxygenase-1/Carbon Monoxide: From Basic Science to Therapeutic Applications. Physiological Reviews *86*, 583-650.

Ryter, S.W., and Choi, A.M.K. (2002). Heme Oxygenase-1: Molecular Mechanisms of Gene Expression in Oxygen-Related Stress. Antioxidants & Redox Signaling *4*, 625-632.

Ryter, S.W., and Choi, A.M.K. (2009). Heme Oxygenase-1/Carbon Monoxide: From Metabolism to Molecular Therapy. American Journal of Respiratory Cell and Molecular Biology *41*, 251-260.

Ryter, S.W., and Tyrrell, R.M. (2000). The heme synthesis and degradation pathways: role in oxidant sensitivity: Heme oxygenase has both pro- and antioxidant properties. Free Radical Biology and Medicine *28*, 289-309.

Sack, B., and Herzog, R. (2009). Evading the immune response upon in vivo gene therapy with viral vectors. Current opinion in molecular therapeutics *11*, 493-503.

Salom, M.G., Nieto Ceron, S., Rodriguez, F., Lopez, B., Hernandez, I., Gil Martinez, J., Martinez Losa, A., and Fenoy, F.J. (2007). Heme oxygenase-1 induction improves ischemic renal failure: role of nitric oxide and peroxynitrite. American Journal of Physiology - Heart and Circulatory Physiology *293*, 3542-3549.

Sardana, M.K., and Kappas, A. (1987). Dual control mechanism for heme oxygenase: tin(IV)-protoporphyrin potently inhibits enzyme activity while markedly increasing content of enzyme protein in liver. Proceedings of the National Academy of Sciences of the United States of America *84*, 2464-2468.

Sawle, P., Foresti, R., Mann, B., Johnson, T., Green, C., and Motterlini, R. (2005). Carbon monoxide-releasing molecules (CO-RMs) attenuate the inflammatory

response elicited by lipopolysaccharide in RAW264.7 murine macrophages. British Journal of Pharmacology *145*, 800-810.

Senju, S., Haruta, M., Matsumura, K., Matsunaga, Y., Fukushima, S., Ikeda, T., Takamatsu, K., Irie, A., and Nishimura, Y. (2011). Generation of dendritic cells and macrophages from human induced pluripotent stem cells aiming at cell therapy. Gene Therapy *18*, 874-883.

Shen, X., Ke, B., Uchida, Y., Ji, H., Gao, F., Zhai, Y., Busuttil, R., and JW, K.-W. (2011). Native macrophages genetically modified to express heme oxygenase 1 protect rat liver transplants from ischemia/reperfusion injury. Liver Transplant *17*, 201-210.

Sheridan, A.M., and Bonventre, J.V. (2000). Cell biology and molecular mechanisms of injury in ischemic acute renal failure. Current Opinion in Nephrology and Hypertension *9*, 427-434.

Shimizu, H., Takahasi, T., Suzuki, T., Yamasaki, A., Fujiwara, T., Odaka, Y., Hirakawa, M., Fujita, H., and Akagi, R. (2000). Protective effect of heme oxygenase induction in ischemic acute renal failure. Crit Care Med *28*, 809-817.

Shiraishi, F., Curtis, L., Truong, L., Poss, K., Visner, G., Madsen, K., Nick, H., and Agarwal, A. (2000). Heme oxygenase-1 gene ablation or expression modulates cisplatin-induced renal tubular apoptosis. American Journal of Physiology Renal Physiology *278*, 726-736.

Siamon, G. (2007). The macrophage: Past, present and future. European Journal of Immunology *37*, S9-S17.

Silk, K.M., Leishman, A.J., Nishimoto, K.P., Reddy, A., and Fairchild, P.J. (2012). Rapamycin Conditioning of Dendritic Cells Differentiated from Human ES Cells Promotes a Tolerogenic Phenotype. Journal of Biomedicine and Biotechnology *2012*, 11.

Soares, M.P., and Bach, F.H. (2009). Heme oxygenase-1: from biology to therapeutic potential. Trends in Molecular Medicine *15*, 50-58.

Stein, M., Keshav, S., Harris, N., and Gordon, S. (1992). Interleukin 4 potently enhances murine macrophage mannose receptor activity: a marker of alternative immunologic macrophage activation. The Journal of Experimental Medicine *176*, 287-292.

Ströfer, M., Jelkmann, W., and Depping, R. (2011). Curcumin decreases survival of Hep3B liver and MCF-7 breast cancer cells: the role of HIF. Strahlentherapie und Onkologie *187*, 393-400.

Suttner, D.M., and Dennery, P.A. (1999). Reversal of HO-1 related cytoprotection with increased expression is due to reactive iron. FASEB J. *13*, 1800-1809.

Sutton, T., CJ., F., and Molitoris, B. (2002). Microvascular endothelial injury and dysfunction during ischemic acute renal failure. Kidney International *62*, 1539-1549.

Tadagavadi, R., and Reeves, W. (2010). Renal dendritic cells ameliorate nephrotoxic acute kidney injury. Journal of the American Society of Nephrology *21*, 53-63.

Takeda, Y., Takeno, M., Iwasaki, M., Kobayashi, H., Kirino, Y., Ueda, A., Nagahama, K., Aoki, I., and Ishigatsubo, Y. (2004). Chemical induction of HO-1 suppresses lupus nephritis by reucing local iNOS expression and synthesis of anti-dsDNA antibody. Clinical and Experimental Immunology *138*, 237-244.

Tenhunen R, Tokola O, and Lindén IB (1987). Haem arginate: a new stable haem compound. J Pharm Pharmacol *39*, 780-786.

Tenhunen, R., Marver, H.S., and Schmid, R. (1969). Microsomal Heme Oxygenase, Characterisation of the Enzyme. The Journal of Biological Chemistry *244*, 6388-6394.

Thomson, J., J, I.-E., Shapiro, S., Waknitz, M., Swiergiel, J., Marshall, V., and Jones, J. (1998). Embryonic stem cell lines derived from human blastocysts. Science *282*, 1145-1147.

Tsubokawa, T., Yagi, K., Nakanishi, C., Zuka, M., Nohara, A., Ino, H., Fujino, N., Konno, T., Kawashiri, M., Ishibashi-Ueda, H., *et al.* (2010). Impact of anti-apoptotic and anti-oxidative effects of bone marrow mesenchymal stem cells with transient overexpression of heme oxygenase-1 on myocrdial ischemia. American Journal of Physiology Heart and Circulatory Physiology *285*, 1320-1329.

Tullius, S.G., Nieminen-Kelh‰, M., Bachmann, U., Reutzel-Selke, A., Jonas, S., Pratschke, J., Bechstein, W.O., Reinke, P., Buelow, R., Neuhaus, P., and Volk, H.-D. (2001). Induction of heme-oxygenase-1 prevents ischemia/reperfusion injury and improves long-term graft outcome in rat renal allografts. Transplantation Proceedings *33*, 1286-1287.

Vera, T., Henegar, J., Drummond, H., Rimoldi, J., and Stec, D. (2005). Protective effect of carbon monoxide-releasing compounds in ischemia-induced acute renal failure. Journal of the American Society of Nephrology *16*, 950-958.

Vinuesa, E., Hotter, G., Jung, M., Herrero-Fresneda, I., Torras, J., and Sola, A. (2008). Macrophage involvement in the kidney repair phase after ischaemia/reperfusion injury. The Journal of Pathology *214*, 104-113.

Wagener, F.A.D.T.G., Volk, H.-D., Willis, D., Abraham, N.G., Soares, M.P., Adema, G.J., and Figdor, C.G. (2003). Different Faces of the Heme-Heme Oxygenase System in Inflammation. Pharmacol Rev *55*, 551-571.

Wang, Y., Wang, Y.P., Zheng, G., Lee, V.W.S., Ouyang, L., Chang, D.H.H., Mahajan, D., Coombs, J., Wang, Y.M., Alexander, S.I., and Harris, D.C.H. (2007). Ex vivo programmed macrophages ameliorate experimental chronic inflammatory renal disease. Kidney International *72*, 290-299.

Weis, N., A Weigert, A., von Knethen, A., and Brune, B. (2009). Heme Oxygenase-1 Contributes to an Alternative Macrophage Activation Profile Induced by Apoptotic Cell Supernatants. Molecular Biology of the Cell *20*, 1280-1288.

Wiesel, P., Patel, A., Carvajal, I., Wang, Z., Pellacani, A., Maemura, K., DiFonzo, N., Rennke, H., Layne, M., Yet, S., *et al.* (2001). Exacerbation of Chronic Renovascular Hypertension and Acute Renal Failure in Heme Oxygenase-1-Deficient Mice. Circulation Research *88*, 1088-1094.

William, K.M., Jr., Huang, T.J., and Mahin, D.M. (1997). Isolation and Characterization of a cDNA from the Rat Brain that Encodes Hemoprotein Heme Oxygenase-3. European Journal of Biochemistry *247*, 725-732.

Wilson, H., Stewart, K., Brown, P., Anegon, I., Chettibi, S., Rees, A., and Kluth, D. (2002). Bone-marrow-derived macrophages genetically modified to produce IL-10 reduce injury in experimental glomerulonephritis. Molecular Therapy *6*, 710-717.

Wu, C.-C., Lu, K.-C., Chen, J.-S., Hsieh, H.-Y., Lin, S.-H., Chu, P., Wang, J.-Y., Sytwu, H.-K., and Lin, Y.-F. (2008). HO-1 induction ameliorates experimental murine membranous nephropathy: anti-oxidative, anti-apoptotic and immunomodulatory effects. Nephrology Dialysis Transplantation *23*, 3082-3090.

Xue, H., Guo, H., Li, Y.-C., and Hao, Z.-M. (2007). Heme oxygenase-1 induction by hemin protects liver cells from ischemia/reperfusion injury in cirrhotic rats. Wolrd Journal of Gastroenterology *13*, 5384-5390.

Yamagishi, H., Yokoo, T., Imasawa, T., Mitarai, T., Kawamura, T., and Utsunomiya, Y. (2001). Genetically modified bone marrow-derived vehicle cells site specifically deliver an anti-inflammatory cytokine to inflamed interstitium of obsrtuctive nephropathy. Journal of Immunology *166*, 609-616.

Yang, C., Zhang, X., Fan, H., and Liu, Y. (2009). Curcumin upregulates transcription factor Nrf2, HO-1 expression and protects rat brains against focal ischemia. Brain Research *1282*, 133-141.

Yoneya, R., Ozasa, H., Nagashima, Y., Koike, Y., Teraoka, H., Hagiwara, K., and Horikawa, S. (2000). Hemin pretreatment ameliorates aspects of the nephropathy induced by mercuric chloride in the rat. Toxicology Letters *116*, 223-229.

Zheng, D., Wang, Y., Cao, Q., Lee, V., Zheng, G., Sun, Y., Tan, T., Wang, Y., Alexander, S., and Harris, D. (2011). Transfused macrophages ameliorate pancreatic and renal injury in murine diabetes mellitus. Nephron. Experimental Nephrology *118*, e87-99.

Zhong, F., Chen, H., Han, L., Jin, Y., and Wang, W. (2011). Curcumin attenuates lipopolysaccharide-induced renal inflammation. Biological and Pharmaceutical Bulletin *34*, 226-232.

Zhong, L., Li, B., Mah, C., Govindasamy, L., Agbandje-McKenna, M., Cooper, M., Herzog, R., Zolotukhin, I., Warrington, K.J., Weigel-Van Aken, K., *et al.* (2008). Next generation of adeno-associated virus 2 vectors: point mutations in tyrosines lead to high-efficiency transduction at lower doses. Proceedings of the National Academy of Sciences of the United States of America *105*, 7827-7832.

Zhou, H., Ramiya, V., and Visner, G. (2006). Bone marrow stem cells as a vehicle for delivery of heme oxygenase-1 gene. Stem Cells and Development *15*, 79-86.

Zhuang, L., Pound, J., Willems, J., Taylor, A., Forrester, L., and Gregory, C. (2012). Pure populations of murine macrophages from cultured embryonic stem cells. Application to studies of chemotaxis and apoptotic cell clearance. Journal of Immunological Methods *385*, 1-14.